

S.L. Codd, Mechanical and Industrial Engineering, Montana State University.

NMR basics will be very briefly introduced, as will the use of gradients to encode the NMR signal for position. However, most of this educational presentation will be devoted to exploring the range of NMR techniques that can be used to encode for the flow and diffusion of fluids.

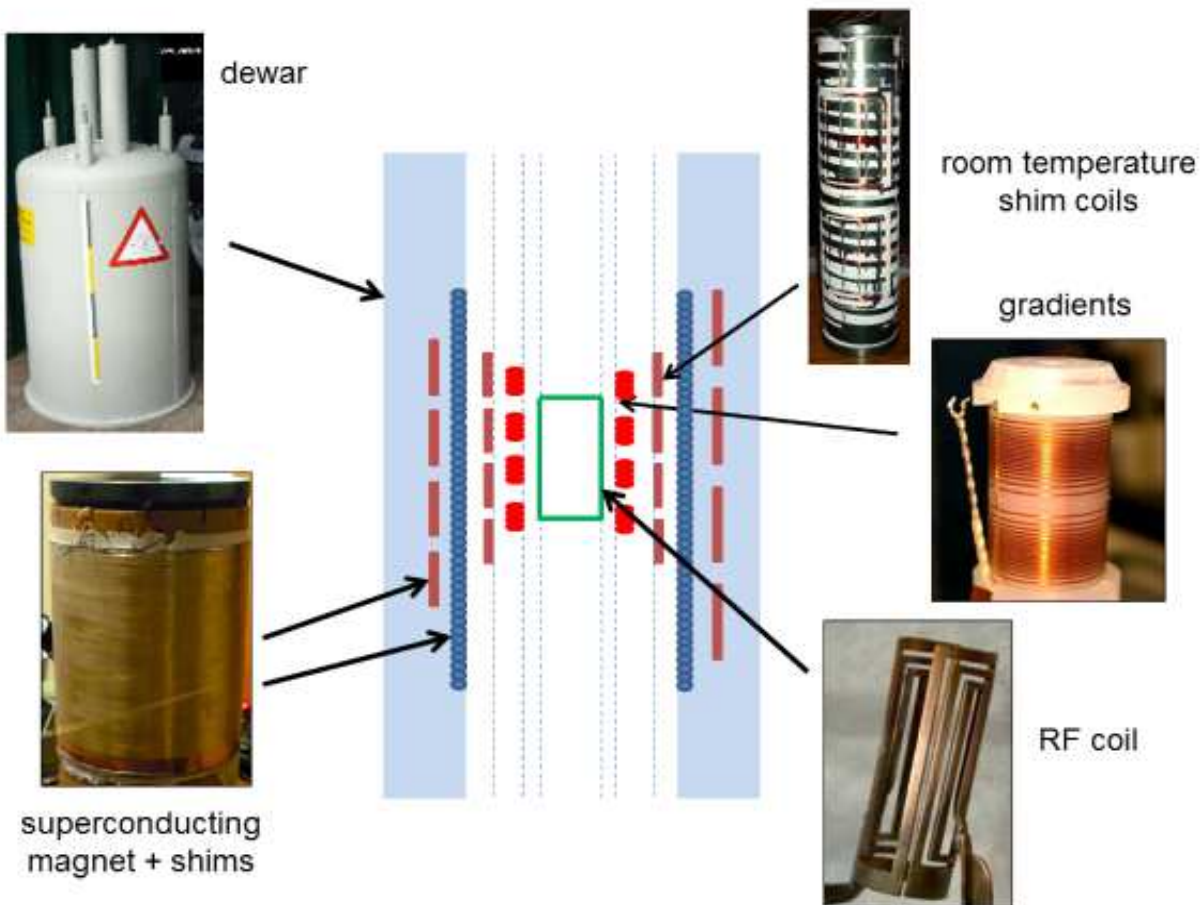
The use of spin echoes to determine diffusive molecular motion was first demonstrated in 1950. In 1965 pulsed gradients (PGSE) were added and highlighted a direct relationship between the echo amplitude and the self-diffusion coefficient of the spins. This was the start of an exciting exploration into what information could be accessed by non-invasively measuring and comparing the average motion of fluids over various time windows. PGSE sequences have been developed to explore progressively shorter times and smaller distances, and to separate coherent and stochastic motion over a spectrum of times. In particular, unique information has been yielded in turbulent flows, rheology of complex fluids such as polymers, emulsions and colloids, liquid flow in porous materials, and gas transport in porous media.

**MR/MRI Hardware**

A.G. Webb, Gorter Center for High Field MRI, Department of Radiology, Leiden University Medical Center, The Netherlands.

Magnetic resonance systems are used in almost every academic and industrial chemistry, physics and biochemistry department, as well as being one of the most important imaging modalities in clinical radiology. The design of such systems has become increasingly sophisticated over the years. Static magnetic fields increase continuously, large-scale arrays of receive elements are now ubiquitous in clinical MRI, cryogenic technology has become commonplace in high resolution NMR and is expanding rapidly in preclinical MRI, specialized high strength magnetic field gradients have been designed for studying the human connectome, and the commercial advent of ultra-high field human imaging has required new types of RF coils and static shim coils together with extensive electromagnetic simulations to ensure patient safety.

This talk will cover the hardware and engineering that constitutes a magnetic resonance system, whether that be a high-resolution liquid or solid state system for NMR spectroscopy, a preclinical system for imaging animals or a clinical system used for human imaging.



**A Hitchhikers Guide to Small Animal MRI/MRS**

J.F. Dunn<sup>a,b,c</sup>, <sup>a</sup>Experimental Imaging Centre; <sup>b</sup>Cumming School of Medicine; <sup>c</sup>University of Calgary.

Animal research has been a cornerstone in the development of MRI, from the early days of spectroscopy and imaging, through the development of BOLD and a range of commonly used methods. Moving forward, what does the future hold? We are at a junction in the use of small animals for MRI and MRS research. There is a strong sentiment in some corners of the galaxy, in support of the idea that animal research is not as relevant as it once was. This educational talk will take us on a journey from the past to the future. I will discuss some of the early applications and success of small animal MRI/MRS. I will provide some insight as to what constitutes both good and bad questions to be addressed using animal research. In pre-clinical research it is critical to choose the correct model for the correct question. Animal model research falls largely into 4 types of studies: one is to develop and validate MRI methods that are sensitive and specific to a life process (disease, tissue structure, physiology); a second is to increase our understanding of how life works (development, anatomy, physiology, molecular and biochemical processes); third is to study disease processes (triggers and pathophysiology of disease), and the fourth is to use animal models for research into treatment options (diet, drugs, etc.). Be clear on your goals. Included will be comments about knowledge translation. I will discuss some of the problems, advantages, and challenges of using animal models from motion correction to anesthesia. I will provide information on some of the current technologies (magnets etc.) for animal work. This talk will provide an overview of the role that small animal research can play in technology development, and life science applications, with the premise that the field will continue to thrive. That is, as long as the Vogons don't decide to destroy Earth to create a hyperspace bypass.

**Compact Magnetic Resonance: Frontiers and Challenges**

D. Sakellariou<sup>\*</sup>, Center of Surface Chemistry and Catalysis, Faculty of Bioscience Engineering, KU Leuven, Belgium.

Magnetic Resonance spectroscopy (NMR) and imaging (MRI) have revolutionized science and medicine by their capacity to analyze matter in a non-invasive, three dimensional and localized manner. Applications cover very broad areas from chemical analysis, material characterization, bio-molecular structure and dynamics, anatomic and functional in vivo imaging. This extremely powerful technique has however several limitations, which reduce its widespread use in society, in view of industrial and bio-medical applications. Low signal sensitivity, high-cost and limited availability are three of the main challenges for the next generation of modern magnetic resonance devices and technologies.

Several options for pushing the current limits will be discussed with particular emphasis on miniaturization for the magnet and the detector system. I will introduce fundamental ideas behind intuitive and optimized permanent magnet design, present and comment on several examples from single-sided portable magnetic resonance sensors and desktop NMR magnet systems. Several directions towards novel magnet technologies will be discussed with particular focus on MRI localized spectroscopy in the presence of rotating fields, on and on variable magnetic fields high-resolution relaxometry. These instrumental and methodological approaches are aiming at applications in chemistry and chemical engineering for in situ analysis, in industry for on-line non-destructive monitoring and quality control, in personalized medicine for metabolic profiling of tissue extracts or organisms in vivo, in the study and optimization of contrast agents, and open the way for modern magnetic resonance devices for dedicated use.

**Quantitative MR Evolution or Revolution?**

[RS Hinks](#)<sup>§</sup>, GE Healthcare.

The history of MR Imaging, from its earliest conception in the early '70s through commercialization in the '80s and on to the present day has been replete with promises that Quantitative MR (qMR) Imaging would radically change diagnosis, treatment, and staging of diseases. This hope arises from the recognition that the NMR signal in the human body is sensitive to a wide range of phenomena such as relaxation times, chemical shift, magnetization transfer, motion, and flow, in addition to concepts such as shape and volume afforded by the increasingly precise localization of MR Imaging. Some key enablers of quantitative MR include:

- Advances in MR system engineering enable MR experiments to more correctly match physics theory.
- Better compute capability improves image quality and the ability to model more complex systems.
- Phantoms for ensuring standardization in qMR are being developed and becoming commercially available.
- Increasing standardization between systems allows improved multi-site trials.
- Modern trends in data analysis including machine learning allow identification of significant patterns in complex data sets.

This talk will build a context of MR imaging based on historical development, with the hope of providing insight into future trends in Quantitative MR.

**Uncommon Journey Through the Land of Spins**

E. Fukushima, ABQMR, Albuquerque, New Mexico, USA.

I will describe my journey through the Land of Spins. There were many encounters with people, places, and activities. Memorable people include Erwin Hahn, Edwin Uehling, Irv Lowe, Jasper Jackson, Bill Rollwitz, Al Garroway, Paul Lauterbur, Janez Stepisnik, Bernhard Bluemich, and Paul Callaghan. Places and activities that come to mind include building a pulse NMR rig in the '60s (with vacuum tubes), a front row seat in the '70s to watch the development of carbon-13 distillation facility at Los Alamos, flow measurements of non-Newtonian fluids including grains, Siberian field-trips while looking for aquifers and leaked gasoline, launching our NMR research activity as a small business, and building a helicopter-borne Earth's field NMR for use on Arctic Sea.

P.J. Basser<sup>\*,§</sup>, Eunice Kennedy Shriver National Institute of Child Health and Human Development, NIH.

While diffusion tensor MRI(1) has provided a quantitative means to characterize macroscopically isotropic and anisotropic tissues, such as brain gray matter (GM) and white matter (WM), respectively, following its invention and development, there has been a trend toward using more advanced diffusion MRI methods to "drill deeper into the voxel"--to extract additional anatomical features and morphological details, such as intra and extracellular volume fractions, and features of cell size, shape and orientation, to aid in assessment of pathology or to follow changes in development. Formerly, we called this activity "in vivo MRI histology", but increasingly the term "microstructure imaging" has been applied. Model-based displacement MR approaches have been used to estimate distinct features of neural tissue. One method treats the extra-axonal space in WM as hindered and anisotropic, described by a DTI model, and the intra-axonal space as restricted tubes (2, 3). This composite hindered and restricted model of diffusion (CHARMED) MRI framework was then extended to measure the diameter distribution of a pack of cylindrical axons in WM (AxCaliber) (4), by adapting the particle sizing method proposed by Packer et al. to estimate the diameter distribution of spherical droplets using NMR PFG methods (5). Viewing dendrites in GM as an ensemble of restricted tubes, Komlosh et al. applied multiple PFG-MR and MRI sequences to measure and characterize microscopic diffusion anisotropy in GM phantoms and GM (6-8). The classic "k-space and q-space imaging" method for estimating a 3-D average propagator in each voxel without assuming a Gaussian displacement distribution (9) was adopted and adapted by Wedeen (as diffusion spectrum imaging or DSI) (10, 11) to obtain information about crossing fibers in WM(12, 13). The primary bottleneck for in vivo applications of these methods is the need to densely sample 3-D q-space in order to reconstruct the average propagator using a 3-D FFT. One strategy we employed was to use efficient CT reconstruction algorithms and a priori information about the average propagator and of  $E(q)$  (14). Another promising approach was developed by Özarlsan et al.(15), who used orthogonal Hermite functions to efficiently represent  $E(q)$ . More recently, it has become apparent that information about tissue water compartments (microdynamics) in tissue could be biologically and clinically useful, particularly in conjunction with diffusion MRI data. Again, porous media NMR approaches applied for decades to sandstones and concrete, have the potential to reveal distinct water compartments within tissues. The primary obstacle for biological and clinical translation of these approaches is again the preponderance of MR data required. We addressed this problem systematically, first by applying compressed sensing to reduce the data required for 2D spectroscopic/relaxometric MRI ten-fold (16), and then employing experimental design and reconstruction innovations, allowing Benjamini et al. to reduce data acquisition requirements by almost another factor of ten (17), making these approaches clinically practicable/feasible for the first time. Other isotropic diffusion MRI spectroscopy methods are potentially promising to identify different water compartments in WM and GM. We expect that in the coming decade, porous media concepts will inform the assessment of normal and abnormal development and aging, and disease and degeneration processes in animal models and in the clinic.

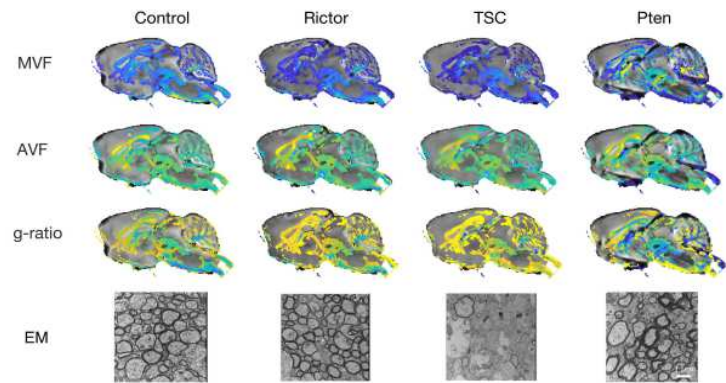
1.Basser et al., *Biophys J* 66, 259 (1994). 2.Assaf Y, et al., *Magn Reson Med* 52, 965 (2004). 3.Assaf Y, et al. *Neuroimage* 27, 48 (2005). 4.Assaf Y, et al., *Magn Reson Med* 59, 1347 (2008). 5.Packer K J, et al., *J. Colloid Interface Sci.* 40, 206 (1972). 6.Komlosh M E, et al., 47th ENC. (Asilomar, CA, 2006), pp. E060077. 7.Komlosh M E, et al., *J Magn Reson* 189, 38 (2007). 8.Komlosh M E, et al., *Magn. Reson. Med*, (2008). 9.Callaghan P T, et al.. *J. Phys. E: Sci. Instrum.* 21, 820 (1988). 10.Wedeen V J, et al., 8th Annual ISMRM. (Denver, 2000), pp. 82.11.Wedeen V J, et al., *Magn Reson Med* 54, 1377 (2005).12.Wedeen V J, et al., *Biophys J* 80, 1024 (2001).13.Wedeen V J, et al. *Neuroimage* 41, 1267 (2008). 14.Pickalov V, et al., 3rd IEEE ISBI'06: From Macro to Nano. (Arlington, VA, 2006), pp. 710-713.15.Ozarlsan E, et al. *Neuroimage* 78, 16 (2013). 16.Bai R, et al. *J Magn Reson* 255, 88 (2015). 17. Benjamini D, et al. *J Magn Reson* 271, 40 (2016).

## MRI Characterization of White Matter in Rodent Brain

MD Does<sup>§</sup>, Vanderbilt University.

MRI provides contrast that is sensitive to the microstructure and composition of many tissues, including cerebral white matter. Efforts to develop methods that also provide *specific* characterizations of white matter, such as the volume fraction of myelin or the mean axon diameter, are ongoing. For in vivo human imaging, such methods may offer unique windows into neurological and psychiatric disorders and have the potential to serve as important clinical biomarkers. Presently, the development of such methods is limited by scan time/signal-to-noise ratio and lack of gold standard validation.

However, for the purpose of ex vivo imaging of mice, these limitations can be largely overcome. That is, MRI is already well suited to be a routine tool for the quantitative evaluation of white matter in mouse models of neurologic and psychiatric disorders. This presentation will cover the development and experimental evaluation of a number of quantitative MRI measures, applied to select mouse models of abnormal white matter microstructure. Example images of myelin volume fraction (MVF), axon volume fraction (AVF), and g-ratio, along with electron microscopy, are shown for four different types of genetic mouse strains, each exhibiting different white matter characteristics.





## Low-field MRI studies of Enhanced Oil Recovery processes

E.J.Fordham<sup>\*</sup> and J Mitchell<sup>§</sup>, Schlumberger Gould Research, Cambridge CB3 0EL, UK.

MRI has long been of interest as a laboratory tool for flows in porous media [1], because of its insensitivity to the solid matrix and the potential for robust discrimination of immiscible phases as found ubiquitously in petroleum reservoirs. Enhanced Oil Recovery (EOR) processes are defined as recovery processes involving "substances not naturally present in the reservoir" [2], increasing the physico-chemical complexity of the system and process studied. They are high-value processes for which laboratory screening of some kind is a mandatory stage. For laboratory core floods, MRI has not achieved high acceptance in comparison to X-ray absorption, in spite of the latter's requirement for chemical doping and sometimes disappointing quantitative accuracy [3]. We show that quantitative NMR can be successfully used for EOR core floods, given suitable specification of NMR hardware and sample holders, and furthermore with simple and straightforward pulse sequences [4].

This talk will summarise work over several years on several different types of EOR process, using straightforward MRI methods (typically one dimension only of spatial resolution) and low-field NMR hardware (2 or 12 MHz <sup>1</sup>H resonance), and sample holders appropriate to the system investigated. Applications, with comparison to available oilfield pilot study measurements [5,6], will cover the following categories of EOR process: Alkali-Surfactant-Polymer (ASP) [7], Alkali-Surfactant (AS) [8], Polymer EOR [9], and Miscible Gas [10] recoveries. Physical and petrophysical considerations underlying the hardware specification and experimental design will be discussed, and particular opportunities for MRI methods will be highlighted.

### References:

- [1] J. Mitchell, T.C. Chandrasekera, D.J. Holland, L.F. Gladden & E.J. Fordham (2013). Magnetic resonance imaging in laboratory petrophysical core analysis. *Physics Reports*, **526** (3) 165225.
- [2] L. W. Lake (1989). *Enhanced Oil Recovery*. Prentice-Hall.
- [3] A.W. Cense, H.A. van der Linder, N. Brussee, J. Beljaars & A. Schwing (2014). How reliable is In Situ Saturation Monitoring (ISSM) using X-ray? *Int. Symp. Soc. Core Analysts*, Avignon, France, Sept. 2014. Paper **SCA2014-009**
- [4] J. Mitchell, L.F. Gladden, T.C. Chandrasekera & E. J. Fordham (2014). Low-field permanent magnets for industrial process and quality control. *Prog. Nucl. Magn. Reson. Spectroscopy* **76**, 160.
- [5] J. Edwards *et al.* (2011). Single-well in-situ measure of oil saturation remaining in carbonate after an EOR chemical flood. *SPE Middle East Oil and Gas Show*, Manama, Bahrain, 25-28 September, Paper **SPE141091**.
- [6] J. Mitchell *et al.* (2012). Quantitative remaining oil saturation using magnetic resonance: From the laboratory to the pilot. *SPE EOR Conf at Oil & Gas West Asia*, Muscat, Oman, April 2012. Paper **SPE154704**
- [7] J. Mitchell, J. Staniland, R. Chassagne & E.J. Fordham (2012). Quantitative in situ enhanced oil recovery monitoring using nuclear magnetic resonance. *Trans. Porous Media*, **94**, 683786
- [8] J. Mitchell *et al.* (2012). Magnetic resonance imaging of chemical EOR in core to complement field pilot studies. *Int. Symp. Soc. Core Analysts*, Aberdeen, Scotland, Aug. 2012 Paper **SCA2012-30**
- [9] A. Clarke, A. Howe, J. Mitchell, J. Staniland, L. Hawkes & K. Leeper (2015). Mechanism of anomalously increased oil displacement with aqueous viscoelastic polymer solutions. *Soft Matter* **11**, 35363541.
- [10] J. Edwards *et al.* (2012). Time-lapse diffusion logs to discriminate reservoir oil from Miscible gas. *SPE EOR Conf at Oil & Gas West Asia*, Muscat, Oman, April 2012. Paper **SPE154616**.

**MR and multi-modal contrast agent development**

P. Caravan<sup>\*§</sup>, Athinoula A. Martinos Center for Biomedical Imaging, Massachusetts General Hospital & Harvard Medical School.

Contrast agents are widely used in clinical MRI with about 50% of all procedures employing a gadolinium-based contrast agent. Contrast agents can provide better delineation of pathology, functional information such as organ perfusion or permeability, shorten exam times, and yield greater diagnostic confidence. While clinical contrast agents provide information based solely on their distribution and pharmacokinetics, newer contrast agents in development can provide more specificity for pathology, taking a so-called molecular MR approach. One mechanism is conjugate a targeting group, a peptide or small molecule that recognizes and binds to a protein associated with disease, to a MR-active reporter like a gadolinium-chelate. Another approach is to have the relaxivity of the contrast agent change in response to an environmental stimulus such as pH change or the presence of a specific enzyme. It is also possible to incorporate other imaging reporters (gamma or positron emitters, fluorophores) into the contrast agent to create multimodal contrast agents that can be detected with different imaging devices. This educational lecture will describe these varied approaches, including the strengths and limitations of each, drawing on the state of the art for examples.

## Complementary Imaging of Cartilage by $\mu$ MRI, $\mu$ CT, and Optical Microscopies

Y. Xia<sup>\*</sup>, Department of Physics and Center for Biomedical Research, , Oakland University, , Rochester, MI 48309, USA.

As articular cartilage is the load-bearing tissue in a complex organ (the joint) that offers mechanical functions to the body, biomechanical properties of the tissue (e.g., compressive modulus) should be the ultimate measures of the tissue's health. These biomechanical properties of cartilage, however, are determined at the molecular level by the amounts and spatial arrangements of biomolecules as well as the interactions among them. Furthermore, the environment in which these biomolecules exist is regulated at the cellular level by the cartilage cells, chondrocytes. In cartilage, these cells are also spatially confined at the morphological level by the architectures of the extracellular matrices.

Gradual degradation of articular cartilage is the hallmark of osteoarthritis (OA), a musculoskeletal disease that is the number one cause of disability in most countries. Although the disease always results in the same end-stage symptom (loss of joint function), the degradation of the tissue can have different early-stage characteristics and be either idiopathic or linked to different initiation events or risk factors, such as trauma, obesity, or biomechanical instability. Currently, an accurate diagnosis of OA, at a time when an interventional procedure is potentially beneficial, remains elusive in current clinical practice.

The multiscale features of cartilage biology and cartilage degradation mandate the need for a wide range of research tools and approaches that extend beyond the traditional boundaries of research. This presentation describes our research journey at Oakland University, from a small lab in 1994 with a single technology (microscopic MRI,  $\mu$ MRI) to our current multidisciplinary microscopic imaging lab. We have  $\mu$ MRI (which offers a direct translation pathway to clinical MRI), polarized light microscopy (PLM, which is the gold standard in biology and clinical pathology), Fourier-transform infrared imaging (FTIRI, which offers a true capability in chemical imaging), and microscopic computer tomography ( $\mu$ CT, which enables the study of cartilage-bone interface). Together with biochemical assays (which quantifies molecular contents) and biomechanical testing (which calibrates the mechanical health of cartilage), we examine the influence of the molecular and microscopic changes on tissue's functional integrity, providing critical information towards the understanding, and ultimately, management of early arthritic diseases.

In this presentation, the physics and capabilities of these imaging tools will be briefly described, together with some recent results. With a spatial resolution from a fraction of a micron to tens of microns in these microscopic imaging tools, some non-cartilage examples will also be introduced to demonstrate the salient nature of these tools in application to projects in science and engineering.

## Magnetic Resonance Imaging with Hyperpolarized and Inert Gas Contrast Agents and Xenon Biosensor Molecular MRI

MS Albert<sup>a,b,c</sup>, <sup>a</sup>Department of Chemistry, Lakehead University, Thunder Bay, ON, Canada; <sup>b</sup>Thunder Bay Regional Health Research Institute, , Thunder Bay, ON, Canada; <sup>c</sup>Northern Ontario School of Medicine, Thunder Bay, ON, Canada.

Hyperpolarized noble gases and inert fluorinated gases are combined with magnetic resonance imaging (MRI) to image the internal structures of the body with much greater sensitivity than current imaging technology. Applications include lung imaging, brain imaging, and the use of molecular biomarkers to target disease. A particularly useful application of this technology is for lung imaging. Fluorine-19 (<sup>19</sup>F) technology is currently being tested to determine if the quality of <sup>19</sup>F lung images obtained can be used to provide clinical information beyond the capability of current imaging technology. Due to its low-cost and abundance, this technology could be easily implemented in every MRI scanner in the world. Our group has recently made substantial progress in the field of brain imaging. For the first time, volunteers with Alzheimer's disease have been imaged using the hyperpolarized xenon-129 (HP <sup>129</sup>Xe) MRI technology and HP <sup>129</sup>Xe functional MRI. Preliminary results have shown to be promising for potential early detection of Alzheimer's disease and could also have implications for drug treatment and monitoring of the disease. Molecular biosensors are a useful tool for identification of disease sites in the body. Despite the lack of direct specificity of noble gases for biological receptors, they can be delivered to a target by means of molecular systems that can encapsulate the noble gas. Our team has successfully obtained the first ever in vivo images of cucurbit[6]uril, for a HP <sup>129</sup>Xe biosensor to image the vascular system throughout a living animal model. Future work will determine the potential to detect various disease target sites in the body. Overall, there is a wide range of applications for HP noble and inert fluorinated gas MRI in the diagnosis and treatment monitoring of human disease. Our research program continues to strive toward the ultimate goal of clinical translation.

## Breakdown of Carr-Purcell-Meiboom-Gill spin echoes in inhomogeneous fields

L-S Bouchard<sup>\*s</sup> and NN Jarenwattanon, Department of Chemistry and Biochemistry, University of California Los Angeles.

We have found unexpected behavior of NMR signals in gases, with respect to the temperature dependence of linewidth [1, 2] as well as behavior of CPMG echoes. The NMR signal decay for uncoupled spins in an external field gradient  $g$  follows [3]

$$S(\tau) = \exp(-2\tau/T_2) \exp(-2\tau^3\gamma^2g^2D/3) \quad (1)$$

in which  $2\tau$  is the evolution time,  $T_2$  is the spin-spin relaxation time,  $\gamma$  is the nuclear gyromagnetic ratio, and  $D$  is the self-diffusion coefficient. In the absence of a large magnetic field inhomogeneity and large diffusion rate, the expression collapses to  $\exp(-2\tau/T_2)$ . The CPMG train eliminates the  $\tau^3$  term [4, 5] in a train of  $n$  echoes, where  $2\tau$  is the interpulse spacing:

$$S(t) = \exp(-n2\tau/T_2) \exp[-\tau^2\gamma^2g^2D(n2\tau)/3] \quad (2)$$

In the limit of short interpulse spacing ( $\tau \rightarrow 0$ , but holding  $n2\tau$  constant), CPMG minimizes the effect of molecular self-diffusion on nuclear spin decoherence in inhomogeneous magnetic fields. The contribution of the inhomogeneous term becomes negligible as  $\tau^2 \rightarrow 0$ , recovering  $\exp(-2\tau/T_2)$ . This expression works well in liquids.

However, in gases the situation is different. We used the CPMG sequence to probe NMR signal decay in liquids and gases and found different behaviors of the decay function in a magnetic field gradient (Fig. 1). In gases, we find that CPMG is unable to eliminate signal decay in the limit of short interpulse spacings ( $\tau \rightarrow 0$ ), making it impossible to recover the true  $T_2$  time in that limit. The  $T_2$  time recovered in the limit  $\tau \rightarrow 0$  depends on the applied gradient  $g$ . This is to be contrasted to the case of liquids, where the true  $T_2$  value is recovered in the limit  $\tau \rightarrow 0$  regardless of the applied  $g$ . This behavior is due to nature of motional averaging of gases, which is fundamentally different than motional averaging in liquids. In a gas, the Einstein-Fick approximation does not apply. For a gas, the correct expression for signal decay is:  $\exp[-\gamma^2g^2\kappa\tau]$ , where  $\kappa$  is a temperature-dependent term [1, 2]. Application of the CPMG sequence with  $n$  echoes leads to a decay function proportional to:

$$\exp[-\gamma^2g^2\kappa(2n\tau)] \quad (3)$$

Taking the limit  $\tau \rightarrow 0$  while keeping  $2n\tau$  fixed does not eliminate the signal decay. This demonstrates a fundamentally different behavior in inhomogeneous fields: with gases, shortening the interpulse spacing does not eliminate the signal decay. Many NMR/MRI experiments, where field gradients are applied during the signal readout, could be impacted by this effect.

### References

- [1] N. N. Jarenwattanon *et al.*, "Thermal maps of gases in heterogeneous reactions," *Nature*, **502**, 537540, 2013.
- [2] N. N. Jarenwattanon and L.-S. Bouchard, "Motional averaging of nuclear resonance in a field gradient," *Phys. Rev. Lett.*, **114**, 197601, 2015.
- [3] E. L. Hahn, "Spin echoes," *Phys. Rev.*, **80**, 580594, 1950.
- [4] H. Y. Carr and E. M. Purcell, "Effects of diffusion on free precession in nuclear magnetic resonance experiments," *Phys. Rev.*, **94**, 630638, 1954.
- [5] S. Meiboom and D. Gill, "Modified spin-echo method for measuring nuclear relaxation times," *Rev. Sci. Instrum.*, **29**, 688691, 1958.

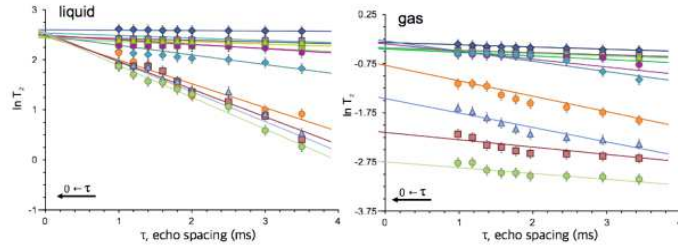


Fig. 1: For a liquid, short interpulse spacing in the CPMG sequence minimizes the effect of magnetic field inhomogeneity on nuclear spin decoherence. As  $\tau \rightarrow 0$ ,  $T_2$  approaches a single value. However, for gases, short interpulse spacing in CPMG cannot eliminate signal decay originating from field inhomogeneity. For each plot, the different colors represent applied gradients ( $g$ ) of different magnitudes;  $g$  ranges from 0 G/cm (dark blue diamonds) to 1 G/cm (light green circles).

## *In situ* NMR Imaging of Ion Transport in Li-Ion Batteries

G.R. Goward<sup>\*§</sup>, S.A. Krachkovskiy and J.D. Bazak, Department of Chemistry, McMaster University; B.J. Balcom, Department of Physics, University of New Brunswick; I.C. Halalay, General Motors Global R & D.

Effective modeling the performance of automotive Li-ion batteries requires the knowledge of electrolyte transport properties: specific conductivity,  $\text{Li}^+$  transference number and salt diffusion coefficient, as functions of temperature and salt concentration. An accurate determination of these parameters is not a trivial task, due to the fact that the values of ionic diffusion coefficients in an electrolyte solution depend on the salt concentration. At the same time, the salt concentration inside a battery is neither stationary nor homogeneous at high charging or discharging rates, as experienced during vehicle acceleration or braking; rather, it is a function of current density, time and distance from the electrodes. In contrast to commonly used methods, such as PFG-NMR and electrochemical techniques, MRI can provide spatially resolved details about the chemical and dynamic features of solution species.

Using *in situ* MRI, we have unambiguously demonstrated that the electrolyte solutions can experience large concentration polarizations during battery operation. Because of this situation, the difference in ionic diffusivities at opposite ends of the cell can be as large as 60% (Fig. 1b), which must be taken into account in the description of mass transport. Moreover, one can directly both the salt diffusivity and the  $\text{Li}^+$  transference number, by carrying out experiments under conditions of a steady-state concentration gradient and by combining the PFG-NMR diffusion measurement with *in situ* MRI techniques into single pseudo-3D experiment, [1]. Furthermore, implementation of pure phase-encoding MRI methods, e.g. centric scan SPRITE [2], allows the mapping of not only the transport of ions through the electrolyte solution, but also the lithiation of electrodes (Fig. 1c), which leads to the next level of battery performance characterization by NMR techniques.

### References

- [1] S. A. Krachkovskiy, J. D. Bazak, P. Werhun, B. J. Balcom, I. C. Halalay, and G. R. Goward, *J. Am. Chem. Soc.*, 138 (2016), 7992.  
 [2] M. Halse, J. Rioux, S. Romanzetti, J. Kaffanke, B. MacMillan, I. Mastikhin, N. J. Shah, E. Aubanel, and B. J. Balcom, *J. Magn. Reson.*, 169 (2004), 102.

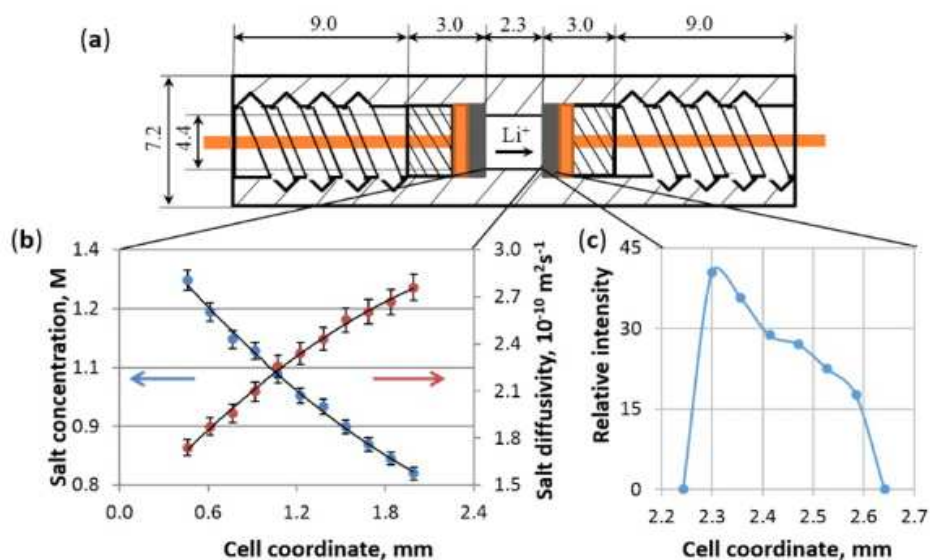


**Fig. 1.** (a) *In-situ* electrophoretic NMR cell design (dimensions in mm). (b) Steady-state lithium salt concentration (blue) and diffusivity (maroon) profiles in 1M  $\text{LiPF}_6$  / EC:DMC (1:1 v/v) at a current density of 9  $\text{A/m}^2$ . (c) Lithium profile in a graphite electrode charged to a voltage of 0.03 V at current density of 1.5  $\text{A/m}^2$ .

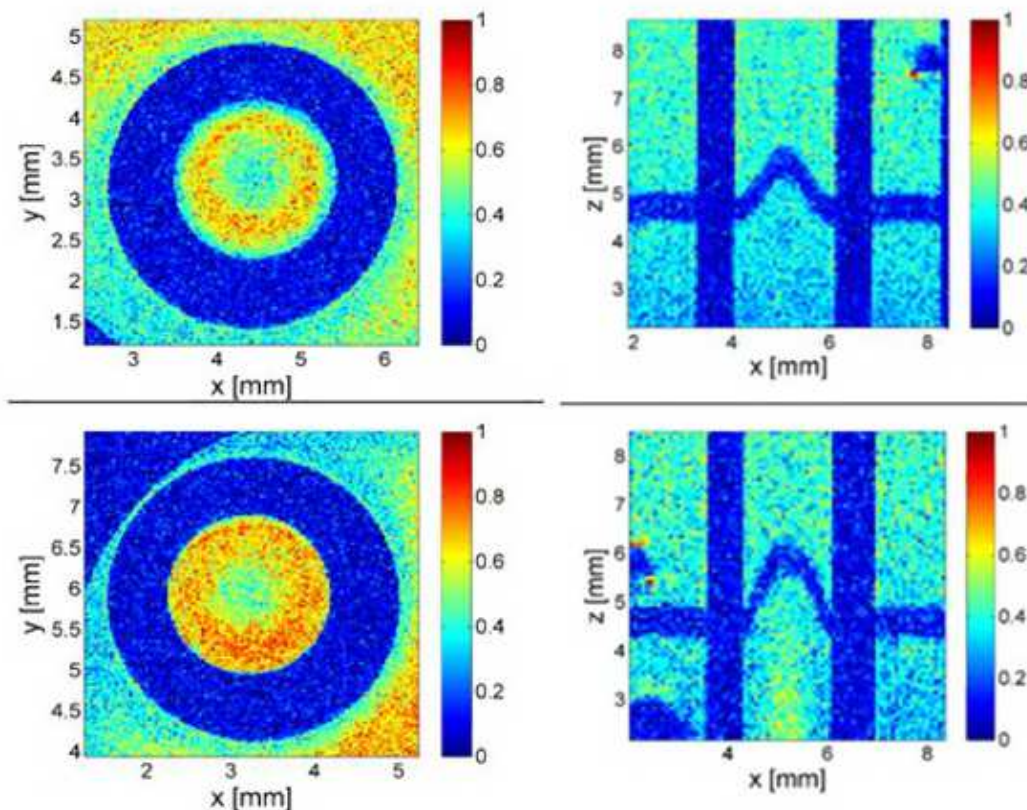


## MRI of macromolecular filtration

G. Guthausen<sup>a,b</sup>, F. Arndt, N. Schork, S. Schuhmann and H. Nirschl, <sup>a</sup>Institute of Mechanical Process Engineering and Mechanics; <sup>b</sup>EBI, Water Chemistry and Technology, Karlsruhe Institute of Technology (KIT), Karlsruhe, Germany.

Ultrafiltration of macromolecular substances is a widely spread process technology applied for example in water treatment and in food engineering. An accumulation of the often colloidal substances on the membrane surface occurs during filtration. For example in water filtration, extracellular polymeric substances (EPS) are known to be a main source for deposit formation which can be modeled by sodium alginate. This polyanionic polysaccharide is known to form a macromolecular solution in the absence of bivalent cations, but to form gel structures in the presence of bivalent cations, with an impact on the fouling mechanisms in a filtration process.

MRI was used to explore the filtration mechanisms in ceramic hollow fiber membranes during in-situ ultrafiltration. Time and spatially resolved measurements were performed to get detailed insight into structure and kinetics of deposit formation. Other than in filtration of particles or of milk, an aqueous solution of alginate shows similar relaxation and diffusion properties as water. Therefore, gel layer and concentration polarization are observed by exploiting paramagnetic relaxation enhancement as MRI contrast mechanism. This approach allows for a quantification and detailed analysis of the deposit. Additionally, flow profiles confirm the findings of structural MRI: The different filtration mechanisms determine also the hydrodynamic conditions in the membrane lumen. Analyzing the flow profiles provides further information of the factors leading to fouling layer formation and the characterizing physical parameters.



Alginate filtration without  $\text{Ca}^{2+}$  (top) and with  $\text{Ca}^{2+}$  (bottom): fouling structures via RARE (left) and velocity along the fiber axis via saturation tagging (right).

## Cell Tracking with Magnetic Resonance Imaging

P. Foster<sup>s</sup>, Robarts Research Institute, Western University, Canada.

To detect cells using MRI they must be labeled with MR contrast material to make them distinct from the surrounding tissues. The majority of preclinical cellular MRI studies have utilized iron oxide nanoparticles for the cell label. A variety of iron oxide-based labels are available including superparamagnetic iron oxide particles (SPIO, 60-120 nm), ultra-small iron oxide agents (USPIO, 10-30 nm) and micron-sized iron oxide particles (MPIO, 0.75  $\mu\text{m}$  and larger). Areas containing iron-labeled cells appear as regions of signal loss (or regions of signal hypointensity) on MR images, creating negative contrast. More recently,  $^{19}\text{F}$  based nanoemulsions have been used for cellular MRI.

For experimental cell tracking, cells are typically loaded with iron or  $^{19}\text{F}$  agents prior to their injection or implantation. To image inflammation, cells are labeled *in situ* via an intravenous administration of the agents. The resulting signal can be tracked *in vivo* providing information about the presence, location and migration of the labeled cells. This presentation will compare iron- and  $^{19}\text{F}$ -based cellular MRI and give various examples of how these technologies are used in preclinical investigations of disease. Special focus will be given to the tracking of cancer cells and cancer cell therapies.

This presentation will also describe the current limitations of cell tracking with MRI which are important to our understanding of what advances and improvements are crucial to move this field forward. Some of these limitations include: the potential for transfer of label from the original cell to bystander cells, dilution of the label in proliferating cells, misinterpretation of the signal from iron-labeled cells due to other sources of signal loss and quantification. We will also cover advances in this field related to both the cell labels and labeling and the MRI hardware and software for detection of cells.



## Combining MRI with other imaging and measurement modalities: applications to pharmaceutical and catalysis research.

M.D. Mantle, , Department of Chemical Engineering & Biotechnology, Philippa Fawcett Drive, , Univeristy of Cambridge, , Cambridge U.K. CB3 0AS.

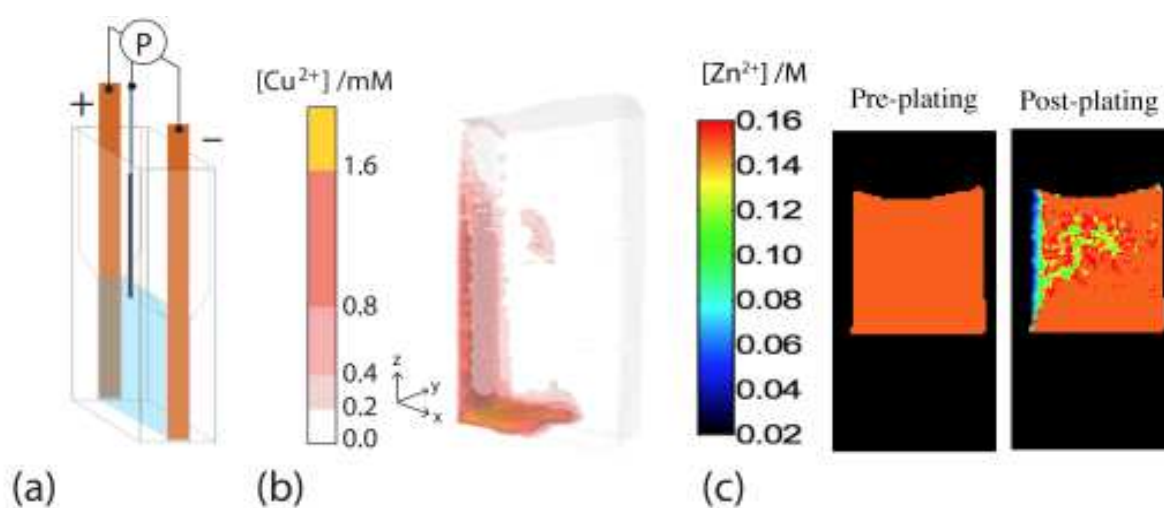
This talk will begin with recent developments from our group focussing on the application and development of combining MRI with other imaging and measurement modalities to address important problems in pharmaceutical and catalysis research. In particular, we describe how MRI may be combined with Terahertz Pulsed Imaging (TPI) techniques to better understand the microscopic behaviour of extended release pharmaceutical tablets during pharmacopeial dissolution testing. Two MRI/TPI studies are described: (1) The stability of a pharmaceutical product during transport and subsequent storage is a key issue for assessing its longevity and hence shelf-life. In order to speed-up pre-clinical research and development, and minimise the associated costs, accelerated stress testing conditions are often employed. Here we show how a combination of TPI and MRI can further our understanding of standard dissolution stability test results for commercially available drug products. TPI data for pre- and post-stress tested Lescol® XL tablets showed significant physical changes in the tablet coating thickness and density; however, MRI data for pre- and post-stress tested Lescol® XL tablets during dissolution showed no real changes in the internal micro structure, which agreed well with the results from the standard drug release curves; (2) Precise control of drug release kinetics from an extended release solid matrix is often facilitated by coating a tablet with a well-defined polymer film. Here we report results from a combined TPI/MRI study which helps explain the different drug release kinetics from laboratory and pilot scale tablet coating processes.

Finally, the talk will finish by describing the initial results from a benchtop low-field NMR spectrometer designed to work inside the vacuum chamber of the NIMROD neutron diffractometer (Rutherford Appleton Labs, UK) to address mechanistic problems in heterogeneous catalytic hydrogenation reactions. Here NMR spectroscopy provides chemical speciation and mass transport information with neutron diffraction providing simultaneous information regarding reactant/product structuring during chemical reaction.

MM Britton, School of Chemistry, University of Birmingham, Birmingham, B15 2TT, UK.

The design and development of improved electrochemical technologies, such as batteries, anti-corrosion, and electroplating, requires detailed understanding of the electrochemical reactions, ion transport and concentration gradients within these systems. However, there are few methods that are able to visualise and quantify these non-invasively, spatially, in situ and in real time. Magnetic resonance imaging (MRI) has proved to be an excellent tool for non-invasively studying complex, spatially heterogeneous chemical systems in materials, engineering and chemical research [1]. While, MRI has enormous potential for in situ investigation of the spatial distribution, speciation, and mobility of molecules and ions in electrochemical devices, there are currently very few examples of MRI being used to probe such systems. This is largely due to the experimental challenges associated with setting up an electrochemical cell inside a strong magnetic field and the imaging artefacts caused by the presence of metals that lead to undesirable variations in the radiofrequency (RF) and magnetic fields across the sample [2]. However, it has been found, recently, that such technical issues can be overcome and that it is possible to collect viable data [3] in electrochemical systems. This talk will present the challenges for studying electrochemical systems by MRI and demonstrate how they can be overcome to enable the collection of unique and quantitative data during the electrodisolution and deposition of metal ions in a range of electrochemical cells. Results will be presented, visualising the discharge process in a model Zn-air battery [4], corrosion of metallic copper in an aqueous electrolyte [5] and the electroplating of zinc in a room temperature ionic liquid (RTIL).

[1] M.M. Britton, *Prog. Nucl. Magn. Reson. Spec.*, 101 (2017) 51-70. [2] L.H. Bennett, P.S. Wang, M.J. Donahue, *J. App. Phys.*, 79 (1996) 4712-4714. [3] A.J. Davenport, M. Forsyth, M.M. Britton, *Electrochem. Comm.*, 12 (2010) 44-47. [4] M.M. Britton, P.M. Bayley, P.C. Howlett, A.J. Davenport, M. Forsyth, *J. Phys. Chem. Lett.*, 4 (2013) 3019-3023. [5] J.M. Bray, A.J. Davenport, K.S. Ryder, M.M. Britton, *Angew. Chem. Int. Ed.*, 55 (2016) 9394-9397.



(a) Electrochemical MRI cell (b) 3D  $\text{Cu}^{2+}$  concentration map<sup>7</sup> during electrodisolution of metallic copper (c) 2D  $\text{Zn}^{2+}$  concentration map before and after zinc electroplating in a RTIL.

# Spatially resolved and clinically feasible relaxation-diffusion correlation spectroscopy in the spinal cord

Dan Benjamini and Peter J Basser

Section on Quantitative Imaging and Tissue Sciences, NICHD, National Institutes of Health, Bethesda, MD 20892, USA

**Introduction:** Combining and correlating multidimensional magnetic resonance (MR) contrast mechanisms, e.g.,  $D$ - $T_2$ , would provide novel and complementary information about dynamic molecular processes and microscopic physical and chemical environments within tissue. To date, these multidimensional relaxation-diffusion correlation (REDCO) experiments have been primarily relegated to applications involving NMR spectrometry and spectroscopy studies in homogeneous samples [1–3]. However, these methods have not been widely used in MRI applications owing to the vast amount of scan time and acquired MR data required to reconstruct a single multidimensional spectrum. To overcome this bottleneck we recently proposed the marginal distributions constrained optimization (MADCO) method for accelerated multidimensional MRI [4]. The concept in this approach is to use the more accessible 1D information (i.e., the marginal distributions) to enforce physical constraints on the multidimensional distribution, resulting in a dramatic reduction in the number of data samples required and a concomitant reduction in MRI acquisition times [4]. Here, by using MADCO, we introduce a new MR imaging framework—which we term magnetic resonance microdynamic imaging (MRMI)—that permits the simultaneous noninvasive quantification of multiple cellular, interstitial, and subcellular tissue components within tissue. This unique information is obtained without imposing *a priori* tissue models, and in a clinically or biologically feasible time period.

**Materials and Methods:** Although it can be used to investigate other types of biological tissue, we chose to apply MRMI on a fixed ferret spinal cord specimen because its microstructure and organization are well known and highly ordered. MRI data were collected on a 7 T Bruker wide-bore vertical magnet with an AVANCE III MRI spectrometer equipped with a Micro2.5 microimaging probe and three GREAT60 gradient amplifiers. MRI data were acquired with an inversion recovery spin-echo diffusion-weighted echo planar imaging (IR-DWI-EPI) sequence, in which the diffusion gradient amplitude,  $G$ , the inversion period,  $\tau_1$ , and the echo time,  $\tau_2$ , governed the diffusion,  $T_1$ , and  $T_2$  weightings, respectively. The three 1D distributions of  $T_1$ ,  $T_2$ , and  $D$ , were first estimated using a total of 52 acquisitions in the  $G$ - $\tau_1$ - $\tau_2$  space. The MADCO framework was then used with the *a priori* obtained 1D distributions as constraints to estimate the  $D$ - $T_1$ ,  $D$ - $T_2$ , and  $T_1$ - $T_2$  spectra, using an additional 36 acquisitions. For all types of acquisitions, TR = inversion time + 4 s. A single 2.5 mm axial slice with in-plane resolution of  $101 \times 101 \mu\text{m}^2$  was acquired with 2 averages and 8 segments. Each image took 1 minute to acquire, leading to a total experimental time of 88 min.

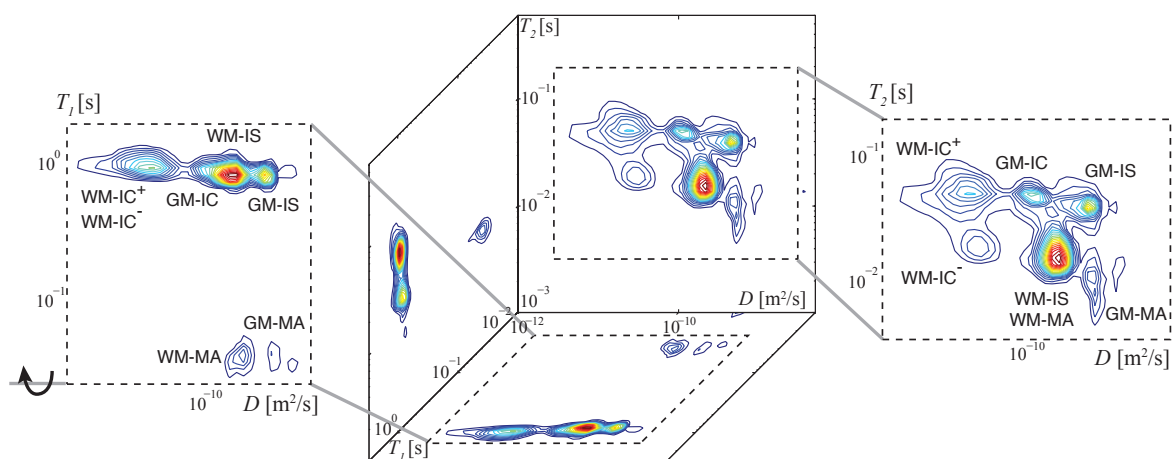


Figure 1: Microscopic compartmental analysis of a mixture of the representative gray and white matter ROIs, which yield a gray–white matter “mixed volume”. To the right is the most informative  $D$ - $T_2$  spectrum with four peaks, corresponding to four unique microscopic nervous components that can be unequivocally assigned (WM-IC<sup>+</sup>, WM-IC<sup>-</sup>, GM-IC, and GM-IS). Having similar  $T_2$  and  $D$  values, the WM-IS, WM-MA, and GM-MA peaks are well separated by their  $T_1$  value, reflected in the  $D$ - $T_1$  spectrum to the left.

**Results and Discussion:** In most cases, a typical MRI brain voxel would include gray and white matter (GM and WM), and would contain a mixture of axons, neurons, different types of glia, myelin, interstitial spaces, and proteins. One of the greatest challenges facing quantitative MRI methods is distinguishing between at least a subset of these components within an imaging voxel. The strength of microdynamic imaging in this context was demonstrated by analyzing a mixture of spectra from GM and WM regions of interest (ROIs). The resulting REDCO spectra are shown in **Fig. 1**, in which the microdynamic information from the  $D$ - $T_2$  and  $D$ - $T_1$  spectra reveals seven unique

peaks: (1) WM interstitial (WM-IS); WM intracellular (WM-IC), which has two subpopulations – with (2) long  $T_2$  (WM-IC<sup>+</sup>) and (3) short  $T_2$  (WM-IC<sup>-</sup>) values; a low diffusivity short-lived  $T_1$  and  $T_2$  peak that is assigned to (4) WM myelin-associated (WM-MA) water; (5) GM intracellular (GM-IC); (6) GM interstitial space (GM-IS); and a short  $T_1$ - $T_2$  GM component is identified as a (7) GM myelin-associated (GM-MA) component. To associate the REDCO peaks to their correct *macroenvironment* (i.e., WM or GM), “pure” WM and GM ROIs were first selected and analyzed separately.

Summing over the REDCO peaks resulted in the *apparent volume fraction* (AVF) images of the nervous tissue components, which exhibit unique contrasts and are shown in **Fig. 2**. First, let us examine the spatial distribution of all the intracellular components we identified: WM-IC<sup>+</sup>, WM-IC<sup>-</sup>, and GM-IC. The difference between the intracellular images is clear, with the practical absence of WM-IC<sup>-</sup> in the gray column (**Fig. 2a**). On the other hand, the GM-IC is mainly present in the GM (**Fig. 2b**). The third IC component, the WM-IC<sup>+</sup> image, reveals a more uniform spatial distribution of intensities, with higher AVFs in WM (**Fig. 2c**). We note that very few axons, if any, are expected to reside in the cervical portion of the spinal cord GM, while neurons should be mostly present there and not in the WM [5]. On the other hand, glia range in size and shape (i.e., microglia and macroglia) and are distributed in all CNS tissue types, with more in WM than in other tissue types [6]. Apart from the known neuroanatomy, it is visible from **Fig. 1** that the GM-IC component has the highest diffusivity among the three cellular components, which means that GM-IC water resides in the biggest physical compartment. It is also evident that the WM-IC<sup>+</sup> peak spans a wide range of diffusivities, suggesting a broad size distribution. With this in mind, and with the clear difference in the image contrasts, the WM-IC<sup>-</sup>, WM-IC<sup>+</sup>, and GM-IC components can be hypothesized to originate from intraaxonal, intragial, and intraneuronal water, respectively. As anticipated, WM-IS image intensity is mainly limited to WM (**Fig. 2d**) and is complementary to the GM-IS image, whose intensity is almost exclusively present in the gray column (**Fig. 2e**). The total myelin-associated content (WM-MA + GM-MA) MRI stain suggests a higher concentration in WM, but non negligible presence in the GM as well (**Fig. 2f**). Myelin-associated proteins, such as myelin basic protein and myelin oligodendrocyte glycoprotein, are present in both myelin and in oligodendrocytes. While myelin is almost exclusively present in WM, oligodendrocytes are present in GM as well, which is consistent with the observed MA image contrast.

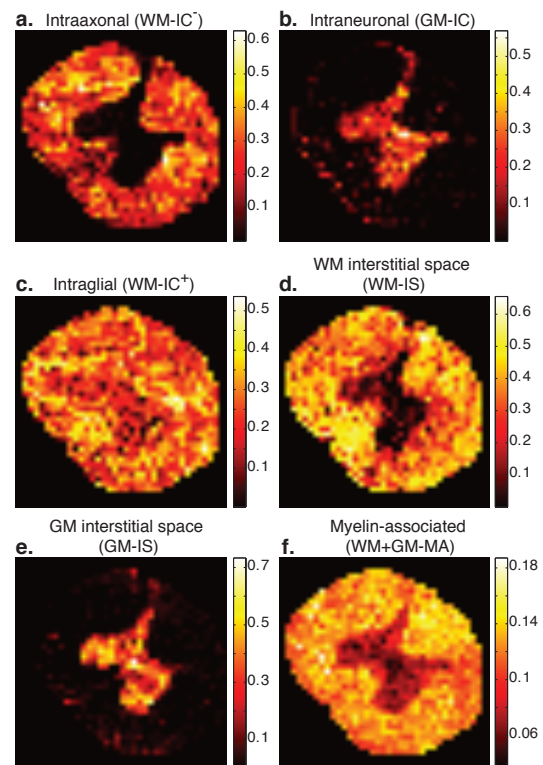


Figure 2: Generated quantitative images of the identified microscopic neuroanatomical tissue components. Note that the AVFs are additive and normalized, and therefore sum to 1.

**Conclusions:** Using MRMI, we identified specific tissue components on the basis of their multispectral signature within individual imaging voxels. The spatially resolved images obtained by combining REDCO and MRI allowed us, for the first time, to detect and distinguish between different intracellular components: axons, neurons, and glia. Interstitial spaces and myelin-associated water, which are additional distinct microenvironments within gray and white matter, were also identified and imaged. These seven cellular, interstitial, and extracellular components may be present in any single MRMI spinal cord voxel. MRMI delivers unprecedented microdynamic imaging data, which could have only been obtained by using laborious histological procedures on fixed specimen. MRMI is clearly not limited to applications within the CNS; it can be used on any type of tissue or material in which relaxation, diffusion, and transport properties can be measured, providing exciting opportunities for investigators in a range of disciplines.

## References

- [1] A. E. English *et al.* Quantitative Two-Dimensional time Correlation Relaxometry. *Magn Reson Med*, 22(2):425–434, 1991.
- [2] Mark D. Does *et al.* Multi-component T1 relaxation and magnetisation transfer in peripheral nerve. *Magn Reson Imaging*, 16(9):1033–1041, 1998.
- [3] Yi-Qiao Song *et al.* T1-T2 Correlation Spectra Obtained Using a Fast Two-Dimensional Laplace Inversion. *J Magn Reson*, 154(2):261–268, 2002.
- [4] Dan Benjamini and Peter J. Basser. Use of marginal distributions constrained optimization (MADCO) for accelerated 2D MRI relaxometry and diffusometry. *J Magn Reson*, 271:40–45, 2016.
- [5] Susan Standring. *Gray’s Anatomy: The Anatomical Basis of Clinical Practice*. Elsevier, 41 edition, 2015.
- [6] Richard S Snell. *Clinical Neuroanatomy*. Lippincott Williams & Wilkins, Philadelphia, PA, 7th edition, 2009.

## Oxygen Profile Characterization in Biofilm Systems Using $^{19}\text{F}$ Nuclear Magnetic Resonance Oximetry

JW Simkins, JD Seymour, KE Keepseagle and PJ Stewart, Chemical & Biological Engineering Department, Montana State University, Bozeman, MT, USA 59718

$^{19}\text{F}$  magnetic resonance has become a popular method in the medical field for quantifying oxygenation in blood, tissues, and tumors<sup>1-3</sup>. The technique, called  $^{19}\text{F}$  NMR oximetry, exploits the strong affinity of molecular oxygen for liquid fluorocarbon phases<sup>4</sup>, and the resulting strong linear dependence of  $^{19}\text{F}$  spin-lattice relaxation rate  $R_1$  on local oxygen concentration. The success of  $^{19}\text{F}$  NMR oximetry in clinical contexts naturally introduces the possibility of repurposing this method to measure oxygen in different systems.

Bacterial biofilms, aggregates of bacteria encased in a self-secreted matrix of metabolic products, are ubiquitous in industrial and clinical settings and, in both cases, oxygen gradients are a critical parameter in biofilm behavior. In the clinic, biofilms manipulate oxygen gradients to not only undermine host defenses but also dramatically reduce bacterial susceptibility to antibiotics, making them extremely difficult or impossible to treat<sup>5,6</sup>. For this reason, chronic wound oxygenation is known to be a significant predictor of clinical outcome<sup>7</sup>. In industry, regardless of whether biofilms are considered useful (e.g. wastewater treatment, bioremediation, or biofuel production) or deleterious (e.g. drinking water distribution systems, desalination, and food processing), oxygen represents one of the most important factors governing biofilm behavior. Optimization of such biofilm systems thus requires an in-depth understanding of how the biofilm establishes and responds to oxygen gradients.

However, measurement of oxygen distributions in biofilms is often cumbersome and in some cases intractable. In systems that permit it, such as a planar biofilm, the gold standard for oxygen quantification is the microelectrode, which is inserted to various depths within the biofilm and a 1D oxygen profile is constructed. The microelectrode has two hallmark drawbacks: first, the technique is limited to acquisition of one point at a time<sup>8</sup>, making it extremely time consuming, and second, insertion of the electrode is fundamentally invasive, and can cast doubt on obtain values<sup>9</sup>. In systems such as a biofilm growing in a packed bed column, spatially-resolving oxygen concentration becomes unmanageable. NMR, entirely non-invasive and permitting spatial resolution, provides the potential to overcome these boundaries.

In the present work we develop methodology for quantifying oxygen distributions in different biofilm systems, focusing primarily on planar *Staphylococcus aureus* biofilms grown on agarose gel, a model of a chronic wound infection, and biofilms grown on packed bed columns, of which the porous geometry models, for instance, wastewater and soil biofilms. We explore the applicability of different fluorocarbons for different biofilm systems, based on properties such as signal density, fractional sensitivity to oxygen, emulsion stability, and volatility.

Construction of a calibration curve detailing the response of  $^{19}\text{F}$   $R_1$  to oxygen concentration is accomplished by bubbling gases of variable oxygen concentration through pure-phase fluorocarbon and allowing the system to reach equilibrium before measuring  $R_1$ <sup>3</sup>.  $R_1$  mapping is accomplished using inversion recovery in combination with a spin-echo imaging sequence. When a fluorocarbon with multiple peaks is used as the oxygen sensor, the excitation  $90^\circ$  pulse is used to chemically select the dominant spectral peak and the refocusing  $180^\circ$  pulse is used for the slice selection.

In the planar biofilm case, we demonstrate that injection of a stream of pure liquid hexafluorobenzene (HFB), a fluorocarbon with high signal density, into the growth medium immediately before measurement allows for observation of the oxygen-depth profile. Similarly, injection of a bolus of HFB into the medium records the exact oxygen concentration at that point. Following further development, this technique could be used in the clinic to evaluate oxygen penetration in chronic wounds, a metric which has been shown to be a strong predictor of clinical outcome.

For porous media biofilms, we incorporate the oxygen-sensing fluorocarbon into the matrix material itself. We use perfluorooctylbromide (PFOB), which readily forms stable emulsions, and



incorporate the PFOB emulsion into 3 mm alginate beads by dripping an emulsion of PFOB-in-sodium alginate into a calcium chloride solution. In a subset of beads, biofilm growth is stimulated by inoculating with *Escherichia coli* before dripping. The effect of biofilm growth is investigated by packing a mixture of sterile and inoculated beads into a 10 mm inner diameter column and recording  $R_1$  profile (bulk, 1D longitudinal profile, 2D longitudinal, and 2D radial) over the course of microbial development. We correlate these measurements with  $^1\text{H}$  velocity maps to yield, for the first time to our knowledge, a comprehensive comparison of fluid flow distribution and resulting oxygen distribution in a packed bed system. In addition to bacterial experiments, we also probe the timescale of oxygen depletion, both axially down the column and from within individual beads, when the transition is made from oxygen-saturated feed water to oxygen-depleted via nitrogen sparging. The PFOB bead system is modular, and can be modified as desired to alter conditions in the packed bed and observe subsequent changes on the system.

Finally, we report progress toward encapsulation of hydrofluorether (HFE) in 300  $\mu\text{m}$  diameter alginate beads using a microfluidic device. HFE affords much higher signal-to-noise ratio than PFOB and is a frequently used fluorocarbon phase in microfluidic technologies. The small size and high signal afforded by these make them easy to incorporate into systems where oxygen levels are of concern and facilitate the measurement.

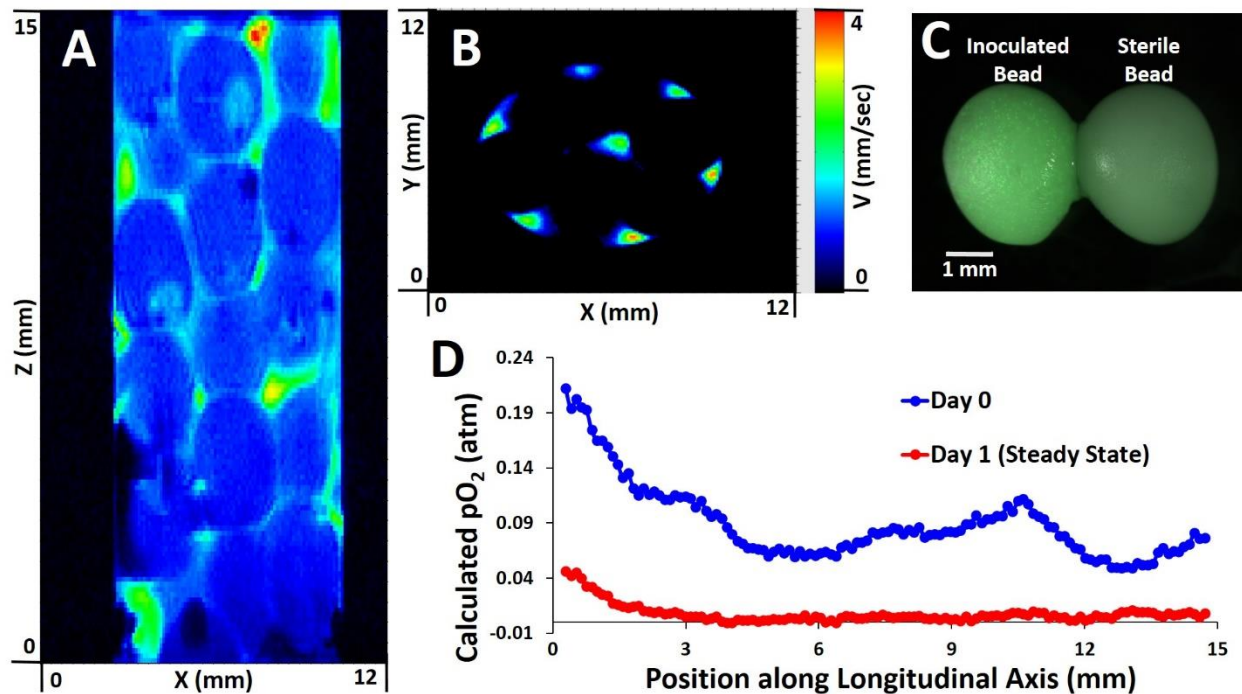


**Fig 1.** (A)  $^1\text{H}$  sagittal image of water flowing at 50mL/hr through a column containing PFOB-laden alginate beads. (B)  $^1\text{H}$  axial velocity map showing flow streamlines. (C) Fluorescent image of individual beads, with the inoculated bead exhibiting green fluorescence due to growth of *S. aureus*. (D) Longitudinal oxygen profile over course of bacterial growth calculated via  $^{19}\text{F}$   $R_1$  of PFOB.

#### References:

- [1] Eidelberg, D, *et al.* (1988). *Magn Reson Med* 6, 344-352. [2] Liu, S, *et al.* (2011). *Magn Reson Med* 66, 1722-1730. [3] Mason, RP, *et al.* (1996). *NMR Biomed* 9, 125-134. [4] Delpuech, JJ, *et al.* (1979). *J Chem Phys* 70, 2680-2687. [5] Jesaitis, AJ, *et al.* (2003). *J Immunol* 171, 4329-4339. [6] Tresse, O, *et al.* (1995). *J Antimicrob Chemother* 36, 521-526. [7] Ueno, T, *et al.* (2014). *Journal of Nippon Medical School* 81, 4-11. [8] Davies, PW, *et al.* (1942). *Rev Sci Instrum* 13, 524-533. [9] Silver, IA (1973). *Chem Eng in Med* 118, 343-352.

# Application of an Earth's Field NMR Flow Meter to Multiphase Flow Measurements

K.T. O'Neill<sup>1</sup>, P.L. Stanwix<sup>1</sup>, E.O. Fridjonsson<sup>1</sup> and M.L. Johns<sup>1</sup>

<sup>1</sup>School of Mechanical and Chemical Engineering  
University of Western Australia, Perth, Western Australia 6009, Australia.

## Introduction

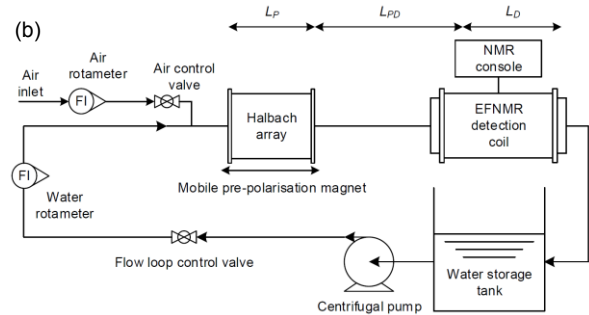
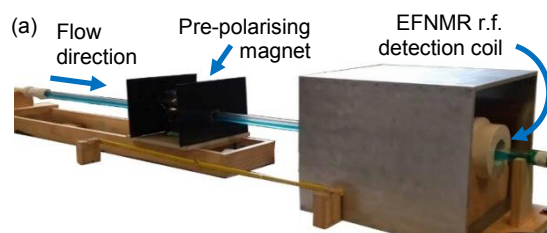
Instantaneous measurements of multiphase fluid flows has significant potential in a number of industries; particularly in the oil and gas industry in assisting the development of marginal fields and monitoring subsea processing [1]. The accurate quantification of component flowrates for industrial flows (typically consisting of oil, gas, condensate and water) using multiphase flow meters provides considerable benefits with respect to process safety, production monitoring and reservoir management [1, 2].

## Materials and Methods

We present the novel use of an Earth's Field nuclear magnetic resonance (EFNMR) multiphase flow metering system (illustrated in Figure 1) [3]. The apparatus consists of a pre-polarising permanent magnet (0.3 T Halbach array) upstream of an EFNMR radio frequency (r.f.) detection coil (Magritek, New Zealand) which is used to excite and detect a  $\sim 2260$  Hz  $^1\text{H}$  NMR signal from the flowing fluid stream. The flow loop can accommodate two phase air/water flows in both the stratified and slug flow regimes. Single phase in-line rotameters are used to provide accurate measurement of the individual component flowrates in order to validate NMR measurements.

A simple r.f. 'pulse and collect' sequence is used to acquire the free induction decay (FID) signal from the flowing fluid stream. A model for the FID signal (Equation 1 in Figure 1) is used and is a composite of three contributions; (i) signal polarisation in the permanent magnet, (ii) intermediate signal attenuation between polarisation and detection, and (iii) signal decay and flush-out during detection [3, 4]. The NMR flow meter model is fit (via Tikhonov regularisation) to experimentally acquired FID signals in order to determine the relevant velocity probability distribution of the flowing fluid stream.

For two-phase NMR measurements only the liquid contributes to the measurable NMR signal, which implies; (i) the resultant velocity distribution is representative of the liquid velocity distribution alone, and (ii) the overall level of signal magnetisation ( $S_0$ ) is directly proportional to the liquid holdup present in the EFNMR detection region. The second observation is used to estimate the liquid holdup during two phase measurements.



$$S(v, t_e) = S_0 \left( 1 - e^{-\frac{L_p}{vT_1}} e^{-\frac{L_{pD}}{vT_1}} 1 - \frac{t_e v}{L_D} e^{-\frac{t_e}{T_2}} \right)$$

Figure 1(a) Photo of measurement section of the flow loop. (b) Schematic of the flow metering apparatus. The flow meter model which has been developed is also presented (equation 1) [4], where  $S$  is the measured FID signal at velocity  $v$  and time since excitation  $t_e$ , and the relevant lengths ( $L_p$ ,  $L_{pD}$  and  $L_D$ ) are all indicated in the schematic.

## Results and Discussion

NMR measurements of single phase (water) flows at mean velocities ( $V_M$ ) of 0.09 to 1.15 m/s were conducted. The velocity probability distributions ( $P(v)$ ) which have been determined from the regularised fit of Equation 1 to measured time-averaged FID signals is presented in Figure 2(a) whilst the comparison of the NMR measured mean velocity to the rotameter measured mean velocity is illustrated in Figure 2(b).

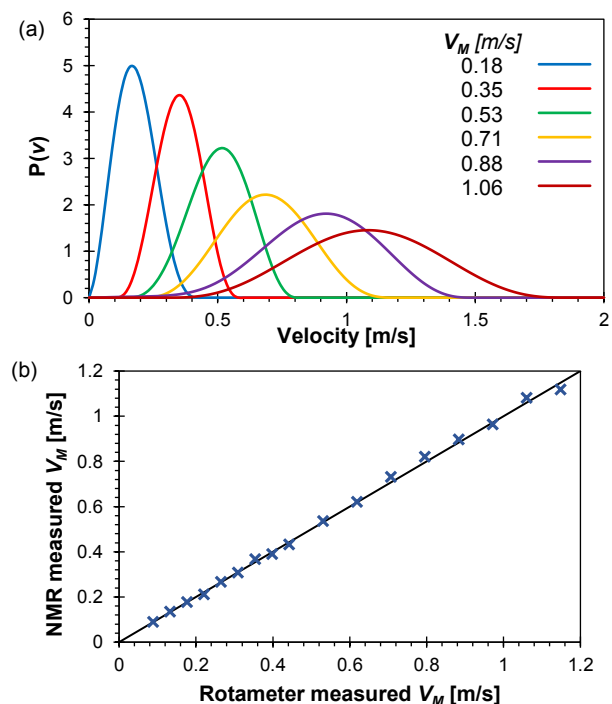


Figure 2(a) Velocity probability distributions determined from fitting Equation 1 to FID signals acquired from single phase water flows. (b) Comparison of NMR measured mean velocity to the measured mean velocity from the in-line rotameter.

The NMR measured mean velocity shows excellent agreement to the rotameter measured mean velocity. The mean absolute error for the seventeen velocity measurements in Figure 2(b) is 1.9 %

Similar measurements are conducted for two-phase air/water experiments at liquid superficial velocities ( $U_{SL}$ ) of 0.09 – 0.26 m/s and superficial gas velocities ( $U_{SG}$ ) of 0.22, 0.44 and 0.88 m/s. These flowrates result in either stratified or slug flow regimes. The NMR measured liquid velocity probability distributions which are determined from the regularised fit of Equation 1 to

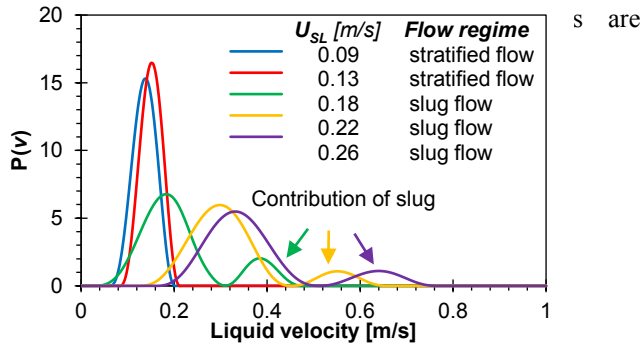


Figure 3 Liquid velocity distributions determined from fitting Equation 1 to FID signals from two phase air/water flows. The visually observed flow regime for each measurement is indicated. Note  $U_{SG} = 0.44$  m/s for all trials.

The stratified flow experiments ( $U_{SL} = 0.09$  and  $0.13$  m/s) show a single peak corresponding to the continuous liquid linear velocity distribution anticipated for time-invariant flow. The slug flow experiments ( $U_{SL} = 0.18, 0.22$  and  $0.26$  m/s) clearly exhibit a bimodal velocity distribution, with the larger lower velocity peak corresponding to the background stratified liquid layer whilst the smaller higher velocity peak corresponds to the faster moving slugs.

Further time variant information can be determined from two-phase flows if instead of analysing time-averaged FID signals, the individual FID scans are interpreted in a repeated ‘single-shot’ analysis. Figure 4(a) shows example time resolved liquid holdup tracks (with the visually observed flow regime indicated), whilst Figure 4(b) shows the

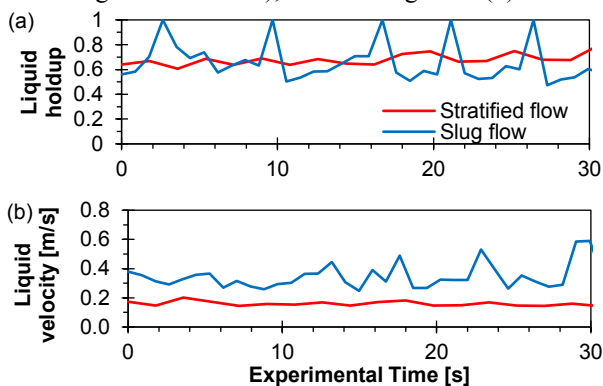


Figure 4(a) Liquid holdup tracks for NMR measurements in the stratified flow ( $U_{SL} = 0.09$  m/s,  $U_{SG} = 0.44$  m/s) and slug flow ( $U_{SL} = 0.26$  m/s,  $U_{SG} = 0.44$  m/s). (b) The corresponding liquid velocity tracks.

The holdup and velocity tracks are observed to be relatively constant in the stratified flow experiment, whilst clear

fluctuations can be observed in the liquid holdup and velocity tracks for the slug flow experiment.

Finally, the results from air/water experiments are summarised in the following figure with comparison of the NMR measured average liquid superficial velocity to the in-line rotameter measurement of superficial liquid velocity.

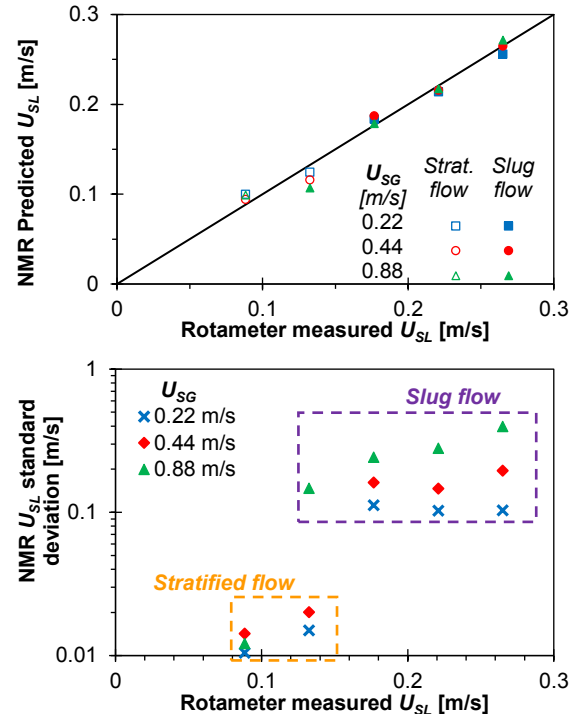


Figure 5(a) Comparison of NMR measured superficial liquid velocity to rotameter measured superficial liquid velocity. (b) Standard deviation of superficial liquid velocity used to distinguish flow regimes.

Figure 5 demonstrates the NMR measurement procedure is both accurate and can be used to distinguish stratified and slug flow for two phase gas/liquid flows.

## Conclusions

We have presented the novel use of an Earth’s Field NMR multiphase flow metering system. The system is capable of resolving velocity distributions and liquid hold-up in near real time. These parameters were successfully validated against known volumetric flowrates as well as visual observation of liquid hold-up. Currently the focus is on adaptation of the apparatus to accommodate oil-water-gas flow, which will necessitate the inclusion of multiple polarisation positions.

## References

- [1] Thorn, R., Johansen G.A and Hjertaker, B.T., Three-phase flow measurement in the petroleum industry, *Meas. Sci. Technol.*, **24**, 2013, 012003.
- [2] G. Falcone, G.F. Hewitt, C. Alimonti, B. Harrison, Multiphase flow metering: current trends and future developments, *J. Petrol. Technol.* **54**, 2002, 77–84.
- [3] Fridjonsson E.O., Stanwix P.L., Johns M.L., Earth’s field NMR flow meter: Preliminary quantitative measurements, *J. Magn. Reson.*, **245**, 2014, 110-115.
- [4] O’Neill, K.T., Stanwix, P.L., Johns, M.L. and Fridjonsson, E.O., Quantitative Velocity Distributions via Nuclear Magnetic Resonance Flow Metering, *J. Magn. Reson.*, **269**, 2016, 179–185.



## Measurement of rotational and translational motion in granular Couette flow using MRI

*D.A. Clarke<sup>1</sup>, H.T. Fabich<sup>2</sup>, T.I. Brox<sup>3</sup>, J.R. Brown<sup>4</sup>,  
S.L. Codd<sup>4</sup>, J.D. Seymour<sup>4</sup>, P. Galvosas<sup>3</sup>, and D.J. Holland<sup>1</sup>*

*1. University of Canterbury, New Zealand; 2. ABQMR, Albuquerque, New Mexico;  
3. Victoria University of Wellington, New Zealand; 4. Montana State University, Montana*

Granular materials exhibit compressibility analogous to gases, gravitational flow analogous to liquids and a yield stress analogous to solids. These characteristics arise from the contact forces between individual particles, in other words localized interactions determine the macroscopic flow properties in granular materials. Thus, if we are to understand natural or industrial granular flows, we must understand the motion of individual granules, and how these influence the rheology of the granular flow. For example, translational motion of individual particles is induced from external forcing of a system and by inelastic collisions between particles, while rotational motion arises from sliding frictional contacts between particles. Granular temperature describes the translational fluctuations about the mean velocity within a sample and is an important variable in kinetic theory continuum models that describe granular flow [1]; relatively little is known about the effects of rotational motion on the granular dynamics. One of the challenges here is the lack of techniques to characterize the rotational and translational motion experimentally. MRI is a promising tool in this regard as it is able to recover the mean and distribution of velocities in opaque flows [2, 3].

Motion is encoded in pulsed field gradient (PFG) MRI experiments according to:

$$S(\mathbf{p}) = \int \eta \exp(i\mathbf{p}(\mathbf{v} + \mathbf{v}')) d\mathbf{v}', \quad (1)$$

where the inverse variable  $\mathbf{p}$  is defined as  $\mathbf{p} = \gamma \int \mathbf{g}(t) t dt$ ,  $\mathbf{v}$  represents the local mean velocity and  $\mathbf{v}'$  is the fluctuation about this mean, and  $\eta$  is the distribution of velocities of particles [4]. However, derivations based on this equation assume individual granules are point sources, effectively ignoring any contribution arising from the rotation of granules.

In this work, a model is developed to relate the *translational and rotational* components of the motion to the velocity distribution measured by MRI. We show that the rotational granular temperature,  $T_{rotation}$  is related to the variance of the angular velocity,  $\langle \omega^2 \rangle$  by:

$$T_{rotation} = \frac{2}{5} R^2 \langle \omega^2 \rangle \quad (2)$$

where  $R$  is the particle radius. In order to test the new model, pulsed field gradient MRI experiments of granular flow were simulated using the discrete element method (DEM) [5, 6]. DEM is a computational fluid dynamics framework for granular flow in which the motion (translational and rotational) of each granule is tracked using Newton's laws of motion. To simulate the PFG measurement, a signal arising from each particle was calculated by numerically integrating the displacement of the particles with respect to time, including effects of both rotation and translation. The granular temperature was estimated by a

parabolic fit of the natural logarithm of the signal data against the gradient strength [3]. This computational method has the advantage of being able to include or exclude the contribution that rotational motion of the particles made to the signal. Thus, the mean and variance of velocity may be extracted from the simulation with or without the contribution from particle rotation. The model was applied to an assembly of particles in an annular shear cell, which was also measured experimentally by MRI.

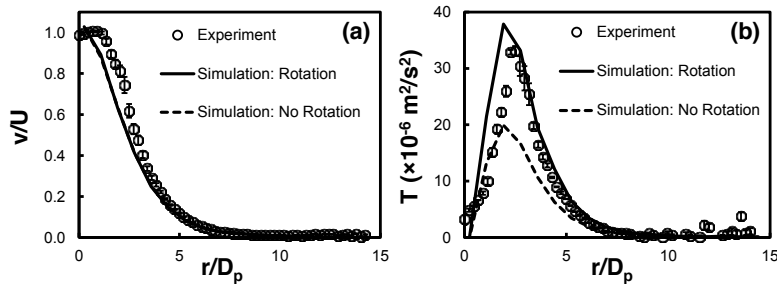


**Figure 1(a) Local mean velocity and (b) Granular temperature for Couette flow of  $D_p = 0.6$  mm particles.**

The DEM model was first validated by comparison with the velocity and granular temperature measured by MRI, as shown in Figure 1. The velocity measured experimentally is in excellent agreement with the translational velocity predicted from the simulations (Fig. 1a). The measured granular temperature is approximately double the translational component of granular temperature from the simulations (Fig. 1b). However, if the effect of both rotational and translation granular temperature are combined, the experiments are in excellent agreement with the numerical simulations, validating the DEM model. The results also demonstrate that rotation does not influence the measurement of the mean translational velocity, in agreement with theoretical predictions.

The numerically simulated rotational granular temperature was then calculated and compared with Equation 2 (Fig. 2). The results demonstrate that for a wide range of contact parameters characterizing the particle-particle interactions, the model accurately estimates the rotational granular temperature based solely on the local variance of the angular velocity distribution with no empirical parameters. Thus, if we measure the rotational granular temperature, it is possible to estimate the local rotational component of granular motion. Such measurements are not possible using other experimental techniques. We are now extending this analysis to extract both translational and rotational components of the granular temperature experimentally using more complex PFG sequences, such as repeated or refocused PFG and Modulated Gradient Spin Echo.

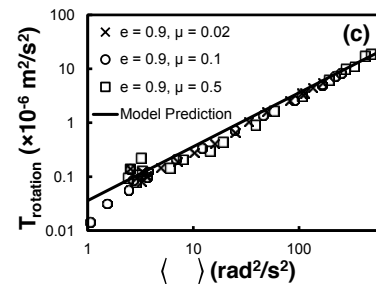


**Figure 2. Comparison of model prediction with DEM MRI simulations.**

1. Jenkins, J.T. and M.W. Richman, *Physics of Fluids*, 1985. **28**(12): p. 3485-3494.
2. Seymour, J.D., et al., *Phys. Rev. Lett.*, 2000. **84**(2): p. 266-269.
3. Holland, D.J., et al., *Powder Technol.*, 2008. **182**(2): p. 171-181.
4. Callaghan, P.T., *Principles of nuclear magnetic resonance microscopy*. 1991.
5. Cundall, P.A. and O.D.L. Strack, *Géotechnique*, 1979. **29**(1): p. 47-65.
6. Kloss, C., et al., *Prog. Comput. Fluid Dyn.*, 2012. **12**(2-3): p. 140-152.

## Local $T_1$ - $T_2$ Distribution Measurements in Porous Media

S. Vashae<sup>1</sup>, B. Newling<sup>1</sup>, B. MacMillan<sup>1</sup>, F. Marica<sup>1</sup>, M. Li<sup>1</sup>, B.J. Balcom<sup>1</sup>, <sup>2</sup>H.T. Kwak, <sup>2</sup>J. Gao, <sup>2</sup>A.M. AlHarbi

<sup>1</sup>UNB MRI Centre, Department of Physics, University of New Brunswick, Fredericton, New Brunswick, E3B 5A3, Canada

<sup>2</sup>Saudi Aramco EXPEC Advanced Research Center, Reservoir Engineering Technology Division, Pore Scale Physics Focus Area, Bldg. 2291, #GA-168

Magnetic resonance (MR) is a well-recognised, non-invasive method for investigating fluid behaviour in reservoir cores and core plugs. 2D MR methods [1, 2] are commonly employed to identify and quantify oil and gas saturation. In comparison with conventional 1D  $T_2$  distribution measurement techniques, 2D MR improves one's ability to distinguish different fluid phases by mapping proton density as a function of the  $T_2$  relaxation time in one dimension and the  $T_1$  relaxation time in a second dimension.

Bulk  $T_1$ - $T_2$  correlations provide the relaxation time ratio  $T_1/T_2$  for reservoir cores and core plugs [2]. The ratio  $T_1/T_2$  is beneficial as an indicator of wettability. The basic  $T_1$ - $T_2$  correlation experiment is advantageous for the study of fluids in porous media; the experiment is robust and works well both in low and inhomogeneous magnetic fields [3, 4].

Bulk  $T_1$ - $T_2$  measurements generate information from entire sample. In some cases spatially resolved  $T_1$ - $T_2$  measurement of the sample is preferred. For example water flooding experiments in reservoir rock cores and core plugs, where the efficiency of the flooding is examined by monitoring water and oil displacement as a function of space along the core plug.

Spatially resolved  $T_1$ - $T_2$  measurement is introduced for the first time here. A spatially-selective adiabatic inversion pulse [5] in the presence of a slice-selective magnetic field gradient is combined with a CPMG measurement to measure  $T_1$ - $T_2$  for slices of interest.  $T_1$  weighting is introduced during recovery from the inversion associated with slice-selection. The slice-selective  $T_1$ - $T_2$  method does not employ conventional selective excitation, but rather employs a subtraction method based on measurements acquired with and without an adiabatic inversion slice-selection.

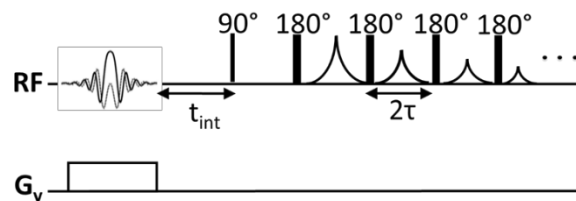


**Fig 1.** Adiabatic inversion  $T_1$ - $T_2$  for slice-selective  $T_1$ - $T_2$  measurements of regions of interest. The longitudinal recovery time  $t_{int}$  is increased in successive experiments.

The  $180^\circ$  pulse in a simple  $T_1$  inversion recovery measurement is replaced by an adiabatic inversion pulse to make the  $T_1$ - $T_2$  measurement slice-selective (Fig. 1). The adiabatic inversion pulse is applied in the presence of a slice-selective magnetic field gradient. The slice-selective  $T_1$ - $T_2$  experiment consists of two successive scans: during the 1<sup>st</sup> scan (Fig. 1) the magnetization is inverted from  $z$  to  $-z$  inside a desired frequency band (Fig. 2a). The 2<sup>nd</sup> scan (Fig. 1 without slice-selection) is a simple CPMG experiment with all magnetization maintained along  $z$  at the

beginning of the measurement (Fig. 2b). Subtracting the signals from those two scans leaves only the selected frequency band, as shown in Fig. 2c.

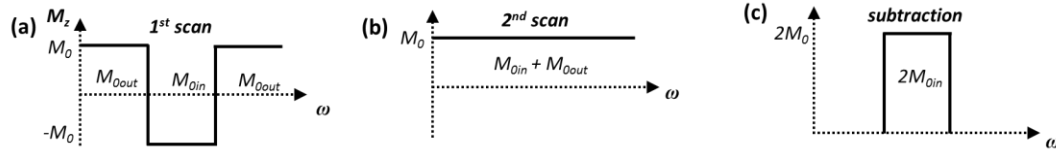


**Fig 2.** An illustration of the adiabatic inversion scheme for slice-selection. (a) During the first scan, the adiabatic inversion pulse rotates the selected frequencies inside the slice of interest by  $180^\circ$ . (b) During the second scan all magnetization is maintained along the  $+z$  direction. (c) The acquired signal is the difference between the two scans.

The slice-selective  $T_1$ - $T_2$  approach (Fig. 1) was implemented to measure oil saturation during a model flooding measurement. The experiment was undertaken on a brine saturated Bentheimer core plug which was injected with crude oil in four stages to displace brine.  $T_1$ - $T_2$  distribution plots for a slice of sample for different oil saturation stages, are shown in Figs. 3a-3e.

The new spatially resolved  $T_1$ - $T_2$  technique is quantitative and robust and can be utilized to identify oil and water and quantify oil saturation in specific areas along the sample, during flooding measurements.

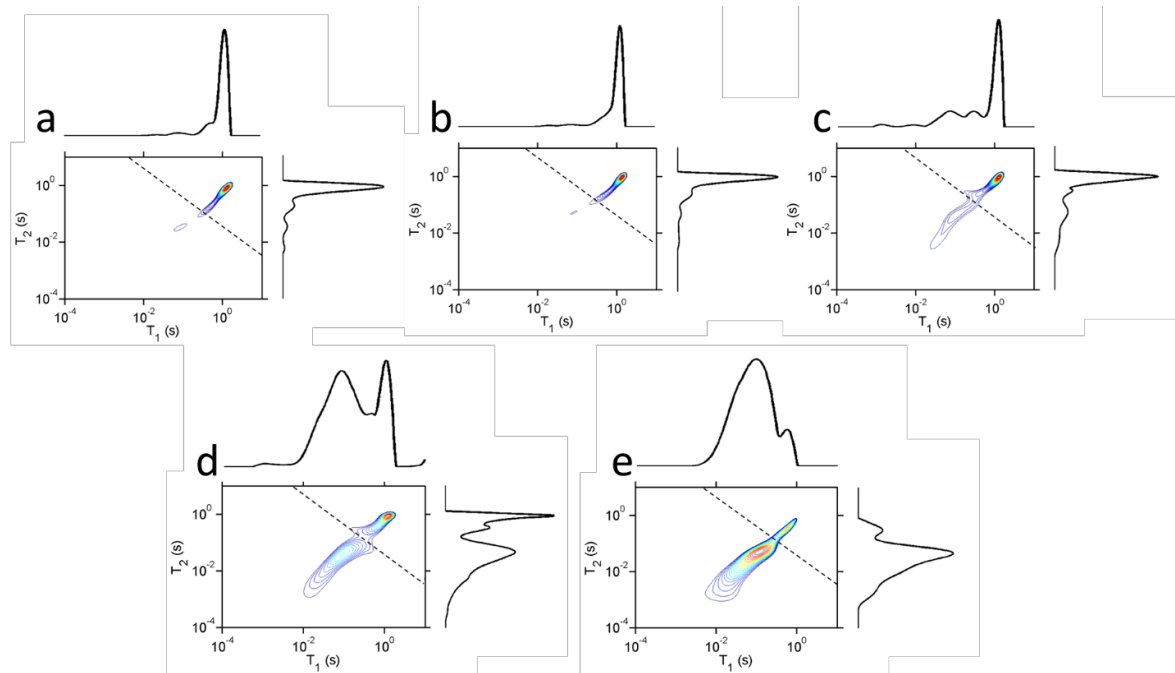


**Fig 3.** Slice-selective  $T_1$ - $T_2$  contour plots for fluids in the Bentheimer core plug at different crude oil saturation stages (same slice): (a) No crude oil (100% brine), (b) 31% crude oil, (c) 53% crude oil, (d) 68% crude oil and (e) 86% crude oil. (---) indicates the  $T_1$ - $T_2$  cut-off. The region left to the (---) is associated with oil and also brine in small pores. The region to the right of (---) corresponds to brine.

#### References:

1. M.D. Hurlimann et al., J. Chem. Phys. 117 (2002) 10223-10232.
2. Y.Q. Song et al., J. Mag. Reson. 154 (2002) 261-268.
3. J. Mitchell et al., Prog. Nucl. Magn. Reson. Spectrosc. 76 (2014) 1-60.
4. M. Fleury et al., J. Petrol Sci. Eng. 137 (2016) 55-62.
5. A. Tann'us et al., NMR. Biomed. 10 (1997) 423-434.

## Humans: Exchange Models

S.E. Mailh t, Department of Mechanical Engineering, Montana State University, Bozeman, MT, USA; J.E. Maneval, Department of Chemical Engineering, Bucknell University, Lewisburg, PA, USA;

R.K. June, Department of Mechanical Engineering, Montana State University, Bozeman, MT, USA; J.R. Brown, Department of Chemical and Biological Engineering, Montana State University, Bozeman, MT, USA; P. Galvosas, School of Chemical and Physical Sciences, Victoria University of Wellington, Wellington, NZ; S.L. Codd, Department of Mechanical Engineering, Montana State University, Bozeman, MT, USA; J.D. Seymour, Department of Chemical and Biological Engineering, Montana State University, Bozeman, MT, USA.

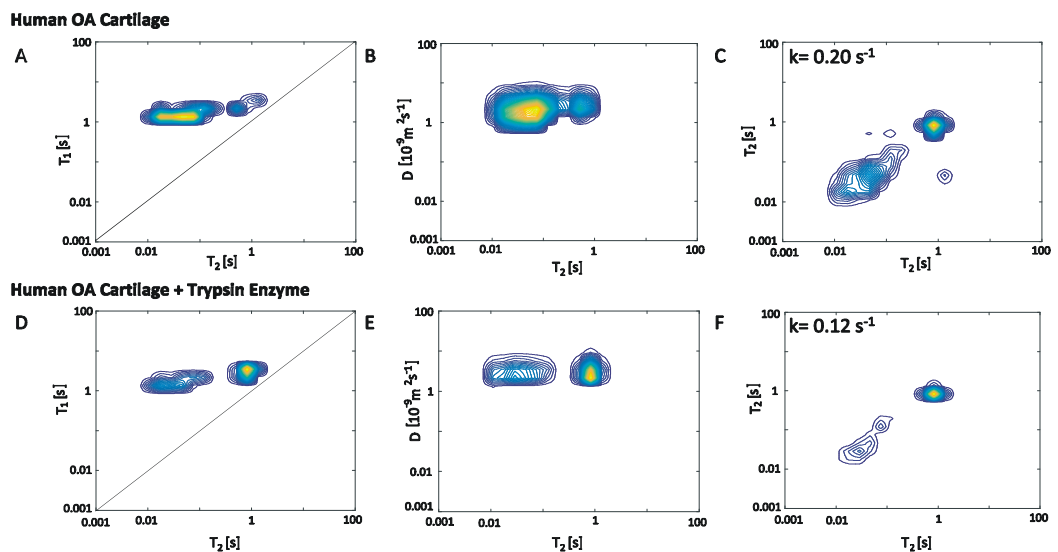
Articular cartilage is the thin, load bearing tissue that lines joint surfaces. Damage to cartilage is correlated to an increase in  $T_2$  and  $D$  of fluid (1, 2). The aim of this study is to characterize the effect of diffusive exchange on observable relaxation rates in cartilage by utilizing  $T_1$ - $T_2$ ,  $D$ - $T_2$  correlation methods, and  $T_2$ - $T_2$  exchange methods.

Specifically, we show that diffusive exchange is based on solvent, enzyme degradation, and sample variation.

Using two site  $T_2$ - $T_2$  exchange time domain data fitting (3-6), the exchange rate was determined for porcine cartilage, human osteoarthritic (OA) cartilage, enzyme digested human cartilage, and human cartilage in three solvents. For porcine cartilage, the characteristic exchange time is 1.54 seconds and commensurate with  $T_1$ . The  $T_1$  relaxation of the two sites has been averaged by exchange. Using the diffusivity of fluid (fig 1 B,D) and the exchange time, the expected diffusion length of fluid is between 100 and 250  $\mu\text{m}$ . This same trend is observed in human OA cartilage cores, where the average exchange time is about 5 seconds (fig 1 A-C), although significant donor variation is observed (data not shown).

To investigate the cause of donor variation, cores were degraded with trypsin and collagenase. Matrix degradation causes a decrease in exchange frequency and an increase in exchange time (fig 1D-F). There is also a dependency on exchange frequency when cartilage cores are soaked in saline, phosphate buffered saline (PBS), and culture media. The addition of ions caused an increase in exchange frequency and decrease in exchange time.

In conclusion, we show that the diffusive exchange rate and observable  $T_1$  and  $T_2$  are dependent on sample preparation, enzyme degradation, and solvent in articular cartilage. We hypothesize that fluid matrix interactions and health of cartilage tissue play a role in determining diffusive exchange rate.



References: References: 1.Xia Y, et al., Arch Biochem Biophys. 1995; 323: 323-8. 2.Alhadaq HA, et al., Ann Rheum Dis. 2004; 63: 709-17. 3.Van Landeghem M, et. al, Concepts in Magnetic Resonance Part A. 2010; 36A: 153-69. 4.Dortch RD, et al., J Chem Phys. 2009; 131: 164502. 5.McDonald PJ, et al., Physical Review E. 2005; 72: 011409. 6.Mitchell J, et al., The Journal of Chemical Physics. 2007; 127: 234701.

## Diffusion MRI in the Aplysia Neuronal Network: Experiments and Numerical Simulations

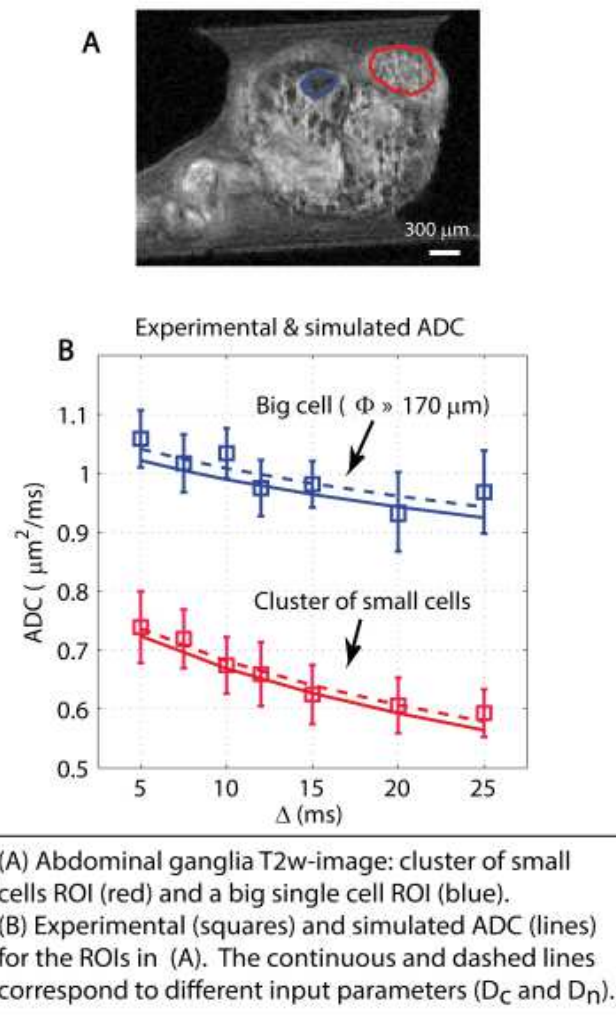
K. Nguyen, D. Le Bihan and L. Ciobanu, Neurospin, CEA-Saclay, Gif-sur-Yvette, France; J.-R. Li, INRIA Saclay-Equipe DEFI CMAP, Ecole Polytechnique, Palaiseau, France.

**Introduction:** In this study we used the *Aplysia* ganglia to investigate the relationship between the biological cellular parameters and the diffusion MRI signal. We simulated the diffusion MRI signal by solving the Bloch-Torrey equation using the geometrical description of *Aplysia* ganglia obtained from high resolution T2-weighted images and matched the simulations with experimental dMRI data.

**Methods:** T2-weighted images of the abdominal ganglia of *Aplysia californica* ( $26\mu\text{m}^3$  resolution) were acquired on a 17.2T imaging system (Fig. 1A). Diffusion-weighted images were obtained on the same samples at 7 diffusion encoding times and 8 b-values. The apparent diffusion coefficients (ADC) were computed in ROIs encompassing large cells (diameters  $\geq 100\mu\text{m}$ ) and clusters of hundreds of small cells (diameters  $\sim 20\mu\text{m}$ ). For the simulations, the large neurons were modeled according to the T2w images, with irregularly shaped nuclei, while the small neurons were considered spheres with smaller concentric spherical nuclei. The numerically simulated dMRI signal was obtained by solving the Bloch-Torrey equation with impermeable boundary conditions between the nucleus and the cytoplasm and at the cell membrane<sup>1</sup>.

**Results:** From the experimental data, when increasing the diffusion time, the ADC was observed to drop by 19.7% in the small neuron clusters and by 9.7% in the large single cells. The unknown parameters of the Bloch-Torrey equation (intrinsic diffusivities, nuclear volume fraction) were calibrated against the experimental data. The best fits between the simulated and the experimental ADCs are shown in Fig. 1B. For the small neurons we established that a linear relationship exists between the ADCs in the nucleus ( $D_n$ ) and the cytoplasm ( $D_c$ ). For the big cells we found necessary to include an irregular nuclear region of high intrinsic diffusivity embedded in the cytoplasm in order to fit the large drop in ADC experimentally observed.

**References:** 1. Li et al. Physics in Medicine and Biology (2013).





## Objective Image Quality Metrics Predict Accuracy of Quantitative Parameters fit to Compressed Sensing Dynamic MRI

N. Murtha<sup>a,b</sup>, J. Rioux<sup>a,b,c</sup>, C. Bowen<sup>a,b,c</sup>, S. Clarke<sup>a,b,c</sup> and S. Beyea<sup>a,b,c</sup>, <sup>a</sup>Physics and Atmospheric Science, Dalhousie University, Halifax, NS, Canada; <sup>b</sup>Biomedical Translational Imaging Centre, QE2 Health Sciences Centre, Halifax, NS, Canada; <sup>c</sup>Diagnostic Radiology, Dalhousie University, Halifax, NS, Canada.

### INTRODUCTION

We propose to use image quality metrics (IQMs) developed in the field of image processing as a means of predicting the accuracy of quantitative parameters recovered using CS dynamic MRI. Image reconstruction quality is typically quantified by the root mean squared error (RMSE). Alternative IQMs, such as the Gradient Magnitude Similarity Deviation (GMSD) [1], the Structural Similarity Index (SSIM) [2], the Multi-Scale SSIM [3] or the Information-Weighted SSIM [4] show superior agreement with perceptual image quality. We investigate the correlation between these IQMs and the accuracy of recovered temporal dynamic parameters in CS dynamic MRI simulations.

### METHODS

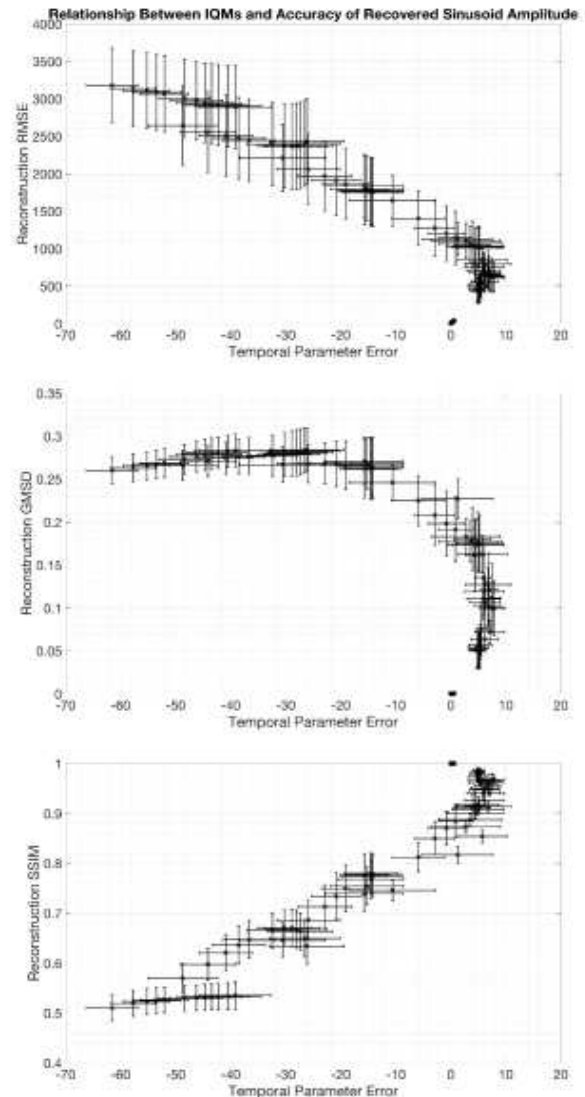
A simulation framework was developed in which numerical phantom features that evolved in contrast according to sinusoidal and exponential timecourses. The simulated k-space was sampled using a modified CIRCULAR Cartesian UnderSampling (CIRCUS) [5] at increasing undersampling factor. CS reconstructions were performed with the Berkeley Advanced Reconstruction Toolbox [6]. Temporal parameters were recovered from the reconstructions using pixel-wise least-squares fitting.

### RESULTS AND CONCLUSIONS

Figure 1 shows exemplar results of the relationship between sinusoidal amplitude and the RMSE, GMSD and SSIM. In each case, a relationship between metric scores and recovered parameter accuracy is observed. The RMSE and SSIM show higher predictive capabilities, whereas the GMSD becomes saturated as parameter error increases. This indicates that, while some metrics may correlate well with human perception, they may not serve as indicators of temporal accuracy. Further simulations are currently being undertaken to examine the relationship between these IQMs and physiologically relevant pharmacokinetic parameters.

### REFERENCES

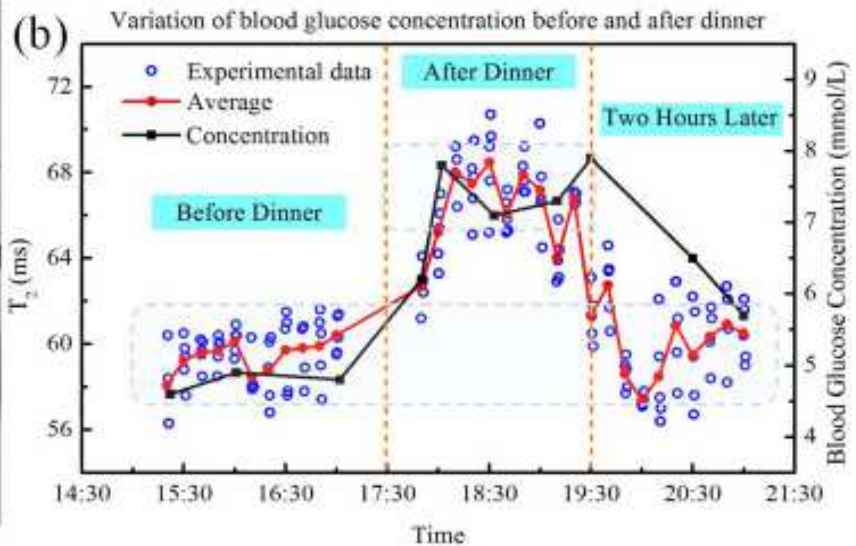
- [1] W. Xue et al. *IEEE Trans. Image Process.* 23(2):684-695 (2014). [2] Z. Wang et al. *IEEE Trans. Image Process.* 13(4):1-14 (2004). [3] Z. Wang et al. *IEEE ASILOMAR* (2003). [4] Z. Wang et al. *IEEE Trans. Image Process.* 20(5):1185-1198 (2011). [5] J. Liu et al. *Quant Imaging Med Surg.* 4(1):57-67 (2014). [6] M. Uecker et al. *Proc. Intl. Soc. Mag. Reson./ Med.* 23:2486 (2015).



## A low field NMR device using multilayer halbach permanent magnet for human finger blood glucose noninvasive monitoring

Rongsheng Lu<sup>\*s</sup>, School of Mechanical Engineering, Southeast University, Nanjing, 211189, P. R. China;  
 Jianxiang Hu, School of Mechanical Engineering, Southeast University, Nanjing, 211189, P. R. China;  
 Junnan Wang, School of Mechanical Engineering, Southeast University, Nanjing, 211189, P. R. China;  
 Ke Chen, School of Mechanical Engineering, Southeast University, Nanjing, 211189, P. R. China;  
 Zhonghua Ni, School of Mechanical Engineering, Southeast University, Nanjing, 211189, P. R. China.

Blood glucose noninvasive NMR detection has the advantages of non-invasive and rapidity. Magnet is an indispensable module to a nuclear magnetic resonance (NMR) device. The magnetic field strength and uniformity in its detection region will directly affect the NMR signal. However, commonly used NMR magnets are too bulky and expensive, restricting the development and promotion of NMR technology for blood glucose noninvasive detection. Therefore, the purpose of this paper is to develop a NMR magnet device for noninvasive glucose monitoring. Firstly, based on the theory of magnetic circuit design and finite element method (FEM), a magnet structure with strong strength, homogeneity in small size is designed, as well as the geometric parameters of magnet are optimized. Then the detection probe is developed and the NMR experimental device is established. Finally, several glucose solutions with different concentrations were detected by the NMR experimental device. The experimental results illustrate that the transverse relaxation time reduces linearly with the increase of solution concentration, which prove that the low field NMR method is feasible to detect small concentration variation. Besides, human finger with different blood glucose level were detected by the NMR experimental and different signals were found. In conclusion, the proposed low field NMR device using multilayer halbach permanent magnet will be an effective tool for human finger blood glucose noninvasive monitoring.





## Helicopter borne detection of oil under ice

S.A. Altobelli<sup>\*</sup>, M.S. Conradi and E. Fukushima<sup>§</sup>, ABQMR, Albuquerque, NM, USA;

T. Nedwed, D. Palandro and H. Thomann, Exxon Mobil.

This contribution describes a project to develop a mobile NMR system for detecting oil immediately under (or in) seasonal sea ice. With such a system, an errant release of oil in the Arctic could be located, tracked, and remedied. Tests were conducted with oil surrogates under one meter-thick foam representing ice.

The project moved North over the years of development from New Mexico to New Hampshire to a pristine pond in Newfoundland, Canada.

We detected the equivalent of a 1 cm thick layer of vegetable oil under a 1m thick GeoFoam raft floating on the pond with an Earth's field NMR system carried by a Sikorsky S-92 helicopter. The system weighs 1200 kg including flight qualified 12V batteries, is 6m in diameter, flew at up to 60 knots and was able to detect the oil surrogate in 4 minutes. The experiments were run by a Tecmag Scout portable spectrometer. The pre-polarization electronics were designed and built at ABQMR. The excitation pulse amplifier was made for automotive applications since the power available, the band pass requirements and the coil impedance were within easy reach of this inexpensive choice.

The system employs pre-polarization which is adiabatically switched off, and AM/FM excitation. At this extremely low frequency, it proved important to simulate the (linearly polarized) excitation in the lab, as opposed to the rotating, frame. The adiabaticity of the pre-polarization switch-off is a concern primarily because there are regions where the polarizing field is anti-parallel to the Earth's field.

The pre-polarization coil was a loop and the NMR coil was a gradiometer. The coils were wound together and enclosed in a fiberglass airframe together with the pre-amp.

The acquisition strategy depends on the difference between the  $T_1$ 's of water (2s) and oil (150ms). The NMR properties of the surrogate oil are closely matched to light crude oil. Signals are collected after pre-polarization periods of 1.1s and 0.3s. The oil is (nearly) fully polarized in both acquisitions, the water is not fully polarized in either. We form a linear combination of the two which suppresses the water signal.

The design and performance of the system will be described.



## NMR Studies of Small (1 liter) and Large (1,000 liter) Metal Containers in Low and High Pressure Factory Environments

M. J. McCarthy, UC Davis Food Science and Technology; M. P. Augustine<sup>§</sup>, UC Davis Chemistry.

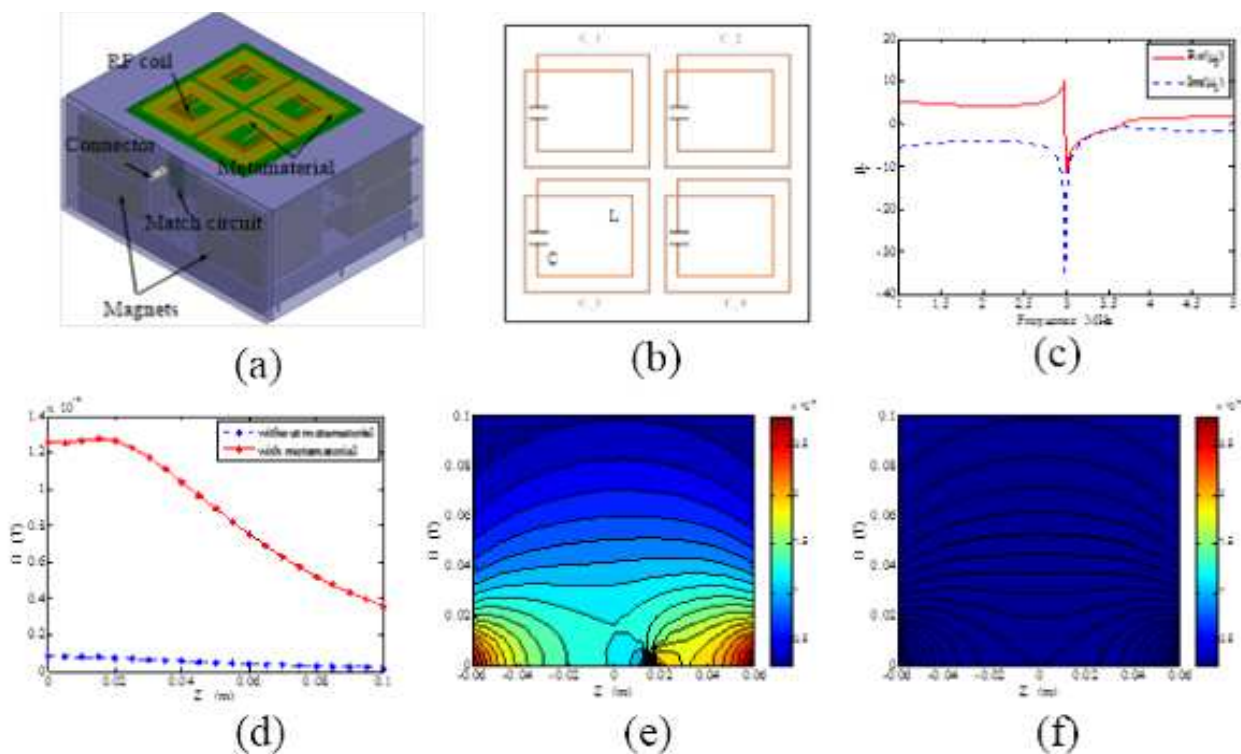
Modern permanent magnet and radio frequency electronics technology now make NMR spectroscopy amenable to process control in real factory environments. In comparison to large, expensive, laboratory anchored superconducting magnet based spectrometers, it is the decreased size and durability of systems based on these technological advances that now allows NMR to provide real time feedback during industrial processes. The factory environment presents an interesting spectrometer building challenge as standard 5 mm diameter, glass tubes containing pure compounds or simple mixtures are rarely encountered. Samples are typically well defined, reproducible complex mixtures presented in metal pipes at ambient or elevated pressure or in large aseptic metal containers. Early work involving the NMR study of industry standard sealed "Coke" cans is extended here to study tomato spoilage in 1,000 liter, 1 ton aseptic containers with single sided magnets of varied construction and coil arrangement. The design and construction of the recently deployed NMR based tomato spoilage detector will be described. Other early NMR work involving the study of aqueous geochemistry at up to 3 GPa pressure is also extended here to study both food and biomass in a high pressure processing (0.5 GPa) situation for the first time.

## Radio Frequency Field Enhancement with Metamaterial for Unilateral Nuclear Magnetic Resonance

Wu Jiamin, Xu Zheng\*, He Yucheng, Zhang Li and Yu Dengjie, State Key Laboratory of Power Transmission Equipment & System Security and New Technology, School of Electrical Engineering, Chongqing University.

Unilateral nuclear magnetic resonance structure as a new type of magnet is widely applied in engineering, but the difficulty of this technology is that the detecting depth is not deep enough, and samples located more distant from sensor surface of can not be measured. To overcome this drawback of unilateral nuclear magnetic resonance instrument, we use metamaterial to enhance RF magnetic field. Metamaterial composed of many resonance coil array added above RF coil, which can change the RF field distribution in the space, so that more energy transmitted to farther region, thereby increase the measuring depth of unilateral nuclear magnetic resonance sensor.

Figure 1 shows the model of unilateral nuclear magnetic resonance sensor and results. Figure 1(a) shows unilateral magnetic resonance sensor. It is composed of magnets, RF coil, metamaterial and match circuit. The frequency of this sensor is 3MHz. Figure 1(b) shows the model of metamaterial with four resonant elements (each capacitor is 300pF), each Sub-unit of metamaterial has 86mm in side length, 1mm in trip width, 1mm in trip space and 10 turns. Figure 1(c) shows the results of relative permeability. We obtained real part of relative permeability equals to -1 while the frequency is about 2.99MHz. At this frequency, we assume voltage of excitation equals to 1V, then calculated the distribution of magnetic field along Z axis with and without metamaterial, respectively, the results is shown in Figure 1(d). Magnetic filed in region with metamaterial is much higher than that without metamaterial. Figure 1(e) and 1(f) are the distribution of magnetic field in plane XOZ with and without metamaterial, respectively. The results show that the metamaterial designed is useful for RF enhancement in NMR system, and some experiments based on the unilateral nuclear magnetic resonance sensor with this metamaterial will be proceed.



## Synergistic Combination of MRI and Neutron Imaging to Shed Light on the Root-Soil Interface

S Haber-Pohlmeier<sup>§</sup>, RWTH Aachen University, Worringer Weg 1, 52074 Aachen, Germany; C. Tötze and S. Oswald, Univ. of Potsdam, Inst. of Earth and Environmental Science, Karl-Liebknecht-Str. 24-25, 14476 Potsdam, Germany; A. Pohlmeier, Research Center Jülich, IBG-3, Wilhelm-Johnen Str., 52425 Jülich, Germany; B. Blümich, RWTH Aachen University, Worringer Weg 1, 52074 Aachen, Germany.

The interface between bulk soil and root is known as the rhizosphere. It is the bottleneck for water and nutrient uptake and forms the part of the soil that is modified actively and dynamically in many ways by root activities and associated microorganisms [1]. Root activities are the exudation of small organic acids, sugars and polymers like mucilage a biohydrogel mainly composed of polysaccharides and a small fraction of lipids. Due to these components, biohydrogels exhibit specific properties, such as swelling and shrinking linked to a considerable water uptake and release. In combination with the solid matrix this leads to a change in mechanical and hydraulic properties and consequently affects water flow and uptake. The understanding of these processes is still incomplete and their study requires 3D non-invasive analytical methods with high resolution since the interface extends only up to a few millimeters. Additionally, static information like the water content is not sufficient. Rather one must consider the local dynamics, because it reflects the interaction between the fluid, the solid, and the polymeric matrix.

In this work we explore the synergy of two non-invasive techniques in a combined study: Neutron imaging (NI), whose strength is the sensitivity to the total hydrogen atom density irrespective of their physical and chemical surroundings [2] and MRI, yielding dynamic information in terms of relaxation times. For the first time we combined the two methods making use of a transportable MRI scanner, which allows the investigation of identical samples with a minimum time lag and consequently minimum changes in the physical state of the plant.

The overall aim of the study is the characterization of the root-soil interface, for which it is mandatory to assess how far transition structures are real or are just due to principal limits of edge detection. Since NI has the higher physical resolution, the limits of both methods are tested with phantoms composed of water filled tubes in a partially saturated sand matrix. Subsequently NI and MRI images of a real root system are co-registered showing unambiguously that MRI detects the root system architecture with the same precision as NI [3]. To explore the pore space in the root-soil interface we measured spatially resolved relaxation time maps with high resolution. Based on the presence of mucilage faster relaxation times are expected due to reduced mobility of water in a soil particle gel conglomerate. The T1 profiles of fine lateral roots show this behavior in a 1 to 2 mm thin zone before approaching the characteristic T1 of bulk soil. Generally, the MRI voxel intensity is controlled by both water content (spin density) and relaxation times. Therefore, we use the NI images to separate relaxation and water content contribution from MRI images to prove the existence of mucilage in the root-soil interface by faster relaxation times. These results indicate that the model of Brownstein-Tarr for relaxation in porous media should be extended by a term describing additional relaxation in the gel phase.

### References:

1. York, L.M., et al., *Journal of Experimental Botany*, 2016, 67(12), 3629-3643.
2. Moradi, A.B., et al., *New Phytologist*, 2012, 192, 653-663.
3. Haber-Pohlmeier, S., et al., *Vadose Zone Journal*, 2017, submitted.

## Unsteady relative permeability measurement considering capillary pressure and saturation profiles from magnetic resonance imaging

J. Gao<sup>\*</sup>, H. Kwak and A. M. Harbi, Saudi Aramco; B.J. Balcom, The University of New Brunswick.

Nuclear magnetic resonance (NMR) and imaging (MRI) play an essential role in formation evaluation and laboratory study on flow in porous media during secondary and tertiary recovery processes. Capillary pressure is present in any immiscible multiphase flow, but it is not properly accounted for in the conventional relative permeability measurement due to analytical difficulty with the Johnson, Bossler, and Neumann (JBN) method or its availability from the same sample in the history matching method.

In this study, unsteady state corefloods for relative permeability are conducted with a Maran GeoSpec12 (~0.3T) characterizing the core plugs at various state and monitoring the oil saturation profiles. Quantitative saturation profiles with sufficient spatial and temporal resolutions are obtained by spin echo single point imaging (SE-SPI) method. A suite of advanced NMR/MRI methods are also conducted on both sandstone and carbonate cores when permitted to correlate the core properties such as heterogeneity and wettability with flow behaviors.

The capillary pressure and nonwetting phase relative permeability are estimated from the saturation profiles at the end of the oil flood, which is solely used to establish the irreducible water state in conventional methods. The measured capillary pressure is inputted as further input in the estimation of relative permeability from the production pressure and saturation profile of consecutive water flooding by using core flood history matching. Other than ignoring the capillary pressure or injecting at a much higher rate than in the reservoir, this study improves the relative permeability measurement by considering the capillary effect adequately from two consecutive displacements on the same core plug and including saturation profiles as additional fitting criteria.

## Probe Performance of the New Downhole Three Dimensional Magnetic Resonance Imaging Tool

Luo Sihui, State Key Laboratory of Petroleum Resources and Prospecting, China University of Petroleum, Beijing 102249, China; Lizhi Xiao<sup>\*</sup>, State Key Laboratory of Petroleum Resources and Prospecting, China University of Petroleum, Beijing 102249, China; Xin Li, State Key Laboratory of Shale Oil and Gas Enrichment Mechanisms and Effective Development, Sinopec Research Institute of Petroleum Engineering, Beijing, China.

In this paper, we will introduce the development of our downhole three dimensional magnetic resonance imaging tool emphasized on probe performance.

The three dimensional downhole measurement consists of depth, radially and azimuthally resolved information of the reservoir. A new centralized probe is designed and implemented in our borehole NMR tool, as shown in Fig.1. In general, only the depth and radial information can be acquired using the currently downhole NMR tools. The azimuthal information is equally important to the depth and radial if they can be measured simultaneously, and three dimensional information then will be achieved. In many cases, information lack due to strong anisotropy or partial invasion of drilling fluid around borehole will cause problems and may have serious impact to applications. Three dimensional measurements is the right direction to solve these problems.

Early version of the azimuthal magnetic resonance tool was designed in 2003 as a decentralized measurement<sup>[1]</sup>. The sensitive volume of Prammer's design can divide the sensitive region from a thin-walled, hollow cylinder as of the MRIL-Prime tool into azimuthally distinguishable quadrants<sup>[2]</sup>. Because of the configuration of azimuthal antenna, quadrants could not be addressed individually, it could lead to overlapped signals, post processing was unable to overcome. And the depth of investigation may decrease dramatically due to  $B_0$  changes.

We have designed and built a new probe which incorporates into Jackson geometry<sup>[3]</sup> as the main magnets assembly a set of adjusted magnets, radial polarization magnets, to produce the  $B_0$  field, as shown in Fig.2. The radially polarized magnets in the middle of main part are used to adjust the homogeneity along with z-axis and increase the height to approximate 20cm of the sensitive region. We employ an array antenna which consists of eight winding coils with uniform performance. The sensitive region of our tool can be divided into eight azimuthally distinguishable units, which give a image of the borehole wall. The received signals will not be overlapped and the simulation result is shown in Fig.3. We will discuss the probe design and test performance in detail.

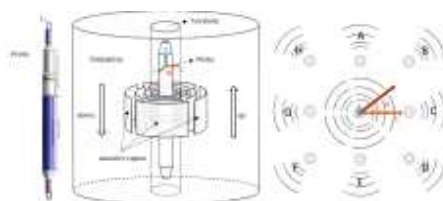


Fig. 1. A new probe designed is run centralized with high azimuthal resolution in the borehole. Under the cylindrical coordinate, three-dimensional scale can be described as depth along z-axis, depth of investigation along with radial direction and azimuthal degree  $\theta$ .

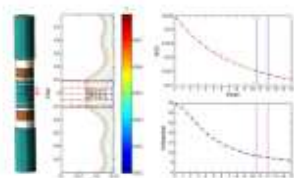


Fig.2. Magnet assembly and its produced magnitude and gradient distribution of  $B_0$ . The gradient in sensitive region is ranged from 8.7 to 7.4 Gauss/cm respect to the depth of investigation ranged from 10.5 to 12cm. The Larmor frequency is 669kHz, 646kHz and 623kHz respectively.

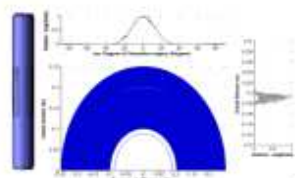


Fig.3. Array antenna and sensitive map based on  $B_0$  and  $B_1$  distribution. All the coils of uniform performance have excited sensitive region of approximate  $45^\circ$  arc degree width and of approximate 1.5cm thickness in transverse plane.

### References

- [1] Prammer, M G, Mueggli, S, et al. Directional resonance: new applications for MRF. SPE Annual Technical Conference and Exhibition, Denver, 2003.
- [2] Prammer, M G, Kozubick, S, Mueggli, S, et al. Systems and methods for deep-looking NMR logging. US 7463127 B2[P]. 2009.
- [3] Jackson J A, Barson J J, Hargrove F. Resonance (inside-out) NMR: III. Detection of nuclear magnetic resonance in a remotely produced region of heterogeneous magnetic field. *J Magn Reson*, 1990; 41(3): 411-421.

## Measuring rock pore shapes with diffusion NMR

J. P. de Almeida Martins<sup>a,b</sup> and D. Topgaard, <sup>a</sup>Division of Physical Chemistry, Lund University, Lund, Sweden; Y.-Q. Song<sup>s</sup>, <sup>b</sup>Schlumberger-Doll Research, Cambridge, U.S.A.

As a source of the majority of the World's primary energy, porous rock formations have been the subject of extensive studies aimed at understanding the pore matrix and fluid flow. NMR measurement of diffusion and relaxation of the pore filling fluids has been widely applied to probe the underlying pore structure [1]. However, conventional diffusion/relaxation methods could not separate distinctive structural properties such as pore sizes, anisotropy, and orientation as they are intrinsically entangled.

Conventional PFG methods measure diffusion along one gradient direction. Thus, for a sample with randomly oriented anisotropic pores, said anisotropy will result in a broad diffusion distribution. Drawing inspiration from solid-state NMR MAS techniques, we recently presented a triple PGSE sequence where diffusion encoding is averaged over the three Cartesian coordinates [2]. Such protocol averages out the effects of anisotropy and orientation, and permits the measurement of isotropic diffusivities. The framework of isotropic diffusion has shown to be able to distinguish different microstructures in human brain [3]. Recently, we also presented a correlation experiment where the heterogeneity of a given material is characterized via the individual values of isotropic and anisotropic diffusivities [4].

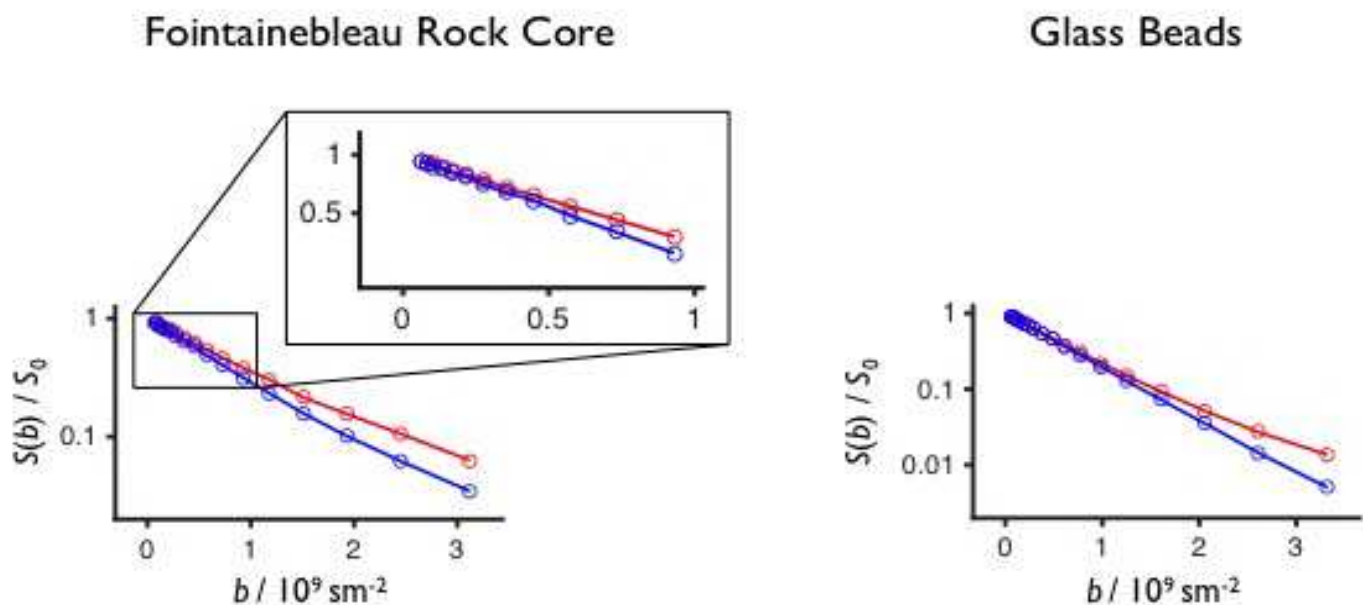
Here, isotropic and directional diffusion encodings are applied to samples of glass beads, and rock cores in order to resolve the effects of pore heterogeneity, anisotropy, and restricted diffusion. Fig. 1 shows the difference between restriction and anisotropy effects. When restricted diffusion is present, such as in a rock core, directional (red) and isotropic (blue) encodings yield different initial decay slopes. A different situation was observed for glass beads, where both encoding schemes result in the same initial slope and the directional decay curves upward at higher gradients. Such behavior signals the existence of anisotropy, which we attempt to quantify using the aforementioned correlation experiment.

[1] Y.-Q. Song, J. Magn. Res. 229, 12 (2013).

[2] D. Topgaard, Microporous Mesoporous Mater. 205, 48 (2015).

[3] F. Szczepankiewicz et al., Neuroimage 104, 241 (2015).

[4] J. P. de Almeida Martins, D. Topgaard, Phys. Rev. Lett. 116, 08761 (2016).





## Magnetic Resonance Imaging (MRI) of Phase Separation in Vesicle-Polymer Mixtures

E. Thompson and M.M. Britton<sup>s</sup>, School of Chemistry, University of Birmingham; E. Robles<sup>r</sup>, P&G UK; P. Saveyn, V. Guida and M. Declercq, P&G Belgium; C. Eads, P&G USA.

Vesicle dispersions are used in consumer products, cosmetics and food.[1] Non-adsorbing polymer is added to these dispersions to enhance properties, such as, flowability.[2] However, adding the polymer induces a depletion attraction between the vesicles, which can lead to the formation of a transient gel network. This transient gel network will be unstable and the system will separate into vesicle-rich and vesicle-poor phases. [3] Unfortunately, it is difficult to predict if phase separation will occur but early identification of unstable formulations will streamline industrial processes. [4]

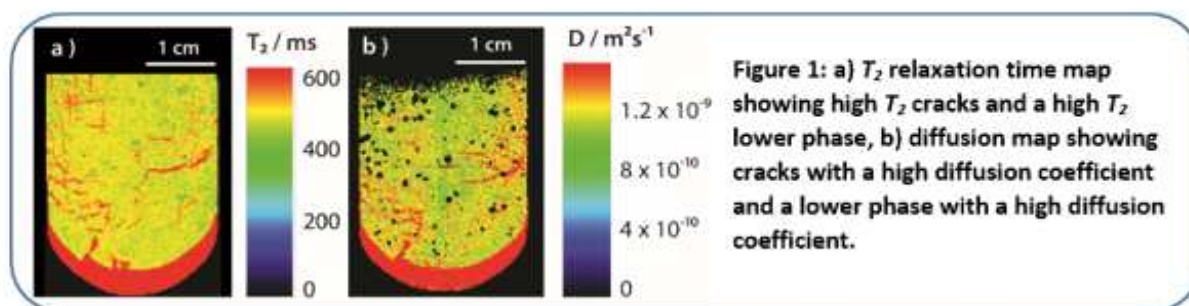
Using magnetic resonance imaging (MRI), phase separation of an opaque vesicle-polymer mixture is monitored overtime.  $T_2$  relaxation time and diffusion maps have been used to visualise the formation of water-rich cracks, in the vesicle-rich phase, over a period of days following polymer addition (Figure 1). Using MRI, these cracks are observed several weeks before any destabilisation can be observed visually. Furthermore, gels with air bubbles trapped inside phase separate approximately five times faster than the same gel with all air bubbles removed.

To better predict phase separation in vesicle-polymer mixtures, the degree of instability in each image must be quantified and monitored over time. Moran's I, a measure of spatial autocorrelation, quantified the cracks and phase separation effectively. [5] Moran's I has previously been applied to clinical MR images, [6,7] but has not been applied to systems which exhibit small heterogeneities like the water-rich cracks formed during phase separation. In this study, Moran's I proved particularly effective at quantifying the small cracks which form early in the phase separation process.

In this project, we have shown that MRI is uniquely placed to identify vesicle-polymer mixtures that will phase separate, which is important when developing new product formulations. MRI can identify unstable mixtures much earlier than visual inspection. It has also helped identify factors, such as the presence of trapped air bubbles, which accelerate phase separation. Finally, by using Moran's I, it has been possible, for the first time, to quantify the degree of instability observed, which will be enormously beneficial for the prediction and modelling of phase separation in these highly complex systems.

### References

1. R. Lipowsky, Nature, 1991, 349, 475-481.
2. R. Harich et al., Soft Matter, 2016, 12, 4300-4308.
3. J. Yeon Huh, PhD, University of Delaware, 2008.
4. J. Yeon Huh, M.L. Lynch and E. M. Furst, Ind. Eng. Chem. Res, 2011, 30, 78-84.
5. P. A. P. Moran, Biometrika, 1950, 37, 17-23.
6. G. Derado, F. D. Bowman, T. D. Ely and C. D. Kilts, Stat. Interface, 2010, 3, 45-58.
7. A. C. Santago et al., Ann. Biomed. Eng., 2016, 44, 2158-2167.

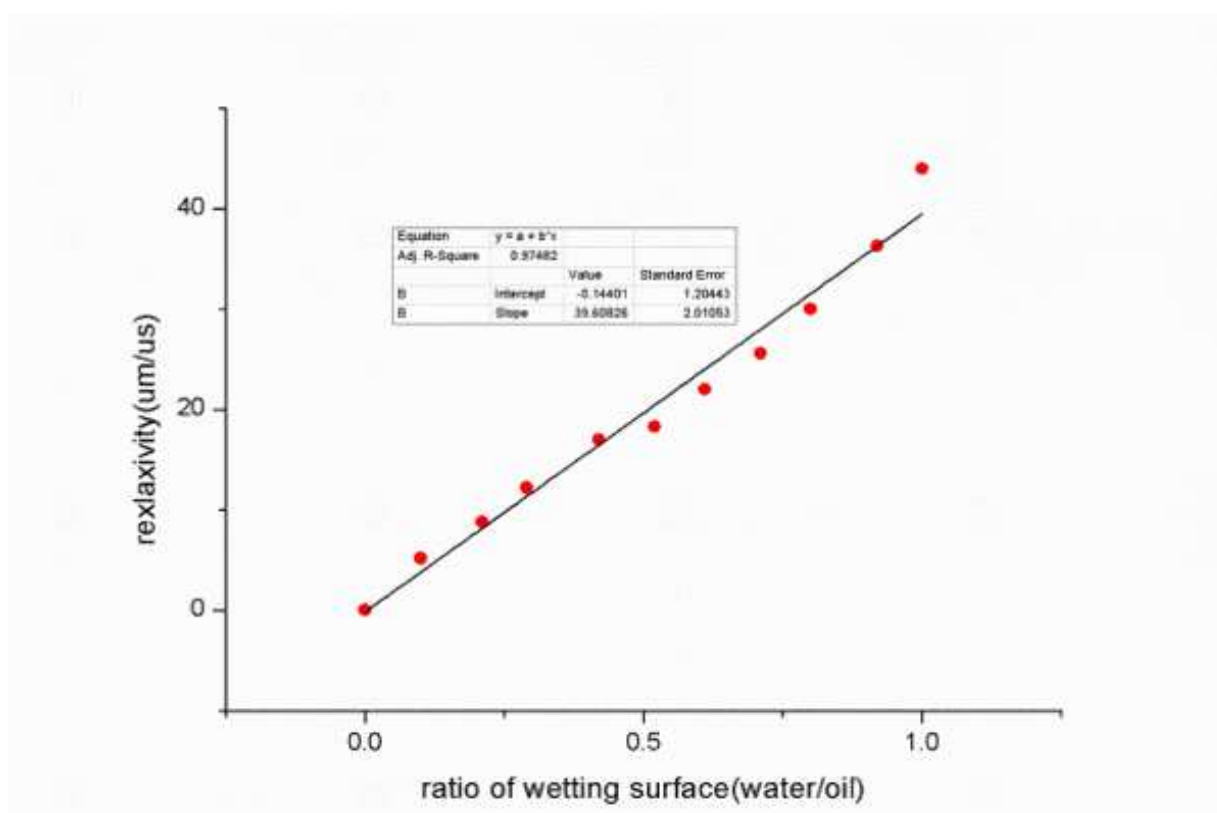




## Theoretical investigation of wettability heterogeneity in porous media with NMR

Jie Wang, Lizhi Xiao<sup>a,b</sup>, Yan Zhang and Guangzhi Liao<sup>§</sup>, <sup>a</sup>State Key Laboratory of Petroleum Resources and Prospecting, China University of Petroleum, Beijing 102249, China; <sup>b</sup>Harvard SEAS-CUPB Joint Laboratory on Petroleum Science, Cambridge, MA 02138, USA.

Understanding heterogeneity of wettability in porous media is of great importance for design catalysis and for enhancing oil recovery. In this paper, we report multi-dimensional nuclear magnetic resonance (NMR) method to characterize wettability for heterogeneous porous media with numerical simulation and experimental results. The apparent contact angle is introduced as the parameter to represent the heterogeneous wettability in porous media. It is determined by the ratio of different wetting pitches and the wetting intensity of each uniform wetting pitch. For the uniform wetting pitches, T1/T2 is applied to probe the local wetting strength of as it represents the intensity of interactions between fluid and solid surface. T2-D is introduced to obtain the effective relaxivity (defined as the ratio of wetting surfaces). To validate this method, here we simplify the porous media as the microstructure constructed with different ratio of wetting balls. Lattice Boltzmann method is applied to simulate the fluid distribution under different wetting conditions and NMR signal is obtained accordingly. Finally, we applied the method introduced above to calculate the apparent contact angle. The result is shown as in figure 1. For the experiment, we build a microstructure sample by mixing glass beads with different wetting properties alerted with chemical method. The MR method is applied to calculate the apparent angle of the microstructure. The flat planes are designed with different ratios of wetting pitches with the same chemical method and used as a control experiment. Optical visualization method is used to detect the contact angle for the flat plane. The results from visualization and NMR method are compared to testify our method. The simulation results and the experiment results match the forward model we construct. Thus, the apparent angle gives us an overall perspective for heterogeneous wetting structure and multidimensional NMR method provides us a method to detect this heterogeneity.



**Novel solid state NMR sequences for shale rocks**

[Ravinath Kausik](#)<sup>\*§</sup> and Yiqiao Song, Schlumberger-Doll Research, 1 Hampshire street, Cambridge, MA 02039, USA; Robert Blum, Department of Physics, Yale University, New Haven, Connecticut 06511; Greg Boutis, City University of New York, Brooklyn College, Department of Physics, Brooklyn, NY, USA.

The reservoir quality (RQ) of tight-oil and gas organic shale formations is a function of the solid kerogen and the heavy viscous bitumen quantities. 2D NMR  $T_1$ - $T_2$  measurements do not provide an accurate measure of the presence of these components due to their short relaxations times. In this presentation, we discuss the performance of a series of line narrowing pulse sequences for the characterization of different components in shale rocks. These sequences include the magic echo, WAHUA sequence, quadratic echo and the solid echo, which were all shown to increase the transverse coherence times of shale rock components in comparison to the CPMG pulse sequence. This is because these different line narrowing sequences average out the dipolar interaction (the primary cause of transverse relaxation) to various degrees. The extension of the transverse coherence times result in a better quantification of the  $^1\text{H}$  nuclei (or total organic hydrogen TOH) in the solid samples, enabling applications such as determining maturity and kerogen hydrogen index. We introduce recent advances for the novel combination of these sequences with traditional spin-lattice or spin-spin relaxation measurements to provide one and multi-dimensional spectroscopy and relaxometry maps. We discuss how these sequences can enable mapping of spacial distributions of the solid components and therefore be used for microscopy of full cores.

## Ultra-short Echo Time Imaging (UTE) with Multiple Echo Refocusing for Porous Media $T_2$ Mapping

D. Xiao<sup>a,b</sup> and B. J. Balcom<sup>s</sup>, <sup>a</sup>University of New Brunswick; <sup>b</sup>University of Windsor.

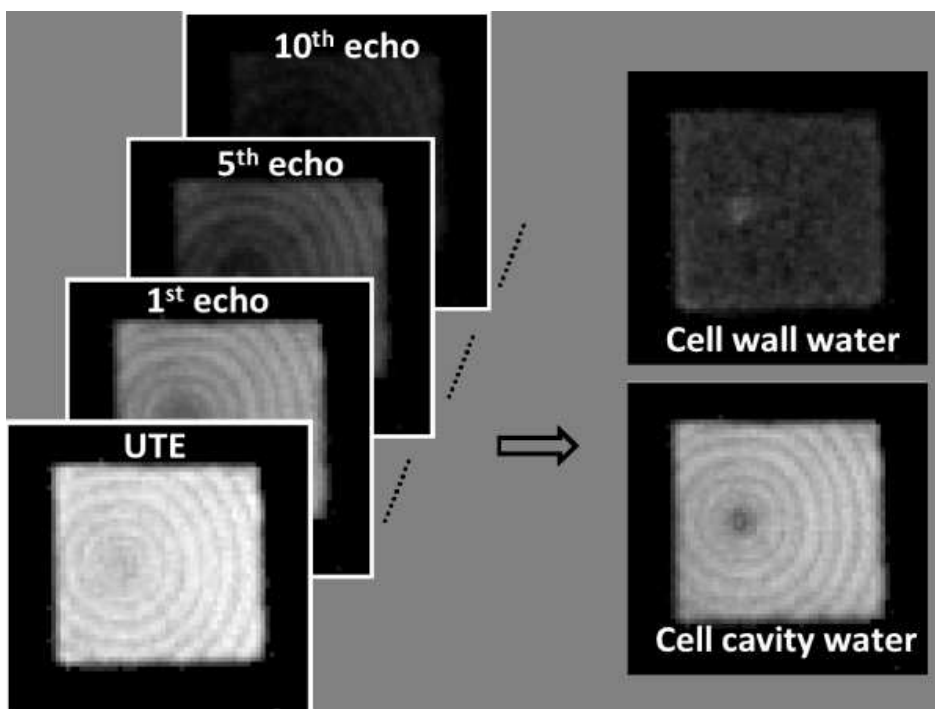
The  $T_2$  relaxation time is well known to provide useful information to distinguish various signal components in porous media. In wood samples, water bound within the cell walls has short  $T_2$  values on the order of milliseconds, while the free lumen water in the cell cavity has relatively long  $T_2$  relaxation times on the order of tens of milliseconds. Differentiating cell wall water and cell cavity water is of considerable importance, as these two components behave differently in moisture desorbing and adsorbing processes, and deeply influence wood properties. Study of water components based on  $T_2$  relaxation times has been reported on bulk wood samples [1], and with one dimensional spatial resolution [2]. Three dimensionally resolved multiple components analysis is necessary due to the inhomogeneous features within wood materials.

We employ an ultra-short echo time sequence to effectively capture the short  $T_2$  component, following a series of  $180^\circ$  refocusing pulses to generate images with various  $T_2$  weightings. The  $T_2$  decay curves for each image voxel can be extracted and fit to multiple relaxation components. Challenges include characterizing gradient waveforms and  $B_0$  shifts, and matching the point spread functions of UTE and echo images.

The method was applied to a black spruce heartwood sample of  $2.2 \text{ cm}^3$ , with a nominal spatial resolution of  $0.5 \text{ mm}^3$ . 32 echo images with an echo spacing of 5 ms were acquired following the UTE image. The extracted two components show that the earlywood, corresponding to the high intensity portion of growth rings in UTE image, has a high lumen water content, while the cell wall water is relatively homogeneous in a freshly cut sample. Applying the measurement during wood drying processes will provide insights into wood properties and inform design of the kiln drying conditions.

[1] C. Lamason, B. MacMillan, B. Balcom, B. Leblon, Z. Pirouz, Water content measurement in black spruce and aspen sapwood with benchtop and portable magnetic resonance devices, *Wood Mater Sci Eng.* 10, 86-93 (2015)

[2] R. S. Menon, A. L. Mackay, S. Flibotte, J. r. T. Hailey, Quantitative separation of NMR images of water in wood on the basis of  $T_2$ , *JMR* 82, 205-210 (1989)



## Hyperpolarized Benchtop NMR for Industrial Applications

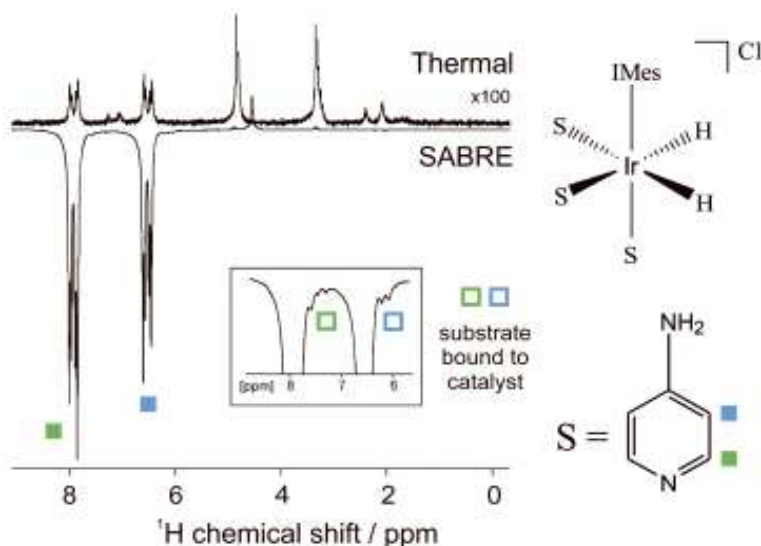
M. E. Halse, P. Richardson, O. Semenova and S. B. Duckett, Centre for Hyperpolarisation in Magnetic Resonance, Department of Chemistry, University of York, York UK YO10 5NY; A Parrott and A Nordon, Department of Pure and Applied Chemistry, University of Strathclyde, 295 Cathedral Street Glasgow UK G1 1XL.

The development of robust, high-resolution benchtop NMR spectrometers based on permanent magnets presents the opportunity for exciting new applications of NMR spectroscopy outside of the typical laboratory environment. One of the significant barriers to progress in this field is the relatively low sensitivity of these devices, which is a direct consequence of the lower magnetic fields (1–2 T) when compared to standard NMR spectrometers (7–23.5 T). Therefore benchtop NMR is an area where hyperpolarisation techniques, which can boost NMR sensitivity by several orders of magnitude, can have a transformative impact. Here we focus on the use of the parahydrogen ( $p\text{-H}_2$ ) induced polarisation (PHIP) approach [1] because  $p\text{-H}_2$  is relatively cheap and easy to produce and so does not significantly compromise the portability and affordability of the benchtop NMR device when compared to other hyperpolarisation methods. PHIP can be achieved either using a hydrogenation reaction or through catalytic transfer of polarisation at a metal centre, the so-called SABRE approach.[2] In this work, we demonstrate that high levels of hyperpolarisation can be observed on a benchtop NMR spectrometer using both hydrogenative PHIP and SABRE and show how a fully integrated flow system can be used to generate reproducible and renewable SABRE hyperpolarisation in seconds. In addition, we explore how these methods can be applied to species identification and reaction monitoring in a process control environment.

## References

[1] C. Bowers and D. Weitekamp, Phys. Rev. Lett. 1986, 57, 2645-2648.

[2] R. Adams et al., Science 2009, 323, 1708-1711.



## Field Switching Coherently Pumps Hyperpolarization to Enhance Signals

W.S. Warren<sup>\*§</sup>, T Theis, S Eriksson and Z Zhou, Duke University, Duke Box 90346, Durham, NC 27708.

The most common hyperpolarization method (dynamic nuclear polarization or DNP) can dramatically increase magnetization in virtually any organic molecule, but the apparatus is complicated and expensive (ca. \$2.5M for clinical systems) and polarization grows slowly. Another approach, called SABRE, was conceived about a decade ago; our work has extended this in the development of LIGHT-SABRE, which permits efficient generation of hyperpolarization directly in a high field magnet, and SABRE-SHEATH, an approach to directly polarize heteroatoms such as  $^{13}\text{C}$  or  $^{15}\text{N}$  using an extremely simple low field apparatus. These papers have led to a wide range of applications: our group alone has polarized about 50 different reagents, including many that are biologically interesting.

This inexpensive, general, and simple method has a few current limitations. The most significant is that hyperpolarization levels are typically lower than in DNP. Here we show that a simple modification—pulsing the low matching field to cause a coherent transfer—can produce very substantial magnetization enhancements. In essence, this is the difference between saturating a transition and giving pulses. In Figure 1, we show the  $^{15}\text{N}$  magnetization induced in acetonitrile by changing moving the field to the exact SABRE-SHEATH resonance for  $x$  ms, moving it off resonance for  $(100-x)$  ms, and repeating many times. The case of  $x=100$  ms (the right side of the curve) corresponds to normal SABRE-SHEATH. In fact, however, magnetization flows through  $2\text{JNH}$  couplings with a predicted near-complete transfer at 20 ms, so pulsing the field (and then allowing time for exchange) generates large magnetization enhancements—over double in some experiments. Theory and experiment are in excellent agreement (Figure 1) and the approach also lets us unravel important details about the magnetization transfer process, including the presence of inactive states in the catalytic process. Extensions to more complex "field pulses" and to arbitrary field profiles will be discussed.

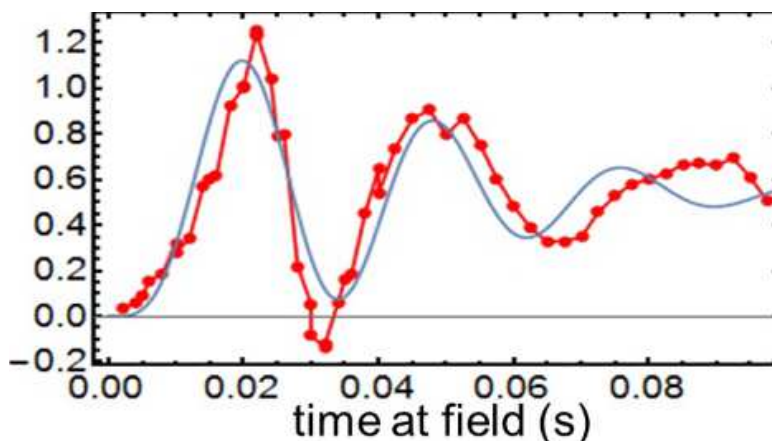


**Fig. 1.** SABRE-SHEATH intensity versus pulse length in acetonitrile (experimental red, simulated blue). The field is cycled between the correct SABRE-SHEATH matching field and a mismatched field, with the sequence repeated after 100 ms. The right hand side corresponds to normal SABRE-SHEATH. The maximum occurs at much shorter times, because scalar couplings across the iridium bond cause coherent transfer.

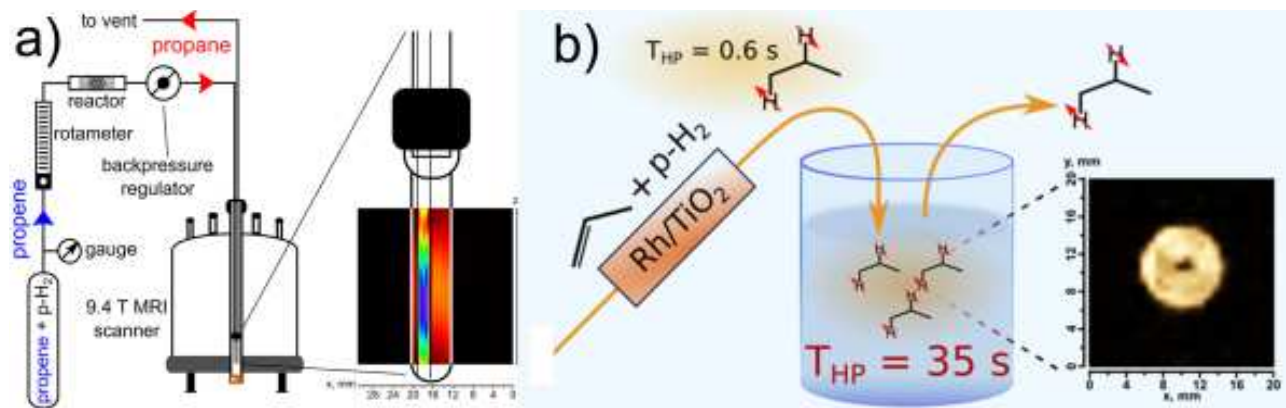
## Parahydrogen and heterogeneous catalysis for enhanced MRI

V.V. Zhivonitko, K.V. Kovtunov and I.V. Koptug\*, International Tomography Center SB RAS, 3A Institutskaya St., Novosibirsk, 630090, Russia.

Parahydrogen-induced polarization (PHIP), including its most recent variants such as SABRE, is arguably the simplest and technically least demanding hyperpolarization technique which in recent years attracts significant attention of the magnetic resonance community. PHIP was first demonstrated unambiguously in 1987, but until 2007 observation of PHIP effects was associated exclusively with homogeneous processes in solution, such as H<sub>2</sub> activation and catalytic hydrogenation of unsaturated compounds by dissolved transition metal complexes. However, during the past decade PHIP effects in liquid and gas phase hydrogenations of alkenes and alkynes have been also demonstrated with numerous heterogeneous hydrogenation catalysts, including transition metal complexes immobilized on solid supports, supported and unsupported metals, metal oxides, metal sulfides, etc. Further extension to other catalyst types such as single-site and/or molecularly defined heterogeneous hydrogenation catalysts was also demonstrated. Representative recent examples of such studies will be discussed.

The ability to produce and observe PHIP and SABRE effects in heterogeneous catalytic processes significantly expands the range of potential applications of parahydrogen-derived signal enhancement in NMR and especially in MRI. We currently pursue several directions in PHIP and SABRE research. One of them involves the development of advanced heterogeneous catalysts with the aim to maximize the degree of achievable spin polarization in both HET-PHIP and HET-SABRE experiments. Another encompasses the utilization of PHIP-derived signal enhancement in MRI to obtain new valuable knowledge about the dynamic processes in operating reactors. Thus, combining the unique chemical specificity of NMR spectroscopy and the non-invasive nature of MRI with the strong parahydrogen-based signal enhancement is clearly beneficial for catalytic and chemical engineering applications of magnetic resonance.

Another major direction of HET-PHIP research is the production of hyperpolarized molecular markers for biomedical applications of MRI and MRS. Such applications require the availability of biocompatible hyperpolarized samples. Thus, if a hydrogenation catalyst contains transition metals or other toxic ingredients, it needs to be rapidly removed from the sample after reaction completion. Unlike homogeneous catalysts, the heterogeneous ones can be easily filtered out after the reaction. Furthermore, heterogeneous catalytic hydrogenation can be performed in a continuous flow mode, providing a constant stream of hyperpolarized fluid. While an ultimate catalyst with the highest HET-PHIP production efficiency is yet to be identified, we have taken decisive steps toward biomedical applications of this methodology. Examples of the use of liquid and gas phase hydrogenations of unsaturated compounds with parahydrogen to produce catalyst-free hyperpolarized substances for potential in vivo use and to prolong polarization lifetime will be described. The figure below exemplifies the use of HET-PHIP to produce hyperpolarized propane and its imaging in the gas phase (a) and in solution (b).

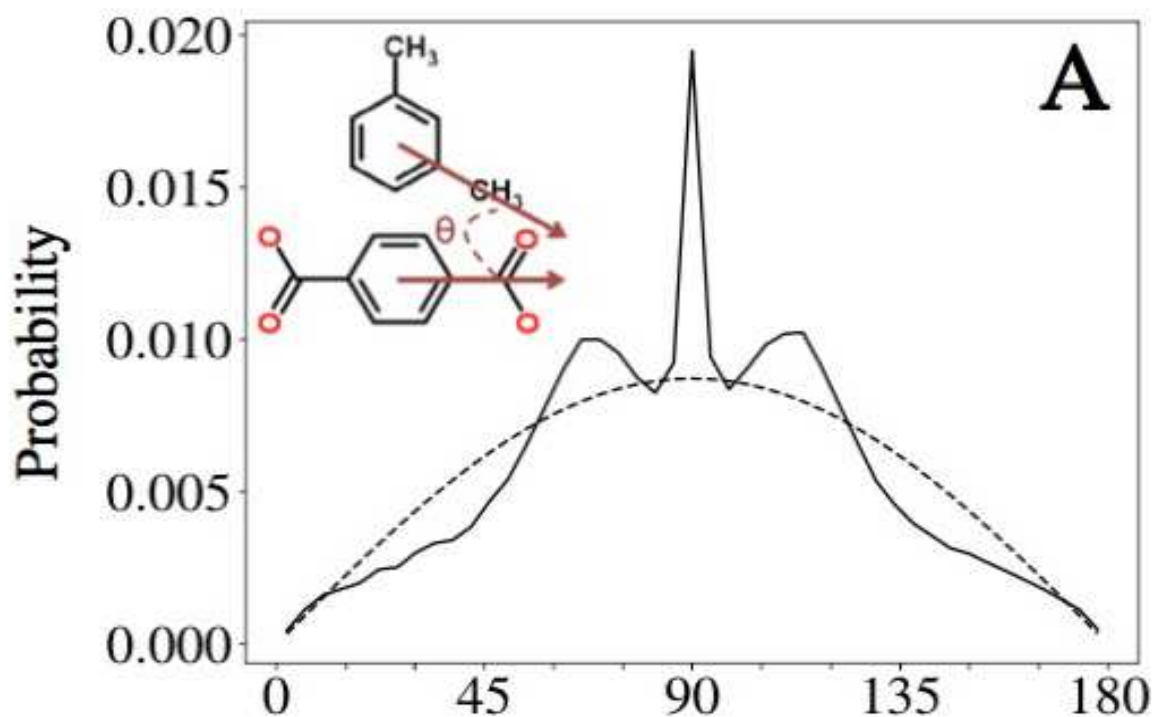




## Relaxometry and Diffusometry of Small Molecules in MOFs

J. Reimer<sup>§</sup> and V Witherspoon, Dept Chem and BioM Engr, UC Berkeley, Berkeley CA USA 94720.

We employed NMR diffusometry and relaxometry techniques to quantify the self-diffusion coefficients ( $D_s$ ) and the relaxation times ( $T_1$  and  $T_2$ ) of small molecules in MOF-5 and the MOF-74 series  $M_2(\text{dobdc})$  series ( $M = \text{Mg}, \text{Ni}, \text{Zn}$ ). When matched with molecular dynamics simulations, these studies reveal the Gibbs free energies changes for motion, the magnitude of internal pore gradients, and role of open-metal site adsorption strength on the self-diffusivity of gases. This work comes from the PhD thesis of Velencia Witherspoon and was supported in part by the Center for Gas Separations Relevant to Clean Energy Technologies, as an Energy Frontier Research Center funded by the U.S. Department of Energy, Office of Science, Basic Energy Sciences under Award DE- SC0001015.



## Scaling exponent and absolute molecular mass of polymers in solution by PGSE NMR

N.H. Williamson\*, Future Industries Institute, University of South Australia, Mawson Lakes, SA 5095, Australia; M. Röding, SP Agrifood and Bioscience, Frans Perssons väg 6, 402 29 Göteborg, Sweden; S.J. Miklavcic, Phenomics and Bioinformatics Research Centre, School of Information Technology and Mathematical Sciences, University of South Australia, Mawson Lakes, SA 5095, Australia; M. Nydén, School of Energy and Resources, University College London, 220 Victoria Square, Adelaide, SA 5000, Australia.

Although molecular mass controls the performance of a polymer in its application, traditional characterization methods do not always work. Molecular mass distribution (MMD) measurements of polymers in solution by pulsed gradient spin echo (PGSE) NMR are advantageous with respect to other methods due to the access to chemical shift information and ease of sample preparation. However, converting from polymer self-diffusion coefficient,  $D$ , to molecular mass,  $M$ , requires prior knowledge of parameters in a scaling law,  $D=KM^{-\nu}$ . In this talk we show that the scaling exponent,  $\nu$ , can be directly estimated from a PGSE experiment in which the extremity (end-group) polymer signal can be spectrally resolved by a chemical shift from the polymer main-chain signal [1]. The method builds on the work of Viéville et al. [2] who showed that the distribution of  $D$  is mass-weighted for the main-chain signal and number-weighted for the end-group signal. The key to directly obtaining  $\nu$  is our use of parametric distribution models to fit these two signals. The method is developed using lognormal and gamma distribution models, which are known to be good model choices for PGSE NMR measurements of MMDs [3,4], in part because gamma and lognormal MMDs are theoretically predicted for many polymerization processes.

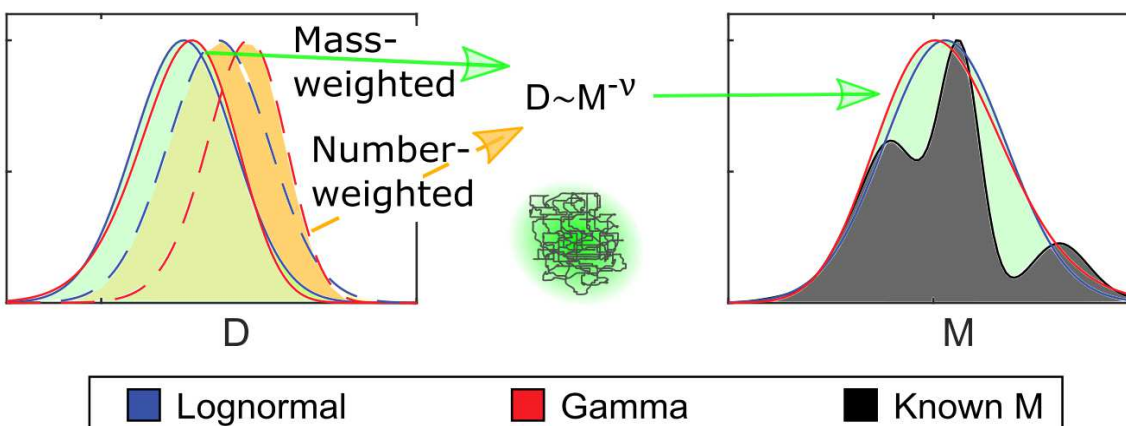
The scaling exponent is, on its own, a useful measure of polymer conformation and solvent quality. The same PGSE experiment provides the information necessary to estimate the other scaling parameter,  $K$ , and therefore the absolute MMD. We tested the method on mixtures of polyethylene glycol standards and obtained excellent agreement to known values for both the scaling exponent and absolute MMD characteristics. The methods can be applied to newly synthesized polymers for which the MMD is unknown and otherwise unobtainable.

[1] N.H. Williamson et al., *J. Colloid Interface Sci.* 493 (2017)

[2] J. Viéville et al., *J. Mag. Reson.* 212 (2011)

[3] N.H. Williamson et al., *J. Mag. Reson.* 267 (2016)

[4] X. Guo et al., *Macromol. Chem. Phys.* 218 (2016)



**Nuclear Magnetic Resonance Relaxation and Diffusion Measurements to Monitor Phase Change**

L. W. Thrane and S. L. Codd, Mechanical and Industrial Engineering, Montana State University; J. D. Seymour, Chemical and Biological Engineering, Montana State University.

State of the art multi-dimensional nuclear magnetic resonance (NMR) relaxometry and diffusometry techniques along with magnetic resonance imaging (MRI) are applied to explore and characterize phase change in complex systems. High-field NMR techniques are highly sensitive to the thermodynamic phase of the system as well as restrictions on molecular motion. High resolution imaging along with T1-T2 relaxation correlation experiments and pulsed gradient spin echo (PGSE) NMR methods are demonstrated to characterize hydrate formation. The NMR techniques are applied to monitor the hydrate formation process in a model water-cyclopentane system at various sub cooling temperatures. Using T1-T2 correlation NMR, the transition from mobile to restricted dynamics is observed simultaneously for both water and cyclopentane throughout the formation process by examining the magnetization decay as a function of  $1/\tau$  at multiple  $\tau$  times. Spectrally resolved diffusion measurements allow monitoring of the hydrate formation process by measurement of the area under the liquid water peak as it disappears due to solidification of the water in the hydrate. Also, restriction in diffusive motion due to boundaries between solid-liquid or immiscible liquid-liquid phases provides a means to characterize structure by the size of particles or pore spaces. Magnetic resonance imaging (MRI) data monitors total hydrate formation rate based on cyclopentane saturation and temperature, as well as the spatial heterogeneity within the system. The combination of these MR techniques allows for exploration of the complex molecular dynamics involved in hydrate formation processes.

## Solid state multi-nuclei magic angle spinning micro-imaging of materials and hard tissues at very high field

M. Yon<sup>\*§</sup>, V. Sarou-Kanian, D. Massiot and F. Fayon, CEMHTI, CNRS, 1D av. Recherche Scientifique, 45071 Orléans Cedex2, France; U. Scheler, Leibniz-Institut für Polymerforschung Dresden, Hohe Str. 6, Dresden, Germany.

Magnetic Resonance Imaging is a powerful tool which offers high resolution spatial localization of mobile species in soft tissues. However, the application of MRI in rigid solids remains challenging as they usually exhibit short transverse relaxation time which prohibits the use of spin echo MRI sequences and strong line broadening which decreases both the sensitivity and the resolution obtained with frequency encoding.

Magic Angle Spinning (MAS), which averages anisotropic interactions through a macroscopic rotation of the sample, allows obtaining narrow resonances in the solid-state. We show the potentiality of combining MAS and MRI<sup>1-3</sup> to carry out multi-nuclei ( $^1\text{H}$ ,  $^{31}\text{P}$ ,  $^{27}\text{Al}$  or  $^{51}\text{V}$ ) three dimensional micro-imaging in rigid solid, at very high magnetic field (17.6 T) with greatly improved SNR and spatial resolution when compared to static conditions. These will be exemplified on a wide range of materials: polymers, oxide ceramics, biomaterials and hard tissues with spatial resolutions ranging from 30 to 300  $\mu\text{m}$ , at MAS spinning frequencies up to 20 kHz using classical MRI spin-echo or Zero Echo Time (ZTE) sequences.

In hard tissues, very high magnetic field and moderate MAS spinning rate provide high spectral resolution and enable the use of various frequency selective excitation schemes for  $^1\text{H}$  chemically selective imaging. This allows us to record for the first time a 3D image probing the spatial distribution of apatitic hydroxyl protons inside a mouse tooth with attached jaw bone with a nominal isotropic resolution nearing 100  $\mu\text{m}$ .

1. D. G. Cory, J. W. M. Van Os, and W. S. Veeman, J. Magn. Res. 1988 76 543-547

2. U. Scheler, B. Blumich and H.W. Spiess, Solid State Nuclear Magn. Res. 1993 2 105-110

3. D.E. Demco and B. Blumich, Concepts in magn. resonance 2000 12 269-288.

M. Yon, V. Sarou-Kanian, U. Scheler, J-M. Boulter, B. Bujoli, D. Massiot, F. Fayon *submitted to scientific reports*

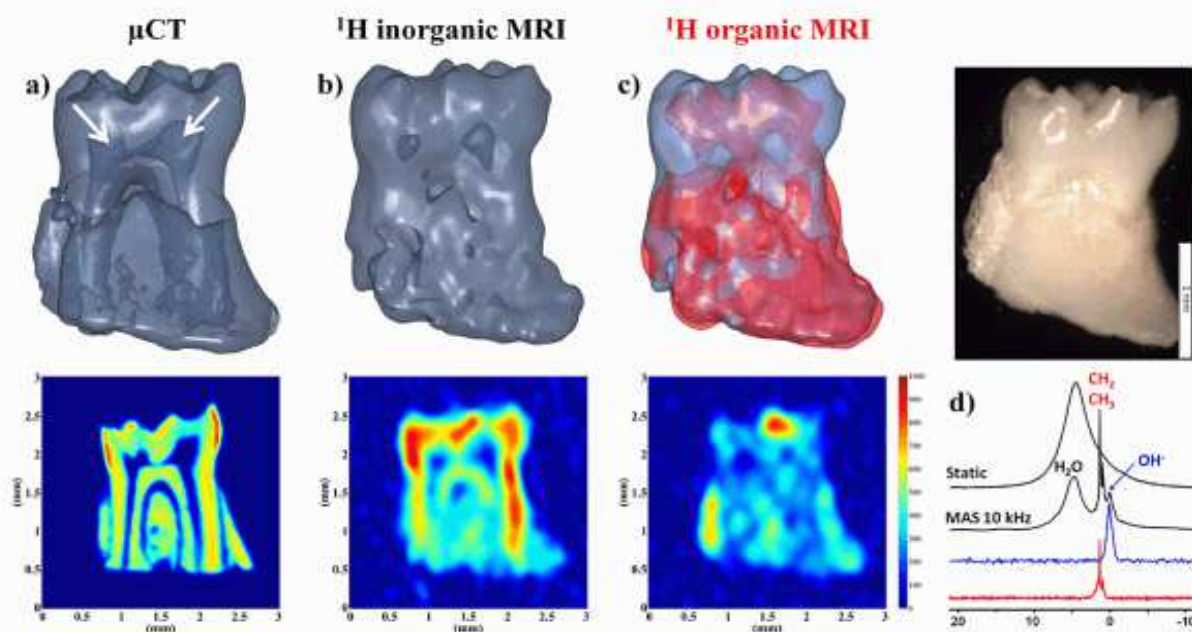


**Figure 1:** a)  $\mu\text{CT}$  3D isosurface representation and 2D slice of the mouse tooth, the white arrows show the pulp channel of the tooth b-c) chemically selective  $^1\text{H}$  MAS-MRI images of the same sample recorded with a spin echo sequence at a spinning frequency of 10 kHz. The red image is obtained with the aliphatic resonances (red component) and the blue image with the inorganic resonance (blue component) of the MAS spectra. d) Overlay of the static, MAS at 10 kHz and selected region of the  $^1\text{H}$  spectra of the mouse tooth at very high field (17.6 T).

## Magnetic Resonance Probing Ensemble Dynamics in k-Space

V. Herold\*, T. Kampf and P.M. Jakob, , Experimentelle Physik, Julius-Maximilians-Universität Würzburg; Germany.

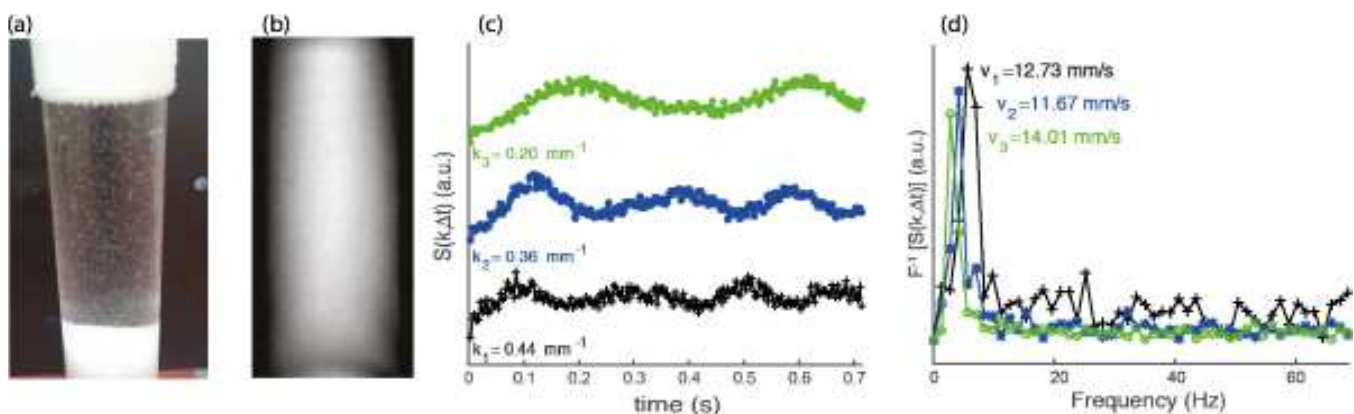
We demonstrate the use of spatial encoded magnetic resonance to quantify ensemble dynamics of dispersed microscopic particles below the spatial resolution. By evaluating time series of single k-space data-points, k-dependent motion patterns can be revealed in short measurement time. The signal generation can be described analogously to the theory of dynamic light scattering [1]. Ensemble dynamics was measured by examining time correlations in the k-space signal using the autocorrelation function or structure function [2].

To proof the feasibility of this new technique we have simulated the MR measurement with samples producing particle drift and brownian motion. MR experiments with sedimenting microspheres ( $D = 100 \mu\text{m}$ ) verified the results of the simulations. A typical CINE-FLASH-(fast-low-angle-shot)-sequence with  $N = 200$  time-frames and a repetition time of  $TR = 3.6 \text{ ms}$  was applied first with and then without spatial phase encoding [3]. Fig. 1a shows a photography of the sedimenting glass spheres ( $D = 100 \mu\text{m}$ ). For the limited temporal and spatial resolution ( $0.4 \times 0.4 \text{ mm}^2$ ) the reconstructed CINE-MR-images reveal no details about the particle size, distribution and dynamics as shown in Fig. 1b. When picking out the time course of a single  $k_x$ -encoded data-point (without spatial phase encoding), and examining the temporal correlation in the signal, the imprint of the ensemble motion gets visible. In the case of drifting particles the motion is reflected in the signal oscillation, as shown for three different k-space-values in Fig. 1c. The corresponding spectra of the structure functions allow the quantification of the drift motion as shown in Fig. 1d [2]. The mathematical description of this new method is very similar to the well known q-space encoding, it allows to quantify particle motion below the spatial resolution almost in real-time [4]. Since this new approach does not directly encode the particle displacement such as done with q-space encoding it is not limited by relaxation times and covers a wide field of applications for particle motion in opaque media.

### References:

- [1] B. J. Berne and R. Pecora, Dynamic light scattering: with applications to chemistry, biology, and physics (Courier Corporation, 1976).
- [2] R. Cerbino and V. Trappe, Phys Rev Lett 100, 188102 (2008).
- [3] A. Haase, J. Frahm, D. Matthaei, W. Hanicke, and K.-D. Merboldt, Journal of Magnetic Resonance (1969) 67, 258 (1986).
- [4] P. T. Callaghan, Translational dynamics and magnetic resonance: principles of pulsed gradient spin echo NMR (Oxford University Press, 2011).

Figure 1:



**Ultra-high field MRM and MRS of biological systems**

JR Krug<sup>a,b</sup>, FM Vergeldt<sup>a,d</sup>, E Golovina<sup>a,c</sup> and H Van As<sup>a,d</sup>, <sup>a</sup>Lab of Biophysics, Wageningen University, Stippeneng 4, 6708 WE Wageningen, NL; <sup>b</sup>BioNanoTechnology, Wageningen University, Bornse Weilanden 9, 6708 WG, Wageningen, NL; <sup>c</sup>Lab for Plant Physiology, Wageningen University, Droeveldalsesteeg 1, 6708 PB, Wageningen, NL; <sup>d</sup>Wageningen NMR Centre, Wageningen University and Research, Wageningen, NL.

MRMicroscopy (MRM) concerns imaging of small-scale samples at high spatial resolution. With MRSpectroscopy (MRS) we obtain localized information on i.e. metabolites present in a sample. The sensitivity and resolution of both MRM and MRS increase with increasing magnetic field strength. At the same time susceptibility and chemical shift artefacts can become limiting at (ultra-)high fields. Here we report on first results obtained at a 950 MHz NMR spectrometer (Dutch national facility at Utrecht uNMR-NL, funded by NWO Roadmap program), currently one of the highest magnetic field strengths available. It allows us to non-invasively detect low concentrated compounds. In this research, we tested the resolution and detection limits of the 950MHz system with a 5 mm coil, using a phantom, consisting of capillaries filled with different sucrose concentrations. MRM images could be obtained with voxel resolutions of 12x12x100  $\mu\text{m}^3$  within 9 minutes of measurement time, while by localised spectroscopy we were able to detect 10 mM sucrose in a volume of 125 nL within 11 minutes of measurement time. A number of biological samples has been explored as well. In small cabbage and Arabidopsis seeds we were successful to image the embryonic axis. Possibilities to image the redox state of the embryonic tissues observed in the seeds during rehydration in relation to seed viability/longevity will be discussed. Also MRM and MRS of other biological systems like leaves and complex granular biofilm systems have been explored. Susceptibility artefacts and contrast observed in these systems will be discussed and compared to results obtained at lower field (14 and 7 T) systems. We conclude that these first results demonstrate the very promising possibilities of ultra-high field MRM and MRS.



**Remote detection MRI of microfluidic flow, chemical reactions and adsorption**

V.-V. Telkki<sup>\*§</sup> and A. Selent, NMR Research Unit, University of Oulu, Finland; V. V. Zhivonitko and I. Koptug, Laboratory of Magnetic Resonance Microimaging, International Tomography Center SB RAS, Novosibirsk, Russia; S. Franssila, Department of Materials Science and Engineering, Aalto University, Finland.

Microfluidics offers new technological capabilities due to the precise and flexible channel design, efficient heat exchange, high mechanical stability and economical use of reactants. Nuclear magnetic resonance (NMR) spectroscopy is a promising, versatile technique for monitoring microfluidic processes. However, non-standard NMR techniques are required due to low quantities of substances.

Remote detection (RD) NMR method, in which the encoding of spin coherences of fluid flowing through a microfluidic chip is performed by a large coil around the chip and the signal is detected by another, much smaller and sensitive coil outside the chip, provides an elegant solution to the sensitivity issue [1,2]. In addition, the method enables one to measure time-of-flight flow images.

In this presentation, we show that combined RD MRI and parahydrogen-induced polarization (PHIP) methods allow gas flow profiling in microfluidic chips [3,4] and detailed analysis of performance of microfluidic packed-bed reactors [5]. We introduce the concept of remote detection exchange spectroscopy (RD-EXSY), and show that, along with indirect spatial information extracted from TOF data, it provides unique information about the active regions, reaction pathways and intermediate products in a microfluidic reactor. Furthermore, we demonstrate that RD-EXSY can be combined with direct spatial encoding efficiently by applying the principles of Hadamard spectroscopy [6]. We show also that RD MRI provides an efficient means to quantify the adsorption of flowing gas mixtures in situ [5,7].

- [1] A. J. Moule et al., Proc. Natl. Acad. Sci. U.S.A. 2003, 100, 9122.
- [2] C. Hilty et al., Proc. Natl. Acad. Sci. USA 2005, 102, 14960.
- [3] V.-V. Telkki et al., Angew. Chem. Int. Ed. 2010, 49, 8363.
- [4] V. V. Zhivonitko et al., Angew. Chem. Int. Ed. 2012, 51, 8054.
- [5] V. V. Zhivonitko et al., Lab Chip 2013, 13, 1554.
- [6] V.-V. Telkki et al., Angew. Chem. Int. Ed. 2015, 53, 11289.
- [7] A. Selent et al., submitted for publication in Micropor. Mesopor. Mat.

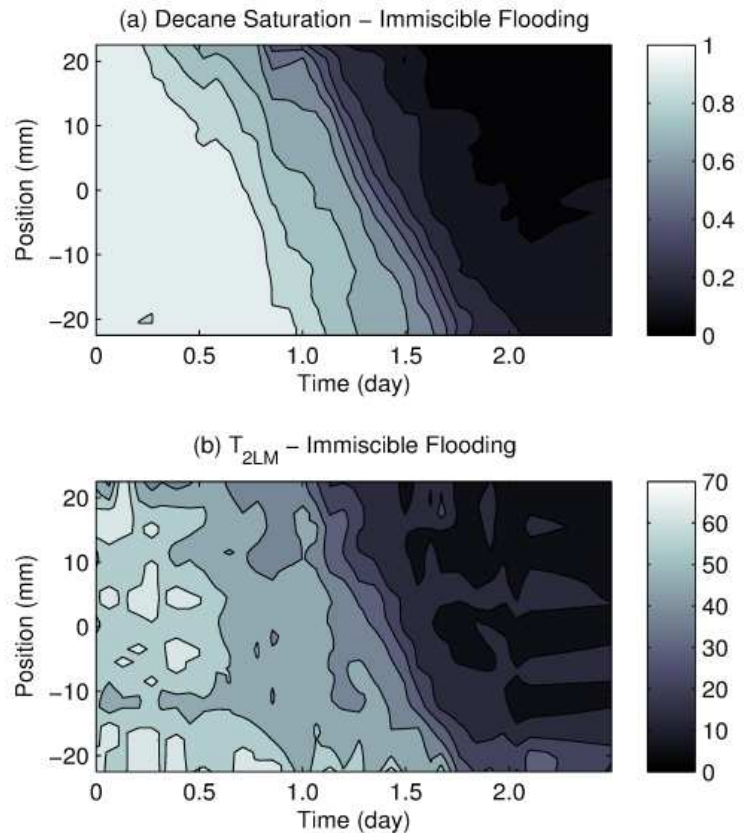
## MRI of High Pressure Carbon Dioxide Displacement: Fluid/Surface Interaction and Fluid Behavior

A. Afrough, M Shakerian, M S Zamiri, B MacMillan, F Marica, B Newling, L Romero-Zerón and B J Balcom<sup>\*§</sup>, University of New Brunswick.

The transverse relaxation rate can report on the properties of fluids and surface bound layer in porous materials. Such pore level information can potentially increase petroleum recovery through a better understanding of petroleum flooding

displacement mechanisms. Pure phase-encoding magnetic resonance methods, such as  $T_2$ -mapping SE-SPI, and 1D double half  $k$ -space SPRITE (Muir and Balcom, 2012, In *Annual Reports on NMR Spectroscopy*, Vol. 77) were employed at a magnetic field of 0.2 T to quantitatively measure the transverse relaxation rate and fluid content spatially and temporally in  $\text{CO}_2$  flooding experiments. Carbon dioxide enhanced oil recovery is a method of contemporary interest because of mitigating the climate change impact of  $\text{CO}_2$ . In miscible and immiscible flooding experiments, at 9 MPa and 6 MPa respectively,  $\text{CO}_2$  displaced decane and heavy oil from Berea sandstone core plugs. The experiments were performed at 40°C in a non-magnetic metallic core holder (Shakerian et al., 2017, Rev Sci Instrum, submitted), including an integrated radiofrequency probe, capable of withstanding a maximum pressure of 35 MPa and temperatures of 170°C. The correlation between transverse relaxation rate and fluid saturation revealed the contrast in

decane/pore-surface interaction between miscible and immiscible drainage of decane by  $\text{CO}_2$ . The density of decane in the pore surface bound layer decreased during the miscible drainage of decane by  $\text{CO}_2$ . In immiscible displacement of decane by  $\text{CO}_2$ , the pore surface area wetted by decane monotonically decreased at saturations less than 0.25 (residual saturation). This behavior potentially demonstrates the development of a non-continuous wetting film on the pore surface. The transverse relaxation rate profiles demonstrated changes in the composition and viscosity of the heavy oil caused by the extraction of light components by  $\text{CO}_2$ .  $\text{CO}_2$  flooding of heavy oil shows an initial increase in  $T_2$  caused by increased fluid mobility. Later,  $T_2$  decreased consistent with the extraction of light components from the heavy oil that enriched the displacing  $\text{CO}_2$  phase.



## Multi-component quantitative magnetic resonance imaging by phasor representation

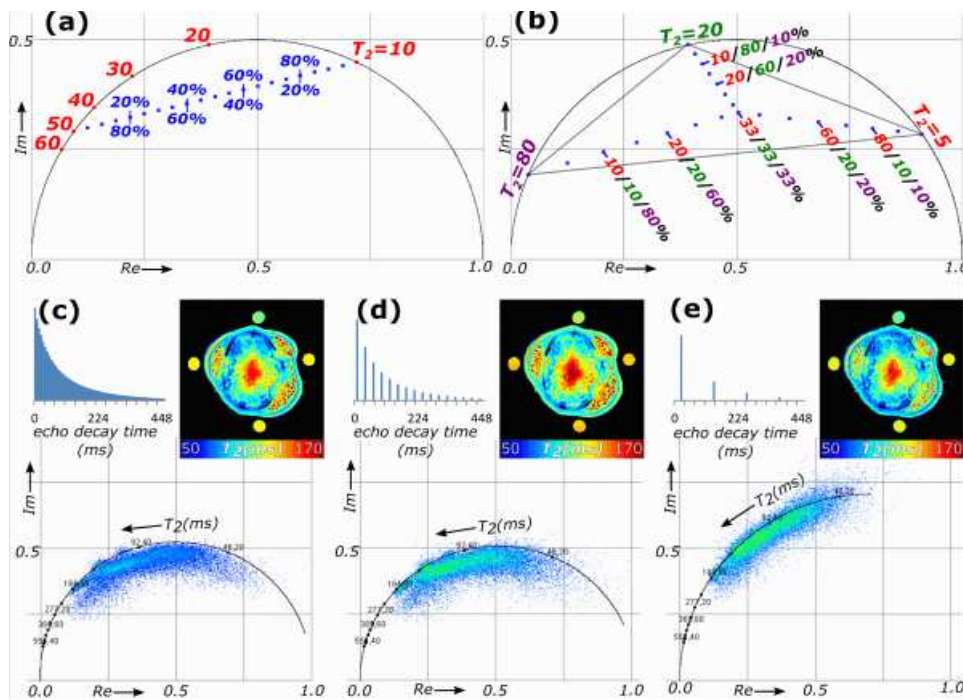
F.J. Vergeldt<sup>a,b</sup>, A.N. Bader<sup>a,c</sup>, H. van Amerongen<sup>a,c</sup> and H. Van As<sup>a,b</sup>, <sup>a</sup>Laboratory of Biophysics, Wageningen University & Research, The Netherlands; <sup>b</sup>Wageningen NMR Centre, Wageningen University & Research, The Netherlands; <sup>c</sup>MicroSpectroscopy Centre, Wageningen University & Research, The Netherlands; F. Fereidouni, Department of Pathology and Laboratory Medicine, UC Davis Medical Center, Sacramento, CA, USA; T.W.J. Scheenen, Department of Radiology and Nuclear Medicine, Radboud University Medical Centre, Nijmegen, The Netherlands.

Quantitative magnetic resonance imaging (qMRI) is a versatile tool in life, material, and medical sciences. When multiple components contribute to the signal in a single pixel, however, it is difficult to quantify their individual contributions and characteristic parameters. Here we introduce qMRI based on phasor representation to disentangle the signals from multiple components.<sup>1</sup> In this approach, the non-spatial information in the pixels is represented as vectors: the phasors. Plotting the phasors allows decomposition, unmixing, segmentation and quantification of very diverse qMRI data. The presented phasor analysis is model-free, fast, accurate, unbiased and also works for undersampled data. It simplifies the inherent complexity of qMRI data analysis for multi-component imaging.

The concept is demonstrated with modelled multi-echo relaxation curves. Mono-exponential decays are located on a semicircle in a phasor plot (Fig. 1a). The phasor of a bi-exponential decay is a linear combination of the phasors of the mono-exponentials (Fig. 1b). A mixture of three decays is located inside a triangle connecting the individual components on the semicircle (Fig. 1b). The phasor approach is demonstrated with a T<sub>2</sub>-MRI measurement of a plant stem (Fig. 1c-e). For this dataset an extended cloud of phasors was located inside the semicircle (Fig. 1c). The insert shows the average T<sub>2</sub> map calculated from the phasors.

Many applications of qMRI use undersampling to reduce measurement time. Undersampling was simulated by reducing the original 64 echoes to e.g. 16 or 4 (Fig. 1d-e). Compared to the original data, the low number of echoes and the truncation of the exponential decay resulted in a deviated semicircle. The cloud of phasors retained its shape and location inside the new semicircle. As undersampling was achieved by discarding echoes, the total SNR decreased, which resulted in more scatter in the phasor plot. The average T<sub>2</sub> maps, however, were not notably affected by the undersampling and lower SNR.

1) Vergeldt, et al. Sci. Rep. 7 (2017) 861.



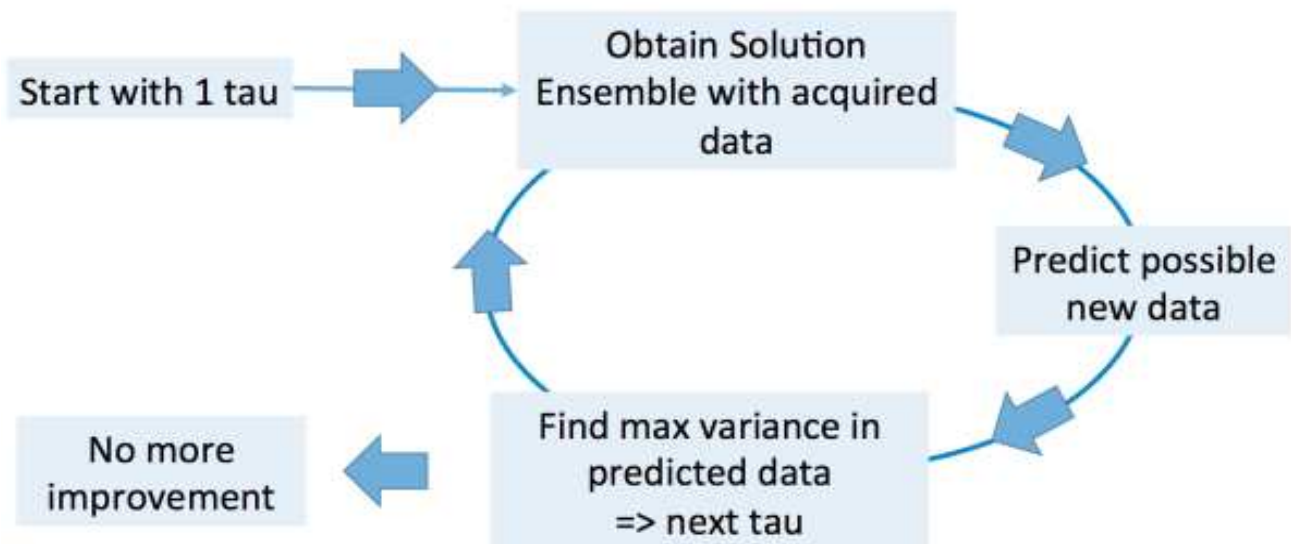
**A machine-learning based adaptive method for multiparametric NMR experiments**

Y Tang and Y\_Song, Schlumberger-Doll Research,.

An NMR experiment is defined by a time sequence of RF pulses, gradient pulses, and data acquisitions. Conventionally, the time sequence is pre-set prior to an experiment, oftentimes resulting in suboptimal results and prolonged acquisition time for a particular sample. In this work, we demonstrate a new approach, in which NMR acquisition parameters are optimized dynamically, with the incremental knowledge of the sample under investigation, over the course of an experiment.

Based on a machine learning (ML) algorithm, we take an adaptive approach to analyze the acquired data in real time, make data-driven predictions, and from which determine the most suitable acquisition parameters for subsequent measurements. Such an adaptive optimization process allows efficient data acquisition with minimal operator interference, raising exciting possibilities of a fast, streamlined and automated workflow for many NMR pulse sequences and applications. The idea of this ML algorithm is shown in the Figure.

We will show theory and experiments based on this algorithm to perform several experiments and different samples. For example, we have examined experiment with one parameter, such as a T2 decay experiment demonstrating automatic real-time optimization of data acquisition. In practical experiments, however, there are often several parameters that require adjustment. For example, recycle delay (RD) is a common parameter for all experiments. Typically, experimentalist tends to adjust RD so that it is much longer than the relevant T1. We will show that this process can be automated efficiently with the machine learning algorithm in both theory and experiments. In addition, we show that our ML algorithm for 1 parameter can be adapted to optimize two experimental parameters simultaneously. Both parameters are included in the signal equation and their value for the next acquisition is obtained from the optimization in 2D (2D error map as a function of the two parameters).

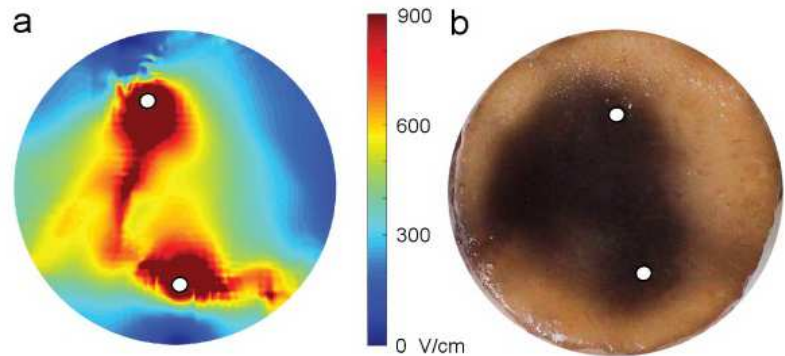


## Magnetic Resonance Imaging of Electric Field Distribution in Samples During Pulsed Electric Field Treatment

I. Sersa\* and F. Bajd, Jozef Stefan Institute, Ljubljana, Slovenia; M. Kranjc and D. Miklavcic, University of Ljubljana, Faculty of Electrical Engineering, Ljubljana, Slovenia.

Pulsed electric field (PEF) treatment in food processing industry and electroporation in medicine are essentially two identical processes in which cell membranes are temporarily made permeable due to their exposure to a high electric field. PEF treatment helps saving energy, preserving vitamins and significantly increases yield in processes of juice and nutrient extraction from fruits and vegetables, while reversible electroporation is applied in medicine for increasing uptake of drugs into the cells and is successfully used in tumor treatment of patients with cancer [1].

However, success of both processes critically depends on the local electric field. If the field is too low, usually less than 400 V/cm, the treatment has no effect. On the other hand, if the field is too high, usually more than 900 V/cm, the cells are irreversibly damaged and will die because of the excessively high electric field (irreversible electroporation). Just when the field is in the right range (between 400 and 900 V/cm), the treatment is reversible (reversible electroporation) and the cells can fully recover from the effects of the field. Therefore, an efficient method for monitoring the electric field during PEF or electroporation treatment of cells in a tissue is of a high importance. For that purpose, magnetic resonance electrical impedance tomography (MREIT) was found efficient [2]. MREIT is an upgrade of current density imaging (CDI), which uses current density maps along with sample geometry data and known electric potentials on the electrodes to calculate, sample's impedance and also the electric field in it.



Feasibility of MREIT to monitor PEF (electroporation) treatment was tested on various samples such as potato tubers [3] and mice with tumors [4]. In all cases two needle platinum-iridium electrodes were inserted in the sample in orientation aligned with the static magnetic field and perpendicular to the imaging slice. Up to eight 100  $\mu$ s long electric pulses separated by 100  $\mu$ s intervals were delivered to the electrodes. Voltages of the pulses were up to 3000 V depending on the separation between the electrodes (4 - 15 mm). The electric pulses were executed between the excitation and the first refocusing RF pulse of the single-shot RARE sequence. Effects of the pulses were recorded as phase shifts of the acquired image. These were then used to calculate the current-induced magnetic field change map and from it the current density map by using Ampere's law. The final step of the MREIT procedure was the use of the J-substitution algorithm [2] to obtain the map of electric field during delivery of electric pulses. In all cases, the map was found very useful for prediction of treatment effects and its outcome.

The figure on the top shows a map of electric field in a potato tuber during the PEF treatment (a) and the corresponding optical photography image of the sample taken 18 h after the treatment (b). In the photography, the electroporated region darkened due to oxidation of phenolic compounds released from the successfully electroporated cells. The darkened region coincides well with the region of electric field  $E > 400$  V/cm.

[1] Yarmush M.L. et al., *Annu. Rev. Biomed. Eng.* **16**, 295-320 (2014).

[2] Kwon O. et al., *IEEE Trans. Biomed. Eng.*, **49**, 160-167 (2002).

[3] Kranjc M. et al., *Innov. Food Sci. & Emerg. Tech.*, **37**, 384-390 (2016).

[4] Kranjc M. et al., *Radiology*, **274**, 1151-123 (2015).

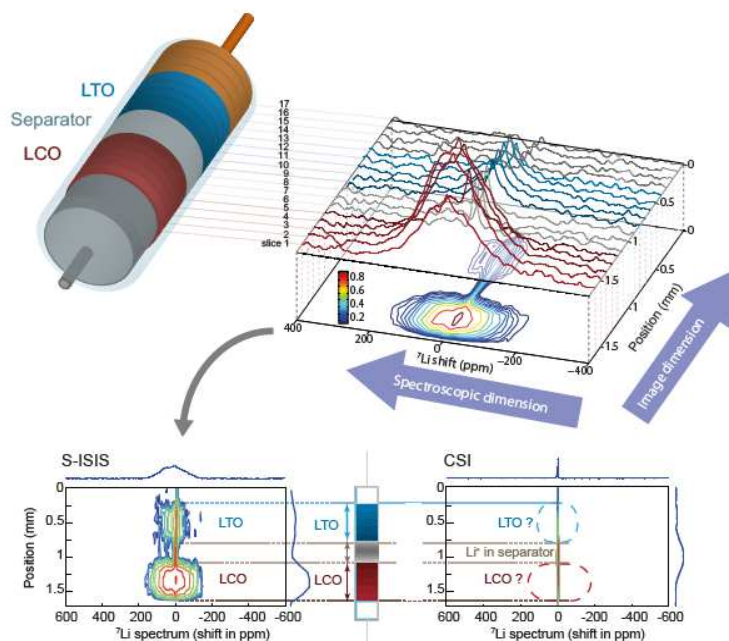


## NMR SPECTROSCOPIC IMAGING FOR THE STUDY OF LITHIUM-ION BATTERIES

V. SAROU-KANIAN\*, M. TANG, C.E. DUTOIT, M. DESCHAMPS and E. SALAGER<sup>§</sup>, CNRS, CEMHTI UPR 3079, Université d'Orléans, 1D avenue de la recherche scientifique, , 45071 Orléans Cedex 2, France; M. MENETRIER, ICMCB, CNRS UPR9048, Université de Bordeaux, ENSCPB, 87 avenue du Dr A. Schweitzer, , 33608 Pessac Cedex, France; J.M. TARASCON, Chimie du Solide et de l'Energie, FRE 3677, Collège de France, 75231 Paris Cedex 05, France.

The development of renewable energies, inherently intermittent, as well as the development of electrical cars call for efficient energy storage. Electrochemical storage is performed with lithium-ion batteries or supercapacitors depending on application. A better understanding of the phenomena limiting the energy storage capacity and the rate at which it can be stored is essential to enhance the characteristics of those devices.

We combine NMR spectroscopy and imaging to study Li-ion batteries operando, i.e. while they are functioning. Classical spectroscopic imaging methods work well for the characterization of the components with a sharp spectrum, like electrolyte in supercapacitors<sup>[1]</sup>, electrolyte in batteries<sup>[2]</sup> or metallic lithium<sup>[3]</sup>. Conversely, the signal of the active material in the solid electrodes of batteries is in general not detected with standard spectroscopic imaging techniques. The transition metal centers in the electrodes are indeed paramagnetic in some stages of the charging-discharging process and result in very short lifetimes of the NMR signal. We recently developed S-ISIS, a way to retrieve this signal in a functioning 5-mm diameter Li-ion battery<sup>[4]</sup>. It was inspired by the ISIS localized spectroscopy concept<sup>[5]</sup> that takes advantage of the longer longitudinal relaxation time of those materials. We could reconstruct, for the first time, the full 1D <sup>7</sup>Li spectroscopic image of a battery, including the solid paramagnetic electrodes ( $\text{Li}_{1-x}\text{CoO}_2$ ,  $0 < x < 0.5$  and  $\text{Li}_{4+y}\text{Ti}_5\text{O}_{12}$ ,  $0 < y < 3$ ), with a resolution of 100  $\mu\text{m}$ . As a result the lithiation fronts formed in those 400- $\mu\text{m}$  thick electrodes can now be studied in situ for various (dis)charging conditions. We will discuss the constraints on spatial, temporal and spectral resolution in the framework of in situ or operando characterization of functioning batteries.



### References

- [1] A. J. Iltott, N. M. Trease, C. P. Grey, A. Jerschow, Nat. Commun. 2014, 5, DOI 10.1038/ncomms5536.
- [2] E. Salager, V. Sarou-Kanian, M. Sathiya, M. Tang, J.-B. Leriche, P. Melin, Z. Wang, H. Vezin, C. Bessada, M. Deschamps, et al., Chem. Mater. 2014, 26, 70097019.
- [3] R. Bhattacharyya, B. Key, H. Chen, A. S. Best, A. F. Hollenkamp, C. P. Grey, Nat. Mater. 2010, 9, 504510.
- [4] M. Tang, V. Sarou-Kanian, P. Melin, J.-B. Leriche, M. Ménétrier, J.-M. Tarascon, M. Deschamps, E. Salager, Nat. Commun. 2016, 7, 13284.
- [5] R. J. Ordidge, A. Connelly, J. A. B. Lohman, J. Magn. Reson. 1969 1986, 66, 283294.



***In Situ* MRI Investigation of Ion Transport in Graphite Anodes of Li-Ion Batteries**

S.A. Krachkovskiy<sup>\*</sup>, J.D. Bazak, C. Hewitt and G.R. Goward<sup>§</sup>, Department of Chemistry, McMaster University, Hamilton, Ontario, Canada; J.M. Foster, Department of Mathematics, University of Portsmouth, Portsmouth, UK; B.J. Balcom, Department of Physics, University of New Brunswick, New Brunswick, Canada.

Thicker electrode layers for lithium ion cells are presently getting increased attention from industry because they can provide higher energy density at lower production cost, due to a favourable electrode-to-current collector ratio per stack volume [1]. It appears, however, that the transport of lithium ions through such electrodes is becoming the limiting step during high-rate charging and discharging, leading to significant cell polarization and capacity reduction.

*In situ* MRI can be used for accurate characterization of mass transport in battery materials [2]. It is a non-invasive analytical method, which, in contrast to commonly used routines, such as NMR and electrochemical techniques, provides spatially resolved details about chemical and dynamic features of the investigated species. However, taking into account the low gyromagnetic ratio of <sup>7</sup>Li nuclei and the small transverse relaxation time of intercalated lithium in composite electrodes (typically < 100 μs), it is challenging to collect high-resolution images within a reasonably short experimental time [3].

We report herein implementation of the centric scan SPRITE MRI technique [4], which effectively overcomes the limitations stated above. This is a pure phase-encoding MRI method; therefore, it provides images free from distortions caused by magnetic field inhomogeneity and susceptibility variations between different battery components. One can use an extremely short phase encoding time (e.g. 30 μs) to avoid signal loss due to the fast relaxation, while collection of multiple FID points (10 in our case) significantly boosts the image intensity. As the result, high quality 1D MR images of the electrochemical cell under operational conditions with a resolution of 50 μm can be collected within an hour. By this approach, we can unambiguously monitor non-uniform lithiation of the graphite anode (350 μm thickness), and the rearrangement of Li ions within the electrode that follows, during the working cycle of the battery, providing an essential advance for the next level of battery performance characterization.

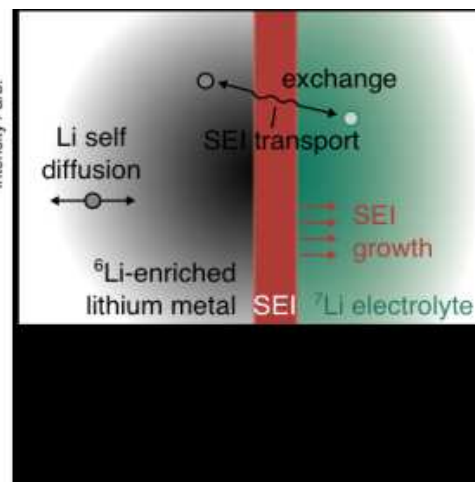
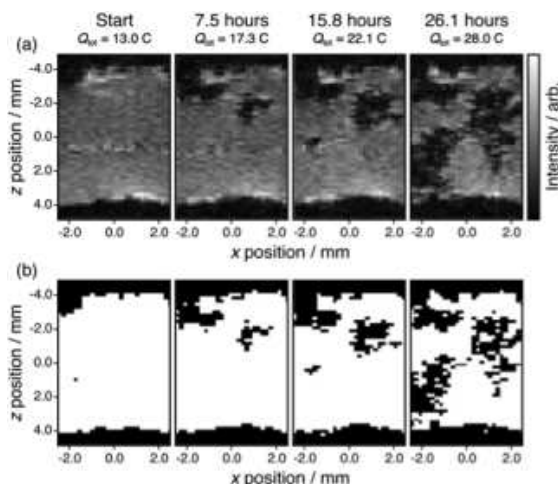
## References:

- 1.M. Singh, J. Kaiser and H. Hahn, J. Electrochem. Soc., 162 (7), A1196 (2015)
- 2.S. A. Krachkovskiy, J. D. Bazak, P. Werhun, B. J. Balcom, I. C. Halalay and G. R. Goward, J. Am. Chem. Soc., 138, 7992 (2016).
- 3.M. Tang, V. Sarou-Kanian, P. Melin, J. B. Leriche, M. Menetrier, J. M. Tarascon, M. Deschamps and E. Salager, Nat. Commun., 7, 13284 (2016).
- 4.M. Halse, D. J. Goodyear, B. MacMillan, P. Szomolanyi, D. Matheson and B. J. Balcom, J Magn Reson, 165, 219 (2003).

## Indirect MRI detection of critical electrochemical device parameters

A. Jerschow<sup>\*s</sup>, New York University.

We will describe our work on the development of techniques for assessment of Li-ion batteries and battery materials via magnetic resonance imaging (MRI). The goal of these studies is to analyze battery degradation and energy storage mechanisms in situ during charging or



discharging conditions by imaging changes in both the electrolyte and the electrodes in a noninvasive fashion. In situ NMR/MRI have proven to be a useful tool to probe the structure of Li-ion batteries during real-time charge and discharge. Ex situ studies of batteries are limited by self-relaxation of the electrode materials before a measurement can be obtained. The application of advanced magnetic resonance techniques, such as MRI and complex NMR experiments, in situ has the potential to monitor dynamics and visually monitor changes in functioning electrochemical systems in real time. The functionality of some energy storage devices where only the electrolyte is involved in the electrochemical process (such as supercapacitors) can only be studied in situ, as the electrolyte concentration gradients will relax as a potential is removed from the cell. Here we present techniques for in situ MRI of batteries and supercapacitors and discuss findings obtained from these studies [1,2]. It will be discussed how the rf field is perturbed by the presence of conducting materials in the probe [2], how susceptibility shifts can be used for assessing the morphology of microstructure buildup on electrodes [3]. The location and concentration of both cations and anions can be followed separately [4]. The figure shows sections through 3D images of Li metal obtained from an intact cell [5], at different times after initiation of charging. We will also discuss the opportunities for indirectly monitoring SEI layer properties. Further opportunities are provided by imaging both electrolyte and electrode at the same time in order to study Lithium dendrite growth models [6]. If there is time, recent results on MRI of commercial-type cells will be discussed.

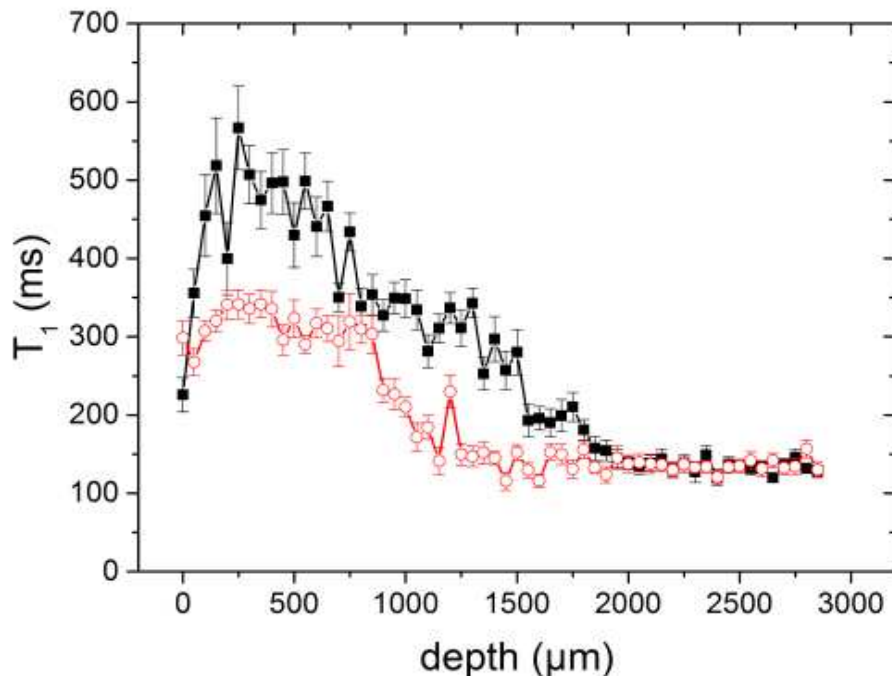
1. S. Chandrashekar, N. M. Trease, H. J. Chang, L.-S. Du, C. P. Grey, A. Jerschow, *Nat. Mater.*, 2012, 11, 311-315.
2. A. J. Ilott, S. Chandrashekar, A. Klöckner, H. J. Chang, N. M. Trease, C. P. Grey, L. Greengard, A. Jerschow, *J. Magn. Reson.* 2014, 245, 143149.
3. H. J. Chang, N. M. Trease, A. J. Ilott, D. Zeng, L.-S. Du, A. Jerschow, C. P. Grey, *J. Phys. Chem. C*, 2015, 119, 1644316451.
4. A. J. Ilott, N. M. Trease, C. P. Grey, A. Jerschow, *Nat. Comm.* 5, 2014, 4536.
5. A. J. Ilott, H.-J. Chang, C. P. Grey, A. Jerschow, Real time 3D imaging of microstructure growth in battery cells using indirect MRI, *Proc. Natl. Acad. Sci. USA*, 2016, 113, 10779-84.
6. H. J. Chang, A. J. Ilott, N. M. Trease, M. Mohammadi, A. Jerschow, C. P. Grey, *J. Am. Chem. Soc.* 2015, 137, 1520915216.

## Low-field NMR profiling and relaxation dispersion as new biomarkers for osteoarthritis in articular cartilage

OV Petrov, E Rossler, C Mattea and S. Stapf, TU Ilmenau, Dept. of Technical Physics II.

The dependence of the proton NMR relaxation times on field strength and on location within the tissue has been determined for a number of bovine and human articular cartilage samples. While the strong variation of  $T_2$  across the triple-layered cartilage structure as well as its orientation dependence are well known from clinical and laboratory high-field studies,  $T_1$  shows similar behavior only in low magnetic fields. At 0.27 T, the ratio of longest to shortest  $T_1$  has been found to cover a ratio of about 3-5 in healthy tissue, less in osteoarthritic tissue (see figure). At the same time, the average  $T_1$  was found to be strongly field dependent in the range down to 0.25 mT, but no spatially resolved data are available under these conditions.

Parameters obtained from a low-field and variable-field study are correlated with the severity of osteoarthritis and interpreted based on models of biomolecular mobility. Furthermore, by correlating the spatially resolved  $T_1$  distribution obtained at field strengths of 0.27 T with mathematical decompositions of the signal recovery function into multiexponential components, an attempt is made to quantify the width of  $P(T_1)$  for variable field strengths, and to identify the field value where this distribution is widest. This field is optimally situated for obtaining  $P(T_1)$  as a biomarker for laboratory studies or preclinical low-field investigations where spatial resolution is absent or insufficient to resolve the cartilage layer structure.



## Relaxation under pressure and elevated temperatures sorting out some stumbling stones on the way to compact NMR in process analytics

N.Nestle and S Arenz, BASF SE Materials Physics and Analytics RAA Ludwigshafen, D- 67056 Ludwigshafen, Germany; P Buhl, ZJ Lim, T Böhringer<sup>a,b</sup> and F Leinweber, <sup>a</sup>BASF SE Technical Equipment and Materials FTT/EP Ludwigshafen, D- 67056 Ludwigshafen, Germany; <sup>b</sup>Nanalysis Corp., Bay 4, 4500 5 Street NE Calgary, Alberta, Canada T2E 7C3.

With affordable, rugged magnets and an acceptable spatial footprint, compact NMR has the potential for industrial process control applications. A major challenge in online and inline analytics of processes in the chemical industry comes from harsh pressure and temperature conditions that are needed for many reactions. Bridging the gap between such process conditions and NMR equipment originally developed for desktop use is one of the main challenges on the way to successful use of compact NMR in process analytics.

Walking down this road, we have tested a range of design options for flow-through probe heads compatible with elevated temperatures. Design changes in the newest generation of compact NMR instruments available from Nanalysis have considerably extended the options for working at elevated temperatures and will be addresses as well.

Furthermore, we constructed a test setup for measurements at elevated pressures up to 300 bar in which we studied the effect of pressure on the spectra of selected solvents and a pressure-dependent chemical equilibrium known from literature [1]. In accordance with earlier findings, a notable pressure sensitivity for T1 was observed for most solvents in the pressure range under study while T2 was much less pressure-dependent. With the exception of water, elevated pressure lead to a shortening of the solvent T1 times which in connection with no notable effect on expected line widths can be expected to be rather helpful for possible online NMR analytics under pressure.

[1] Noble, W.J.L., 1960. The Keto-Enol Equilibrium of Ethyl Acetoacetate Under High Pressure. Journal of the American Chemical Society [online]. 82(19). S. 5253-5253.

**Quantitative  $T_1$  saturation - recovery measurements in inhomogeneous fields**

M. D. Hurlimann<sup>\*§</sup>, C. Duan<sup>a,b</sup>, S. Utsuzawa, Y. Q. Song and C. Ryan<sup>a,c</sup>, <sup>a</sup>Schlumberger - Doll Research, Cambridge MA 02139, USA; <sup>b</sup>Washington University, Saint Louis MO 63110, USA; <sup>c</sup>Rigetti Computing, Berkeley CA 94710, USA.

Saturation-recovery measurements with Carr-Purcell-Meiboom-Gill sequences are commonly employed to measure the longitudinal relaxation time constant,  $T_1$ , in grossly inhomogeneous fields. We show that off-resonant effects generates unexpected extra signals in the  $T_1$  measurement. In the present study, we derive a modified  $T_1$  kernel that accounts for this off-resonance effect quantitatively. The new kernel, based on analytical results, has been tested with numerical simulations and experiments, and excellent agreement is found. We also discuss the design of crusher pulses that mitigates this effect.

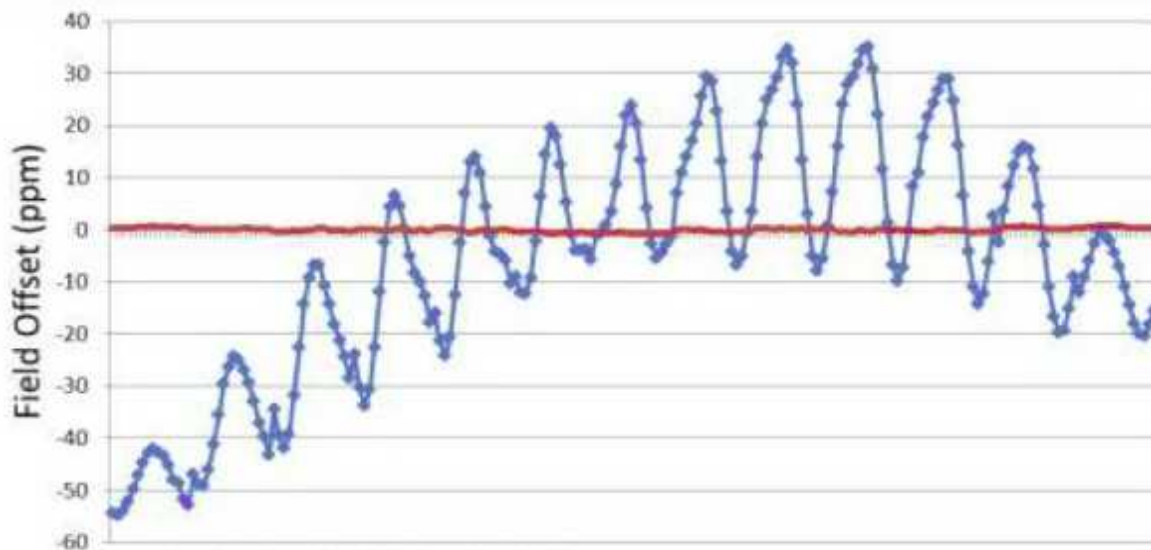
## Passive shims for small, high-resolution dipole magnets

[AF McDowell](#)<sup>§</sup>, NuevoMR, LLC, 617 Amherst NE, Albuquerque, NM 87106, USA.

Shimming small-scale magnets is a challenge because the materials and methods used to improve field quality add to the overall size, weight, and cost of the instrument. We have been developing new approaches to shimming small magnets so that a high degree of homogeneity can be achieved while requiring a minimum of space for the shimming apparatus. At the previous ICMRM, we presented our work on space-efficient *active* shim coils. Here, we discuss recent advances in *passive* shims.

Passive shimming of dipole magnets is usually accomplished through the use of small pieces of magnetic material, either permanent magnet or soft iron "buttons," that are placed at strategic positions on or near the pole pieces. Two problems present themselves when trying to passively shim small high-resolution magnets. The first is the achievement of high-resolution. Often, it is difficult to arrange a limited set of relatively large button sizes to achieve a homogeneity better than 10 ppm, which may be too much for the active shims to correct. The second challenge is the limited space in the gap of a small magnet for installing and holding the buttons.

We have developed a new approach to passive shimming to meet these challenges. Instead of using localized buttons, we use large, very flat, extended regions of passive shim material. To construct our shims, we use a simple additive process that allows us to build shims whose strength we can control in a continuous way. The passive shims occupy less than 0.5 mm, half of which is their support structure. Below is an example of the field measured at points on the surface of a 12 mm diameter sphere in a 20 mm gap 60 MHz magnet. The peak-peak span in the field is improved from 90 ppm to less than 2 ppm. We will discuss how these shims are designed and constructed.





## Towards quantification of SPIO-labelled cells with TurboSPI and bSSFP

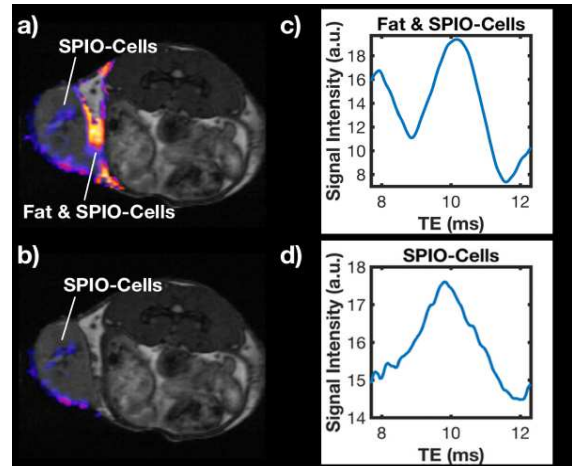
Z O'Brien-Moran<sup>\*</sup>, JA Rioux<sup>a,c</sup> and KD Brewer<sup>a,b,c</sup>, <sup>a</sup>Dalhousie University; ML Tremblay, CB Davis, <sup>b</sup>IWK Health Centre; <sup>c</sup>QEII Health Sciences Centre.

**Introduction:** Quantitative *in vivo* cell tracking offers the potential to increase our understanding of cellular dynamics. Common cell tracking sequences such as bSSFP are sensitive to the effects of superparamagnetic iron oxide (SPIO)<sup>1</sup>, but offer only semi-quantitative analysis. Additionally, bSSFP has limited specificity, with both labeled cells and necrotic tissue causing negative contrast. TurboSPI<sup>2,3</sup>, a multi-echo single point imaging (SPI) sequence, has been proposed recently for SPIO-cell quantification. TurboSPI is purely phase-encoded and has high temporal resolution for  $R_2^*$  mapping. The addition of compressed sensing allows for feasible *in vivo* imaging with sufficient spatial resolution. Unfortunately, initial *in vivo* studies revealed that the current  $R_2^*$  fitting techniques used could not reliably distinguish signal evolution of labeled cells from off-resonance oscillations, i.e. fat (see Figure), and elimination of voxels containing fat ("fat elimination") results in underestimating the number of labeled cells. This study therefore uses simulations and modeling techniques to better understand and account for the fat contribution.

**Methods:** *In vivo* data were obtained in a model of cervical cancer in C57BL/6 mice. Cytotoxic T cells (CTLs) were loaded with ultra small SPIO (~30 nm) and delivered via tail vein injection. All MR data were obtained on a 3T pre-clinical Agilent scanner. bSSFP was performed first for high-resolution anatomical images (TR/TE = 8/4 ms,  $\alpha = 30^\circ$ , 4 phase cycles, 4 averages, 256x170x170, FOV = 38.4mm x 25.5mm x 25.5mm, t = 64min). TurboSPI (TR/TE<sub>effective</sub> = 250/10 ms, ETL = 8, ESP = 10ms, 96x96x48, FOV = 30mm x 30mm x 30mm, t = 28min) was preceded by a fast spin echo (FSE) pre-scan with matched parameters (TE = TE<sub>effective</sub>, t < 2min) that was used to prescribe an under-sampling pattern and constrain the final reconstruction<sup>3</sup>. The TurboSPI signal was simulated using Monte Carlo methods and modeled in the slow diffusion regime<sup>4</sup>. First, the limits of the model were tested for various R (cell size) and  $\Delta\chi$  (change in susceptibility due to iron loading). The model was compared to the simulation for these parameters analyzed by root mean square error (RMSE). Next, an off-resonance fat signal (3.5 ppm) was added to the simulation and modeled for various fat-water ratios to compare with *in vitro* and *in vivo* data.

**Results:** *In vivo*:  $R_2^*$  maps (Figures a and b) show complimentary cell-tracking information from bSSFP (negative contrast in tumor) and TurboSPI (high  $R_2^*$  in tumor), though the maps show errors in fitting voxels with signal time courses like that in Figure c). *In silico*: The model-simulation agreement was first analyzed without fat. The RMSE improved drastically with particle size up to ~2 $\mu$ m after which the rate of improvement began to slow, while changes were more subtle as a function of  $\Delta\chi$ . Thus, the limits of the model were found, indicating the feasible region (combinations of R and  $\Delta\chi$ ) to explore fat contributions *in silico*. Adding fat to the simulated data gives signal time courses that replicate acquired MR data in voxels such as Figure c).

**Conclusions/Future Work:** While TurboSPI gives more information than bSSFP and offers advanced quantitation by  $R_2^*$  mapping, residual fat contributions result in quantification inaccuracies. Two correction approaches will be studied: adding fat to the analytic model, and an n-point Dixon fat subtraction. Understanding the signal through simulation and more robust modeling should improve accuracy in  $R_2^*$  mapping and therefore cellular quantification.



**References:** 1. Majumdar S et al. Mag Res in Med, 1989; 2. Rioux JA et al. J of Mag Res 2012; 3. Rioux JA et al. MAGMA 2017 30(1):41-55; 4. Rioux JA et al. Proc. ISMRM 20, p. 1712, 2012

**Figure:** Left- bSSFP MRI with  $R_2^*$  map of the ROI (tumor and surrounding tissue) overlaid with a) no fat corrections and b) simple "fat elimination". Right: Signal time course from voxels at c) inner tumor edge and d) tumor center. Both techniques recognize d) as labeled cells while c) suggests a combination of cells and fat. The fat elimination (b) simply ignores voxels like those in c), however the uncorrected technique (a) fits this as "only cells".

## Measuring atrophy in the experimental autoimmune encephalomyelitis mouse model of multiple sclerosis: a 9.4T MRI atlas-based regional brain volumetric study.

Nils D. Forkert<sup>a,b</sup>, James A. Rogers<sup>a,c</sup> and V. Wee Yong<sup>a,c</sup>, <sup>a</sup>Hotchkiss Brain Institute, University of Calgary, Calgary, AB, Canada; <sup>b</sup>Department of Radiology, University of Calgary, Calgary AB, Canada; <sup>c</sup>Department of Clinical Neurosciences, University of Calgary, Calgary, AB, Canada; Jeff. F. Dunn<sup>s</sup>, Experimental Imaging Center, University of Calgary, Calgary, AB, Canada.

**Purpose:** Grey matter (GM) atrophy plays an important role in multiple sclerosis (MS) and has become a clinically relevant marker of degeneration. There is a need for animal models that feature both neuroinflammation and atrophy. One potential model is experimental autoimmune encephalomyelitis (EAE), which is commonly used to study neuroinflammation. We used high-resolution magnetic resonance imaging (MRI), a Bruker cryoprobe, and atlas-based regional brain volumetrics to determine the extent of atrophy in the brains of EAE mice at long-term disease.

**Methods:** Female C57BL/6 mice were induced with EAE. Disease severity was assessed using a 15 point scoring system. Mice were imaged at 66 days post induction (n= 27 EAE, 8 Naïve, 13 CFA (receive immune stimulant but no self targeting myelin antibodies)). Imaging was done using a 9.4T MRI with a helium cooled Bruker cryoprobe using a FLASH sequence (TR/TE/=2000ms/6.5ms/60° voxel=37.5 x 37.5 x 250m<sup>3</sup>) (**Figure 1A**). The N3 algorithm was used to correct for signal drop-off from using a surface coil. Niftyreg was used to register an average brain atlas with 62 segmented brain regions to each dataset to calculate regional volumes (**Figure 1B**). Statistics were performed using an ANCOVA test with body weight as a covariate. Multiple comparisons were controlled used the False Discovery Rate.

**Results:** We obtained a nominal resolution of 37.5 x 37.5 x 250m<sup>3</sup> in 38 minutes in vivo. Cumulative long-term disease scores were averaged and EAE mice were divided into two groups based on whether their scores were above (high score) or below average (low score) (n=13 high score EAE, n=14 low score EAE). After correcting for weight, high score mice displayed smaller volumes for 19 out of the 62 measured structures compared to Naïve, CFA, and low score EAE mice. Atrophied structures include both GM and WM regions such as cerebral cortex (**Figure 2A**), corpus callosum (**Figure 2B**), cerebellum, hippocampus, thalamus, and striatum.

**Discussion/Conclusions:** EAE mice exhibit significant reductions in brain volume in the long-term phase of the disease. The atrophic structures bear similarity to those that feature atrophy in MS. This suggests that the EAE model may be a good model to study the mechanism behind atrophy. The EAE mouse model, with this imaging protocol, has the potential to be a model for studying atrophy and for testing future neuroprotective therapeutic treatments.

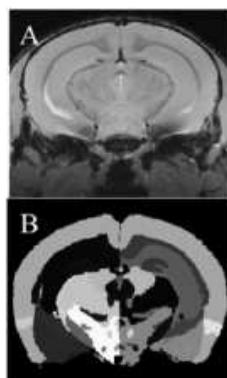


**Figure 1.** Atlas-based regional morphometrics. A) Gradient echo MRI image of an EAE mouse brain 66 days post induction. The N3 algorithm was used to correct for signal drop-off from using a surface coil. B) EAE mouse brain segmented into the 62 measured structures.

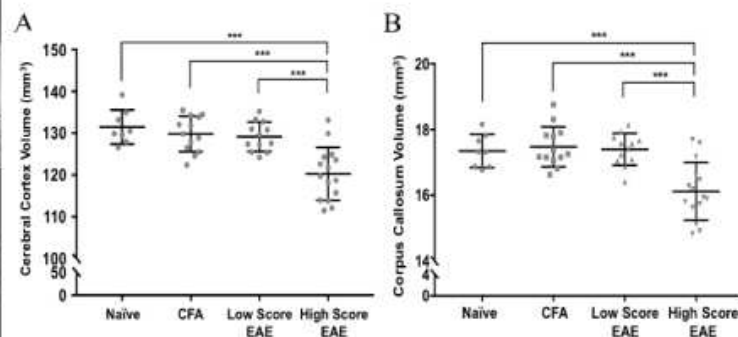


**Figure 2.** Regional volume. A) cerebral cortex, B) corpus callosum. EAE were grouped as below average (Low Score EAE n=12) and above average (High Score EAE n=15) disease scores. Animals imaged at 66 days post disease induction. Middle bar represents group mean with error bars representing +/- standard deviation. p < 0.05\*; <0.01\*\*, <0.001\*\*\*

## Optimization of ultrahigh field $\mu$ MRI methods to monitor brain disorders in Zebrafish model of depression.

Upasana Roy<sup>a,b</sup>, A. Alia<sup>b,c</sup> and Jörg Matysik<sup>§</sup>, <sup>a</sup>Universität Leipzig, Institut für Analytische Chemie, Linnéstr. 3, D-04103 Leipzig, Germany; <sup>b</sup>Universität Leipzig, Institut für Medizinische Physik und Biophysik, Härtelstr. 16, D-04107 Leipzig, Germany; Marcel Schaaf<sup>\*</sup>, <sup>c</sup>Institute of Biology Leiden, University of Leiden, Sylviusweg 72, 2333 BE Leiden, The Netherlands.

### Introduction

In this study, we have optimized and applied high resolution micro-MRI methods to investigate whether glucocorticoid induced depression can cause any specific structural changes in the brain. On our quest, we have used adult zebrafish as model organism (1). Zebrafish model is increasingly used for understanding brain diseases including neurodegenerative disorders. However due to small size of the brain, non-invasive imaging methods with zebrafish are challenging. In our case, we have been able to characterize the anatomical details of the adult zebrafish brain and found changes which could be attributed to the depression.

### Subjects and Methods

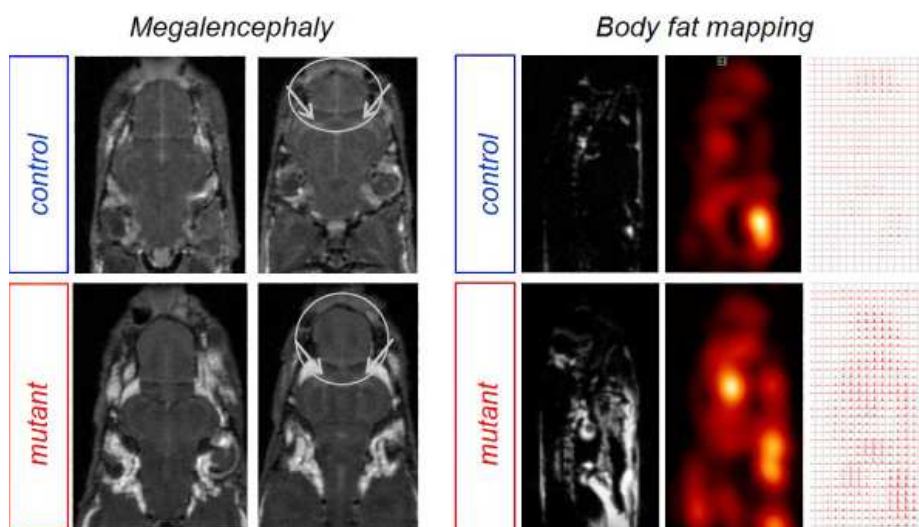
MRI measurements were performed at 9.4 T vertical bore system, using a birdcage radiofrequency coil [diameter 10 mm] and a  $1 \text{ Tm}^{-1}$  gradient insert (2).  $T_2$ -weighted MR images were acquired by RARE sequence [echo time (TE) = 10.567 ms (22.45 ms effective), repetition time (TR) = 5s, averages = 64, echo train length = 4, FOV =  $1.2^2 \text{ cm}^2$ , matrix =  $256^2$ , resolution  $47 \mu\text{m}$ ]. For  $T_2$  relaxation measurement, MSME sequence was used. The whole-body fat mapping was done using CHES sequence [TR=1s, TE=3.4 ms, FOV= $2^2 \text{ cm}^2$  and matrix =  $128^2$ ].  $^1\text{H}$  chemical shift imaging (CSI) was performed at 7.0 T magnet with TE=15 ms, TR=1.5 s and NS=256.

### Results and discussion

Optimized RARE sequence provided sufficient resolution to identify specific markers in both sagittal and coronal direction from adult zebrafish brains. Some structural differences were seen in the two groups. CSI and CHES measurements map fat in the control and GR mutant fish. Signals between 0.80 to 1.25 ppm were chosen to map fat signals. Furthermore, this study demonstrates that micro-MRI is an efficient tool to successfully visualize human diseases in zebrafish models.

### References

(1) Ziv L *et al.* (2013) *Mol Psychiatry* 18: 681. (2) Kabli *et al.* (2010) *Zebrafish* 7: 143.



### Measurement of transverse relaxation properties of whole blood at low magnetic fields

Y. C. Tzeng, Wellington Medical Technology Group, Centre for Translational Physiology, University of Otago Wellington, New Zealand; D. G. Thomas and P. Galvosas<sup>a,b</sup>, <sup>a</sup>Victoria University of Wellington, SCPS, New Zealand; <sup>b</sup>MacDiarmid Institute for Advanced Materials and Nanotechnology, New Zealand; S. Obruchkov, Robinson Research Institute, Victoria University of Wellington, New Zealand; P.D. Teal, Victoria University of Wellington, ECS, Wellington, New Zealand.

**Purpose:** We set out to determine whether changes in physiologically important blood parameters can be derived from transverse relaxation  $T_2$  measurements at low fields.

The relationship between the oxygenation of blood, and the transverse relaxation rate of water protons has been previously investigated by many researchers e.g. Thulborn and Ogawa [1,2]. This blood oxygen level dependent (BOLD) effect is caused by the susceptibility change of oxy/deoxy-hemoglobin, creating magnetic field inhomogeneities, which affect the relaxation of water protons diffusing through those regions. Because the oxy/deoxy-hemoglobin fraction is directly linked to the partial pressure of oxygen (pO<sub>2</sub>) in blood, the relaxation rate of blood, which increases quadratically with the deoxyhemoglobin fraction [1,3], can be used as an indirect proxy of blood and therefore tissue oxygenation.

This relaxation effect has been well characterised at fields greater than 1.5 T, mainly due to its importance in clinical studies (e.g. fMRI). It is known that the size of the relaxation change is proportional to  $B^2$ , and that the observed relaxation rate follows a similar dependency on CPMG echo time to chemical exchange type systems (Luz-Meiboom equation)[1,4-7]. However, at lower fields there have only been a handful of experimental studies of this effect, and they have been limited to measurements at extreme levels of oxygenation/ deoxygenation [6,7].

In this study, we investigated this oxygenation dependent relaxation of blood at fields ranging from 0.05 to 1.5 T using a variable field magnet system. Whole human blood was continuously pumped through a circuit containing an oxygenation membrane, which provided dynamic control of the oxygenation and other physiologically important parameters before it travelled into the magnet. This allowed us to measure small variations in the blood oxygenation, rather than the two point studies which have been done previously. Additionally, we characterised the effect of different CPMG echo times on the observed relaxation rate, and have compared the results to models which have been developed and tested at higher magnetic fields.

- [1] K. R. Thulborn et al. *Biochim. Biophys. Acta***714** 265270 (1982)
- [2] S. Ogawa et al. *PNAS***87** 98689872 (1990)
- [3] W. M. Spees et al. *Magn. Reson. Med.***45** 533542 (2001)
- [4] B. Stefanovic and G. B. Pike, *Magn. Reson. Med.***52** 716723 (2004)
- [5] K. Grgac et al. *Magnetic Resonance Imaging***38** 234249 (2017)
- [6] J. M. Gomori et al., *J. Comp. Asstd. Tomog.* **11** 684 (1987)
- [7] R. A. Brooks et al., *J. Magn. Reson. Imaging***5** 446450 (1995)

## Short-time magnetization preparation for MRI of sprays

Igor Mastikhin<sup>\*§</sup> and Shahla Ahmadi, MRI Centre, University of New Brunswick, Fredericton, NB Canada; Kyle Bade, Spraying Systems Co., , Spray Analysis and Research Services, , Wheaton, IL USA.

The process of spray atomization, i.e., the transformation of a continuous liquid jet into  $\mu\text{m}$ -sub-mm sized droplets, is ubiquitous in industry. Its efficiency determines how well the liquid is mixed with air (direct injection engines) or spread over a surface (painting, agriculture). At the same time, the process is quite complex to analyze theoretically and study experimentally.

One of the main strengths of MRI is its ability to sensitize spatially-resolved NMR signal to a wide variety of physical and chemical parameters. The sensitization is commonly done at the preparation stage via a specific combination of RF pulses, magnetic field gradients and delays, with a subsequent readout imaging sequence. The separation of the preparation and readout permits a quantitative analysis of contributions of each part into the signal.

However, standard preparation schemes are difficult to employ for studies of sprays due to their fast speeds ( $> 10\text{-}20$  m/s). All steps of the pulse sequence (excitation, preparation, spatial encoding, and readout) must be executed while a significant portion of the sample remains within the sensitivity region of the RF probe. In addition, sprays are usually low-density systems, leading to a poor SNR and a need for massive signal averaging and long acquisition time.

In this paper, we reduced the interval between the preparation and the readout stages down to 0.1 ms by performing SPI encoding on the rising gradients. This also enabled the use of 90-degree flip angles to maximize the signal. For an RF coil length  $L$ , spray speed  $V$ , and sequence repetition times  $TR > L/V$ , the magnetization of the water spray remains unsaturated while the one associated with the stationary water on the setup walls is heavily saturated and thus does not contribute significantly to the acquired image. Finally, the use of gradients during preparation stage was eliminated due to their time-consuming rise and stabilization times. This limited possible preparation schemes to a combination of RF pulses and delays.

The two preparation schemes presented here are Time-of-Flight (TOF) and T1-weighting schemes. The total duration of the sequence (without TR) was 0.24–1.1 ms for the TOF and 0.41 ms for T1. In series of images obtained with the TOF scheme (9 TOF delays), the displacement of the liquid parcel is clearly noticeable; the data can be utilized to measure the spray speeds. The T1 prepared images of the near-atomization region (11 spin-locking frequencies, 0–15 kHz) showed a strong signal attenuation at higher frequencies. This can be explained as a presence of high-frequency vibrations of the liquid sheet in the atomization region.

**Quantitative assessment of mesoscale network structure in  $\kappa$ -carrageenan gels by means of magnetic resonance nanoprobe diffusometry**

J. van Duynhoven<sup>a,b,d</sup> and L Zuidgeest<sup>a,b,d</sup>, <sup>a</sup>Unilever R&D Vlaardingen, Vlaardingen, The Netherlands; H Van As<sup>b,d</sup>, D de Kort<sup>b,d</sup>, J Hohlbein, <sup>b</sup>Laboratory of Biophysics, Wageningen University and Research, Wageningen, The Netherlands; S Han and M Emondts, University of California, Santa Barbara, USA; N Loren<sup>c,d</sup> and E Schuster, <sup>c</sup>Chalmers University, Gotenborg, Sweden; H Janssen, SyMOChem BV, Eindhoven, The Netherlands; <sup>d</sup>TI-COAST, The Netherlands.

Many food systems comprise percolating and tortuous biopolymer networks that are notoriously difficult to describe quantitatively at the sub- $\mu$ m scale. Analysing the self-diffusion behaviour of nanoparticles in these networks, we obtained sub- $\mu$ m structural information that complements microscopic information. For this purpose, we designed and synthesized a suite of spherical nanoparticles with defined diameters in the 3-30 nm range. The designs of these particles were either based on dendrimers or complex coacervate core micelles (C3M). The particles were passivated by PEGylation and functionalized with spectroscopic labels (<sup>19</sup>F, TEMPO) to observe their mobility by <sup>1</sup>H and <sup>19</sup>F Pulsed Field Gradient NMR, and Overhauser Dynamic Nuclear Polarization (ODNP). For demonstrating our nanoprobe diffusometry approach we used  $\kappa$ -carrageenan gels prepared with different Na<sup>+</sup>/K<sup>+</sup> salt strengths as model systems. By using Johnson's model for particle diffusion in fibrous networks, we determined the average network mesh sizes and obtained evidence for the presence of salt strength dependent sub- $\mu$ m network heterogeneity. Optical ensemble (FRAP, FCS, RICS) and single-particle tracking (TIRF microscopy) diffusometric techniques, applied to fluorophore-labelled nanoparticles, validated the gel network structural descriptors derived from NMR nanoprobe diffusometry.



## The Application of Diffusion Tensor Imaging to a Turbulent Gas Flow System

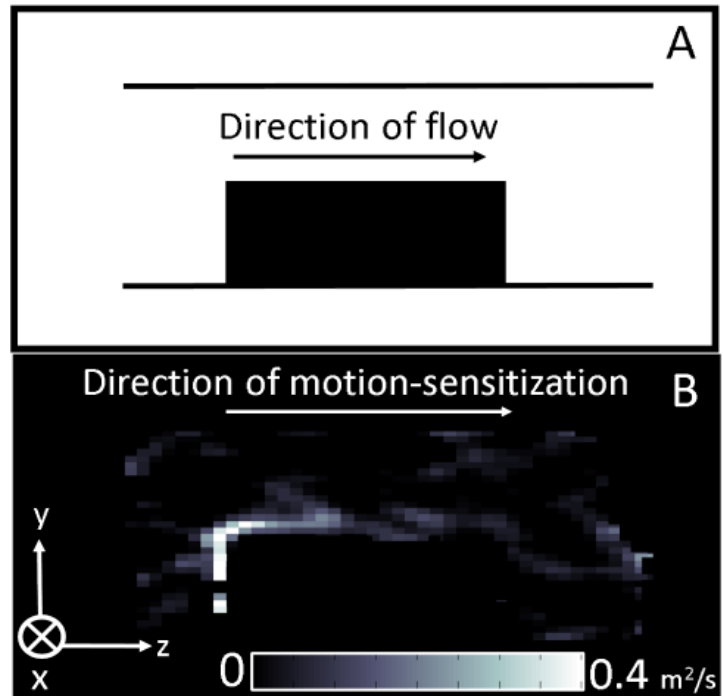
A. Gauthier and B. Newling\*, University of New Brunswick, Fredericton, Canada.

Diffusion tensor imaging (DTI) [1] is a technique used in medical imaging to determine the principal axis along which a fluid is diffusing. This information can then be used to trace fibres in the brain or muscle. Applying this technique to a turbulent gas flow system offers a new perspective on the behaviour of turbulence, which can be described by fluctuations in the velocity field of the fluid [2]. Characterization of turbulence is important for understanding energy loss in systems such as wind turbines, aeroplanes, and pipe flows, as well as for informing numerical solutions to the Navier-Stokes equations. In relatively simple flow systems such as the one used in this experiment, turbulence is often assumed to be isotropic, however use of MRI shows that it is not.

In this experiment, sulfur hexafluoride gas is rapidly flowed ( $\sim 20$  m/s) through a pipe with a hemicylindrical obstruction. The bulk flow is oriented along the z-axis. Turbulence in this system is quantified using the eddy self diffusivity tensor. Eddy self diffusivity describes the fluctuations in the velocity field of the gas, and manifests in an MRI measurement as an attenuation in signal amplitude due to the presence of motion-sensitization. Thus, six separate measurements each with motion-sensitization on a different axis, plus one measurement without motion-sensitization are needed to calculate the full eddy self diffusivity tensor. The SPRITE pulse sequence was used for these measurements [3]. Preliminary results show non-zero eddy self diffusivity only in the x-, y- and z-directions, which suggests that these are the principle axes along which the velocity field is fluctuating. Significant peaks in eddy self diffusivity are observed in each case located in different places in the sample space, which demonstrates that the assumption of isotropic turbulence is not valid for this flow geometry.

### References:

- [1] Bassler, P.J., Özarslan, E., "Anisotropic Diffusion: From the Apparent Diffusion Coefficient to the Apparent Diffusion Tensor", Diffusion MRI: Theory, Methods, and Applications, D. K. Jones, Oxford University Press, 2011
- [2] Ecke, R., "The Turbulence Problem: An Experimentalist's Perspective", Los Alamos Science, 29, 124-141, 2005
- [3] Newling, B., Poirier, C. C., Zhi, Y., Rioux, J. A., Coristine A. J., Roach, D., Balcom, B. J., "Velocity Imaging of Highly Turbulent Gas Flow", Physical Review Letters, 93(15), 2004



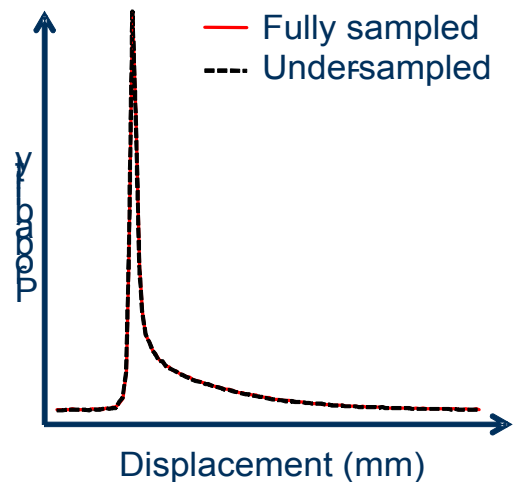
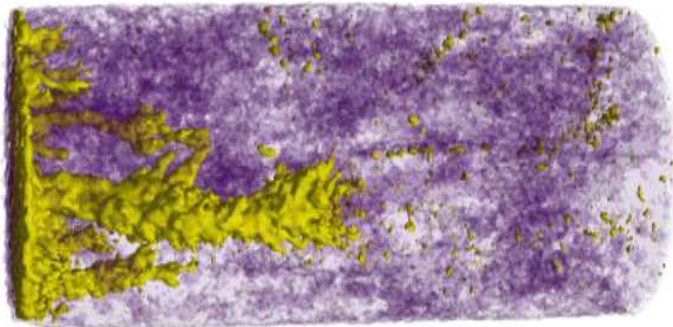
(A) Schematic of the central slice of the cylindrical pipe used in this experiment. The height of the obstruction is half of the diameter of the pipe. (B) The central slice of the map of the zz-component of the eddy self diffusivity tensor

**Monitoring carbonate dissolution using spatially resolved under-sampled propagators and MRI**

A.J. Sederman, A.A. Colbourne, M.D. Mantle and L.F. Gladden, Magnetic Resonance Research Centre, Dept. of Chemical Engineering and Biotechnology, University of Cambridge, Cambridge, CB3 0HE, UK.

The dissolution of a porous rock matrix by an acidic flow causes a change in the pore structure and consequently the pattern of fluid flow and rock permeability. This process is relevant to many areas of practical relevance such as enhanced oil recovery, water contaminant migration and sequestration of supercritical CO<sub>2</sub>. The most important governing factors for the type of change in the pore space are related by the Péclet (Pe) and Damköhler (Da) dimensionless numbers; these compare the transport properties of the fluid in the porous medium with the reactive properties of the solid matrix and the incident fluid respectively. Variation in Pe and Da can cause very different evolution regimes of the pore space and flow can occur, ranging from a uniform dissolution through different "wormholing" regimes (shown on the left hand side of figure 1) to face dissolution.

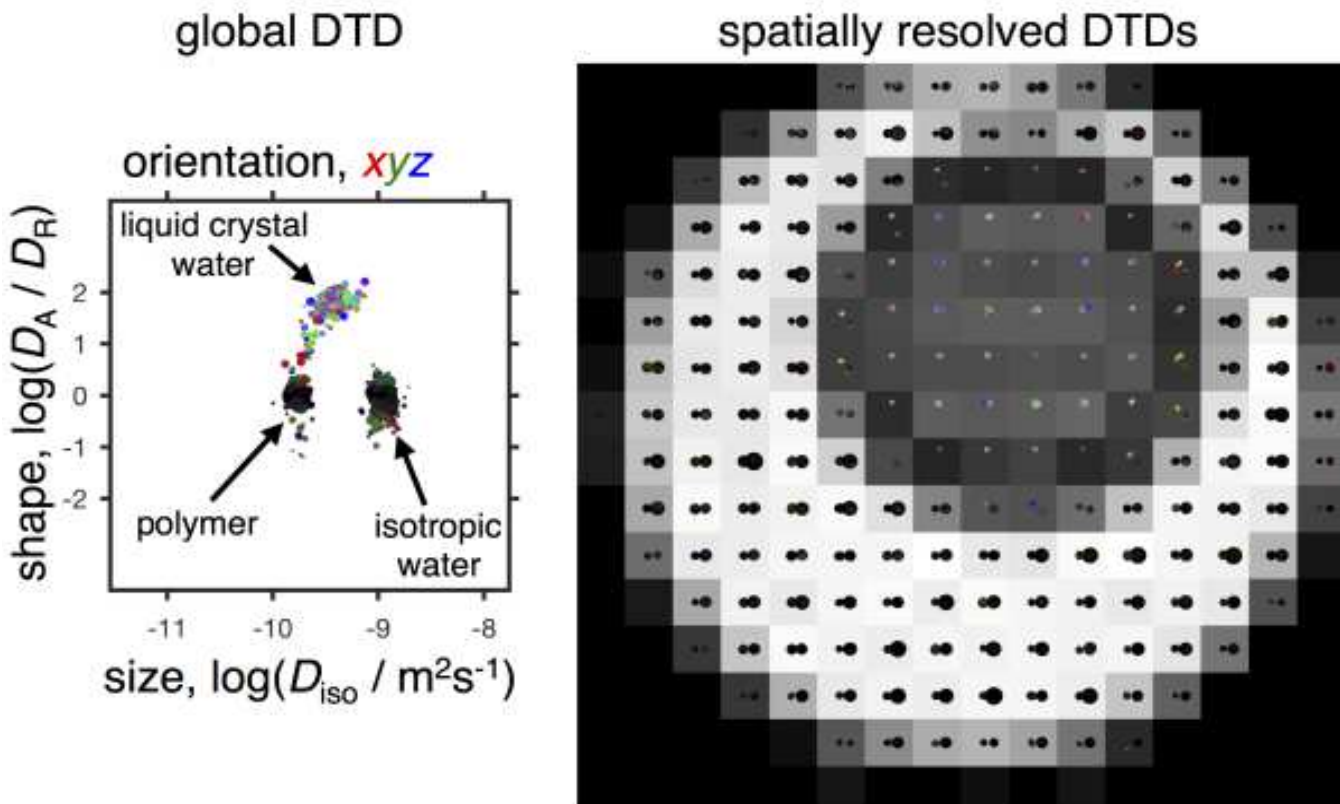
Here, NMR spatially resolved propagators have been used to monitor the evolution of fluid flow during a reactive dissolution rock core flood. A method of under-sampling the q-space data has been developed in order to measure the propagators at sufficient displacement resolution and in a timescale that is short enough to capture the changes in structure and flow. The highly under-sampled (4%) q-space data, which typically reduces the acquisition time from 2 hours to 6 minutes, has been shown to produce equivalent propagator results to the fully sampled experiment (as illustrated in the graph on the right hand side of figure 1). Combining these propagator measurements with quantitative and fast imaging techniques as well as relaxation measurements, a full time-resolved picture of the dissolution reaction is built up. Experiments have been done on for both Ketton and Estailades carbonate rock cores. These rocks possess different pore space topologies which result in very different dissolution behaviours.



## Diffusion tensor distribution imaging

D. Topgaard<sup>\*</sup>, Department of Chemistry, Lund University, Lund, Sweden.

Diffusion tensor imaging (DTI) gives voxel-averaged information about biological tissue properties such as cell density, shape, and orientation. While the conventional DTI parameters sensitively report on changes in any of these properties, they rarely give unambiguous information about which one of them has changed - in particular for heterogeneous voxels containing multiple tissue types. To mitigate this problem, we here introduce a method for quantifying the microstructure of a heterogeneous voxel as a diffusion tensor *distribution* (DTD) that we estimate without any priors or constraints on the number of components or their individual properties. A microscopic diffusion tensor is parameterized with its isotropic average ("size")  $D_{iso}$ , ratio between axial and radial diffusivities ("shape")  $D_A/D_R$ , and orientation - parameters that are given by the local cell density, shape, and orientation. Key for disentangling the information about tensor size, shape, and orientation is to *correlate isotropic and directional diffusion encoding* [Topgaard, J. Magn. Reson. 275, 98 (2017)]. Experiments were performed on a composite phantom constructed from a 5 mm glass tube with a reverse hexagonal liquid crystal inside a 10 mm glass tube with an aqueous polymer solution. Data was acquired on a Bruker 11.7 T microimaging system with single-shot RARE read-out at  $0.6 \times 0.6 \text{ mm}^2$  in-plane spatial resolution,  $16 \times 16$  matrix size, 1 mm slice thickness, and combinations of isotropic and directional diffusion encoding generated by smoothly modulated gradients waveforms. After standard image reconstruction, the DTDs were estimated for each voxel by numerical inversion of the signal data using in-house Matlab code. The experimental results in the figure verifies that our new approach yields data with sufficient information for *unconstrained inversion* into DTDs, which is in stark contrast to all other diffusion MRI methods available today. In neuroimaging, voxel-by-voxel estimation of DTDs will permit mapping of nerve fiber orientation distributions, axial and radial diffusivities of distinct fiber populations, as well as fractions of cerebrospinal fluid, using only a minimum of modeling assumptions.



## Investigation of continuum mechanics models of granular flow by MRI

LA Fullard and C Davies, Massey University, Palmerston North, New Zealand; P Galvosas, Victoria University of Wellington, Wellington, New Zealand; [D.J.Holland](#), University of Canterbury, Christchurch, New Zealand.

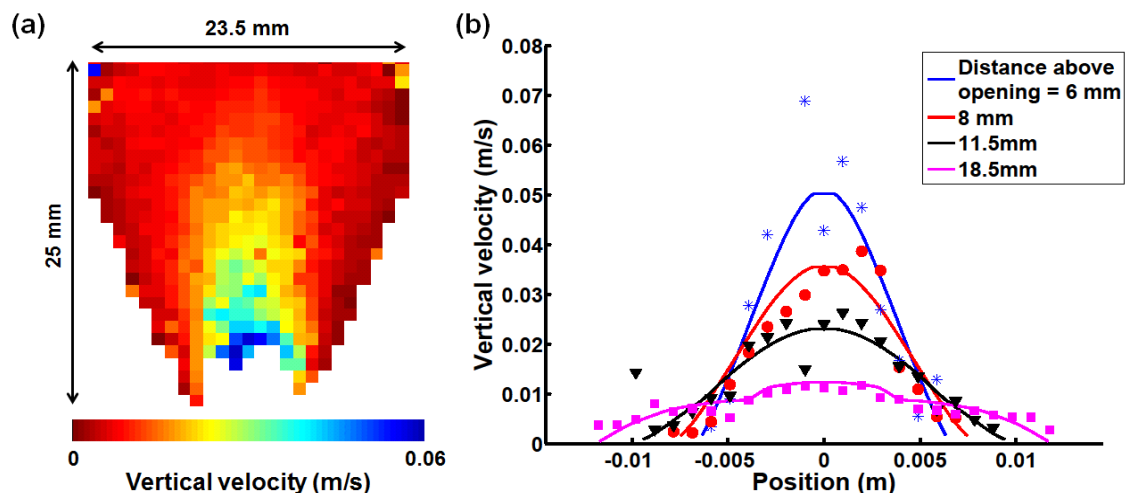
Here we develop an apparatus to permit quantification of the continuum dynamics of a granular flow in three-dimensional (3D) hoppers using MRI. It is desirable to be able to describe granular materials using continuum mechanics, as direct modelling of every individual particle is intractable for realistic flows. However, the shear rate and density dependence of the rheology makes the application of conventional continuum models challenging. The so called " $\mu(I)$ " granular friction law model has been proposed to provide a continuum description of granular flow [1]. Using this law, friction is characterised by three measurable parameters:  $\mu_s$ , the friction for a static bed of grains,  $\mu_1$ , the maximum possible friction in the dense regime, and  $I_0$ , a shape parameter. The  $\mu(I)$  model has shown promise for characterising inclined plane experiments [1], the granular column collapse [2], and others [3]. However, quantitative experimental validation of the model has largely been confined to observations at the wall of quasi-two-dimensional granular flows. MRI permits quantification inside 3D granular flows, providing unique validation data for these numerical models.

Here we study flow in hoppers manufactured using 3D printing to enable easy modification of the geometry of the hopper. The wall friction was increased by fixing particles to the walls of the hopper, or reduced by washing the surface of the hopper with acetone to produce a smooth surface. The seeds flow down from a large reservoir at the top of the magnet, through the hopper and into a bottom reservoir for collection. This arrangement enabled measurements to be taken continuously over a period of several hours by periodically re-filling the upper hopper. Here poppy seeds (diameter  $d_p = 0.5$  mm) were used as they provide a strong signal for MRI. MRI measurements of the velocity in both vertical and horizontal planes were obtained for different hopper configurations using phase contrast velocity imaging. Example data for the velocity in the vertical plane along the centreline of an as-printed hopper (i.e. with no wall friction modification) are shown in (a). The measurements were compared with numerical predictions obtained using the  $\mu(I)$  granular friction law in (b). The model quantitatively recovered the velocity distribution measured by MRI, including the onset of fast flow observed 18 mm above the opening.

[1] P. Jop, Y. Forterre, and O. Pouliquen, *Nature*, vol. 441, no. 7094, pp. 727-730, 2006.

[2] P.-Y. Lagr e, L. Staron, and S. Popinet, *J. Fluid Mech.* vol. 686, pp. 378-408, 2011.

[3] M. Tankeo, P. Richard, and  . Canot, *Granul. Matter*, vol. 15, no. 6, pp. 881-891, 2013.



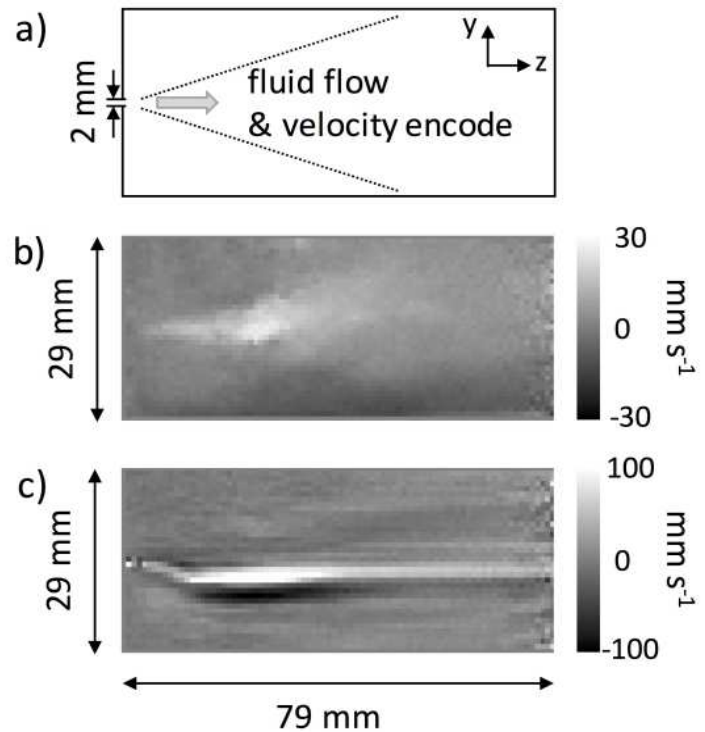
## Jet dynamics in supercritical fluid flow

H.T. Fabich\*, M.S. Conradi, S.A. Altobelli, D.O. Kuethe and E. Fukushima<sup>§</sup>, ABQMR, Inc., Albuquerque, NM, USA.

Jet flow, or fluid flow through a small orifice into a larger vessel, is relevant from hot tubs to diesel injectors. For diesel injectors, high temperatures and pressures are employed meaning the fluids may be supercritical, substantially changing the flow and mixing properties.

The critical point of a fluid is defined by the pressure and temperature ( $P_c$ ,  $T_c$ ) where a liquid and its vapor become indistinguishable. Supercritical fluids, with  $P > P_c$  and  $T > T_c$  are known to have a gas-like viscosity, liquid-like density, and no surface tension.

Preliminary 2D velocity encoded images for jet flow of hexafluoroethane ( $C_2F_6$ ),  $P_c = 3.05$  MPa,  $T_c = 19.9^\circ\text{C}$ , will be presented as depicted in Figure 1a. Figure 1b is a map of longitudinal velocity at 2.07 MPa, subcritical, and Figure 1c at 3.05 MPa, critical. Pressure is measured at the recirculating pump inlet while the temperature was controlled to  $20 \pm 2^\circ\text{C}$ , close to  $T_c$ . For a constant mass flow, the jet velocities are  $400 \text{ mm s}^{-1}$  ( $Re = 8000$ ) and  $130 \text{ mm s}^{-1}$  ( $Re = 4000$ ) for Figure 1b and 1c, respectively, due to a fluid expansion ratio of approximately 3 between the two pressures. The jet in Figure 1b, below the critical point, dissipates more quickly. Even at a lower jet velocity, near the critical point, higher velocities are measured in the vessel as the moving fluid retains a relatively narrow profile throughout the imaging region, as shown in Figure 1c. In addition, Figure 1c shows the jet falling in the gravitational field indicating a density variation between the flowing and non-flowing fluid. These measurements are a start toward better understanding supercritical jet flow and fluid mixing.





## Magnetic resonance angiography at 17.6T resolves blood flow defects and dynamics in AD mouse brain *in vivo*

A. Alia<sup>\*a,b</sup>, <sup>a</sup>Institute of Medical Physics and Biophysics, , University of Leipzig, Leipzig, Germany; F Kara and HJM de Groot, <sup>b</sup>Leiden Institute of Chemistry, , Leiden University, Leiden, Netherlands; S Roßner, Department of Neurochemistry, University of Leipzig, Germany; J Matysik, Institute of Analytical Chemistry, University of Leipzig, Leipzig, Germany.

Magnetic resonance angiography (MRA) provide 3D images of blood vessels *in vivo* and has shown great potential to study blood flow abnormalities non-invasively in many neurodegenerative diseases including Alzheimer's disease (AD). However implication of MRA in small animal models is limited due to sensitivity issues. In AD, the deposition of amyloid peptide in the cerebral vessel walls, known as cerebral amyloid angiopathy is frequently observed, leading to blood flow abnormalities. Visualization of the changes in blood vessel structure is important for early diagnosis and treatment of AD. In this study we optimized high resolution MRA at ultra-high magnetic field (17.6T) to longitudinally monitor changes in brain arteries in living AD mice. To find the optimum combination of parameters for TOF MRA at 17.6 T, radiofrequency pulse repetition time (TR) and pulse flip angle (FA) were steadily varied. Large vessels with relatively high blood flow has excellent visibility at all combination of FA (20°- 50°) and TR (15 - 40ms). However small vessels such as azPA are better delineated at smaller FA (20°). Visual and quantitative analysis of MRA results revealed severe blood flow defects in large and medium sized blood vessels in AD mice brain (Fig. 1). Histological data show that A $\beta$  levels in the vessel wall may be responsible for impaired blood flow, thereby contributing to the early progression of AD. MRA studies at 17.6T provide a powerful non-invasive tool to test the effectiveness of putative disease-modifying therapeutic intervention in Alzheimer's mouse brain.

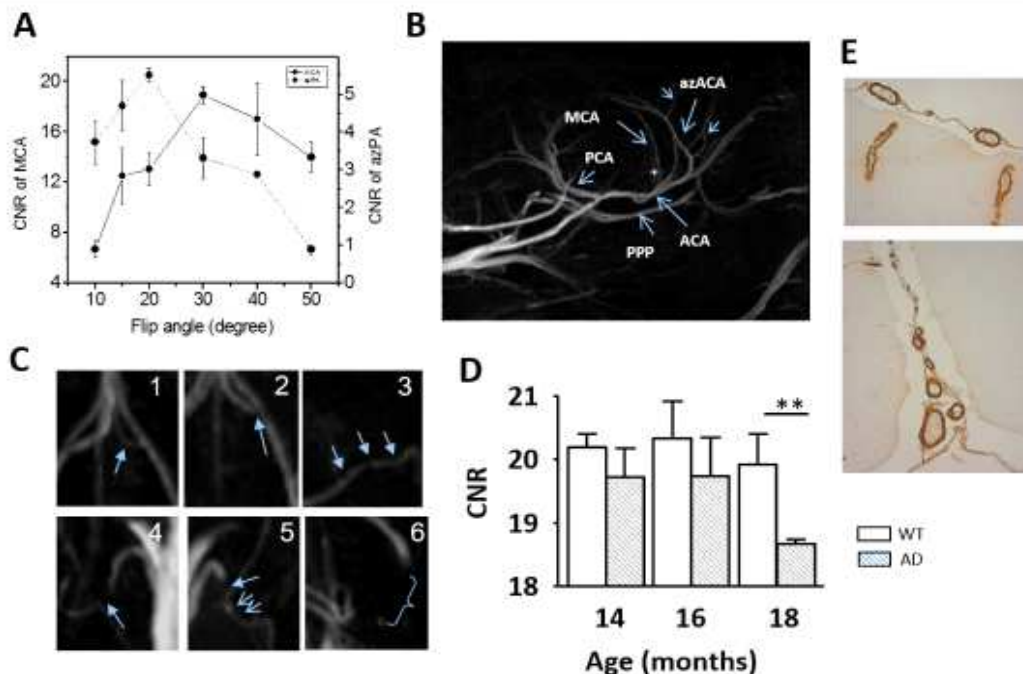


Fig. 1. (A) The effect of varying radiofrequency pulse flip angle (FA) and inflow time (repetition time, TR) evaluated on contrast to noise ratio (CNR) of Middle cerebral artery (MCA) and Azygos pericallosal artery (azPA); (B) Angiogram in transverse view of wild type mouse imaged at 17.6 T; (C) Angiograms of 18 month old transgenic AD mice showing various level of severities of morphological changes appointed in 3D MIP. The number indicates the appointed score to the level of severity of alterations (D) Age dependent changes in contrast-to-noise ratio (CNR) of AComA artery in wild type and AD mice. One tail student T test was used for statistical evaluation. \*  $p < 0.05$ . (E) A $\beta$  deposition in vessel wall detected in the brain sections of AD mouse brain stained with anti A $\beta$ 40.



## A comparative study of site- and zonal-dependent osteoarthritic cartilage changes when using low-resolution and microscopic MRI

F. Badar and Y. Xia<sup>\*§</sup>, Department of Physics and Center for Biomedical Research, Oakland University, Rochester, MI, United States.

**Introduction:** Osteoarthritis (OA) is a common disease of articular cartilage, which has an altered molecular composition (glycosaminoglycan GAG, water) and structural integrity (collagen). These changes can be detected by MRI relaxometry (1), which are site and zonal specific (2). By implementing a new method of zonal analysis on a low resolution T2 map, we show the ability to quantify the complex site-specific depth-dependent relationships between healthy and OA cartilage, using both high- and low-resolution images.

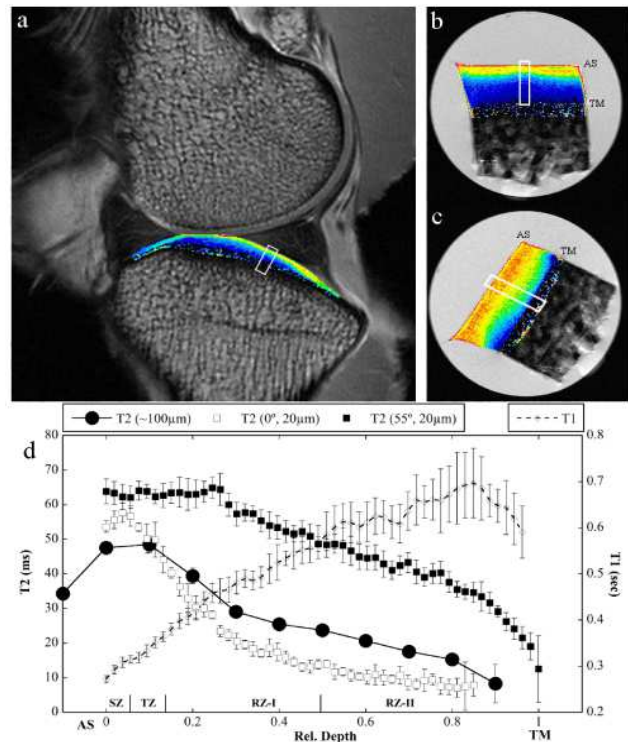
**Methods:** Twelve intact normal (N) canine knee joints were compared to contralateral (C) and osteoarthritis (OA) (six each). Using a 7T/20cm MRI system, T2 maps of the intact joint were constructed at 100 $\mu$ m/pixel. From the medial tibia, T2 profiles of five topographical locations (i.e. sites) were subdivided into three histological zones (SZ, TZ, RZ) (3), with the radial-zone further divided into two equal halves (RZ1, RZ2). After harvesting the individual cartilage-bone blocks from the five topographical sites, T2 (at 0° and 55° from B0) and T1 (55°) images (in gadolinium) were constructed for each specimen at ~ 20  $\mu$ m/pixel using a 7T/9cm  $\mu$ MRI Bruker system.

**Results:** The low-resolution (100  $\mu$ m/pixel) MRI T2 map (a) of a healthy tibia is compared with the high-resolution (20  $\mu$ m/pixel) MRI T2 (0° and 55°) of cartilage from the nearly identical surface location. The depth-dependent profiles (d), from the selected ROI in (a-c), show the specific differences between the low- and high-resolution MRI due to magic angle effect and tissue properties. By comparing the topographical and zonal changes between healthy and OA, a statistical difference can be found in the disease progression from site-to-site. The T2 profiles follow an inverse trend to the T1 profiles, confirming that the decrease in GAG (T1-after) results in an increase of T2. This analysis is zonal specific, with each of the five sites showing different OA progression.

**Conclusions:** Most clinical MRI studies of OA, due to the lack of sufficient resolution, show an average site-, zonal, and unspecified orientational difference between healthy and OA cartilage (2). Hence the sensitivity of MRI towards clinical OA is reduced. Since cartilage has a strong T2 anisotropy that is depth-dependent with a significant topographical variation, our study of cartilage using  $\mu$ MRI can provide the missing information in the low-resolution MRI of OA cartilage. We show a precise zonal division in articular cartilage is important in the clinical management of OA.

**Acknowledgements:** The authors are grateful to Dr. James R Ewing and Dr. Gary Ding (Henry Ford Hospital, Detroit) for their assistance and access to the 7T/20cm MRI system. The authors thank NIH for the R01 grants (AR052353, AR069047).

**References:** (1) App Magn Reson 2017, 48:407. (2) Magn Reson Med 2004, 52:41-6. (3) Quant Imaging Med Surg 2017, 7:227-37.



### Diffusion NMR of Electrolyte Dynamics Confined to Carbon Based Gas Diffusion Electrode Frameworks

S. Merz<sup>\*</sup>, P. Jakes, H. Tempel, S. Eurich, H. Kungl and J. Granwehr<sup>a,b</sup>, <sup>a</sup>Forschungszentrum Jülich GmbH, Institute of Energy and Climate Research, Fundamental Electrochemistry (IEK-9), 52425 Jülich, Germany; <sup>b</sup>RWTH Aachen University, Institute of Technical and Macromolecular Chemistry, 52074 Aachen, Germany.

Dynamics of fluids confined to porous hosts are fundamentally different compared to the bulk state. This aspect plays a key role for the development and enhancement of gas diffusion electrodes (GDE) frameworks since it constitutes a major bottleneck for reaction kinetics, ion and electron transport. The GDE component therefore determines the performance of batteries, fuel cells and electrolyzers. With the advent of ionic liquids (IL) a new class of "green solvents" has been introduced with the potential to replace classical aqueous electrolytes. IL's are liquid salts, solely composed of ions, what results in asymmetry and flexibility with delocalized electrostatic charges. This results in complex interactions of Coulombic forces causing complex diffusion processes in porous hosts that can be contradictive to what is commonly exhibited by molecular fluids. Moreover, properties of IL's are difficult to predict, since theories for property estimations usually do not compensate strong coulomb effects as observed in IL's. In this contribution the dynamics of pyrrolidinium and choline based ionic liquid electrolytes confined to (a) "all green" activated carbon black GDE framework mixtures of different porosities and (b) electrospun carbon cathode frameworks were assessed by PGSTE-NMR and  $T_1$  measurements.

As a first proof of principle the different GDE framework were tested using a model zinc-air-like battery cell based on the classical KOH electrolyte.

The results indicate different IL mobility regimes/environments inside the different carbon frameworks with moderate exchange between different electrolyte environments. Furthermore, diffraction of diffusion patterns were found for certain IL confined to the GDE framework. Therefore, the classical approach for the interpretation of NMR in porous media needs to be rethought for IL in electrospun GDE frameworks. Nevertheless, diffusive diffraction can serve as a proxy for the identification of topological features in the fibrous material.

We gratefully acknowledge funding by the "German Federal Ministry of Education and Research" (BMBF, grant number 03SF0499F "LuZi")

**$^7\text{Li}$  NMR imaging for aluminum-laminated rechargeable lithium ion battery at 4.7/9.4 Tesla**

I. HAISHI<sup>\*</sup>, MRTechnology Inc., Sengen 2-1-6, Tsukuba, JAPAN; S. FUJIKI and Y. AIHARA, Samsung R&D Institute Japan Co. LTD., Osaka, JAPAN.

**Synopsis:**

A feasibility of  $^7\text{Li}$ -NMR imaging for aluminum-laminated rechargeable lithium batteries has been investigated. The NMR/MRI measurement of aluminum-laminated samples was believed impossible because the aluminum-lamination around any Li batteries prevents to penetrate very high radio frequency waves of ordinal NMR excitation and detection to/from a measurement  $^1\text{H}/^7\text{Li}$  subject inside. However, we have discovered that NMR/MRI measurements of the aluminum-laminated lithium objects can be performed in a proper orientation of the  $B_1$  excitation pulse between the sample's lamination planes through a 200  $\mu\text{m}$  sealing gap.

**Experiments and results:**

A 4.7-Tesla wide-bore and 9.4-Tesla narrow-bore NMR magnets, digital NMR/MRI consoles (DTRX6/S7D/ iPlus, MRTe, Japan), home-built 3-axis gradient coils, and rectangle rf solenoid coils (Fig.1) were employed. The TX power for the  $B_1$  excitation was less than 50 W for 120  $\mu\text{s}$ . The aluminum-laminated film of 110  $\mu\text{m}$  was consisted by Al-foil of 30  $\mu\text{m}$  thickness, PET (polyethylene terephthalate), and Nylon. Two laminate films of (28 mm)<sup>2</sup> square with tab thickness of 200  $\mu\text{m}$  and 3 mm sealing width were used to enclose a battery stack. A whole package (Fig.2: 500  $\mu\text{m}$  thickness) with the lamination, a working electrode (e.g., graphite, NCA, LCO), sulfide based all-solid-state electrolyte (Fig.3), Li-foil (Fig.4), of which sizes were (20 mm)<sup>2</sup> square, and Al/Cu current collectors, were successfully measured with NMR or 2D/3D/CSI sequences in seconds to several hours.

**Conclusion:**

$^7\text{Li}$  NMR/MRI measurement of aluminum-laminated Li battery samples were successfully done at 78M / 156MHz. The solid Li foils were visualized. It was confirmed by the standard imaging that the rf signal distribution in the thin laminated battery package was very uniform so that the rf passageway was surely in-parallel to the laminate's planes. We conclude that the proper aluminum lamination makes us possible to proceed a stable in-situ NMR/MRI measurements of Li-batteries beyond delicate plastic packages.

**Reference:**

"Visualizing skin effects in conductors with MRI:  $^7\text{Li}$  MRI experiments and calculations", A. Iotta et al, JMR, Vol. 245, 2014.

"In situ NMR of lithium ion batteries: Bulk susceptibility effects and practical considerations", N. Trease et al, Solid State NMR 42, 2012

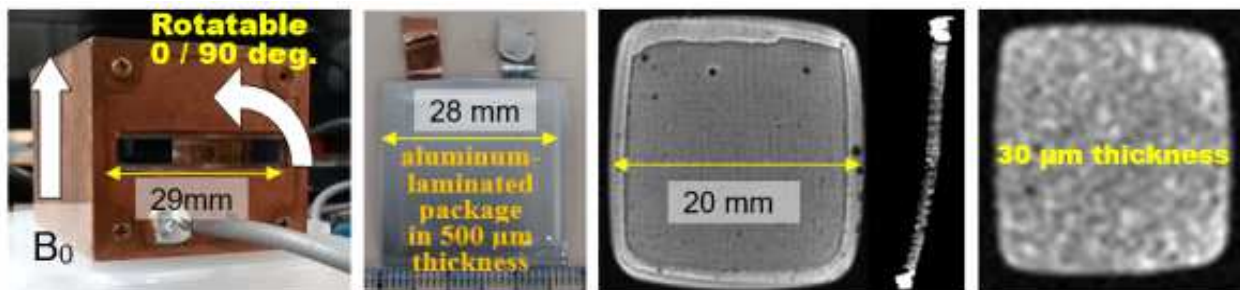


Fig.1 rf-solenoid imaging coil. Fig.2 Li-sample. Fig.3  $^7\text{Li}$ -MRI solid electrolyte. Fig.4 MRI of Li-foil.

## Rheo-NMR and Rheo-SALS using Large Amplitude Oscillatory Shear for the Study of Complex Fluids

S. Kuczera<sup>a,b</sup>, L. Gentile<sup>a,c</sup> and U. Olsson, <sup>a</sup>Division of Physical Chemistry, Lund University, Sweden; T.I. Brox and P. Galvosas<sup>\*</sup>, <sup>b</sup>Victoria University of Wellington, SCPS, MacDiarmid Institute for Advanced Materials and Nanotechnology, New Zealand; <sup>c</sup>Department of Chemistry and Chemical Technologies, University of Calabria, Italy; C. Schmidt, Department of Chemistry, University of Paderborn, Germany.

Rheo-NMR has existed as a tool for studying fluids under mechanical deformation for nearly 25 years [1,2]. It provides spatially and temporally resolved maps of NMR spectra, intrinsic NMR parameters (e.g. relaxation times) or motion (e.g. diffusion or flow). Likewise, Rheo-SALS (Small Angle Light Scattering) is an advanced rheological method which can be used to monitor microscopic changes in the sample due to deformation. Characteristic scattering patterns arise from scattered light intensity as a function of the wave vector, yielding information on microscopic shapes and structures [3]. Both, Rheo-NMR and Rheo-SALS have been established as complementary techniques to conventional rheological measurements.

Shear-induced transformations between oriented planar lamellae and multilamellar vesicles (MLVs) due to steady shear have been studied in the past by Rheo-NMR [4,5]. However, recent advances in Rheo-NMR hardware allow for the application of Large Amplitude Oscillatory Shear (LAOS) deformations in high field NMR magnets for the first time [6]. Here we report on the combined use of Rheo-NMR and Rheo-SALS to study the formation of multilamellar vesicles (MLVs) in a lyotropic surfactant system (C<sub>10</sub>E<sub>3</sub>/water) using LAOS. For the range of investigated strain amplitudes (10-50) and frequencies (1 rad/s, 2 rad/s) MLV formation is observed in all NMR and most SALS cases. For LAOS it was found that the MLV size mainly depends on the frequency as opposed to previous steady shear experiments where the shear rate was the controlling parameter [7]. Additionally, the onset of MLV formation using LAOS was primarily dependent on the applied shear amplitude. Furthermore, the process of onion formation appears to be retarded during LAOS as compared to the steady shear case.

- [1] A. Nakatani et al. *Macromolecules*, **23** 2686 (1990)
- [2] P.T. Callaghan *Rep. Prog. Phys.* **62** 599 (1999)
- [3] J. Samuels *Polym. Sci.* **9** 2165 (1971)
- [4] B. Medronho et al. *Soft Matter* **7** 4938-4947 (2011)
- [5] B. Medronho et al. *Z. Phys. Chem.* **226** 1293-1313 (2012)
- [6] T.I. Brox and P. Galvosas *NZ Patent* 629,361 (2016)
- [7] B. Medronho et al. *Langmuir* **26** 14771481 (2010)

## Planar Couette flow for magnetic resonance microscopy

S. J. Stevenson, T. I. Brox and P. Galvosas<sup>a,b</sup>, <sup>a</sup>Victoria University of Wellington, SCPS, New Zealand; <sup>b</sup>MacDiarmid Institute for Advanced Materials and Nanotechnology, New Zealand.

Many materials in everyday life exhibit peculiar behaviour due to applied mechanical deformations. Rheo-NMR is an established technique which has been used for almost three decades to study these responses by combining methodology from rheometry and nuclear magnetic resonance [1-3]. It enhances standard rheological studies of bulk properties, such as viscosity and elasticity, by exploring the molecular origins and / or local responses within a material.

This contribution reports on the development and application of a novel geometry for magnetic resonance microscopy (MRM) - a planar-cylindrical hybrid (PCH) shear cell - to study fluid mechanics and the complex response of materials under shear. The geometry includes sections of planar Couette flow with the aim to provide a simple homogeneous shear profile. Various geometries to establish planar Couette flow have been used previously to study the fluid mechanics of simple fluids [4-6] but have never been developed for NMR. Generally, they are composed of two parallel sections of planar flow connected by two semicircular sections of circular flow to give a closed flow path in the shape of a racetrack. Shear is applied by rotating a band around the inner section like a conveyer belt. This is another step in recent efforts to enrich the Rheo-NMR toolbox by removing the inhomogeneous flow field conditions as generated by the concentric cylinder / Taylor-Couette (TC) geometries [7] (for which the narrow gap approximation is harder to satisfy as compared to in conventional rheometry).

Previous work on one shear banding wormlike micelle (WLM) solution demonstrated that the curvature of TC cells used during Rheo-NMR experiments influenced the observed rheological response [8]. This work further investigated the influence of curvature by studying the local dynamics of the WLM solution using the PCH in combination with a variant of the RARE pulse sequence [9]. Commonalities and differences of the WLM solution in the PCH when compared to simple fluid systems (e.g. silicone oil) and TC geometries will also be discussed.

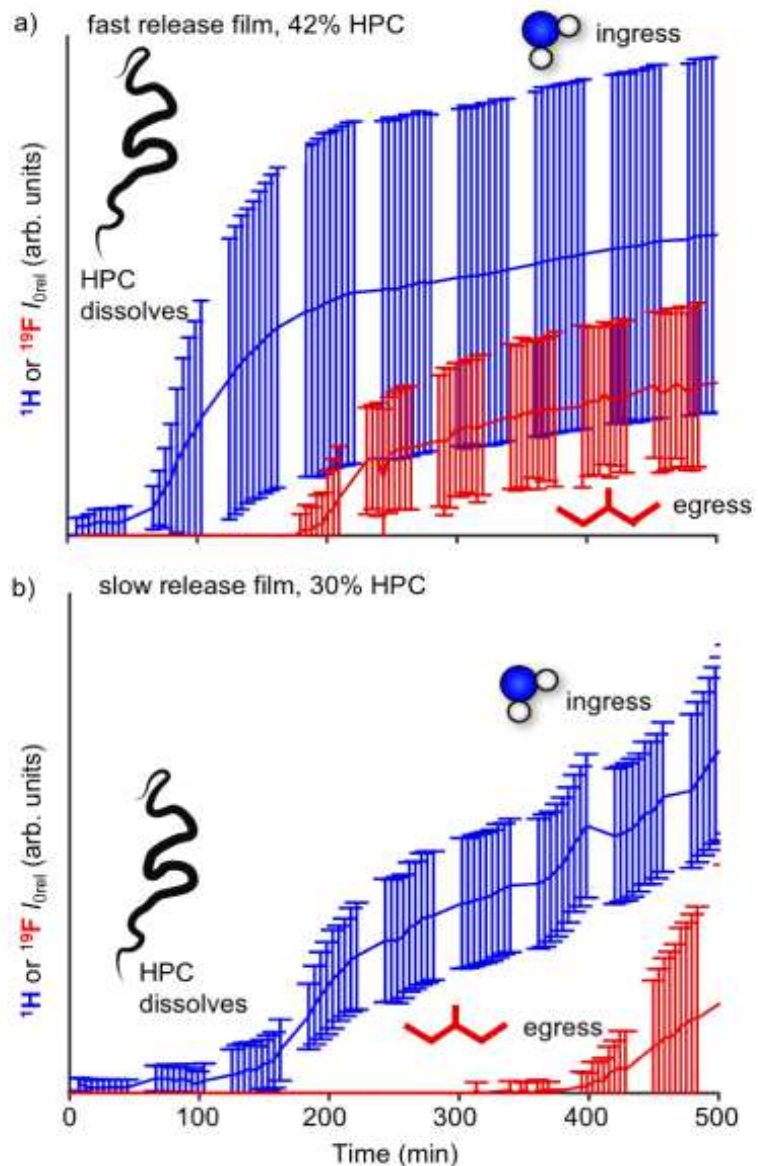
- [1] A.F. Martins et al. *Phys. Rev. Lett.* **57** 1745-1748 (1986)
- [2] A.I. Nakatani et al. *Macromolecules*, **23** 2686-2692 (1990)
- [3] P.T. Callaghan *Rep. Prog. Phys.* **62** 599-670 (1999)
- [4] N. Tillmark et al. *Appl. Sci. Res.* **51** 237-241 (1993)
- [5] J.J. Kobine and T. Mullin *Phys. Fluids*, **13** 1583-1593 (2001)
- [6] D. Krug et al. *Exp. Fluids*, **52** 1349-1360 (2012)
- [7] C.W. Macosko Wiley-VCH (1994)
- [8] T.I. Brox et al. *J. Rheol.* **60** 973-982 (2016)
- [9] S. Kuczera and P. Galvosas *J. Magn. Reson.* **259** 135-145 (2015)



## Release characteristics of extended release films elucidated using real-time 3D MRI

D. Bernin<sup>a,b</sup>, <sup>a</sup>Swedish NMR Centre, Gothenburg University, Gothenburg, Sweden; <sup>b</sup>Department of Chemistry and Chemical Engineering, Chalmers University of Technology, 412 96 Gothenburg, Sweden; C Boissier, J Hjartstam, M Marucci and A Abrahmsen-Alami, AstraZeneca, R&D, Mölndal, Sweden; U Olsson, Department of Chemistry, Lund University, Lund, Sweden.

A common oral extended release administration is a pellet, which is coated with a film of designed permeability controlling the temporal drug release. The permeability is tailored for example with a thin film based on a microscopically phase separated hydroxypropylmethyl cellulose (HPC) and ethylcellulose (EC) mixture. Upon contact with water, HPC dissolves and EC creates a porous network with a pore size being to a large extent proportional to the fraction of HPC. Although the temporal drug release is eventually mainly governed by the pore size of the film, the water ingress, dissolution of HPC and the drug are crucial for the onset of the drug release. A large amount of HPC might form a gel layer or create a heterogeneous pore size distribution complicating a controlled drug release. Fast 3D  $^1\text{H}/^{19}\text{F}$  magnetic resonance imaging (MRI) in combination with a specifically designed release cell was used to monitor the water ingress and the egress of a highly water-soluble  $^{19}\text{F}$ -containing drug through the film in real-time with a spatial resolution of 100 micrometers. The mean non-weighted signal intensity as a function of time is presented in Figure a (fast release film, 42% HPC) and b (slow release film, 30% HPC) revealing that the drug egress ( $^{19}\text{F}$   $I_{0\text{rel}}$ ) and the water ingress ( $^1\text{H}$   $I_{0\text{rel}}$ ) depends strongly on the fraction of HPC. The water ingress is slower for a lower fraction of HPC and for a larger fraction of HPC, water ingress appears to vary strongly throughout the film in contrast to a low amount of HPC. Remarkably for 42% HPC, the position of the film progresses almost 1 mm towards the water phase due to an osmotic pressure build up before the onset of the drug egress in contrast to a lower fraction of HPC.





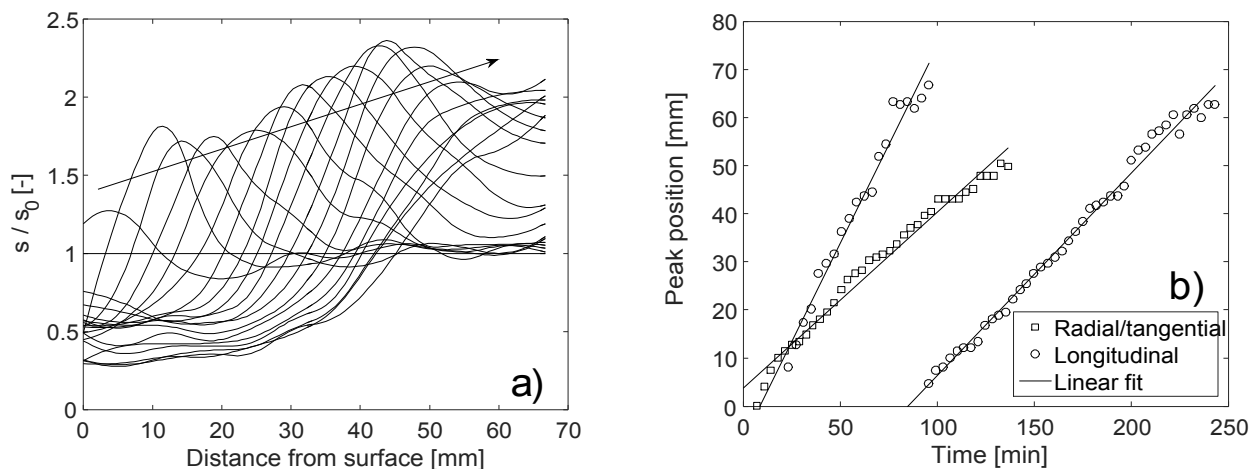
## Fire behavior of wood as studied by NMR

L. Pele and T. Arends, Department of Applied Physics, Eindhoven University of Technology.

Fire can be used advantageously, e.g. for cooking food, but it can also be highly destructive when a wooden structure is concerned. Knowledge on the fire behavior of wood is therefore of large interest not only for personal safety, but also for construction safety. Up to now no fire tests are available in which we get direct insight into the physical phenomena which take place during one-sided heating of a wooden structure. Most often only the temperature is measured. In this study we set out to gain more information by using NMR, as it can give direct access to the moisture transport but also the physical/chemical degradation processes taken place.

In order to measure the moisture transport in a wood sample during fire we have made use of the main magnetic field of a 1.5T whole body MRI scanner, in which a dedicated fire test setup is placed. The samples used are cylinders, 70 mm in diameter and 70 mm in length. The samples are isolated by a Teflon beaker for moisture and heat insulation, leaving one surface exposed. A special birdcage is used which can still operate at high temperatures. In these measurements we only measure one-dimensionally by making use of an anti-Helmholtz coil generating a gradient of 0.2 T/m. In order to heat up the exposed surface of the sample, use is made of an array of halogen lamps, generating a heat flux well over 10 kW/m<sup>2</sup>. As a result the sample can be heated up with a heating rate of ~2 °C per minute up to a maximum temperature in the order of 600 °C.

At the start of the experiment we see with an increase of the temperature in combination with an increase of the NMR signal (Figure 1a). At the same time a strong temperature gradient builds up of well over 10000 K/m. As a result a peak in the moisture content is observed, which travels towards the back linearly in time (Figure 1b). Furthermore, in these experiment we can see that around 270 °C the wood ignites. Moreover these NMR measurement clearly show a difference in fire dynamics depending on the principal direction of wood.



**An adaptive sub-band decomposition approach for high-resolution NMR data analysis**

M.A.R. Anjum\*, [Paul D. Teal](#)<sup>s</sup> and Pawel A. Dmochowski, School of Engineering and Computer Science, Victoria University of Wellington, PO Box 600, Wellington 6140, NEW ZEALAND.

An adaptive sub-band decomposition scheme for high-resolution analysis of Magnetic Resonance Spectroscopy (MRS) data is presented. The scheme is composed of successive filtering, sub-band decomposition and estimation stages. At each stage, signal parameters are extracted for each sub-band. The estimated signal is then subtracted from the target signal to generate a residual and an estimation error. The latter is subjected to Bayesian Information Criterion (BIC) testing in order to decide whether the decomposition process should continue or not. If required, the decomposition process is continued with the residual being the input to the next decomposition/estimation stage. An advantage of this scheme is that it can enhance the performance of the analysis method due to the improved SNR, line-resolution and dynamic range available in individual sub-bands. Secondly, successive removal of the estimated components improves the reliability of the analysis method by reducing the influence of model order and hence reducing the number of false detections. Thirdly, the automated selection of the decomposition level helps to avoid any systematic bias in the estimates introduced by the manual input. Fourthly, the approach reduces processing time by early termination of the decomposition process if the residual does not contain further useful information. The efficacy of the proposed scheme is demonstrated by applying it to multiple sets of recorded NMR spectroscopy data.

## An Application of Spectral Entropy to Functional MRI

C.B.O'Grady<sup>\*</sup>, Department of Medical Physics, Dalhousie University; A. Omisade and J. Hashmi<sup>a,b</sup>,  
<sup>a</sup>Nova Scotia Health Authority; S. Patterson, Nova Scotia Department of Health and Wellness; <sup>b</sup>Department of Anaesthesia, Dalhousie University. J. Rioux, S. Beyea

Functional MRI (fMRI) signals are information-rich but only some of their information is useful. Information theory, introduced in 1948 by Claude Shannon, can be used to determine if such information is present. Applications of information theory in neuroimaging to this point have been varied, from detecting fMRI artifacts<sup>1</sup> to studying information transfer in the brain<sup>2</sup>. Here, we attempt to identify fMRI signals related to task activation by applying entropy in the frequency domain (spectral entropy).

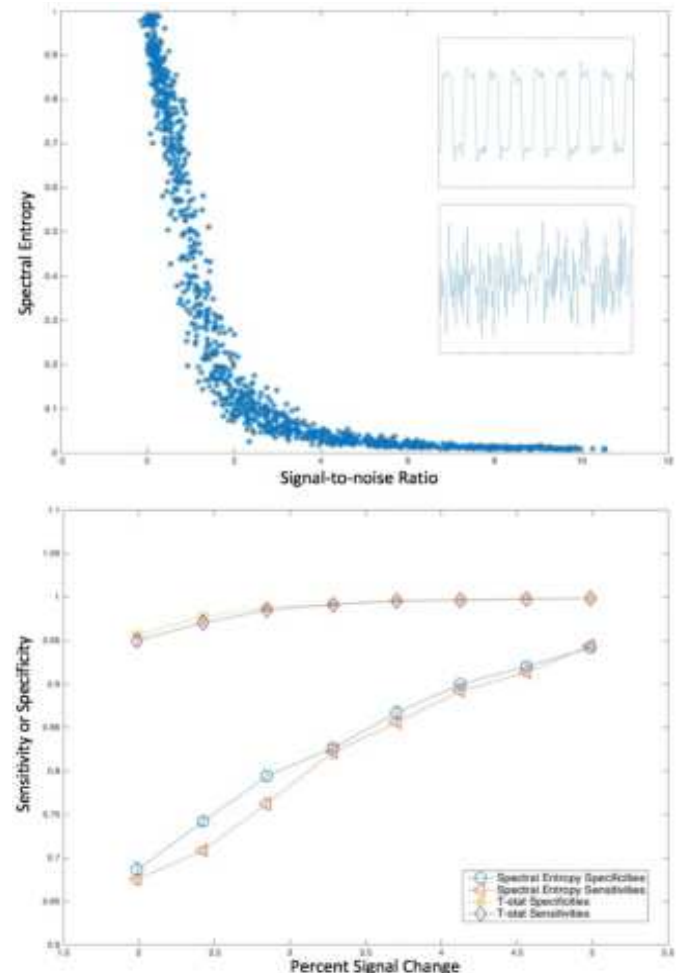
Entropy calculations rely on probability densities (in this case, power spectra values). Low spectral entropy indicates sparsity: only a few frequencies dominate. A high value indicates many interfering frequencies, possibly noise. We applied a regularization scheme to improve the match between the presence of useful task information and the spectral entropy. The regularization is data-driven and its effect is proportional to the relative magnitude of the task frequency. A numerical parameter was added to modulate the regularization. We added noise derived from real data to simulated data to determine this parameter based on sensitivity and specificity for different degrees of known activation.

T-statistic, found with the General Linear Model<sup>3</sup> and used in fMRI interpretation, showed correlation to low-entropy voxels. Similarly, spatial maps corresponded to known areas of activation. Lastly, spectral entropy correlated to SNR in idealized signals. With our regularization method, spectral entropy was sensitive to voxels rich in task information while using minimal a-priori assumptions.

1. McGonigle, J. (2010), 'Automated detection of fMRI artefacts from Shannon entropy distributions', *Proceedings of Medical Image Understanding and Analysis*, pp. 173-178

2. Hinrichs, H., Heinze, H. J., & Schoenfeld, M. A. (2006). 'Causal visual interactions as revealed by an information theoretic measure and fMRI', *NeuroImage*, vol. 31, pp. 1051-1060.

3. Friston, Karl J., et al. (1994). 'Statistical parametric maps in functional imaging: a general linear approach.' *Human brain mapping* vol. 2, no. 4, pp. 189-210



**Top:** a decrease is seen in spectral entropy with increasing SNR of an "ideal fMRI time course" (convolution of the haemodynamic response function to the on/off pattern of the task), demonstrating correlation of spectral entropy to how much of the signal is noise. Inset, top: example ideal time course with SNR=19. Inset, bottom: ideal time course with SNR=1.6.

**Bottom:** t-statistic is often used to measure the likelihood that a voxel's signal is due to task response. Sensitivity and specificity are calculated for t-statistics and spectral entropy using known areas of activation in simulated data. The similarity of curves for t-statistic and spectral entropy indicate that both can correctly identify voxels containing information about the task.

## A Model-based Method for Quantitative Analysis with Benchtop NMR

Y. Matviychuk, J. Yeo and D.J. Holland, University of Canterbury, Christchurch, New Zealand.

NMR spectroscopy is a fast and convenient alternative to standard chemometric methods [1], and recent advances in benchtop NMR make it readily available for use in industrial applications. Unfortunately, at the lower field strengths of benchtop NMR, multiple resonances overlap and baseline distortions are common due to the large solvent peaks located near compounds of interest. These factors, along with a lower spectral resolution, make established integration procedures inapplicable for accurate quantitative analysis in many systems.

In this work, we propose a model-based quantification approach for benchtop NMR and adapt it here for the challenging task of characterizing the composition of sugar mixtures in water. Our method attempts to model the entire spectra for separate chemical species in the mixture, including the effects of chemical shift, j-coupling and relaxation. This allows us to disentangle even highly-overlapping parts of the spectra and accurately quantify the constituents, even when no single unobstructed peaks are present. Our model directly relies on spin system simulations, which makes it invariant to the instrument field strength [2].

We demonstrate our approach by quantifying the composition of sugars in solution. Sugars are the primary constituent of many beverages, such as fruit juices, wine, soft drinks, and milk, however their quantitative analysis poses significant challenges. The four most common of them glucose, fructose, sucrose, and lactose have different chemical properties and sweetness; their relative concentrations (in addition to any acids present) largely determine the final taste of a product. Knowledge of the composition of sugars in beverages provides a means for process monitoring (e.g. fermentation), quality control, or detection of adulteration (e.g. undisclosed sweetening of fruit juices or dilution of them with apple juice [3]). Experimental results on controlled samples and real fruit juices confirm the applicability of our method for quantitative analysis of spectra acquired at 400 MHz as well as 43 MHz.

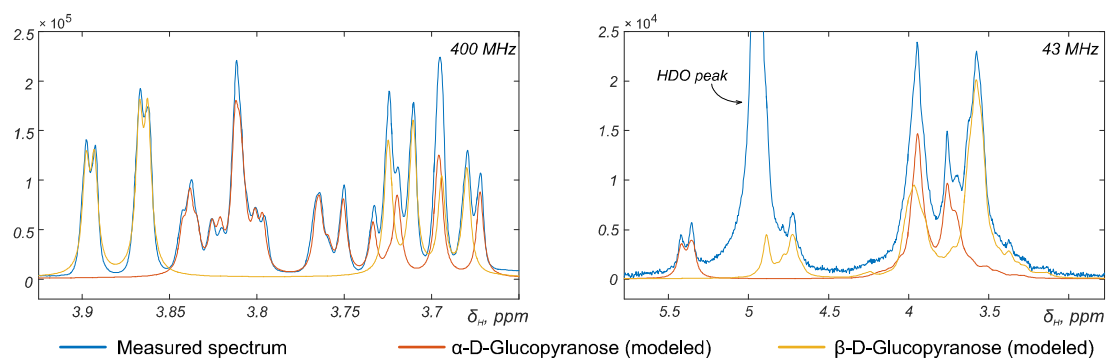
The figure shows an example of modeling the  $^1\text{H}$  NMR spectra of glucose appearing in solution in its two anomeric forms,  $\alpha$ - and  $\beta$ -D-Glucopyranose. The values of chemical shifts and j-coupling constants estimated from the experimental data at 400 MHz (left) are then used in spin system simulations to model the spectra at 43 MHz (right). In both cases, our models closely match experimental measurements obtained on a 0.5M equilibrated solution of glucose in  $\text{D}_2\text{O}$ . The mole fractions of the  $\alpha$ -anomer found with our quantification approach are 0.375 and 0.377 in high- and low-field cases respectively, whereas the value reported in the literature at tautomeric equilibrium is 0.375 [4]. By extension, to analyze mixtures of different sugars, we simulate spectra for their anomers as well. We anticipate our approach will yield quantitative composition information by automated analysis of benchtop NMR measurements.

[1] L. Mannina, A. P. Sobolev, and S. Viel, Prog. Nucl. Mag. Res. Sp., 66, 1-39, 2012.

[2] Kuprov, I. EPR Newsletter., 23(1), 10-11, 2013.

[3] N. Ogrinc, I. J. Kosir, J. E. Spangenberg, and J. Kidric, Anal. Bio.Ch., 376(4), 424-430, 2003.

[4] M. U. Roslund, P. Tahtinen, M. Niemitz, R. Sjoholm, Carbohydr. Res., 343(1) 101-112, 2008.



## A Broadband Nuclear Magnetic Resonance (NMR) System

Mohammad Islam\*, Case Western Reserve University (CWRU), Cleveland, OH 44106, USA; Yi-Qiao Song, Schlumberger-Doll Research, Cambridge, MA 02139, USA; Shin Utsuzawa, Schlumberger-Doll Research, Cambridge, MA 02139, USA; Soumyajit Mandal<sup>§</sup>, Case Western Reserve University (CWRU), Cleveland, OH 44106, USA.

Broadband MR front-ends are useful for real-time process monitoring (e.g. of food), geological prospecting (well-logging for petroleum and mining), detection of explosives and other illicit materials, etc. [1]. Here we present a higher-power version of our earlier design [1] that operates between 250-750kHz. The system components include an untuned transmit and receive coil, a switching power amplifier (H-bridge), a switch-based duplexer, and a transformer-based low noise receiver (as shown in Fig. 1). The coil is wound in three sections with a reversed-polarity central section. The transmitter uses silicon carbide (SiC) FETs because of their high breakdown voltage (1200V), low on-resistance (~31 m), low switching loss, and high temperature rating compared to silicon FETs. In addition, it uses symmetric power supplies (HV+ = HV-) to keep the average voltage at both coil terminals close to zero during pulses. This reduces coupling of the high-current transmitter loop to other circuits; improves safety; and reduces residual coil energy, which reduces receiver settling time. A "freewheeling" FET is also connected in parallel with the coil after each pulse; it acts as a Q-switch and further reduces settling time. Fig. 2(a) shows typical transmitter waveforms. The broadband receiver uses an input noise-matching transformer, low-noise JFET-based preamplifier, and active feedback damping to further reduce settling time. Measurements reveal a voltage gain of 84-90dB (see Fig. 2(b)) and input-referred noise of 0.2-0.3nV/Hz<sup>1/2</sup> (see Figure 2(c)) over the operating frequency range (250-750kHz). The low noise resistance of 2.5-5.5 ensures good NF (comparable to narrowband receivers) for low-to-moderate Q coils. For example, NF 3dB for a 20μH coil with Q = 25 at 500kHz; these values are typical of NMR well-logging systems in highly-conductive surroundings.

References:

[1]S. Mandal, S. Utsuzawa, D. G. Cory, M. Hürlimann, M. Poitzsch, and Y. Q. Song, "An ultra-broadband low-frequency magnetic resonance system," J. Magn. Reson., vol. 242, pp. 113125, 2014.

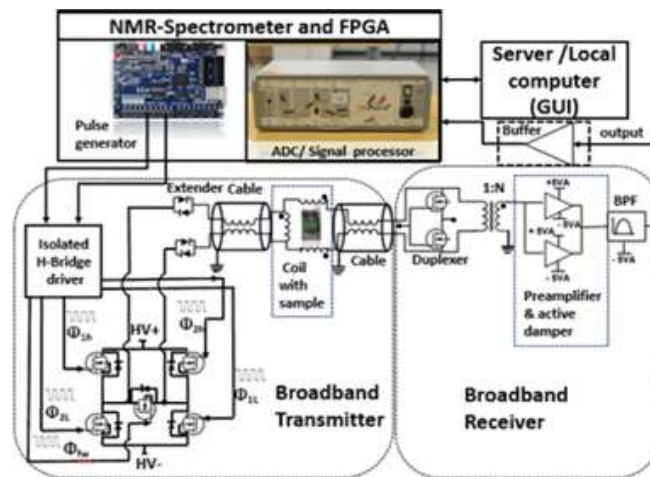


Figure 1: Simplified block diagram of the proposed broadband NMR system.

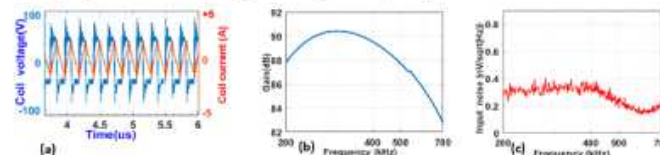


Figure 2: (a) Measured coil current (HV+ = -HV- = 50V, inductance = 12.5μH, frequency = 500 kHz); (

b) small-signal voltage gain and (c) input-referred noise of the receiver.

The turns ratio of the input noise-matching transformer (see Fig. 1)

was set to  $N = 4$  for these measurements.



## An MR/MRI Compatible Core Holder with the RF Probe immersed in the Pressurized Confining Fluid

M. Shakerian<sup>a,b</sup> and B.J. Balcom<sup>\*§</sup>, <sup>a</sup>UNB MRI Centre, Department of Physics, University of New Brunswick, Fredericton, New Brunswick, E3B 5A3, Canada., ; <sup>b</sup>Department of Mechanical Engineering, University of New Brunswick, Fredericton, New Brunswick, E3B 5A3, Canada.

An open frame RF probe for high pressure and high temperature MR/MRI measurements, illustrated in Fig. 1, was designed, fabricated, and tested. The probe was installed in proximity to the sample inside the metallic core holder, increasing sensitivity. The RF probe including the PEEK pillars and copper windings, as shown in Fig. 1a, were immersed in the high pressure confining fluid while MR/MRI measurements were undertaken. This made it possible to design and fabricates an Inconel 718 MR/MRI compatible core holder with a maximum design working pressure of 10000 psi and a maximum operating temperature of 200°C. The heat treated Inconel 718 vessel was certified for an ultimate tensile strength of 210000 psi. The open frame RF probe was tunable for both <sup>1</sup>H and <sup>19</sup>F resonance frequencies at 0.2 T static magnetic fields. The open frame structure greatly simplified fabrication of the RF probe. The fundamental benefits of the open frame RF probe are: (1) reduced MR background signal (2) substantially increased operating pressure, (3) increased maximum operating temperature, (4) improved temperature control efficiency and (5) simplified assembly/disassembly of the core holder and thereby increased robustness of the design.

These improvements arose from (i) employing minimum polymeric materials in the probe fabrication, (ii) submerging the RF probe in the confining fluid, (iii) removing epoxies from the probe structure, and (iv) eliminating a complicated sealing system. 2D XY and XZ density maps of SF<sub>6</sub> saturated Berea were acquired by 2D centric scan SPRITE, as shown in Fig. 2. The experimental system employed the open frame RF probe and a Hastelloy-C MR/MRI compatible core holder, as illustrated by Fig. 1. The two tests were undertaken at a constant temperature of 65°C with a confining fluid pressure of 1500 psi.



FIG.1. The experimental core holder: (a) open frame RF probe, (b) Hastelloy-C metal end cap closure, (c) high pressure BNC connector, (d) MR/MRI compatible metal core holder, including the vessel and the end cap, (e) Berea sample was enclosed by fluid distributors, sleeve and heat shrink tubing. The enclosed sample was placed inside the open frame RF probe during high pressure MR/MRI measurements.

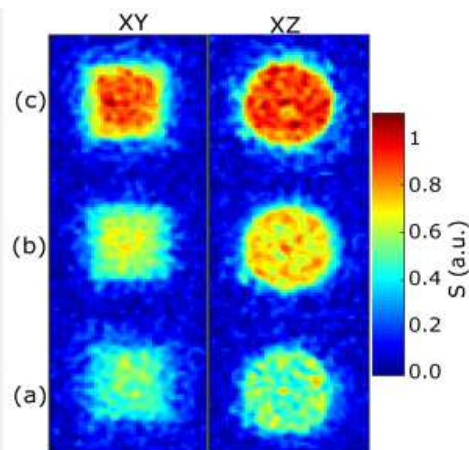


FIG.2. 2D centric scan SPRITE images of SF<sub>6</sub> in a Berea core plug at pressures of (a) 600 psi, (b) 500 psi, and (c) 400 psi, constant temperature 65 °C. 2D images achieved from (a) to (c) show that increasing the pressure increased the signal intensity. Silicon oil was employed as the pressurized confining fluid.



**Crude oil adsorbates on calcite and quartz surfaces investigated by NMR spectroscopy**

H.N. Sjørgård\*, C Totland, W Nerdal and J.G Seland, University of Bergen.

Reservoir rock wettability can have a significant impact on multiphase flow during oil and gas recovery [1, 2]. Adsorption of polar components, present in crude oil, is responsible for wettability alteration of petroleum reservoirs [2-4]. Such components include organic acids, organic bases and asphaltenes. Adsorption of such components, from model oils, have previously been investigated [5-8]. However, the complexity of crude oils may contribute to wettability alteration of petroleum reservoirs in ways that cannot be mimicked by model oils. In this study, various  $^1\text{H}$  NMR techniques were used to investigate the molecular arrangement of crude oil adsorbates on calcite and quartz surfaces due to a wet aging procedure. Solid state magic angle spinning (MAS) NMR techniques were used to directly observe molecules on both surfaces. Liquid state NMR was used to investigate possible differences in the crude oil from before and after the aging procedure. Double-quantum single-quantum coherence spectra were found most valuable for assignment of the quartz surface where the resonances from the entire adsorbate were relatively well resolved. Along with adsorbate molecular positioning, this study also provides quantitative measurements of water present at both surfaces post crude oil aging. Despite traces of aromatic resonances on both surfaces, acid adsorption was determined to be the main mechanism responsible for alteration of wetting state on both the calcite and the quartz surface. NMR experiments show that organic acids adsorb directly onto calcite through electrostatic attraction while the same acids are indirectly adsorbed onto quartz through solubilization in the water phase present at the surface.

## References:

- [1] Jackson, M.D., P.H. Valvatne, and M.J. Blunt, Prediction of wettability variation and its impact on flow using pore-to reservoir-scale simulations. *Journal of Petroleum Science and Engineering*, 2003. 39(3): p. 231-246.
- [2] Morrow, N.R., Wettability and its effect on oil recovery. *Journal of Petroleum Technology*, 1990. 42(12): p. 1,476-1,484.
- [3] Gomari, K.R., R. Denoyel, and A. Hamouda, Wettability of calcite and mica modified by different long-chain fatty acids (C 18 acids). *Journal of colloid and interface science*, 2006. 297(2): p. 470-479.
- [4] Tong, Z., N. Morrow, and X. Xie, Spontaneous imbibition for mixed-wettability states in sandstones induced by adsorption from crude oil. *Journal of Petroleum Science and Engineering*, 2003. 39(3): p. 351-361.
- [5] Jarrahian, K., et al., Wettability alteration of carbonate rocks by surfactants: a mechanistic study. *Colloids and Surfaces A: Physicochemical and Engineering Aspects*, 2012. 410: p. 1-10.
- [6] Tabrizy, V.A., R. Denoyel, and A. Hamouda, Characterization of wettability alteration of calcite, quartz and kaolinite: Surface energy analysis. *Colloids and Surfaces A: Physicochemical and Engineering Aspects*, 2011. 384(1): p. 98-108.
- [7] Totland, C. and R.T. Lewis, Mechanism of calcite wettability alteration by alkyl polyglucoside. *Colloids and Surfaces A: Physicochemical and Engineering Aspects*, 2016. 488: p. 129-137.
- [8] Wu, Y., et al., An experimental study of wetting behavior and surfactant EOR in carbonates with model compounds. *SPE Journal*, 2008. 13(01): p. 26-34.

**Human brain in vivo BSD-DTI - a preliminary study**

K. Klodowski, Faculty of Physics and Applied Computer Science, AGH University of Science and Technology, al. Mickiewicza 30, 30-059 Cracow, Poland; A. T. Krzyzak, Faculty of Geology, Geophysics and Environmental Protection, AGH University of Science and Technology, al. Mickiewicza 30, 30-059 Cracow, Poland.

Diffusion Tensor Imaging (DTI) has led very successful life since its beginning in the early nineties [1]. Over the years its unique properties making possible non-invasive characterization of the tissue microstructure established DTI as a clinical tool for human brain imaging. However, despite the number of valuable contributions aiming to improve this inherently prone to artefacts technique, some problems remained. Precise definition of the b-matrix containing information about diffusion sensitizing gradients is among the most important ones, since errors occurring in the b-matrix propagate to the calculated diffusion tensors.

From the variety of approaches trying to alleviate this troubles, the b-matrix spatial distribution (BSD) calibration seems to be relatively promising [2]. Unlike the standard approach to DTI based on a constant b-matrix for entire volume, BSD derives its spatial distribution. Such calibration is done through DTI measurement of the anisotropic phantom in various orientations within imaging volume [3]. The calibration can improve the precision of the calculated diffusion tensor several times [2-4], however, works only in the limited volume.

The aim of this work was first trial of the clinical application of the BSD-DTI. In order to extrapolate the calibrated b-matrices beyond the phantom volume, smoothing filtering and bivariate polynomial fitting procedures were applied to the spatial distribution of the b-matrix. Several extrapolation methods were validated with anisotropic phantoms. Those giving the best results were applied to the first successful attempt to in vivo BSD-DTI of human brain.

**Acknowledgements**

The work was financed by the National Centre of Research and Development (contract No. STRATEGMED2/265761/10/NCBR/2015).

**References**

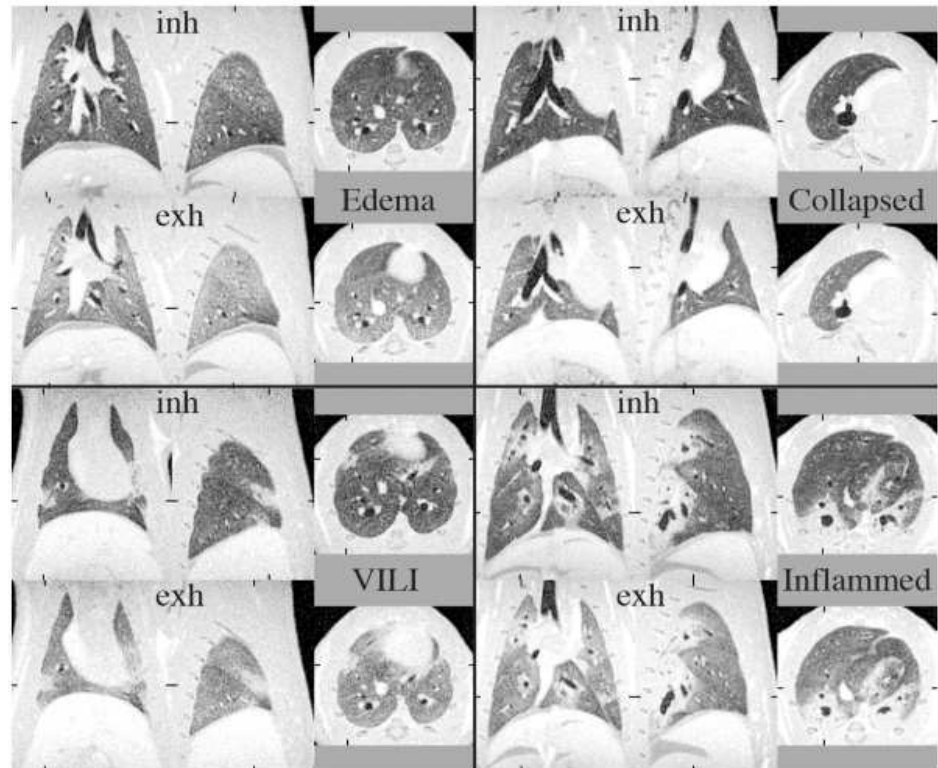
- [1] Basser P. J., Mattiello J., LeBihan D., MR diffusion tensor spectroscopy and imaging, *Biophys. J.* 1994;66:259-267,
- [2] Krzyzak A. T., Olejniczak Z., Improving the accuracy of PGSE DTI experiments using the spatial distribution of b matrix, *MRI* 2015;33:286-295,
- [3] Klodowski K., Krzyzak A. T., Innovative anisotropic phantoms for calibration of diffusion tensor imaging sequences, *MRI* 2016;34:404-409,
- [4] Borkowski K., Klodowski K., Figiel H., Krzyzak A. T., A theoretical validation of the b-matrix spatial distribution approach to diffusion tensor imaging, *MRI* 2017;36:1-6.

### Four Rat Lung Pathologies: Utility of $T_1$ Contrast and Appearance in Ernst-Angle Images

D. O. Kuethe<sup>\*a,b</sup>, <sup>a</sup>ABQMR, Albuquerque, USA; L. E. Fredenburgh, Brigham & Women's Hospital, Boston, USA; J. M. Hix, <sup>b</sup>Lovelace Respiratory Research Institute, Albuquerque, USA.

A major advantage of MRI over X-ray CT is the variety of contrast mechanisms available to MRI. Now that we have overcome issues of inhomogeneous broadening from water-air susceptibility differences and low tissue density to make

CT-quality MRIs of rat lungs it is important to document the utility of relaxation contrast for distinguishing different lung pathologies. For zero echo-time images,  $T_1$ -weighting is the obvious contrast to try first. We measured the bulk  $T_1$  of four pathologies with inversion recovery images and with spoiled steady-state images using different flip angles. We also documented  $T_1$  contrast and the radiologic appearance in images made with the Ernst-angle for healthy lung tissue. Watery edema from isotonic saline lavage has relatively long  $T_1$ ,  $1.75 \pm 0.1$  s. Collapsed lung, ventilator-induced lung injury (VILI), and neutrophilic inflammation from



pseudomonas lipopolysaccharide (LPS) all have  $T_1$ s similar to healthy lung tissue,  $1.24$ ,  $1.40$ ,  $1.21$ ,  $1.24 \pm 0.1$ s, respectively. In short,  $T_1$  weighting is of limited use. Nonetheless, the appearance of the four pathologies in Ernst-angle images (low  $T_1$  contrast, maximum signal for healthy lung) differentiate them well (Figure), much as one would expect from micro X-ray CT. For each pathology, 3 different slice planes are shown, coronal, sagittal, and axial at both the inhaled volume and exhaled volume. The black tick marks on the edges of each frame show the locations of the other two frames. A logical next step is to develop a  $T_2$ -weighted imaging technique that also resolves lung tissue.

## Development Human Anatomy Atlas on MRI

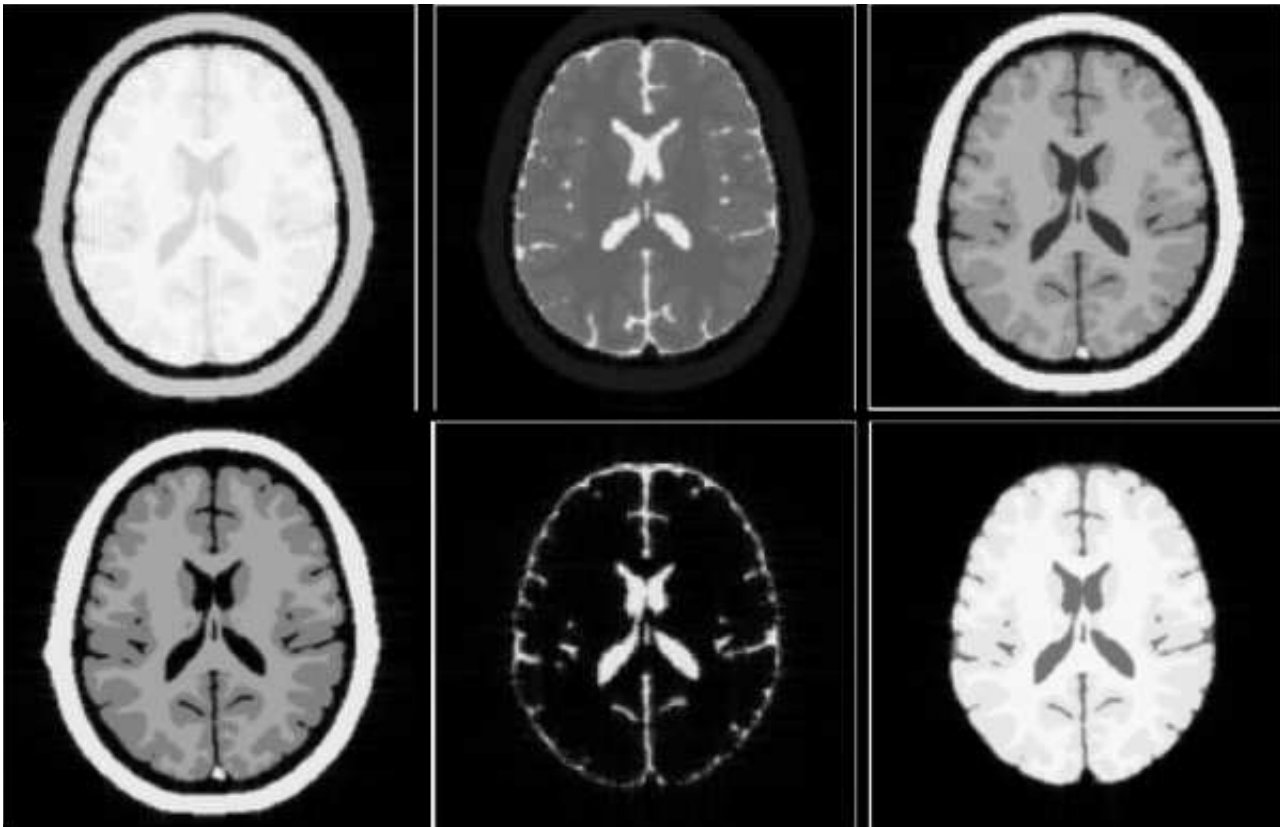
Hongzhi Wang, East China Normal University.

**Purpose:** Human anatomy atlas on MRI (HAAM) often suffers from the limitations in the original images, such as the single type of weighted image, a limited number of fixed sectional image. To solve this problem, a novel approach to build a visible MRI human is presented.

**Methods:** HAAM can be obtained by using the virtual MRI technology to scan a digital human including healthy body or unhealthy body with some typical lesions. Firstly, adopting T1, T2, PD mapping techniques to scan a real human body with 1mm thickness and get the digital human resource. The digital human is a 3D database with the MRI signal parameters such as T1, T2, Diffusion, proton density. Secondly, using the virtual MRI data acquisition and image reconstruction techniques to scan the digital human and get the HAAM with any kinds of contrast. The virtual MRI raw data space, that is K space, can be written as a four integral.

**Results:** The different weighted image with variable contrast of digital human can be acquired in any sectional by different sequence, such as T1-W, T2-W, PD-W, T1-Flair, T2-Flair, STIR (as figure 1).

**Conclusions:** The arbitrary sectional and weighted MRI image can be obtained in real time (less than 0.5s), which is very useful for sectional image anatomy and MRI diagnosis. It has a potential to facilitate the diagnostic atlas matching and the mapping evaluation of radiotherapy treatment plan.



**Constructing local flow curves of complex yield stress fluids based on Rheo-MRI velocity profiles**

I. Nikolaeva, F. Vergeldt, H. Van As and J. van Duynhoven<sup>a,b</sup>, <sup>a</sup>Laboratory of Biophysics, Wageningen University and Research Centre, Wageningen, The Netherlands; P. Venema, Physics and Physical Chemistry of Foods, Wageningen University and Research Centre, Wageningen, The Netherlands; <sup>b</sup>Unilever Discover Vlaardingen, Vlaardingen, The Netherlands.

RheoMRI is a non-intrusive technique that allows a direct and quantitative view on local flow behaviour of complex fluids [1, 2]. Localized rheo-MRI velocimetry is especially helpful for studying flow behaviour of dispersions that display yield stress behaviour, since their flow behaviour cannot be understood from conventional rheological measurements. Of particular interest are dispersions that display shear banding, i.e. co-existing flowing and stationary regions. In our work we have addressed two bottlenecks for fully exploiting the potential of rheo-MRI for studying such systems: heterogeneity of stress in the flowing dispersion and chemical heterogeneity which can lead to chemical shift artefacts.

The Couette geometry, which consists of concentric cylinders with a gap in between them, is most commonly used in rheo-MRI. Although its stress distribution over the gap is well known it has hardly been exploited. The combination of local shear rates (deduced from rheo-MRI velocity profiles), and local shear stress values (derived from the applied torque) allow to construct a local flow curve [3]. Since such a local flow curve can be obtained from a snapshot rheo-MRI velocimetry experiment, it offers unique opportunities to assess transient flow behaviour of dispersions. We constructed a set of Couette geometries with variation of gap sizes (1, 2.5 and 4 mm) that can be mounted in a 300 MHz micro-MRI system and in a conventional rheometer. Several hitherto neglected practical and theoretical aspects of obtaining local flow curves will be discussed, as well as quantitative differences between global and local flow curves that qualitatively may appear similar.

For chemically heterogeneous dispersions such as oil-in-water emulsions the presence of distinct chemical shift can give rise to compromised velocimetry profiles. We have explored the use of chemical shift selective pulses for obtaining clean velocimetry profiles.

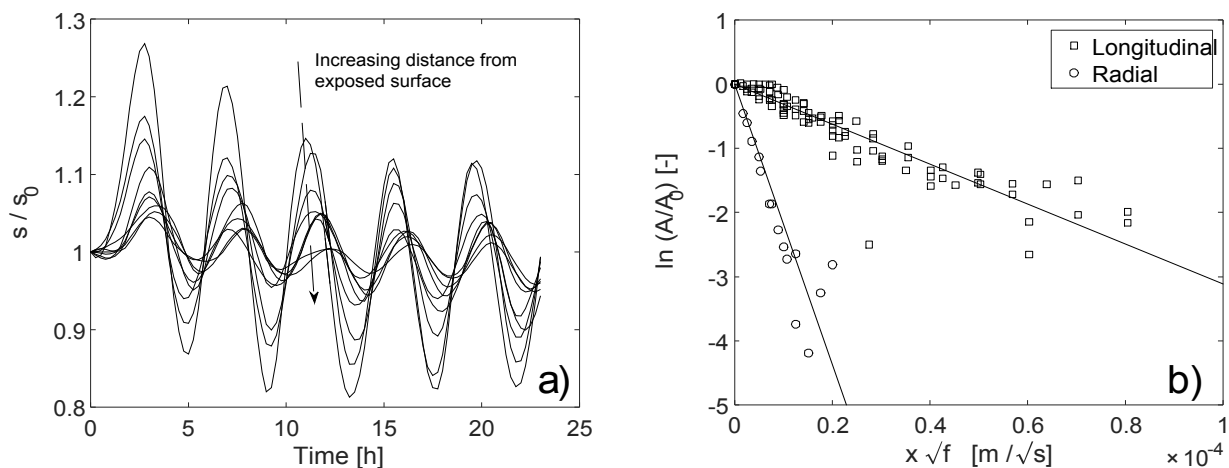
1. Coussot, P. et al., 2009. *Journal of Non-Newtonian Fluid Mechanics*, 158(13), pp.8590.
2. Ovarlez, G. et al., 2008. *Physical Review E - Statistical, Nonlinear, and Soft Matter Physics*, 78(3), pp.113.
3. Ovarlez, G., Bertrand, F. & Rodts, S., 2006. *Journal of Rheology*, 50(3), pp.132.

## Moisture-induced bending of panel paintings as studied by NMR

I. Arends\* and L. Pel, Department of Applied Physics, Eindhoven University of Technology.

Wood has been extensively used in the construction of works of art, e.g. in panel paintings by Rembrandt or Van Eyck. Consequently, these panel paintings form an important part of many museum collections. Panel paintings are generally constructed of a wooden board (often oak), painted on one main side. If the relative humidity of the ambient air changes, moisture exchange takes place between the unpainted wooden surface and the air. The consequent asymmetric moisture content distribution results in unwanted bending of the panel painting. This bending will generate strain in the paint layer, which could result in an irreversible damage of the painting.

Moisture-induced bending of a board is dependent on the penetration depth of the moisture into the board. During sinusoidal fluctuations in relative humidity, the penetration depth depends on the frequency of the changes. Spatially resolved, one-dimensional NMR experiments are performed in which the penetration depth in the different principal directions of wood is studied. An example for the longitudinal direction is shown in Figure 1a. The difference in moisture content amplitude decay between the longitudinal and radial direction is obvious from Figure 1b, since transport in longitudinal direction is faster. Furthermore, bending experiments are performed where the one-dimensional moisture content profile can be related directly to macroscopic bending of the board. Moreover by relaxation measurements we can relate hygroscopic moisture uptake to the wood microstructure.





## Structure and dynamics elucidation of ionic liquids by multidimensional Laplace NMR

M. A. Javed, S. Ahola, P. Håkansson, O. Mankinen, M. K. Aslam and V.-V. Telkki<sup>\*S</sup>, NMR Research Unit, University of Oulu, P. O. Box 3000, 90014 Oulu Finland; A. Filippov, F. U. Shah and O. N. Antzutkin, Chemistry of Interfaces, Luleå University of Technology, SE-97187 Luleå, Sweden; S. Glavatskih, System and Component Design, KTH Royal Institute of Technology, SE-10044 Stockholm, Sweden.

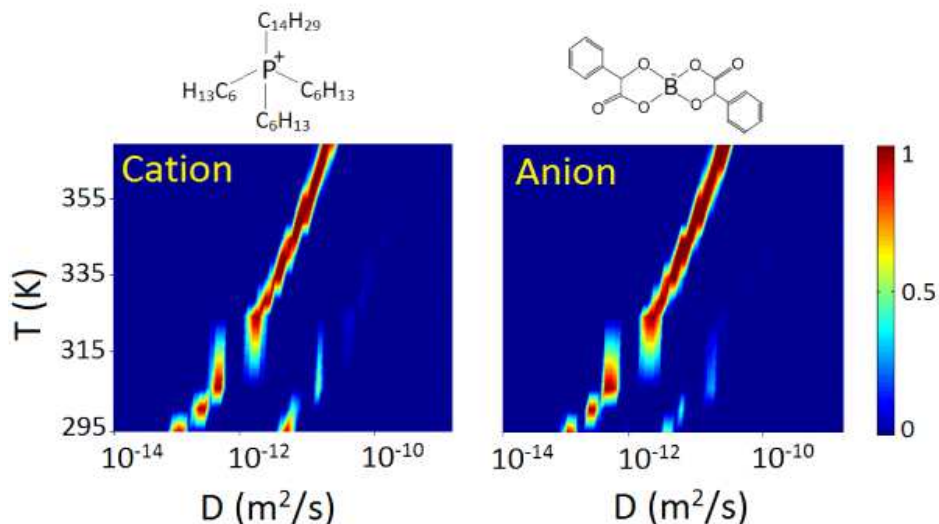
Ionic liquids (ILs) are salts in liquid state that have melting point below 100 °C. They are incorporated with exceptional physical and chemical properties such as high ionic conductivity, negligible vapor pressure, non-flammability, broad liquid range, and excellent thermal stability, which make ILs attractive in many scientific and technological applications [1].

NMR relaxation and diffusion experiments provide versatile information about the dynamics and structure of substances. The relaxation and diffusion data consists of exponentially decaying components and the processing requires a Laplace inversion in order to determine diffusion coefficient and relaxation time distributions. Therefore, these methods are referred as Laplace NMR (LNMR). Like in traditional NMR spectroscopy, multidimensional approach significantly enhances the resolution and information content of LNMR [2].

In this work, we demonstrate that multidimensional LNMR reveal important information about the phase structures and dynamics of ILs that is not observable with conventional NMR spectroscopy or other techniques. One-dimensional diffusion coefficient ( $D$ ) distributions (shown in Figure) of a halogen-free, boron based IL showed two coexisting phases at room temperature. Two-dimensional  $D$ - $T_2$  correlation map enabled us to identify  $T_2$  relaxation times of the slow and fast diffusing phases, and  $T_2$ - $T_2$  exchange maps allowed us to quantify the exchange rates of anions and cations between the phases. Theoretical modeling of the experimental data suggests that the slow diffusing phase is composed of anion-cation aggregates including 10-70 ion pairs, while the fast diffusing phase comprises free anions and cations [3]. These findings provide new opportunities for exploring useful properties of ILs and designing new task specific ILs.

### References

- [1] M. Freemantle, *An introduction to ionic liquids*, Royal Society of Chemistry, Cambridge, 2009.
- [2] D. Bernin, D. Topgaard, *Current Opinion in Colloid & Interface Science*, 18: 166-172, 2013.
- [3] M. A. Javed, S. Ahola, P. Håkansson, O. Mankinen, M. K. Aslam, A. Filippov, F. U. Shah, S. Glavatskih, O. N. Antzutkin, V.-V. Telkki. *Manuscript to be submitted*.



## Effect of motion on CPMG-like measurement in inhomogeneous magnetic field

S. Utsuzawa, C. Ryan<sup>a,b</sup> and M. D. Hürlimann, <sup>a</sup>Schlumberger-Doll Research, Cambridge, MA 02139, USA; <sup>b</sup>Raytheon BBN Technologies, Cambridge, MA 02138, USA.

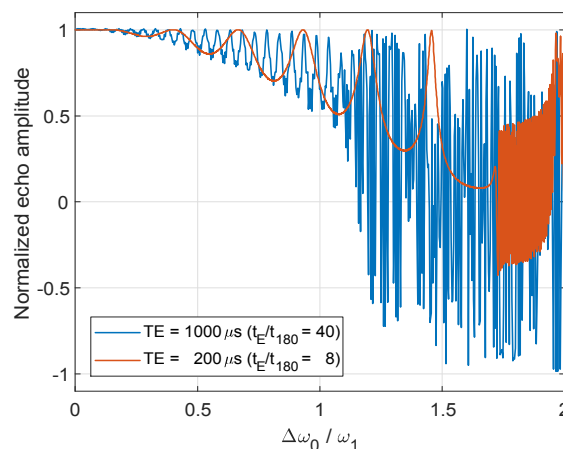
NMR relaxometry using the Carr-Purcell-Meiboom-Gill (CPMG) sequence or its variants is widely used due to its robustness and modest requirement on magnetic field homogeneity. However, variations of the magnetic field during a CPMG measurement introduces signal loss that complicates the quantitative evaluation of sample properties. This effect can be pronounced in NMR well logging where the tool typically moves at a speed of up to 240 m/h or 6.7 cm/s. Tool motion along the magnetic field gradient introduces a fluctuating field for the spins. Consequently, the effective rotation [1] for each CPMG cycle of  $\tau - (\pi)_\phi - \tau$  will change as a function of time, both in the direction of the axis and the rotation angle. Therefore, it is crucial to understand the behavior of nuclear spins under time varying magnetic field for quantitative CPMG measurements.

In this study, we aim to characterize the effect of net relative displacement (i.e. macroscopic motion rather than diffusion) on a CPMG-like measurement in grossly inhomogeneous magnetic fields. We show that the robustness of a given sequence is determined by how well the magnetization can track the effective rotation axis in an adiabatic sense. The initial signal decay introduced by motion is determined mostly by the overlap of the excited region and the detected region (which is typically 10 ~ 20 cm for the NMR well logging tools). At certain critical off-resonance values, the direction of the effective rotation axis swings rapidly. Close to these points, the effective rotation angle goes to zero and the eigenvalues of the rotation matrix are degenerate. At these points, adiabatic tracking becomes effectively impossible, no matter how slow the motion is or how close the echo spacing is. This prevents the refocusing of the echo after exceeding this critical off-resonance value (Figure 1). The result of this study provides a guideline to design magnetic fields for given operating conditions.

### References:

[1]. M. D. Hürlimann and D. D. Griffin, JMR 143 (2000), 120-135.

Fig. 1. Effect of a linear motion on spins in a single voxel. All echo amplitudes would be equal to one in the absence of motion as there is no relaxation process incorporated in the model. At the beginning of the CPMG, the spins are exactly on resonance, and are optimally excited by the initial 90 degree pulse. During subsequent echo formations, the spins are exposed to the  $B_0$  field changing at a rate of 16 G/s. For small enough frequency offset  $\Delta\omega_0$ , the echo amplitudes change in an orderly, reversible manner. Once  $\Delta\omega_0$  exceeds a certain offset that is determined by  $B_1$ , the refocusing pulses are no longer effective and echo amplitudes fluctuate chaotically, and the signal is irreversibly lost. The effect is more pronounced with a large  $t_E/t_{180}$  ratio.



**Preliminary studies on the signal from water sprays using MRI and unilateral NMR**

S. Iyengar and I. Mastikhin<sup>\*§</sup>, University of New Brunswick.

Magnetic resonance experiments have features that are amenable to measuring sprays: unlike optical techniques MRI and NMR acquire information about the entire spray region, as opposed to light which is vulnerable to reflection off the outside of the spray. We measured the signal from a water spray with two different experimental setups to see how NMR signal from water droplets is affected as it transitions into a sub-zero environment. Cold water was sprayed through resonant probes alongside cold nitrogen gas flow with the intention of bringing the droplets towards a frozen state. By saturating the magnetisation of stationary water and the plastic tube, signal from the spray was isolated and examined as temperature in the probe sensitive region dropped. In the first setup a 2.4 Tesla magnet was used, and images were acquired from a 12-centimeter region with a modified SPI sequence. Integrated signal from the center of the probe, where spray is located, was compared to the integrated signal from saturated water in the images. The second setup involved a similar procedure with an 1100 Gauss unilateral NMR instrument, where the CPMG spray signal was analyzed. A second, larger magnet was used to polarise the water before entering the probe to improve signal-to-noise of the low-density sample, leading to a detectable spray signal. The results of these experiments demonstrate that the freezing behaviour of sprays can be examined via MR techniques, and the unilateral NMR measurement demonstrates that, in principle, spray measurements can be done with low-cost, mobile NMR instruments.

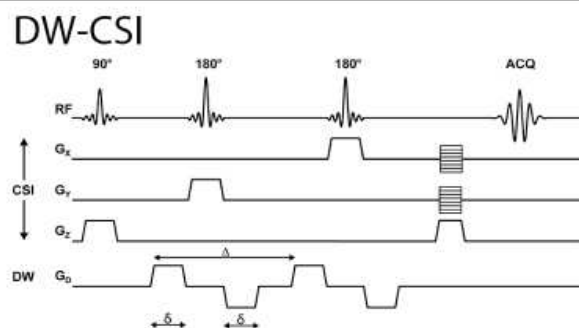
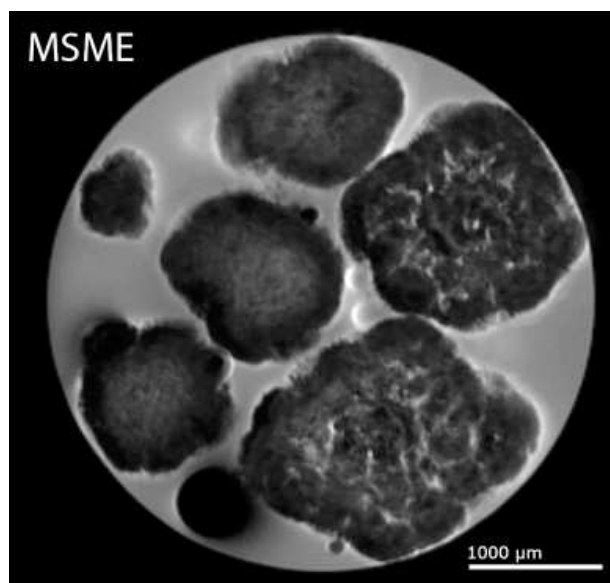
## Non-invasive Magnetic Resonance Imaging of Oils at Ultra High Field in Algae: Chemical Shift Selective and Diffusion Weighted Imaging

R. van Schadewijk, K.B. Sai Sankar Guptra, H.J.M. de Groot and A. Alia<sup>\*§a,b</sup>, <sup>a</sup>Leiden University, Solid-state NMR, The Netherlands; T. van den Berg and R. Croce, VU University Amsterdam, Biophysics of Photosynthesis, The Netherlands; <sup>b</sup>Leipzig University, Institute for Medical Physics and Biophysics, Germany; I. Ronen, Leiden University Medical Centre, Radiology Department, The Netherlands.

We have optimized MR imaging and spectroscopic sequences for 17.6T and 22T to provide in-vivo methods to investigate oil producing green algae (*B. braunii*) Green algae have interested researchers in the biofuels for a long time, especially oleaginous species that can contain significant quantities of oil, such the colony forming species *B. braunii*. However a lack of suitable in vivo methods can make studying green algae difficult.

To study these properties in biological samples in high detail, several imaging sequences including MSME and FLASH have been optimized for ultra-high magnetic field (17.6T and 22T). Birdcage type 5mm volume coils and a solenoid 1000um microcoil were used and advantages and disadvantages will be reviewed. Strategies for dealing with short T2 and local field inhomogeneity caused by magnetic susceptibility will be discussed. Due to the increased spectral separation of oil/fat and water at ultra-high-field, sequences employing fat suppression are less than optimal. Our findings indicate better results can be attained with chemical shift selective techniques when mapping the distribution oil and water in live samples.

Techniques to be covered include Chemical Shift Imaging (CSI), Chemical Shift Selective imaging (CHESS) and Diffusion Weighted Imaging (DWI and DW-CSI) on Ultra-High field in relation to *B. braunii* colonies.



## Capillary Trapping Quantification in Sandstones using NMR Relaxometry

P. R. J. Connolly, S. J. Vogt, E. F. May and M. L. Johns<sup>\*S</sup>, School of Mechanical and Chemical Engineering M050, The University Of Western Australia, 35 Stirling Highway, Crawley WA 6009, Australia; S. Iglauer, Department of Petroleum Engineering, Curtin University, 6151 Kensington, Western Australia, Australia.

Capillary trapping of a non-wetting phase arising from two-phase immiscible flow in sedimentary rocks is critical to many geoscience scenarios, including oil and gas recovery, aquifer recharge and, with increasing interest, carbon sequestration. Critical to quantifying capillary trapping during sequestration is the relatively poorly understood physio-chemical phenomenon of wettability, and how this changes in the presence of supercritical or liquid CO<sub>2</sub>. Here we deploy Nuclear Magnetic Resonance (NMR)  $T_2$  relaxometry to elucidate the pore occupation characteristics of cyclic supercritical CO<sub>2</sub> and N<sub>2</sub> imbibition and drainage processes in a range of rock cores at reservoir conditions, and in the process quantify their respective capillary trapping.

Initially we systematically confirm the relationship between  $T_2$  and pore size by quantifying inter-pore magnetic field gradients due to magnetic susceptibility contrast, and demonstrate that our measurements at all water saturations are relatively unaffected. Diffusion in such field gradients can potentially severely distort the  $T_2$ -pore size relationship, rendering it unusable. Furthermore, it was found that geochemical reactions induced by the presence of CO<sub>2</sub> occur on timescales similar to typical core flooding experiments, which due to the dissolution of paramagnetic ions can reduce bulk fluid  $T_2$  properties appreciably and hence distort the  $T_2$ -pore size relationship. A method of brine 'ageing' was developed which was able to mitigate against this effect.

Sample water  $T_2$  distributions results are shown in the figure below for a single drainage/imbibition cycle for nitrogen/water and CO<sub>2</sub>/brine respectively in a Berea sandstone rock core. In all cases, drainage results in preferential water displacement from larger pores, consistent with a water-wet system. Subsequently imbibition resulted predominately in water re-introduction to the smallest pores available, although this effect was more evident for N<sub>2</sub> than for CO<sub>2</sub>. The amount of consequently residually trapped nitrogen and CO<sub>2</sub> observed was comparable to core flooding data in literature and could be adequately described by the Land Model. Trapping efficiency was observed to increase slightly with repeated imbibition/drainage cycles.

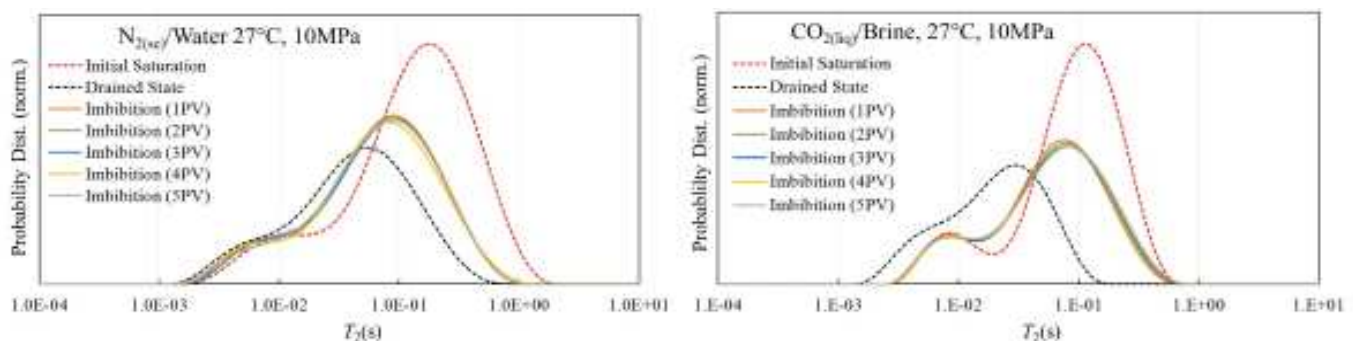


Figure 1 –  $T_2$  distributions of Berea in residual (drained), imbibed and initial saturation states for a) nitrogen/water and b) CO<sub>2</sub>/brine fluid pairs. Distributions are normalized to signal intensity. PV – Pore Volume

## Wet Front Penetration under Unsteady State Wicking and Evaporation in Mortar by Magnetic Resonance Imaging (MRI)

R. Enjilela\* and P. Cano-Barrita<sup>a,b</sup>, <sup>a</sup>Department of Physics, MRI Center, University of New Brunswick, Fredericton, New Brunswick, Canada; <sup>b</sup>, Instituto Politecnico Nacional-CIIDIR Unidad Oaxaca, Oaxaca, Mexico, ; A. Komar and A. J Boyd, , Department of Civil Engineering and Applied Mechanics, McGill University, Montreal, Canada.

The movement of water or water carrying aggressive ions is one of the leading causes of deterioration of concrete structures worldwide. Moisture profiles during water absorption were determined by one dimensional Centric Scan SPRITE MRI [1] in 10 cm mortar specimens under unsteady state wicking and evaporation. Bulk FID and  $T_2^*$  mapping results show a bi-exponential behavior of the MR signal lifetime  $T_2^*$  in all samples, indicating at least two different water populations [2]. The short  $T_2^*$  lifetime, assigned to interlayer water, and its associated amplitude are constant along the sample. The long  $T_2^*$  lifetime, related to water in the pore space, and its associated amplitude change with local moisture content (Fig.1). The wet front was displaced faster into samples with higher w/c ratios. Gravimetric sorptivity measurements show two regimes of water absorption. The two regimes are thought to be related to differences water transport through the pore spaces. In related samples early time capillary absorption is the dominant transport mechanism, whereas at later times ingress of water is also controlled by diffusion-based transport mechanisms [3]. Water front penetration observed with the SPRITE technique, and bulk FID measurement showed a transition in behavior at a similar experimental time to the sorptivity measures. Inverse modeling was conducted to extract transport properties, using the Hydrus program, with moisture content profiles.

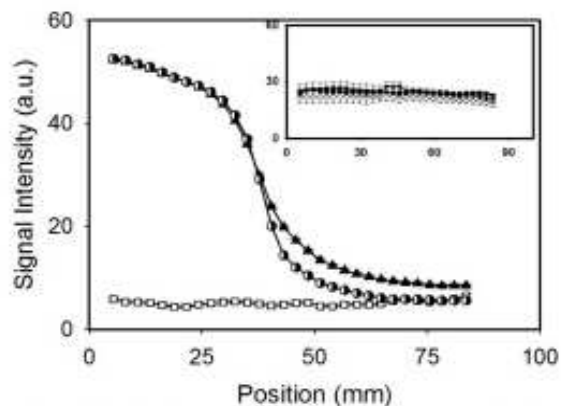


Figure 1. The signal intensity of long  $T_2^*$  lifetime, associated with water content in pore spaces varies with position for mortar w/c = 0.45 of (empty square) nominally dry sample, (semi-filled circle) 30 days, (up triangle) 110 days. The signal intensity of short  $T_2^*$  lifetime, associated with interlayer water, is essentially constant along the sample, (filled square) nominally dry sample, (empty diamond) 30 days, (triangle) 110 days (inset plot).

### References

- [1]. Halse M., Goodyear D. J, MacMillan B., et al (2003). J Magn Reson 165:219–229.
- [2]. Enjilela R., Cano-Barrita P., et al (2017). J Mater Struct 50:151-163.
- [3]. Martys N. S, Ferraris C. F (1997). Cem Concr Res 27:747–760.



## A Continuous Wave Magnetic Resonance Disruption (CW-MaRDi) Technique for the Detection of Magnetic Nanoparticles

S.T. Parslow, M.I. Newton and R.H. Morris<sup>\*§</sup>, Nottingham Trent University, School of Science and Technology, Clifton Lane, Nottingham. NG11 8NS, UK.

Magnetic NanoParticles (MNP), detected by Magnetic Resonance have been used at the heart of a number of devices where the number of MNPs is proportional to the analyte of interest<sup>1</sup>. The systems typically used to measure such surfaces are both complex and expensive which provides significant barriers to market such devices as Point of Care systems. We present a general measurement technique to quantify such assays: Magnetic Resonance Disruption (MaRDi). From previous work incorporating permanent magnet systems and pulsed NMR electronics, it has been shown that the presence of immobilised MNP reduces the echo integral of a fluid placed on top of such immobilised particles<sup>2</sup>.

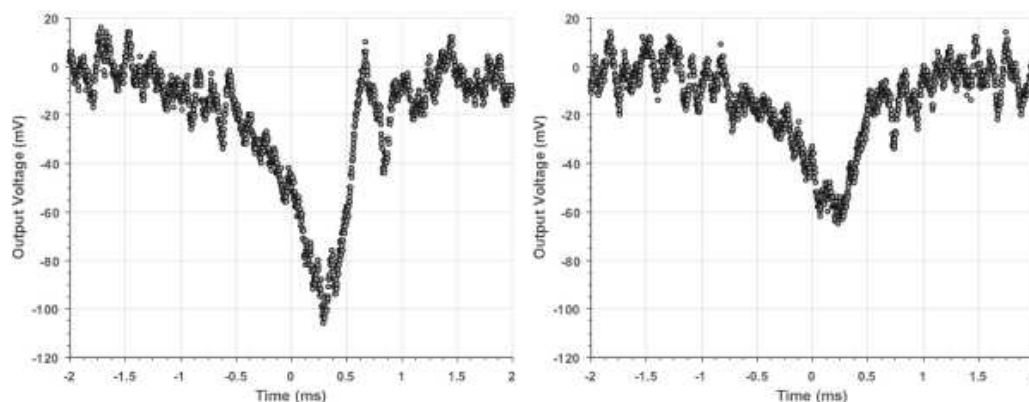
Conceptually simpler, but used far less widely, continuous wave (CW) NMR offers a cost-effective approach to performing MaRDi. Although CW-NMR was first used to demonstrate the phenomenon of nuclear magnetic resonance it has virtually been consigned to the undergraduate laboratory and magnetometers as it is more challenging to reliably determine relaxation parameters compared to pulsed NMR. The equipment required to perform CW-NMR is however significantly less complex and therefore expensive, than that required for pulsed measurements. In this work, we demonstrate proof of principle with a commercial CW-NMR system produced by Leybold-Didactic (Hürth, Germany).

2.8 $\mu$ m diameter avidin coated MNP (M-280 Dynabeads, Thermo Fisher Scientific, Waltham, MA, USA) were immobilised to the surface of biotin coated polystyrene wells (Thermo Fisher Scientific). A 6 $\mu$ L coating of oil was applied and the sample placed inside the commercial CW-NMR system. Analysing the resultant absorption curves we demonstrate a 46% change in peak-to-peak voltage from the addition of 10,000 $\pm$ 1,000 immobilised MNP (Fig. 1). We go on to demonstrate the sensitivity to MNP as a function of binding area and concentration and investigate the influence of particle type and size on the resulting CW-NMR signal. It is likely that the properties of MNP which are optimised for pulsed NMR will not be optimum for CW-NMR and thus extensive characterisation is required before we move towards the development of an affordable, fully automated system capable of rapid and quantitative analysis of MNP concentration suitable for PoC diagnosis.

(1) J. B. Haun, et. al. WIREs Nanomedicine and Nanobiotechnology 2 (2010) 291-304. DOI: 10.1002/wnan.84

(2) S.T.Parslow, et. al. Analytical Methods 9 (2017) 1681-1683 DOI: 10.1039/C7AY00039A

Figure 1: (Left) The absorption curve from 6 $\mu$ L of oil. (Right) The absorption curve from 6 $\mu$ L of oil with the addition of  $\sim$ 10,000 immobilised 2.8 $\mu$ m MNP.



## GPU-optimized 3D fast MRI simulator for non-Cartesian sampling

R. Kose\*, MRTechnology Inc; A Setoi and K Kose<sup>§</sup>, Institute of Applied Physics, University of Tsukuba.

### Introduction

Non-Cartesian (NC) sampling is widely used for advanced imaging such as ultrashort echo-time imaging, compressed sensing, and MR Fingerprinting. In such NC sampling sequences, because the k-space trajectories are usually complicated, effects of system imperfections on the MR images are difficult to understand and analyze. To solve this problem, it is indispensable to simulate the imaging process using the isochromats. In this study, we developed a GPU-optimized 3D fast MRI simulator for NC-sampling.

### Materials and Methods

The MRI simulator was developed based on BlochSolver [1], which was developed for Cartesian sampling. To evaluate the performance and usefulness of the simulator, we performed MRI simulation using a numerical phantom and 3D cones trajectory [2] as shown in Figs.1 and 2. The 3D cones trajectories were designed by combinations of spiral and radial trajectories. The cone angle of the trajectory was varied from 0 to  $\pi$  by 128 equally spaced steps, and one shot scan was used for the signal sampling. The sampling intervals were changed from 5 to 20  $\mu$ s.

### Results and Discussion

Figures 3(a)-(c) show 2D cross-sections selected from 3D image datasets acquired with 5, 10, and 20  $\mu$ s sampling intervals. Because gridding was performed using nearest neighbor points, these images show that finer signal sampling is better for the reconstruction. When the sampling interval was 5 s, the calculation time for the whole k-space data with  $2 \times 2 \times 2$  subvoxels was about 66 s using a single GTX 1070 board, which are comparable to that for Cartesian sampling (48 s) with  $128^3$  k-space data and identical number of subvoxels. Figures 3(d) and (e) are 2D cross-sections selected from 3D image datasets acquired with 5  $\mu$ s sampling intervals under field offset (10 Hz) and inhomogeneous magnetic field. These images clearly show usefulness of our simulator.

### References

[1] Kose R, Kose K, JMR 2017; **281**:165. [2] Gurney PT et al. MRM 2006; **55**:575582.

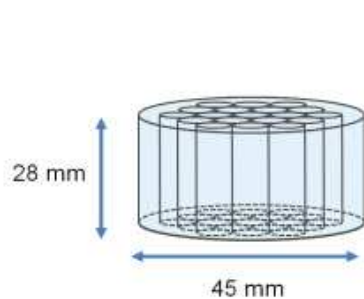


Fig. 1. Numerical phantom in  $(64 \text{ mm})^3$  FOV.

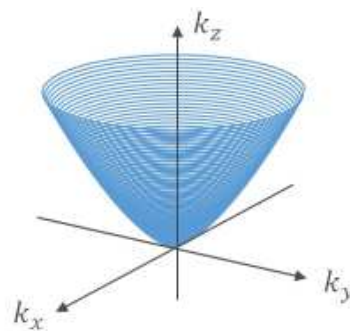


Fig. 2. One of the k-space trajectory.

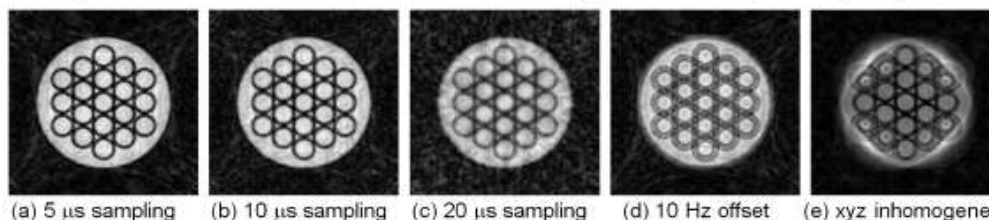


Fig. 3. (a)-(c): 2D cross-sections selected from 3D image datasets acquired with 5, 10, and 20  $\mu$ s sampling intervals. (d) and (e): 2D cross-sections selected from 3D image datasets acquired with 5  $\mu$ s sampling intervals under 10 Hz field offset and spatial inhomogeneity proportional to  $xyz$ .

## Ultrashort echo-time imaging at 1.5 T using insertable gradient coil sets and 3D cones trajectory

A. Seto<sup>1</sup> and K. Kose, Institute of Applied Physics, University of Tsukuba.

### Introduction

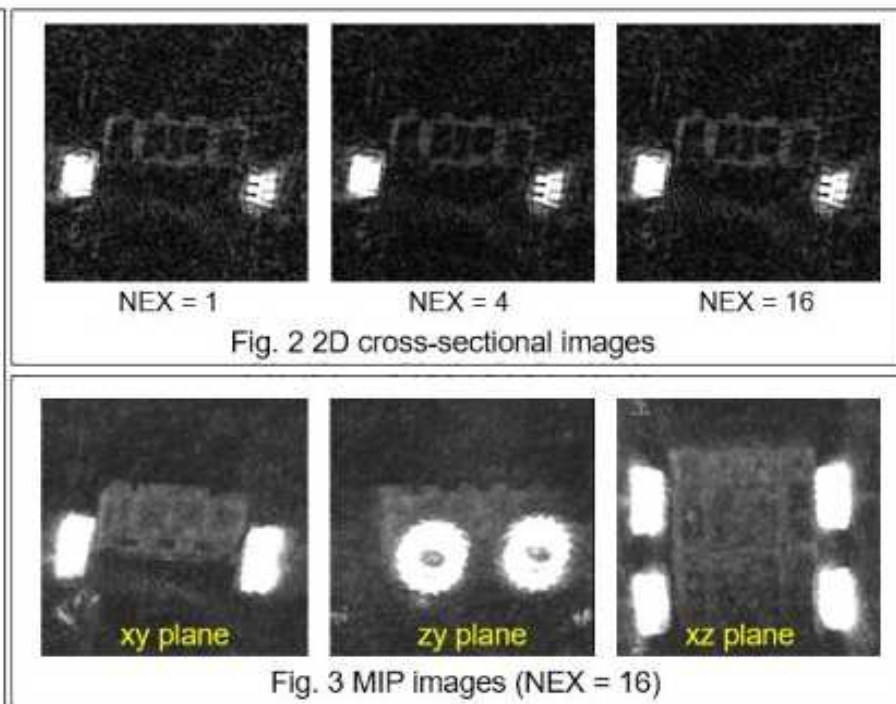
Ultrashort echo time (UTE) imaging is widely used for short  $T_2$  or  $T_2^*$  materials. UTE imaging using 3D cones trajectory has several advantages over 3D radial imaging such as data collection efficiency and flexible trajectory design. However it is difficult to control gradient waveforms and sensitive to magnetic field inhomogeneity. In this study, we developed UTE imaging for a small-bore 1.5 T MRI system using 3D cones trajectory to demonstrate its usefulness for short  $T_2$  materials.

### Material and Methods

We used a home-built compact MRI system consisting of a 1.5 T and 280 mm diameter horizontal bore superconducting magnet, a second-order shim coil, an unshielded gradient coil, an RF coil, and a digital MRI console. Cones trajectory for 3D image acquisition was developed by combining spiral and radial trajectory. The polar angle from z direction was equally divided into 128. The number of shots per cone was 64. TR and TE were 200 and 0.15 ms and the flip angle was  $90^\circ$ . The FOV was  $(64.0 \text{ mm})^3$  and image matrix was  $128^3$ . We used a solid sample consisted of LEGO blocks as shown in Fig.1.

### Results and Discussion

2D cross-sections selected from 3D image datasets of the solid sample acquired with 3D cones trajectory are shown in Fig. 2. Figure 3 shows MIP images acquired with the cones trajectory with NEX = 16. As shown in Figs.2 and 3, the rubber tires showed high image intensity, colored LEGO blocks showed low intensity, and transparent LEGO blocks showed no signal. This is because  $T_2$  of the rubber was about 8 ms,  $T_2^*$  of the colored blocks (supposed to be ABS resin) was about 0.6 ms, and  $T_2$  of the transparent block (supposed to be acrylic resin) was very short. In conclusion, 3D UTE imaging using 3D cones trajectory is useful for 3D MRI of solid-like materials.



## A portable MRI scanner for human brain imaging using an optimized rotating Halbach magnet

C.Z. Cooley\*, J.P. Stockmann, P.C. McDaniel, M.W. Haskell, S.F. Cauley, C. Sappo, C.G. Ha, T. Witzel, C.E. Vaughn and L.L. Wald<sup>§</sup>, A. A. Martinos Center for Biomedical Imaging, Dept. of Radiology, Massachusetts General Hospital, Charlestown, MA, USA.

While MRI is the gold-standard for human brain imaging, the cost, weight, and power requirements of traditional scanners vastly limit the accessibility of the technology. To address this, we introduced a low-cost portable MRI scanner architecture that could facilitate imaging in untraditional sites, like rural clinics, ambulances or a patient's bedside [1]. To enable this, we designed a lightweight, head-only, permanent magnet (fig. 1a).

The magnet size and shape were greatly reduced by allowing the field be low-field ( $< 100\text{mT}$ ) and inhomogeneous. Instead of being viewed as a nuisance, the field variation of the inhomogeneous magnet is leveraged as the MRI spatial encoding magnetic (SEM) field instead of added electromagnetic gradient coil hardware. This built-in encoding field is modulated by mechanical rotation of the magnet, while generalized

projections of the object onto the SEM are acquired in the form of a spin-echo train. To reconstruct images, a general forward model approach is taken, in which an encoding matrix is calculated that relates the image to the data. The image is then estimated using a conjugate gradient method. Although, arbitrary non-linear SEMs can be used to form an image, this results in non-uniform resolution in the image [2], [3]. In addition, spatial extrema in the SEM cause zero gradient areas or "encoding holes" that result in severe image artifacts from small encoding matrix calibration errors. To address this, we designed a Halbach cylinder magnet, made up of an optimized distribution of NdFeB magnet cubes that produces a SEM with a roughly linear field shape. The resulting human head-only magnet weighs 122 kg with a 29 cm bore access (Fig. 1b). Fig. 1c shows the resulting axial field map at iso-center, which is non-linear but contains a dominant 1st order term. This optimized magnet enables 2D imaging with fairly uniform resolution, as demonstrated by the lemon slice image in Fig. 1d.

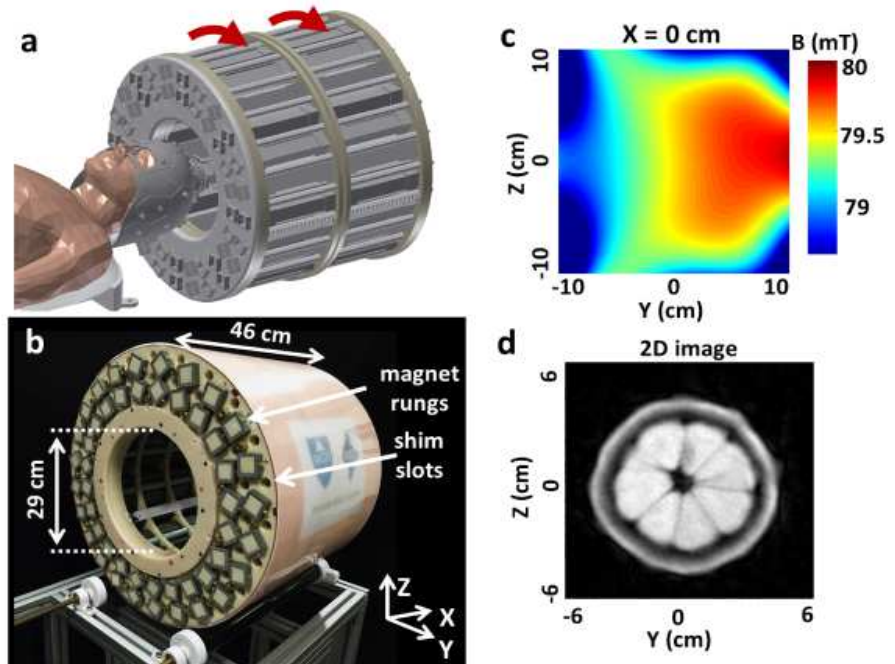


Figure 1: a) CAD model of rotating Halbach magnet with patient for portable MRI scanner. b) Photo of optimized human-size dipole Halbach magnet. c) Measured field map (Y-Z plane) at X = 0 cm. d) 2D image of 1 cm slice of lemon using portable MRI scanner.

- [1]C. Z. Cooley et al., Magn. Reson. Med., 2015.  
 [2]J. Hennig et al., Magn Reson Mater Phy, 2008.  
 [3]J. P. Stockmann, et al., Magn Reson Med, 2010.



**BLIPPED (BLipped Pure Phase EncoDing) High Resolution MRI**

D. Xiao<sup>a,b</sup> and B. J. Balcom, <sup>a</sup>MRI Research Center, Department of Physics, University of New Brunswick, Canada; <sup>b</sup>Department of Physics, University of Windsor, Canada.

MRI image resolution is proportional to the maximum  $k$ -space value, i.e. the time integral of magnetic field gradient. High resolution imaging usually requires high gradient amplitudes and/or longer spatial encoding times. Special gradient coils are often required for high amplitudes and fast switching. We propose a high resolution imaging sequence that employs low amplitude gradients.

This method was inspired by the previously proposed PEPI sequence [1], which replaced the EPI gradient reversals with multiple RF refocusing pulses. It has been shown that when the refocusing RF pulse is of high quality, i.e. sufficiently close to  $180^\circ$ , the phase of magnetization introduced by the spatial encoding magnetic field gradient can be preserved and transferred to the following echo signal without phase rewinding gradients. This phase encoding scheme requires blipped gradients that are identical for each echo, with low and constant amplitude, providing opportunities for high resolution imaging. We now extend the sequence to 3D pure phase encoding with low gradient amplitudes.

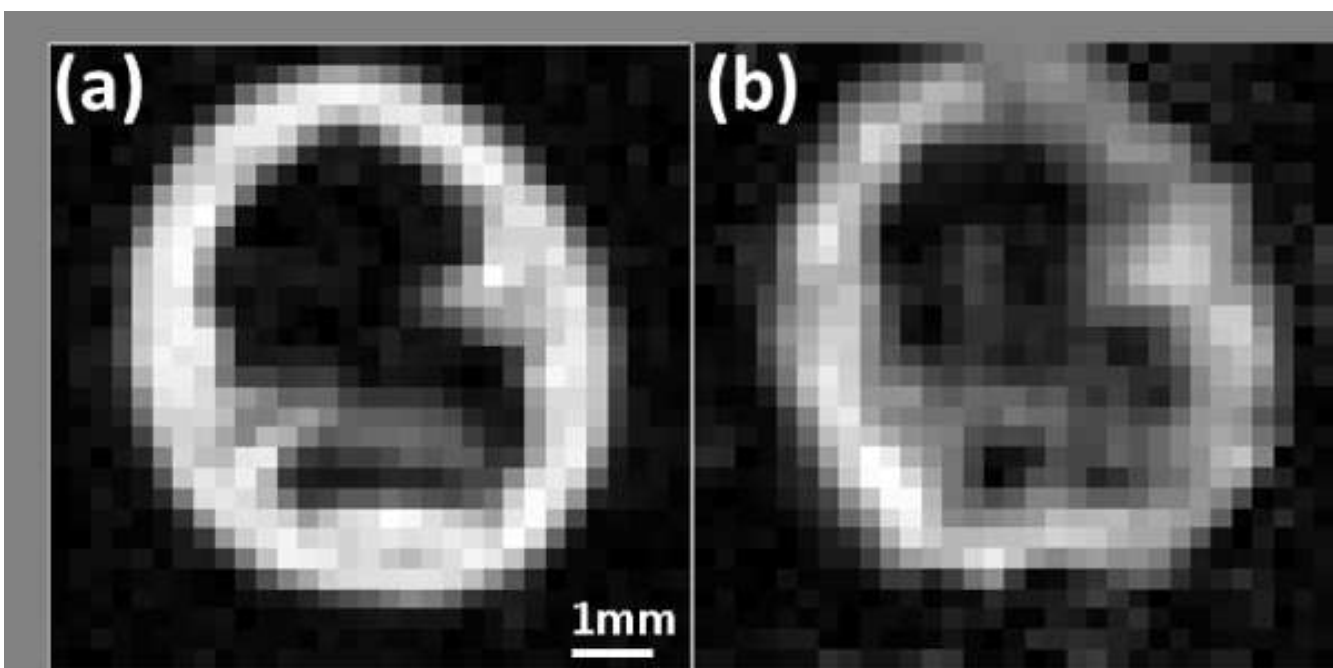
The method was compared with the hybrid-SESPI [2] technique to demonstrate the advantages in terms of low gradient duty cycle, negligible eddy current effects and minimal echo spacing, which lead to superior image quality and high resolution. The 3D imaging method was then applied on a parallel plate resonator [3], achieving a spatial resolution on the order of ten microns.

[1] D. Xiao, B. J. Balcom, echo-planar imaging with concomitant field compensation for porous media MRI. *JMR* 260, 38-45 (2015)

[2] L. Li, H. Han, B. J. Balcom, Spin echo SPI methods for quantitative analysis of fluids in porous media. *JMR* 198, 252-260 (2009)

[3] J. Zhang, B. J. Balcom, Parallel-plate RF resonator imaging of chemical shift resolved capillary flow. *MRI* 28, 826-833 (2010)

Figure 1. 2D slices of 3D images acquired with (a) BLIPPED and (b) hybrid-SESPI. The sample was a section of a red Thai pepper. The nominal image resolution was  $250 \mu\text{m}^3$ .



**Systematic Image Alteration due to Phase Accumulation during RF Pulse Excitation in Pure Phase Encode MRI**

T. McDonald, B. MacMillan, B. Newling and [B. J. Balcom](#)<sup>\*</sup>, UNB MRI Centre, Department of Physics, The University of New Brunswick.

The SPI/SPRITE class of techniques in magnetic resonance imaging are pure phase encode methods that are well established for systems with short transverse signal lifetimes. Applying a broadband radiofrequency pulse in the presence of a magnetic field gradient is unconventional in MRI but fundamental to these methods. Ordinarily it is assumed that the excitation is instantaneous and any possible phase evolution during the RF pulse is ignored. High quality, quantitative imaging of a variety of samples over many years suggests that the off-resonance effects of the RF pulse, with consequent phase accumulation during the pulse, are not significant. However, a reconsideration of the RF pulse behaviour in related work has shown that phase accumulation during the pulse may be non-negligible in some circumstances.

The effect of phase accumulation during the RF pulse is investigated through simulation of one-dimensional SPI experiments and is shown to manifest as a systematic scaling of the image field of view. The field of view scaling effect is also verified experimentally. One-dimensional profiles of a cylindrical elastomer sample were acquired employing a 2.4 T horizontal bore magnet. Experiments were undertaken with variation of the experimental RF pulse duration. Under typical experimental parameters, neglecting the phase accumulation during the RF pulse is acceptable.



## Fast Spectroscopic Imaging with RARE-Type Acceleration

S. Benders\* and B. Blümich<sup>§</sup>, Institut für Technische Chemie, RWTH Aachen University, 52074 Aachen Germany.

Apart from relaxation and spin density contrast, it is of interest to include chemical information in images. Classical chemical-shift imaging [1] suffers from long experimental times as well as from low resolution. There have been approaches to access chemical information with different methods not requiring full phase encoding [2], but these methods often comprise difficult reconstructions. Here, a RARE-type acceleration to a pure phase-encoded chemical-shift imaging sequence is presented. Accelerations of a factor up to 32 are feasible while maintaining the possibility of identifying many species due to their different chemical shifts. Requirements for the application of this approach are good field homogeneity, sufficient dispersion of the chemical shift, and long, yet similar  $T_2$  times of the components. The sequence has been both tested on phantoms and applied to pork skin.

- [1] P.C. Lauterbur, D. M. Kramer, W. V. House, C.-N. Chen, J. Am. Chem. Soc. 97 (1975) 6866-6868.  
 [2] R.V. Mulkern, L. P. Panych, Concepts Magn. Res., 13 (2001) 213-237.

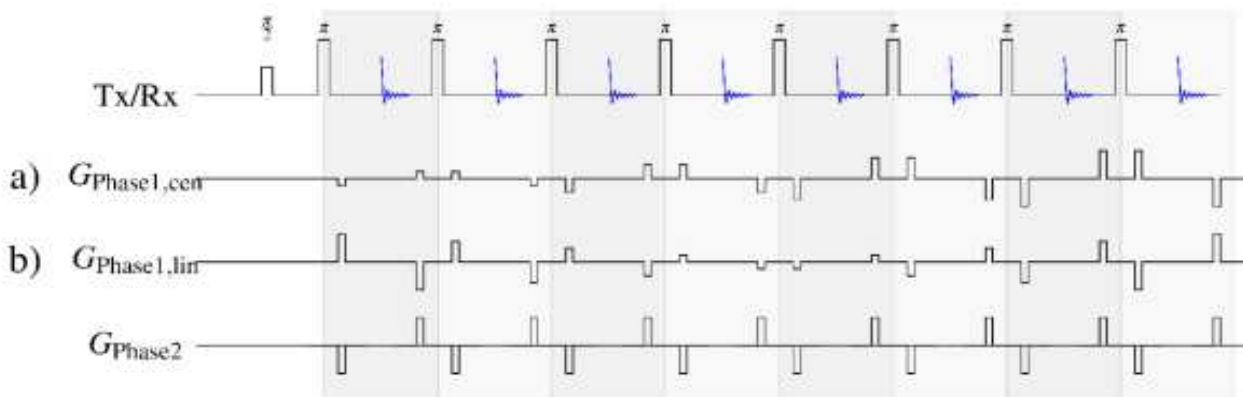


**Figure 1:** CSIRARE Sequence. Phase<sub>1</sub>-direction is encoded in a RARE-like manner with a) centric encoding and b) linear encoding. The gradient amplitude in Phase<sub>2</sub>-direction is changed between experiments.

## Ultra-short Echo (UTE) Imaging of T2 in Calcified Cartilage at Microscopic Resolution

F. Badar and Y. Xia\*, Department of Physics and , Center for Biomedical Research., Oakland University, , Rochester, MI, United States; N. Wang, Center for In Vivo Microscopy, Duke University Medical Center.

**Introduction:** Articular cartilage (AC) is a heterogeneous and load-bearing tissue in joints. Based on the collagen fiber orientation, the non-calcified cartilage is commonly subdivided into three histological zones: the superficial zone (SZ) where the fibers are parallel to surface, the transitional zone (TZ) where the fibers are oriented randomly, and the radial zone (RZ) where the fibers are perpendicular to the surface. Between the non-calcified cartilage and the subchondral bone, there is a thin layer of calcified cartilage (CC), which serves as the structural interface. CC can be damaged in traumatic situation such as sport or battlefield injuries, which accelerates the progression of cartilage degradation that eventually leads to osteoarthritis. Since CC has very short T2, it is commonly invisible in MRI relaxometry measurements (1). Ultra-short echo time (UTE) imaging sequence has the potential to measure T2 as low as one or a fraction of one ms (2).

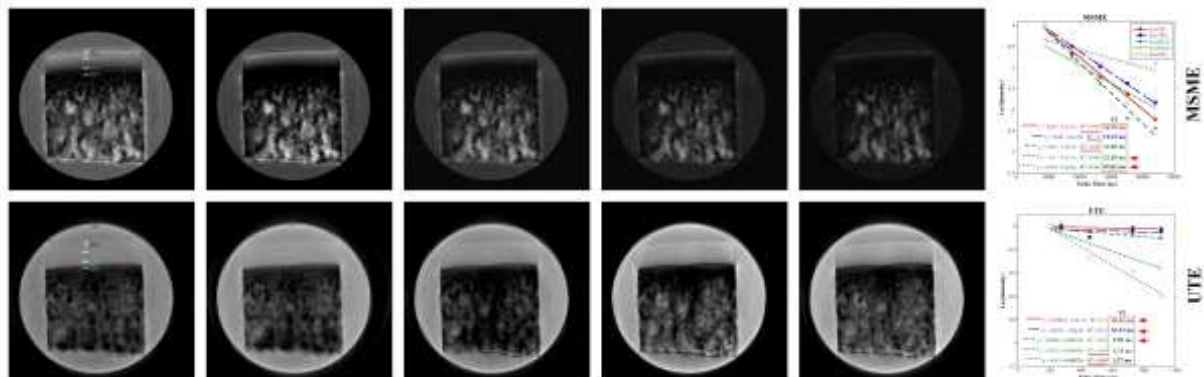
**Material and Methods:** Cartilage blocks from canine humeral head (~3x3x5 mm<sup>3</sup>) were imaged by using MSME and UTE (2D) sequences. A FOV of 5mm and a matrix size of 256x256 were used, which yielded approx. 25 $\mu$ m/pixel resolution. With TR of 100ms, average of 16 scans and a fixed receiver gain, 6 UTE images with echo times at 0.235, 0.3, 0.5, 0.6, and 1 were used for T2 measurements. In addition, a MSME sequence was used with similar geometry settings except with TR of 2000ms and multiple echo times of 8.8, 17.6, 26.4, 35.2 and 43.9ms.

**Results:** The proton maps of cartilage by MSME show the T2 decay of articular cartilage, affirming the heterogeneity of the tissue. Due to the short echo in UTE sequence, UTE images of cartilage have a homogenous appearance of the tissue with relatively constant intensity. A region of interest (colored boxes) was selected in each of the zones including the calcified cartilage region. The signal decay using both sequences are plotted and fit using the natural log fit. As shown on the plots, the MSME sequence at the long echo times give a good exponential fit in the SZ, TZ and RZ1, whereas RZ2 and CC show little change in the decay due to the strong dipolar interaction. UTE in the RZ2 and CC shows a good decay, which yielded a T2 of 1.37ms.

**Conclusions:** UTE can measure the characteristic T2 in the calcified cartilage region of the tissue; while MSME allows the measurement of tissue heterogeneity for most of the non-calcified tissue. It is anticipated that further development and optimization of UTE can capitalize its sensitivity to the calcified cartilage, providing sensitive information toward several specific degradation events in early arthritis.

**Acknowledgements:** The authors are grateful to the National Institutes of Health for the R01 grants (AR052353 and AR069047). The authors thank Dr. Dieter Gross and Saoussan Madi (Bruker, Germany) for helping with the UTE sequence. The authors thank Dr. Hani Sabbah (Henry Ford Hospital, Detroit) for providing the canine specimens.

**Reference:** (1) Magnetic Resonance in Medicine 2002, 48:460-69 (2) Osteoarthritis and Cartilage 2013, 21: 77-85



**X-ray  $\mu$ -CT and MRI of moisture in treated and non-treated wood - imaging the visible and invisible**

N. Nestle and A Sandor, BASF SE Advanced Materials and Systems, D-67056 Ludwigshafen, Germany; M Zlatic Zupanc and M Humar, University of Ljubljana, Biotechnical Faculty, Dept. of Wood Science and Technology Jamnikarjeva 101, 1000 Ljubljana, Slovenia; I Sersa and U Mikac, Jožef Stefan Institute, Jamova 39, 1000 Ljubljana, Slovenia.

Intrusion of liquid water into wood is one of the main reasons for degradation of wooden constructions. A range of different approaches have been developed to avoid or reduce water-induced degradation of wood including biocides, sealing surface treatments and non-sealing treatments with hydrophobic substances such as wax or oil. The latter approach avoids the use of hazardous substances and offers a better tolerance against local defects.

Further improving the performance of non sealing wood treatment with hydrophobic agents requires a better understanding of the spatial and temporal transport patterns of wood during water exposure and subsequent drying. Non-invasive imaging techniques such as MRI and X-ray  $\mu$ CT are especially helpful tools in this context.

Both techniques are complementary in the sense that MRI is especially sensitive to parts of the material containing mobile protons while X-ray  $\mu$ CT is also sensitive to rigid parts of the wood structure and comes with a spatial resolution about a factor of 10 higher than that achievable in MRI. On the other hand, recording of the full wood structure on this length scale results in more complicated images in which a simple separation between liquid and solid phases is less straight forward than in MRI.

In our contribution, we present data obtained on the same specimens of native, oil- and wax-treated wood by both MRI and X-ray  $\mu$ CT along with the experimental conditions used for water exposure and drying in both techniques. Advantages and limitations of both approaches are compared.

## Diffusion and relaxation profiling of skin layers in medical and skin care applications employing the low-field Fourier-MOUSE

J. Flohr<sup>\*</sup>, C. Rehorn, D. Jaschtschuk, M. Küppers and B. Blümich<sup>§</sup>, RWTH Aachen University, Institut für Technische und Makromolekulare Chemie, Worringerweg 2, 52074 Aachen, Germany; K. Borkowski, Jagiellonian University, Gobia 24, Kraków, Poland; K. Momot, Queensland University of Technology, School of Chemistry, Physics & Mechanical Engineering, Brisbane, Australia; C. Kuppe and J. Floege, Aachen University Hospital, Medical Clinic II, Aachen, Germany.

The skin is not only the biggest human organ<sup>[1]</sup> but also a very sensitive organ, which reflects the health and living conditions of a human. The appearance of the skin reveals the age, the physical but also the psychological conditions. Therefore, a whole industry is focused on the enhancement of the aesthetic appeal of the skin. In this study a low-field NMR tool, the Fourier-MOUSE<sup>®</sup>, was applied to get a deeper look into the diffusion and relaxation behavior of the human skin, as it is not yet fully understood. To show the applicability of the Fourier-MOUSE<sup>®</sup> in clinical trials the study not only focused on skin care applications but also on one specific medical topic - the skin properties of dialysis patients.

The Fourier-MOUSE<sup>®</sup> ( $B_0 = 0.4 \text{ T}$ ) is an improved version of the NMR-MOUSE<sup>®</sup>, which exhibits a higher magnetic field homogeneity due to 8 additional, movable magnets, the so called shim unit.<sup>[2]</sup> The sensitive volume encompasses about  $10 \times 10 \text{ mm}^2$ , a penetration depth of 2 mm, and a spatial resolution of  $50 \mu\text{m}$  is achieved. The measurement time can be drastically reduced due to the fact that only one single excitation is necessary to record a 2 mm depth profile by frequency encoding. For example, a  $T_2$ -profile through different skin layers takes about 45 seconds, which qualifies the Fourier-MOUSE<sup>®</sup> as a tool for clinical trials.<sup>[2]</sup>

[1] E. A. Grice, J. A. Segre, *Nat. Rev. Microbiol.* **2011**, 9, 244-253.

[2] M. Van Landeghem, E. Danieli, J. Perlo, B. Blümich, F. Casanova, *J. Magn. Reson.* **2012**, 215, 74-84.

The work was financed by The National Centre for Research and Development in Poland (contract No. STRATEGMED2/265761/10/NCBR/2015).

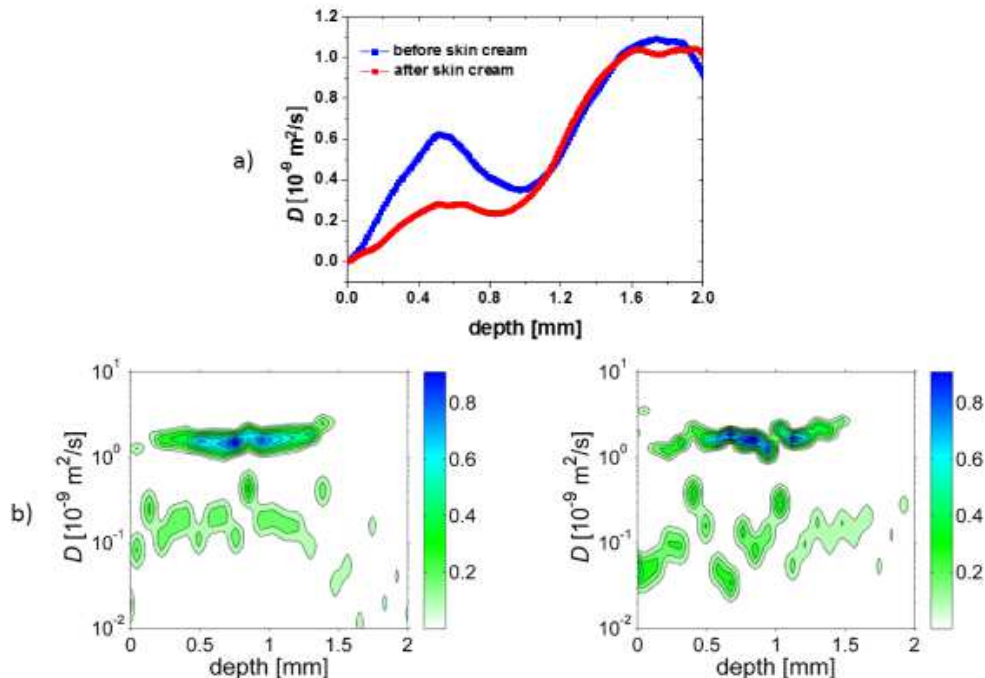


Figure 1: a) 1D-diffusion-profiles through the skin of the forearm before and after skin cream application. b) Diffusion coefficient maps of facial skin of two different volunteers.

## Highly efficient diffusion exchange spectroscopic imaging for biological applications

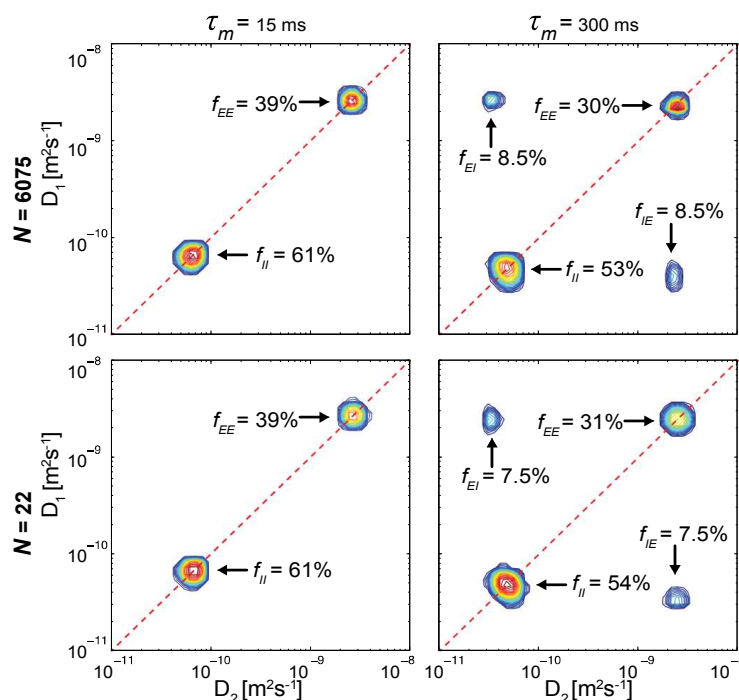
D. Benjamini\*, ME Komlosh<sup>a,b</sup> and PJ Basser<sup>s</sup>, <sup>a</sup>National Institutes of Health; <sup>b</sup>The Henry M. Jackson Foundation for the Advancement of Military Medicine.

Sensitive to local diffusive properties, diffusion exchange spectroscopy (DEXSY) is a powerful two-dimensional nuclear magnetic resonance (NMR) method for measuring the transport of water directly from one microenvironment to another, allowing for exchange processes between numerous compartments. DEXSY is, however, rarely used, especially when combined with magnetic resonance imaging (MRI) in biological applications, because of its exceptionally long scan time requirements.

Using the marginal distributions constrained optimization (MADCO) framework<sup>1</sup>, we present a method to vastly reduce the number of required acquisitions, making DEXSY-MRI feasible for the first time. Experiments are performed on a composite MRI nerve tissue phantom with restricted and free water exchanging compartments. We show that  $N=22$  acquisitions were sufficient to accurately determine the exchange spectrum at three mixing times; this number of acquisitions is  $\sim 276$  times less than what was previously thought to be needed ( $N=6075$ ). The presented framework allows one to add more mixing times at a low data requirement cost (i.e., four acquisitions per additional mixing time). Combined with a fast imaging readout, such as echo planar imaging (EPI), whole human brain imaging using 22 DEXSY acquisitions would take about 22 minutes, which is within the time frame of clinical MRI.

Regarding the diffusion exchange spectrum as a joint probability function and accordingly imposing constraints in the optimization process, provides the opportunity to reliably and feasibly obtain spatially resolved water exchange, as reflected by physical microscopic environments. Cell membrane permeability and active transport processes in healthy and diseased tissue are only partially understood, and currently cannot be directly measured noninvasively and *in vivo*, without imposed restricting assumptions. Fast DEXSY-MRI and NMR can now be beneficial for broad application for heterogeneous materials such as biological tissues, food, plants, and rocks, providing exciting opportunities for investigators in a range of disciplines.

<sup>1</sup>Benjamini D and Basser PJ. Use of marginal distributions constrained optimization (MADCO) for accelerated 2D MRI relaxometry and diffusometry. *J Magn Reson*, 271:40-45, 2016.



### Three-dimensional compressed sensing using two orthogonal readout gradients

D. Tamada\*, U. Motosugi and H. Onishi<sup>§</sup>, Department of Radiology, University of Yamanashi, Chuo, Yamanashi, 409-3898, Japan.

#### Background:

The compressed sensing (CS) enables fast MR imaging using the signal sparsity and randomness of sampling [1]. A Cartesian trajectory along one phase encoding (PE) direction (1D random trajectory) is generally used to achieve pseudo-random sampling. When a large reduction factor with 1D random trajectory is used, acquired MR images suffer from aliasing artifacts along the PE direction [2]. In this study, a three-dimensional random cross sampling (3D cross trajectory), which is achieved by using two orthogonal readout gradients, was proposed to reduce the aliasing artifacts for the compressed sensing.

#### Materials and Methods:

The 3D cross trajectory consists of two orthogonal 1D random trajectories. The sampling density for PE was determined by using the two-dimensional Gaussian function. A CS reconstruction algorithm was developed using the total variation regularized split Bregman method [3]. A phase distortion correction algorithm was used for the reconstruction [2]. Simulation studies were performed to evaluate the quality of MR images obtained using proposed method. Undersampling was simulated by extracting k-space data from fully sampled k-space datasets. The full datasets were acquired using three-dimensional SPGR sequences (TR/TE = 3.5/1.6 ms, FA = 9, FOV = 25×25 cm<sup>2</sup>. Matrix = 160×160×64) with two orthogonal 1D random trajectories. A 3.0 T clinical MRI scanner (MR750, GE Medical Systems, Milwaukee, Wisconsin, USA) and an MRI phantom filled with NiCl<sub>2</sub> was used. The conventional 1D random (R = 6.7) and the 3D cross (R = 6.7) trajectories were used for the CS reconstruction. The image quality was evaluated using Peak Signal to Noise Ratio (PSNR).

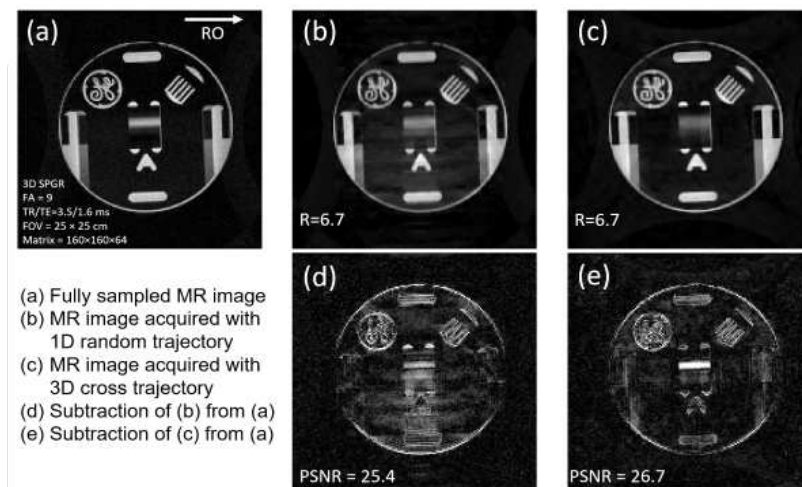
#### Results and Discussion:

Figure (a) shows the MR image reconstructed with the full datasets. Figures (b) and (c) show the CS reconstructed MR images acquired with the 1D random (PSNR = 25.4) and the 3D cross (PSNR = 26.7) trajectories, respectively. Figure (d) and (e) are the subtraction of Figure (b) and (c) from Figure (a), respectively. The MR image obtained with proposed method yields a higher PSNR and less aliasing artifacts compared to the MR image acquired with the 1D random trajectory.

In conclusion, the simulation studies demonstrated the CS reconstruction with the 3D cross trajectory enables fast MR imaging with less aliasing artifacts.

#### Reference:

- [1] Lustig, M., et al. (2007). Magn. Reson. Med., 58(6), 1182-1195.
- [2] Tamada, D., et al. (2014). IEEE Trans. Med. Imaging, 33(9), 1905-1912.
- [3] Goldstein, T., et al. (2009). SIAM J. Imaging Sci., 2(2), 323-343.





## Imperfections of Ultra-short Echo Time Imaging Sequence at Microscopic Resolution

F. Badar, R. Mahar, S. Batool and Y. Xia\*, Department of Physics and Center of Biomedical Research, Oakland University, Rochester, MI, United States.

**Introduction:** Ultra-short Echo (UTE) is a novel technique that is capable of having an echo time as short as a fraction of ms, which has shown its importance in many areas of material and biomedical research. For example, the calcified region of articular cartilage has very short T2s which are commonly invisible in standard imaging sequences (1,2). To facilitate a fast readout, the UTE imaging sequence commonly acquires data during the switching of imaging gradients and utilizes a radial trajectory in k-space.

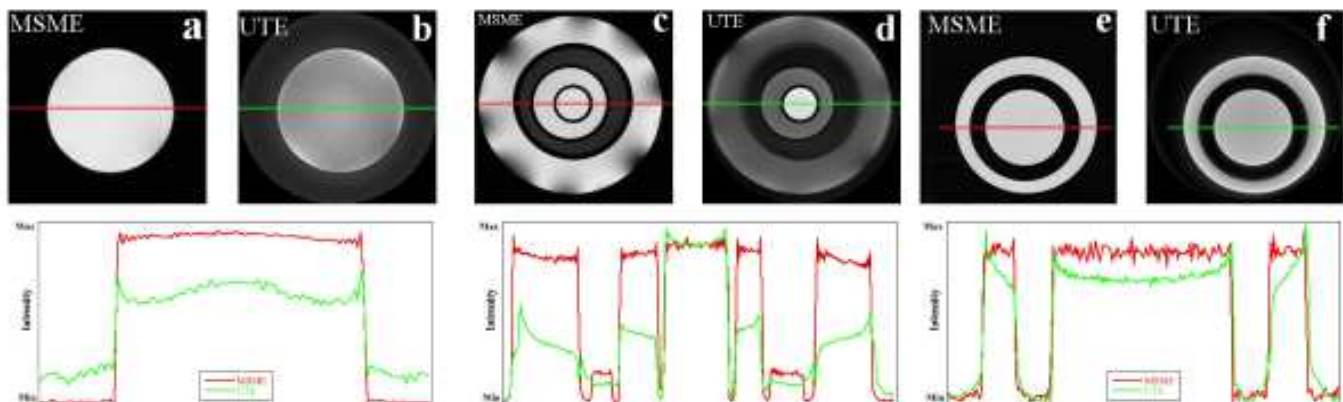
**Material and Methods:** Several phantoms were constructed by using deionized water and doped solutions (0.1% and 1% CuSO<sub>4</sub>) in different sized glass tubes (Wilmad, NJ). These phantoms were placed at the symmetrical center of the receiver coil. A 25mm Bruker vertical birdcage coil and a homemade 5mm horizontal solenoid coil were used to compare the images on a Bruker micro-imager, which has a 7T/9cm vertical bore magnet interfaced with an Avance II console running the Paravision 6.0.1 software. A Bruker UTE (2D) sequence was used, with a TR of 100ms, a shortest echo time (235  $\mu$ s), a bandwidth of 50Khz, and a slice thickness of 1mm. Precise trajectories were measured using for 2D UTE imaging. The same phantoms were also imaged by the MSME sequence (TR 500ms, TE 8ms, and similar matrix size and other settings).

**Results:** A uniform doped solution (CuSO<sub>4</sub>) in glass tubes was imaged using Bruker 25mm coil (a,b,c,d) and the 5mm homemade coil (e,f). The MSME images for the 5mm (solenoid) coil showed uniform signal intensity with the edges of the glass/solution interface showing a sharp edge. However, the UTE images showed a bright ring on the outside of the glass tubes where there is a glass/solution interface. The line profiles across the center of the image (phantoms) clearly show the signal variation and the differences between the MSME and UTE sequences. The inhomogeneity of the rf coil can also be seen between the 25mm Bruker coil (birdcage) and 5mm homemade coil (solenoid).

**Conclusion:** The bright ring shown around the outside edge of all inner rings implies that whenever there is a sudden drop of image intensity, the edge becomes brighter. The question is presented in the UTE imaging when an unknown sample is imaged, whether we can trust the intensity variations on the images as the artifact or true features of the sample. Additional work is in progress to investigate the source of these artifacts and potential improvement in the quality of the UTE images.

**Acknowledgement:** The authors are grateful to the National Institutes of Health for the R01 grants (AR052353 and AR069047). The authors thank Dr. Dieter Gross and Saoussan Madi (Bruker, Germany) for helping with the UTE sequence.

**Reference:** (1) Osteoarthritis and Cartilage 2011, 19:84-88 (2) Clinical Radiology 2004, 59: 720726



## Diffusion and relaxation time mapping of mice/rats with magnetic resonance fingerprinting

Y. Terada<sup>\*§</sup>, Institute of Applied Physics, University of Tsukuba; T Haishi, MRTechnology Inc.

Mice and rats have been widely used as disease models. Many efforts have been made to establish quantitative MRI assessments as biomarkers for detection and progression of the disease models, including quantitative imaging of relaxation times, proton density, perfusion, and diffusion. However, the standard quantification MRI methods mostly need a long scan time, and are subject to multiple sources of error, including motion artifacts, field inhomogeneity, and physiological changes due to extended periods of small animal's gas anesthesia. Therefore, new quantification methods for practical imaging application are needed that are immune to these error sources. A new MR fingerprinting (MRF) methodology [1,2] is a promising candidate. MRF employs a unique acquisition and post-processing strategy that enables multi-parametric imaging in a short measurement time. Here we developed an appropriate MRF acquisition and analysis methods for mapping relaxation times and diffusion coefficient of an anesthetized mouse and rat.

MRF with dual-echo steady states (MRF-DESS) with varying repetition time and flip angle was optimally implemented on a 1.5 T/280 mm horizontal bore SCM system. *In vivo* MRF images were acquired from the brains of an anesthetized mouse (C57BL/6JJcl, 4w, M) and rat (F344/Jcl, 4w, M). Each small animal was anesthetized and positioned in a birdcage volume coil (inner diameter, 25 mm) throughout imaging. Single-slice axial MRF images were acquired (field of view = 3.2 cm x 3.2 cm, slice thickness = 2 mm, measurement time = 26 min). The MRF signal evolution was matched with the pre-determined dictionary to estimate T<sub>1</sub>, T<sub>2</sub>, proton density, and diffusion coefficient values on a per-pixel basis. No respiratory triggering was applied.

Figure 1 shows MRF-based maps of T<sub>1</sub>, T<sub>2</sub>, proton density, and diffusion coefficient of the mouse and rat brains. The relaxation times in cerebrospinal fluid were longer than the other regions. The estimated values agreed with those obtained from the standard methods. The initial MRF results presented here show great promise for quantifying relaxation times and diffusion for a mouse and rat in the very short examination time.

References: [1] Dan Ma et al., Magnetic resonance fingerprinting, *Nature* 2013; 495: 187-193. [2] Y. Gao et al., Preclinical MR fingerprinting (MRF) at 7T: effective quantitative imaging for rodent disease models, *NMR Biomed.* 2015; 28: 384-394.

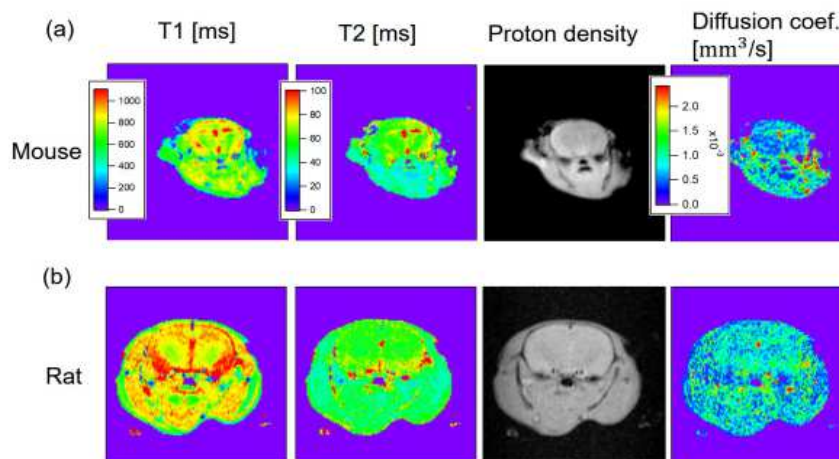


Fig. 1 MRF T<sub>1</sub>, T<sub>2</sub>, proton density, and diffusion coefficient maps from in vivo healthy brains of (a) mouse and (b) rat.

**MRI of Water-Content Changes in Unconsolidated Natural Porous Media with Short  $T_2$** 

A. Görges<sup>\*</sup>, S Haber-Pohlmeier<sup>§</sup> and B Blümich, Institut für Technische and Makromolekulare Chemie, RWTH Aachen University, Worringer Weg 2, 52078 Aachen, Germany; A Pohlmeier, IBG-3, Forschungszentrum Jülich, 52425 Jülich, Germany.

One important methodology of understanding water flow processes in the vadose zone, the unsaturated upper zone of the earth crust, is the reliable imaging and quantification by non-invasive methods. MRI is a suitable technique, since it visualizes water directly and permits non-invasive investigations of continuous sample changes like drying. However, most natural soils exhibit very short relaxation times. In order to overcome this obstacle and to be able to obtain well resolved images from these samples, special pulse sequences have to be utilized. Established imaging pulse sequences like UTE [1], ZTE [2], and SPRITE [3] have been successfully applied in the past on rocks or biological samples with comparable short  $T_2$  relaxation. However, natural soil samples are even more complex due to heterogeneous composition and partial water saturation. They are, in fact three-phase systems. This causes susceptibility artefacts, as well as image blurring due to very short  $T_2^*$  and  $T_2$  values.

The strategy in this work is first to determine all relaxation properties of the principal soil components like sand, silt, and clay as well as those of exemplary soil materials: a sandy loam, a silt loam and a soil conditioner. Since images are acquired with conventional high field scanners, the relaxation experiments cover field strengths from 13 MHz over 24 MHz up to 200 MHz. First images measured with UTE and ZTE will be shown for the soil samples under saturated conditions indicating that these methods are applicable in principle, but parameters controlling the minimum detection time need to be optimized to enable further investigations of the unsaturated state. This is the more interesting state, since the vadose zone is mostly unsaturated. We anticipate that with methodological improvements one will be able to investigate water-content changes during multi-step outflow experiments, the basis for the calculation of the unsaturated hydraulic conductivity parameter, one of the most important quantities for the modelling of water flow in natural soils.

**References**

- [1]Robson, M.D., Magnetic resonance: an introduction to ultrashort TE (UTE) imaging, J. Comput. Assist. Tomo., 27(2003) 825-846.
- [2]Weiger, M., Pruessmann, K., MRI with zero echo time, eMagRes, 311 (2012) 311-321.
- [3]Kennedy, CB, Balcom, BJ, Mastikhin, IV, Three-dimensional magnetic resonance imaging of rigid polymeric materials using single-point ramped imaging with T1 enhancement (SPRITE), Can. J. Chem., 76 (1998) 1753-1765.

## Using Molecular Imaging to Evaluate a Vaccine Immunotherapy in an Ovarian Cancer Model

M.-L. Tremblay<sup>a,b</sup>, V. Gonzalez<sup>a,b,c</sup>, C. Davis<sup>a,b</sup> and K.D. Brewer<sup>\*a,b,c</sup>, <sup>a</sup>Biom edical Translational Im aging Centre (BIOTIC), H alifax, N S; <sup>b</sup>W K H ealth C entre, H alifax, N S; <sup>c</sup>Dalhousie University, Halifax, NS; A. Mackay, A. West, M. M. Stanford and G. Weir, Immunovaccine Inc., Halifax, NS.

**Introduction:** Ovarian cancer is one of the most aggressive cancers among women<sup>1</sup>. It frequently recurs after chemotherapy or radiation treatment, making it an important target for immunotherapy<sup>2</sup>. Pre-clinical PET/MRI provides valuable information when characterizing immunotherapies, particularly in hard to detect cancers like ovarian cancer. Using simultaneous PET/MRI, we can monitor orthotopic ovarian cancer tumor growth and SPIO-labeled immune cell migration via MRI and tumor metabolism via PET in response to an immunotherapy vaccine.

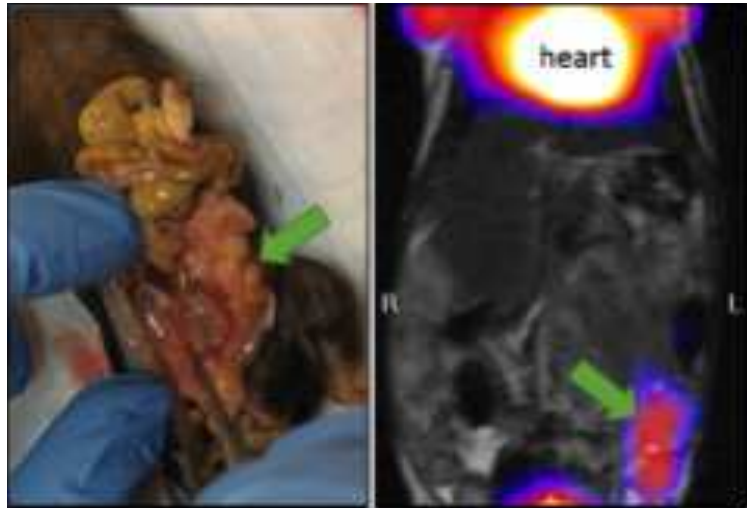
**Methods:** *In vivo* data were obtained in a humanized mouse model of ovarian cancer in HLA-A2.1-/HLA-DR1-transgenic (HHD) H-2 class I/class-II knockout mice. Ovarian surface epithelial cancer cells were implanted (either 0.1, 0.5, 1, or 5x10<sup>5</sup> cells, n=5/group) in the left ovary intrabursally. Tumor growth kinetics were monitored using simultaneous MRI/PET scans every other week beginning 28 days post implantation. Anatomical details and tumor volumetric changes were visualized using a bSSFP pulse sequence (TR/TE = 8/4 ms,  $\alpha = 30^\circ$ , 4 phase cycles, 4 averages, 256x136x136, FOV = 51.2mm x 27.2mm x 27.2mm, t = 41min). Tumor metabolic activity was monitored with a 30 min PET scan beginning 50 min after injection with ~600  $\mu$ Ci of 18F-FDG.

**Results:** Ovarian cancer tumors were detectable on both PET and MRI, with uterine horn swelling also visible on MR images. Tumor progression and spread could be monitored using simultaneous PET/MRI and was compared to necropsies done at endpoint for validation (Fig).

**Conclusion/Future Work:** Simultaneous PET/MRI is an excellent tool for monitoring tumor growth of hard to detect cancer at per-clinical stages. After establishing tumor kinetics, we will use PET/MRI to monitor tumor metabolism and track SPIO-labeled immune cell subsets to understand potential dynamics of recruitment and migration in response to a cancer vaccine immunotherapy.

**References:** 1. Canadian Cancer Society et al. (2015). "Canadian Cancer Statistics 2014." 2. Syrios J., et al. (2014). *Anticancer Res* 34(5):2069-2077.

**Figure:** Left : Necropsy of an untreated mouse at day 49. Right: Corresponding PET/MRI. Green arrows indicate the tumor. R = right and L = left.



### Imaging of $^{23}\text{Na}$ accumulation in the soil-root region due to root water uptake

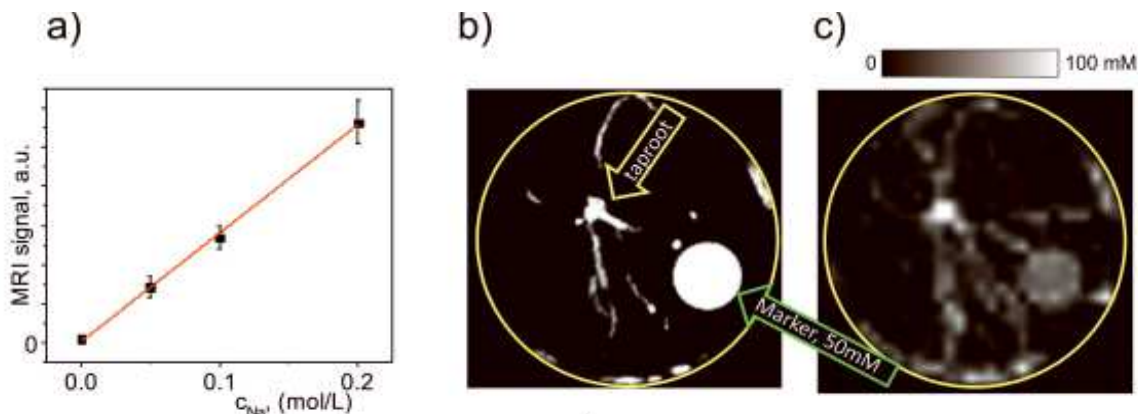
A. Pohlmeier<sup>\*</sup> and J. Vanderborght<sup>§</sup>, Institute for Bio- and Geosciences 3, Research Center Jülich, Germany; A. Perelman and N. Lazarovich, Jacob Blaustein Institute for Desert Research, Ben-Gurion University of the Negev, Sede Boqer, Israel; S. Haber-Pohlmeier, Institute for Technical and Macromolecular Chemistry, RWTH Aachen University, Germany.

Root water uptake may lead to salt accumulation at the root-soil interface, resulting in local salt concentrations much higher than in the bulk soil. This salt accumulation is caused by mass flow through the soil, followed by preferential absorption of specific nutrients by active uptake, thereby excluding most other salts at the root-soil interface or in the root apoplast. The salinity build-up can lead to large osmotic pressure gradients across the roots, thus effectively reducing root water uptake and crop production. Therefore, an understanding and a description of the processes taking place are required, in terms of parametrizing soil physical models. To start with, reliable 3D imaging measurements of the salt accumulation in the soil and the roots are needed.

While common in medical research,  $^{23}\text{Na}$ -MRI is not very well developed for unsaturated porous media such as soils [1]. Therefore we first determined in this study  $T_1$  and  $T_2$  relaxation times of  $^{23}\text{Na}$  in natural sands and a typical soil material as basis for setting up parameters for convenient 3D imaging pulse sequences. Since the typical concentration range of NaCl in soils is with 20 mmol/L to 500 mmol/L relatively low, the next step is checking the linearity between MRI signal intensity and Na concentration. We decided to use a RARE sequence with only a few number of echos to optimize the relation between measurement time, number of scans and signal decay due to  $T_2$  relaxation. With this setup we could reliably determine concentrations of few 10s mmol/L in unsaturated sand with mm resolution. Finally we were able to investigate the NaCl enrichment in the root system of tomatos by a combination of  $^1\text{H}$ -MRI for the root system architecture [2] and  $^{23}\text{Na}$  MRI. For low transpiration rates the enrichment rate is low and the distribution pattern is wide, whereas for high transpiration rates a localized high enrichment near the roots was observed. We could also image a considerable uptake of Na into the roots and even transport and further enrichment in the leaves. This will allow conclusions on the plant's strategy to deal with the salinity.

[1] Rijners et al. JMR 167 25-30 (2004)

[2] Pohlmeier et al. SSSA Special Publ. 61 135-153 (2013), doi:10.2136/sssaspecpub61.c7



$^{23}\text{Na}$  imaging in natural sand by 3D fast spin echo. a) The MRI-RARE signal is proportional to Na concentration in saturated sand. b) Central slice through the root system ( $^1\text{H}$ -MRI). c) Same slice,  $^{23}\text{Na}$ -MRI

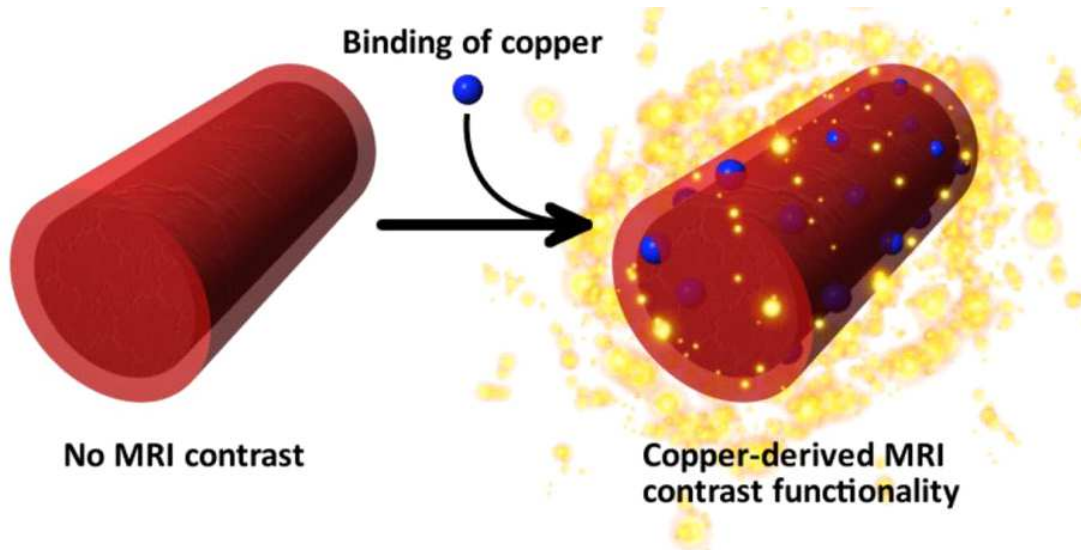


**Copper-binding polymer coatings for enhanced MRI contrast of prostate tumor radiotherapy seeds**

NH Williamson, AA Cavallaro, M Larsson<sup>a,b</sup> and M Nydén<sup>a,b</sup>, <sup>a</sup>Future Industries Institute, University of South Australia, Mawson Lakes, SA 5095, Australia; <sup>b</sup>University College London, UCL – Australia, 220 Victoria Square, Adelaide, SA 5000, Australia.

In the commonly used prostate cancer treatment *permanent low dose brachytherapy*, radioactive seeds are inserted in the close vicinity of the tumor to achieve local radiation therapy. The positioning of the seeds is critical for treatment outcomes and a current problem is to reliably determine the location of the seeds in relation to the prostate. Seeds with magnetic resonance imaging (MRI) contrast would be highly beneficial as MRI would then enable high quality simultaneous imaging of the prostate and the seeds. Here brachytherapy seeds have been modified for MRI contrast with a copper-binding polymeric coating which reduces the  $T_1$  relaxation time of nearby water. The enhanced contrast in MR images may help to identify and locate seeds during initial placement, as well as during the following months of radiotherapy, thus leading to more informed radiotherapy treatment plans and improved patient outcomes.

This poster details our initial work and findings, including the coating of model titanium and (non-therapeutic) nylon seeds with crosslinked Polyethylenimine polymer, Copper uptake, toxicology study, and in particular MRI microimaging of the seeds *ex-vivo* as a function of copper loading. With titanium seeds, effects of susceptibility gradients overpowered the effects of the surface coating, indicating that the coating cannot be used for all seed materials. With nylon seeds, increasing contrast at the surface was observed with increasing copper loading, indicating that the polymeric surface coating can be used to increase contrast in MRI.





**Towards  $T_{1\rho}$  Imaging of Porcine Intervertebral Discs Under Loading**

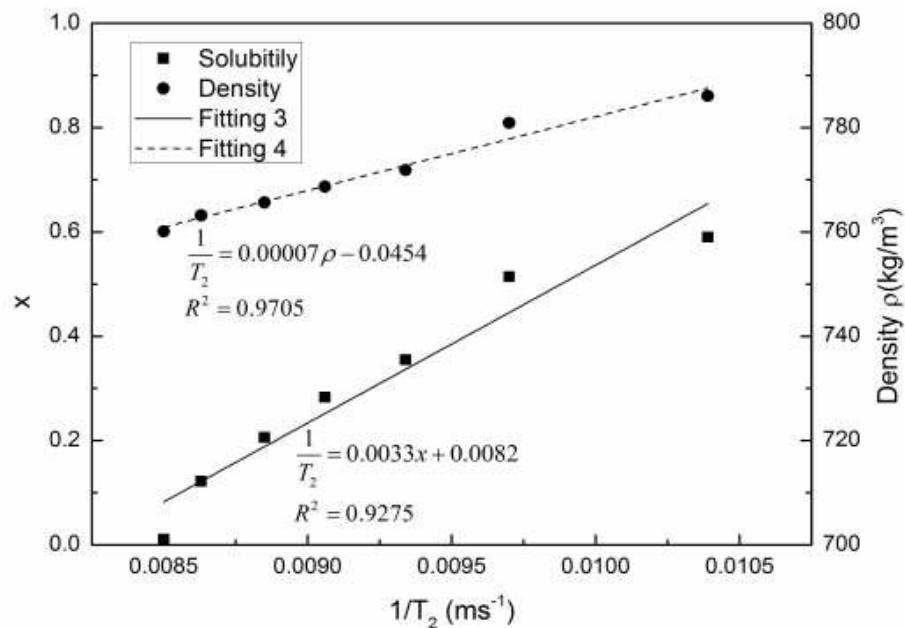
J.H. Walton<sup>\*</sup>, NMR Facility, University of California Davis, Davis, CA, 95616, USA; J. Zhou and F. Fathallah<sup>§</sup>, Department of Biological and Agricultural Engineering, University of California Davis, Davis, CA, 95616, USA.

Intervertebral disc (IVD) is a loci of Lower Back Pain (LBP). The health and functions of the IVD are determined by the inherent biomechanical properties and their interaction with both the magnitude and time-distribution of loading. Recently advances in quantitative Magnetic Resonance Imaging (MRI) techniques have the potential in detecting loading induced mechanical property changes in the IVD. MRI parameters such as  $T_2$ , ADC,  $T_1$ ,  $T_{1\rho}$ , and MTR are sensitive to loading and thus have the potential to detect changes in the mechanical properties of the IVD due to external loading conditions that may increase the risk of injury to IVD. Here we present preliminary  $T_{1\rho}$  measurements on porcine cervical spine IVDs in response to different compressive loading schemes.

## Estimate of physical parameters of CO<sub>2</sub>/ hydrocarbon mixture based on NMR relaxivity

Yuechao Zhao<sup>\*</sup>, Dalian University of Technology; Junlin Chen, Institute of Engineering Thermophysics, Chinese Academy of Sciences; Mingjun Yang, Dalian University of Technology; Yongchen Song, Dalian University of Technology.

Accurate estimate of the physical parameters of CO<sub>2</sub>/hydrocarbon mixture in reservoir, such as solution concentration, density, diffusivity, MMP (Minimum Miscible Pressure), are necessary for reliable reservoir simulations and sequestration engineering design in CO<sub>2</sub> enhanced oil recovery (EOR) project. These parameters are manifested in nuclear magnetic resonance (NMR) relaxivity. NMR relaxivity is of critical importance in core analysis and well logging. In this study, the relationship between NMR relaxation signal, CO<sub>2</sub> solubility, density, MMP of CO<sub>2</sub>/n-hexadecane mixture, and the diffusivity in hexadecane-saturated porous media was investigated experimentally. The <sup>1</sup>H longitudinal relaxation time (T<sub>1</sub>) and transverse relaxation time (T<sub>2</sub>) of CO<sub>2</sub> in liquid hexadecane were measured. An exponential relation was found between the relaxivity and the pressure of the CO<sub>2</sub>/n-hexadecane system, moreover the MMP could be predicted by this relation. The experimental results showed that the T<sub>1</sub> was lengthened by the dissolution of CO<sub>2</sub> while the T<sub>2</sub> was shortened. The solubility and density of CO<sub>2</sub> in liquid hydrocarbon were fitted as a function of 1/T<sub>1</sub> and 1/T<sub>2</sub>. The relaxivity of 1/T<sub>1</sub> and 1/T<sub>2</sub> had a linear relation with elevated solubility and density. Moreover, through the measurement of relaxivity, synchronous measurement of solubility and density and MMP can be realized. The CO<sub>2</sub> diffusivity and the relaxivity 1/T<sub>1</sub> were found to be related exponentially. The experimental findings have a significant impact on developing potential NMR logging techniques to monitor CO<sub>2</sub> migration, stability and capacity in reservoirs, and to provide parameters such as density, MMP and diffusivity for projects of CO<sub>2</sub> enhanced oil recovery (CO<sub>2</sub>-EOR) and geological sequestration.



## Flow Velocity Maps Measured by Nuclear Magnetic Resonance in Medical Needleless Catheter Connectors

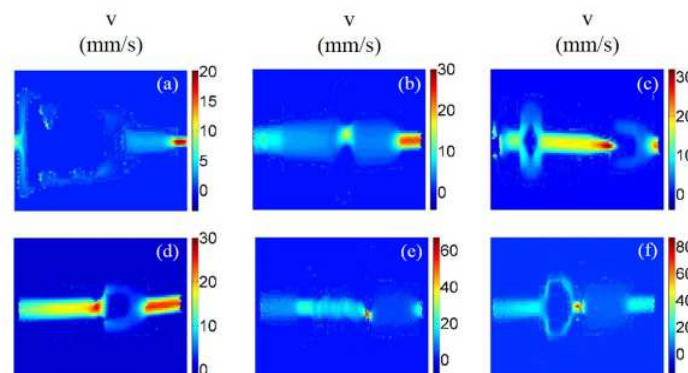
E. Nybo<sup>a</sup> and J. D. Seymour<sup>a,b</sup>, <sup>a</sup>Department of Chemical and Biological Engineering, Montana State University, Bozeman, MT, USA; J. E. Maneval, Department of Chemical Engineering, Bucknell University, Lewisburg, PA, USA; S. L. Codd, Department of Mechanical Engineering, Montana State University, Bozeman, MT, USA; M. A. Ryder, Ryder Science, Inc., Brentwood, TN, USA; G. A. James, <sup>b</sup>Center for Biofilm Engineering, Montana State University, Bozeman, MT, USA; J. Woodbury, ICU Medical, Inc., San Clemente, CA, USA.

Mapping fluid flow patterns in complicated geometries is of interest for diverse biomedical, pharmaceutical and engineering applications. Needleless connectors (NCs) are broadly used medical devices with complicated internal design. Structural features such as complicated geometric surfaces which generate tortuous fluid flow paths lead to flow complexity that may cause undesirable blood reflux [1], bacterial deposition and biofilm formation [2], followed by an increased risk of blood stream infections in patients [3]. Magnetic resonance imaging (MRI) is applied as a non-invasive and non-destructive technique to evaluate the fluid dynamics associated with various internal designs of the NC. Spatial velocity maps of fluid flow at various positions of the devices are acquired. A series of MRI longitudinal and cross-sectional velocity images showing the velocity magnitude  $v = (v_x^2 + v_y^2 + v_z^2)^{1/2}$  and  $v_x$ ,  $v_y$ ,  $v_z$  velocity components for 6 NCs are obtained. Velocity distributions of  $v_x$  and  $v_y$  components quantify the secondary flows caused by the structure of the NCs. MRI velocimetry is demonstrated as an effective method to quantify flow patterns and fluid dynamic dependence on structural features of NCs. The data provides a basis for ground truthing computational fluid dynamics (CFD) methods that could impact design of NCs.

### References:

1. Hadaway, L., Needleless Connectors for IV Catheters. American Journal of Nursing, 2012. 112(11): p. 32-44.
2. Yazdi, S. and A.M. Ardekani, Bacterial aggregation and biofilm formation in a vortical flow. Biomicrofluidics, 2012. 6(4).
3. Donlan, R.M., Biofilms and device-associated infections. Emerging Infectious Diseases, 2001. 7(2): p. 277-281.

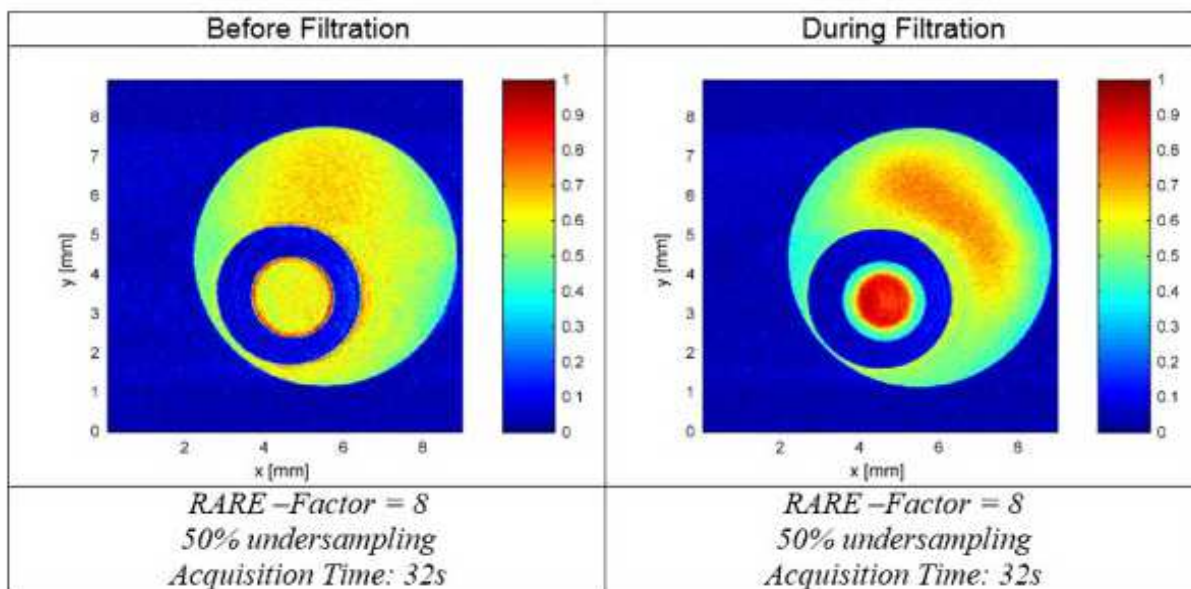
Fig.1: Velocity amplitude maps using MRI. Images show velocities of water flowing from right to left in the longitudinal slice of 0.3 mm thickness, through (a) MaxPlus (CareFusion Inc.), (b) BD Q-Syte (Becton Dickinson), (c) Neutron (ICU Medical Inc.), (d) MicroClave Neutral (ICU Medical Inc.), (e) SmartSite (CareFusion Inc.), (f) OneLink (Baxter Healthcare Corp.).



## In situ observation of fouling layer formation in ceramic hollow fiber membranes using compressed sensing RARE MRI

S. Schuhmann, F. Arndt, N. Schork, H. Nirschl and G. Guthausen<sup>a,b</sup>, <sup>a</sup>Institute for Mechanical Process Engineering and Mechanics, Process Machines, KIT, 76131 Karlsruhe, Germany; <sup>b</sup>Engler-Bunte-Institute, Chair of Water Chemistry and Water Technology, KIT, 76131 Karlsruhe, Germany.

Ceramic hollow fiber membranes are used in several industrial applications. The main problem of the filtration process is the membrane fouling, which is due to the accumulation of mainly colloidal substances on the membrane surface and which is investigated by MRI. Especially the initial fouling process is rather fast on the usually available time scale of MRI in the order of several minutes. A RARE 2D pulse sequence with a compressed sensing scheme was used to reduce the measurement time while keeping the image quality constant. In the present study the formation of the fouling layer was detected during the filtration with a time resolution of 32s. To overcome the lack of contrast between alginate and surrounding water, specific magnetic iron oxide nanocrystallites (MIONs) were applied as paramagnetic contrast agents. The geometric parameters of the fouling were extracted quantitatively from the images and the fouling mechanisms were studied in detail as a function of filtration time.



**The High-field Field-Cycler: A high-resolution high-sensitivity NMR field-cycling device for full range T1 relaxation measurements**

C-Y. Chou, A. Guiga and D. Sakellariou\*<sup>a,b</sup>, <sup>a</sup>CEA Saclay, France; M. Chu and T-H. Huang, Academia Sinica, Taiwan; <sup>b</sup>Center for Surface Chemistry and Catalysis, Faculty of Bioscience Engineering, KU Leuven, Belgium; M. Abdesselem, C. Bouzigues, T. Gacoin and A. Alexandrou, Ecole Polytechnique, France.

$T_1$  relaxation can be a major contrast mechanism in Magnetic Resonance Imaging. Today the  $T_1$ -weighted images are acquired at the center of superconducting magnets and therefore benefit from high-polarization and high-detection sensitivity. Their contrast can be however not optimal. The reason is that  $T_1$ -contrast increases with decreasing magnetic fields, which is contradictory to the trend of going to ever higher magnetic fields.

Here we present a fast field cycling sample shuttling device that is coupled to a high-field superconducting micro-MRI detection probe and allows us to acquire high-resolution, high-sensitivity images with contrast coming from a variety of magnetic fields.

## Longitudinal flow measurement for a living tree using an outdoor MRI

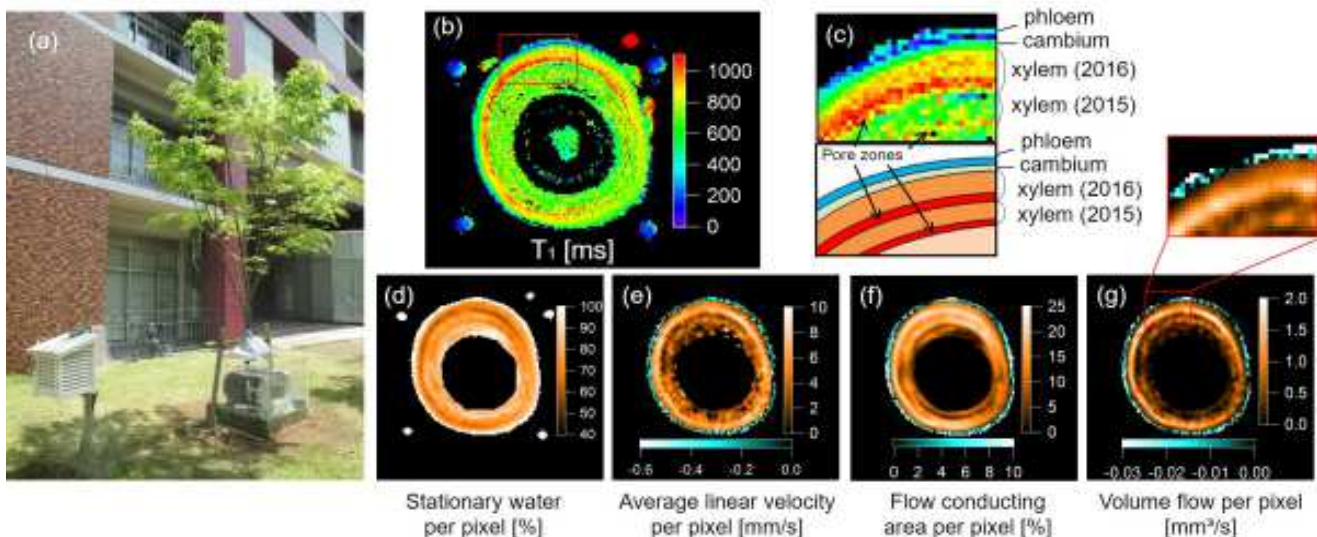
A Nagata, K Kose and Y. Terada<sup>\*</sup>, Institute of Applied Physics, University of Tsukuba.

The water dynamics of plants is important for understanding plant physiology, and flow imaging of an intact tree using MRI has attracted great attention. Outdoor MRI has potential to visualize physiological processes of plants growing in their natural environment, but it still remains a challenge because of the difficulty in settling the MRI system outside for a long time. We recently developed an outdoor MRI system that is robust enough for long-term measurements and allows q-space imaging (QSI) of an intact tree [1]. In this study, flow measurements were performed for several consecutive days in summer and autumn, and the diurnal and seasonal changes in xylem and phloem flow were observed.

Fig. 1(a) shows a tree and the MRI system with a 0.2 T/16 cm-gap permanent magnet (NEOMAX Engineering, 520 kg). The magnet, gradient coil set, RF probe, and other electronics were waterproofed by a box made of acrylic plates. The trunk of the Zelkova serrata at 40 cm above ground was measured. The xylem flow was measured using a pulsed field gradient-spin echo (PFG-SE) sequences for xylem flow ( $TE/TR = 40/800$  ms, slice = 4 cm, Matrix =  $256 \times 64$ , FOV =  $25.6$  cm  $\times$   $12.8$  cm,  $\delta = 8$  ms,  $\Delta = 20$  ms,  $q_{max} = 2.27 \times 10^4$  m<sup>-1</sup> and  $\Delta q = 360$  m<sup>-1</sup>), and phloem flow was measured using PFG-stimulated echo (STE) ( $\delta = 10$  ms,  $\Delta = 200$  ms,  $q_{max} = 2.70 \times 10^4$  m<sup>-1</sup>, and  $\Delta q = 1800$  m<sup>-1</sup>). The flow velocity was calculated as described in Ref. [2].

The anatomical structures in the trunk were visualized in the  $T_1$  image (Fig. 1(b,c)). The xylem and phloem were distinguished. The flow maps (Fig. 1(d-g)) showed upward-flowing xylem sap and downward-flowing phloem. The diurnal and seasonal changes in xylem and phloem flow were observed. The xylem flow was greatest at midday, lowest at night and was proportional to vapor pressure deficit in the air. The xylem flow velocity and flow-conducting area in summer were greatest in the pore zone of the current-year annual ring where large vessels are functional. The xylem flow-conducting area increased as the season progressed from summer to autumn. The downward phloem flow measured in summer was almost constant throughout the day. Phloem flow became negligible in the autumn.

References: 1. A. Nagata, K. Kose, and Y. Terada, Development of an outdoor MRI system for measuring flow in a living tree, *J. Magn. Reson.* 265 (2016) 129-138.  
2. T. W. J. Scheenen, F. J. Vergeldt, C. W. Windt, P. A. de Jager, and H. Van As, Microscopic Imaging of Slow Flow and Diffusion: A Pulsed Field Gradient Stimulated Echo Sequence Combined with Turbo Spin Echo Imaging: *J. Magn. Reson.* 151 (2001) 94.



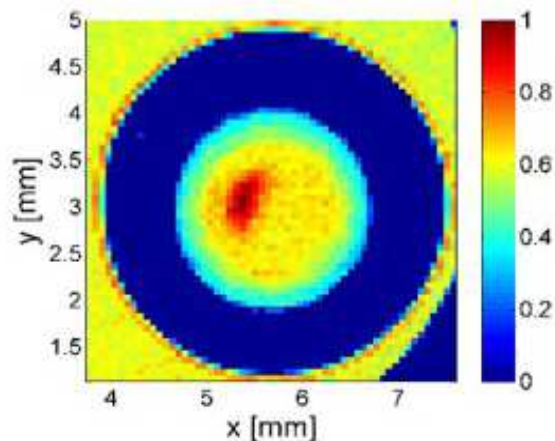


### MRI contrast mechanisms and fouling layer formation during skim milk filtration

N. Schork, F. Arndt, S. Schuhmann, G. Guthausen<sup>a,b</sup> and H. Nirschl, <sup>a</sup>Institute of Mechanical Process Engineering and Mechanics, KIT, Karlsruhe, Germany; <sup>b</sup>EBI, Water Chemistry and Technology, KIT, Karlsruhe, Germany.

An important application of membrane filtration is the separation of casein micelles and whey proteins from skim milk with micro- or ultrafiltration. These protein fractions have different nutritive and techno-functional properties and are therefore added in a variety of food products. An advantage of applying a filtration process instead of conventionally used acid or alkali precipitation is that the filtrated proteins remain in their native state. The colloidal calcium phosphate concentration remains constant which is embedded in the casein micelle. Because of the size of the casein micelles (ca. 200 nm) which are of a magnitude bigger than the pore size of the used hollow fiber membrane ( $d_{\text{mean}} = 40 \text{ nm}$ ), a deposit layer is formed on the membrane surface. A steep decrease in permeate flux is observed with filtration time. Additionally, the small whey protein fraction which should permeate the membrane is retained by the casein deposit layer resulting a poor yield of whey proteins in the permeate.

In order to gain detailed insight to the filtration process, the phenomena and mechanisms which are responsible for deposit layer formation, a filtration process is observed in-situ by MRI. Time and spatially resolved measurements of the fractionation of micellar caseins reveal the complex deposit layer formation during the filtration. An in-depth understanding of the physical principles, i.e. the image contrast, is essential for the interpretation of the MRI results. The different components of skim milk differ in their physical and relaxation properties. MRI filtration results were analyzed in terms of these properties, leading to a detailed description of the skim milk filtration process.



Photograph of the ceramic hollow fiber membrane (left) and axial MRI image during a dead-end filtration with the fouling layer (cyan, right).

### Imaging of a Gas-Liquid Reaction in a Bubble Tail

S. Benders<sup>\*</sup>, B. Fenger, M. Küppers<sup>§</sup> and B. Blümich, Institut für Technische und Makromolekulare Chemie, RWTH Aachen University, 52074 Aachen Germany; F. Strassl and S. Herres-Pawlis, Institut für Anorganische Chemie, RWTH Aachen University, 52074 Aachen Germany.

Bubble-column reactors are one of the most commonly used reactor types for gas-liquid reactions [1]. Although being widely utilized in the production of batch chemicals, the underlying physics, especially at the interface, that lead to their advantageous properties, are not well understood [2]. In this study, Magnetic Resonance Imaging (MRI) is applied to investigate these processes. The reaction system is tailored to fit the needs of MRI. Contrast is achieved by the reaction system, which transforms from a diamagnetic to a paramagnetic state within seconds on contact with oxygen [3]. The different magnetic properties induce significant changes on the relaxation rates. In a first step, the ingress of oxygen into a static solution was investigated. Vortices can be observed while the reaction proceeds from top to bottom.

Since the approach enables easy visualization of gas-liquid reactions, the fluid dynamics in the bubble tail was probed in a further step. Due to the high velocity of the bubble rising in a standard solvent, the viscosity is increased by addition of polyethylene glycol. The images show the rising bubbles (Figure 1). In the tail of the bubble the signal intensity increases due to the change from the diamagnetic to the paramagnetic state. Additionally, the consumption of the oxygen within the bubble can be observed by its shrinking.

[1] A. Behr, D. Agar, J. Jörissen, "Einführung in die Technische Chemie", 2010, Spektrum

[2] P. Rollbusch, M. Bother, M. Becker, M. Ludwig, M. Grünwald, M. Schlüter, R. Franke, Chem. Eng. Sci., 126 (2015) 660-678

[3] D. Schurr, F. Strassl, P. Liebhäuser, G. Rinke, R. Dittmeyer, S. Herres-Pawlis, React. Chem. Eng., 1 (2016) 485-493.

**The work was financed by The National Centre for Research and Development in Poland (contract No. STRATEGMED2/265761/10/NCBR/2015).**

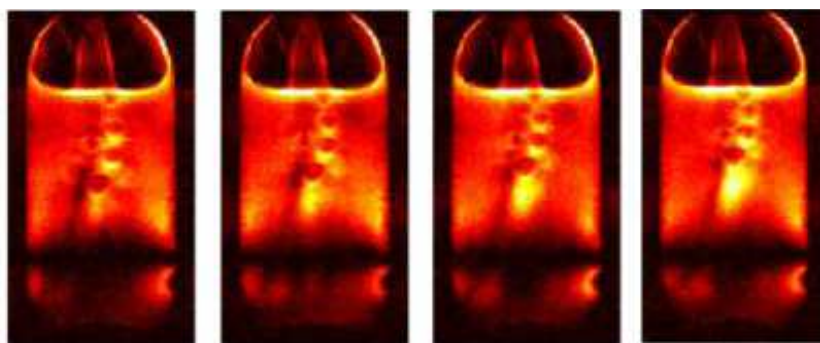


**Figure 1:** Bubbling oxygen through a solution of  $\text{Cu}[\text{btmgp}]\text{I}$  in acetonitrile/PEG. The time resolution is 3.2 s.

**Analysis of Diffusion Effects on T1-T2 Experiments in Multi-phase Systems**

J. Maneval, Department of Chemical Engineering, Bucknell University; M Nelson, Department of Physics, Montana State University; A Mailhot, L Thrane and S Codd, Department of Mechanical Engineering, Montana State University; J Seymour, Department of Chemical and Biological Engineering, Montana State University.

Multi-dimensional NMR relaxation experiments such as T1T2 and T2T2 (aka REXSY) are well known methods for investigating the structure and dynamics of complex systems and materials. A complete theory for explaining the results of these methods is available in terms of multi-site exchange models (Dortch, et al. 2009; van Landeghem, et al., 2010) so long as the dynamics of the underlying system conforms to the condition of "fast diffusion". When this condition is not met, an approach based on the diffusion equation, the so-called Brownstein-Tarr (BT) formulation, is a more appropriate starting place (Brownstein and Tarr, 1979; Song, et al., 2008). Since the diffusion-based approach to modeling these sequences has the potential to provide a predictive theory for the measurements compared to the multi-site approach, there is further motivation to pursue development in this direction.

In this study, we apply the BT approach to address observations of unexpected increases in the inversion-recovery signal at short values of the CPMG-time in some T1T2 experiments. First reported for a macropore-micropore system in porous media (Song et al. (2014)), this phenomenon is also observed in a wide range of other settings, including hydrates, cartilage, and pharmaceutical compounds.

The work presented here develops an extension of the BT formulation to modeling the T1T2 sequence along the lines of that proposed by Bytchenkoff and Rodts (2011). The approach explicitly considers two (or more) physical phases and allows for the interaction of the phases through inter-phase mass transfer processes and phase-equilibrium relations at the interfaces. The approach has the potential to give rise to a wide range of interactions between interacting regions in a material that could be measurable by multi-dimensional NMR methods.

In summary, by accounting for a wider range of dynamics and by explicitly considering interacting physical regions, we hope to develop a more complete and flexible framework for interpreting results of these multi-dimensional sequences in complex materials.

**NMR investigation of the microphysical structure of ice-regolith mixtures**

S.L. Codd and L.W. Thrane, Mechanical and Industrial Engineering, Montana State University; P. Lei, J.R. Brown and J.D. Seymour, Chemical and Biological Engineering, Montana State University; D.E. Stillman, Southwest Research Institute, Boulder.

Ice-regolith is found on Mars and is composed of fine rock and dust particulates mixed in briny ice. The exact cause of the ice structures found on Mars are unknown but some mechanisms have been proposed (Stillman et al, 2014). A likely mechanism is cryosuction, a process in which horizontally segregated ice forms via migration of unfrozen water (Sizemore et al., 2014). However, quantitative cryosuction modeling is difficult because models estimating unfrozen water content and permeability of Mars-like brines within ice-regolith mixtures as a function of temperature are in early stages of development and lack laboratory verification. Hydraulic modeling of these systems is therefore difficult since water ice forms as temperature decreases, significantly reducing subsurface permeability. This project aims to provide the direct measurements of permeability of briny liquid within ice-regolith mixtures to improve modeling. The primary objective is to measure unfrozen water content and permeability of briny ice-regolith mixtures as a function of temperature to determine if martian excess ice could have been formed via cryosuction. A further goal is to determine if liquid networks within the martian subsurface can be detected via orbital and surface remote measurements. For the first time, magnetic resonance (MR) techniques and dielectric spectroscopy (DS) are being used together to study the hydraulic, microstructural and electrical properties created by liquid networks within ice-regolith mixtures. Specifically NMR is used to measure temperature-dependent unfrozen water content, surface area-to-volume ratio, and tortuosity of liquid networks in ice-regolith mixtures with varying salt type, and salt and regolith concentrations. Results were obtained using the methods previously reported for bacterial impact on ice structure (Brown et al, 2012; Brown et al, 2014, Brox et al, 2015).

**References**

- Brown, J. R., T.I. Brox, S.J. Vogt, J.D. Seymour, M.L. Skidmore, S.L. Codd (2012), *Journal of Magnetic Resonance*, 225, 17-24.
- Brown, J.R., J.D. Seymour, T.I. Brox, M.L. Skidmore, C. Wang, B.C. Christner, B. Luo, S.L. Codd (2014), *Biotechnology Reports*, 3: p. 60-64.
- Brox, T.I., M.L. Skidmore and J.R. Brown (2015), *Journal of Glaciology* 61:225.
- Sizemore, H.G., A.P. Zent, and A.W. Rempel (2014), *Icarus*, 51, 191210
- Stillman, D.E., T.I. Michaels, R.E. Grimm, and K.P. Harrison (2014), *Icarus*, 233, 328-341.

## Hyperpolarized and Inert Gas MRI Physics and Medical Applications

MS Albert<sup>a,b,c</sup>, <sup>a</sup>Department of Chemistry, Lakehead University, Thunder Bay, ON, Canada; <sup>b</sup>Thunder Bay Regional Health Research Institute, Thunder Bay, ON, Canada; <sup>c</sup>Northern Ontario School of Medicine, Thunder Bay, ON, Canada.

Hyperpolarized gas and inert gas MRI provide special opportunities for imaging the body than do other currently available technologies. As a co-inventor of hyperpolarized gas technology, we have grown with the field and have expanded our research program to include lung imaging, brain imaging, and the use of biomarkers to detect pathological molecules in the body.

**Lung Imaging** - Conventional MRI technology relies on hydrogen molecules in the body (i.e. water molecules), which are scarce in the lungs. This creates a significant limitation for determining structural and functional information without the use of ionizing radiation. Hyperpolarized gas and inert fluorinated gas can be safely inhaled by humans, provide structural and functional information, and generate signal enhancement of up to 100,000 times over conventionally thermally polarized MRI.

**Brain Imaging** - Hyperpolarized xenon-129 (HP <sup>129</sup>Xe) has the ability to cross the blood-brain barrier and is currently being used in our lab to study Alzheimer's disease. For the first time, functional MR images (fMRI) have been obtained using this technology in both healthy volunteers and participants with Alzheimer's disease. The preliminary results have been promising for use of this technology for early detection and disease staging.

**Biosensors** - HP <sup>129</sup>Xe biosensors are useful for identification of disease sites in the body. This technology works through use of a molecular system that encapsulates the xenon gas, a biological receptor, and an MR technique known as Hyperpolarized Chemical Exchange Saturation Transfer (HyperCEST). Our lab has successfully obtained the first *in vivo* images of a HP <sup>129</sup>Xe MRI biosensor, cucurbit[6]uril. Future work will look at the functionalization of various molecules and their potential to target disease sites in the body.

Hyperpolarized and inert gas MRI offers unique advantages for imaging the body that may lead to improved health outcomes.

**MOISTURE CONTENT MEASUREMENT OF BLACK SPRUCE SAPWOOD AND HEARTWOOD WITH LOW FIELD MAGNETIC RESONANCE**

Clevan Lamason, Bryce MacMillan and Bruce Balcom, Magnetic Resonance Imaging Center, University of New Brunswick (UNB), NB, CANADA; Brigitte Leblon, Faculty of Forestry and Environmental Management, UNB, NB, CANADA; C Zarin Pirouz, FPInnovations, Vancouver, CANADA.

In this study, a low field magnetic resonance (MR) method was employed to measure moisture content (MC) in black spruce (*Picea mariana Mill.*) sapwood and heartwood plugs. The technique employed distinguished signal from both the solid wood matrix and liquid water. We propose a new approach to measure MC by utilizing the liquid to solid  $^1\text{H}$  MR ratio without the use of a reference sample of known MC. Results show that the relationship between predicted and gravimetric MC is linear with a slope that is close to unity. While the method has been developed based on black spruce it should have general applicability to a wide range of wood species.



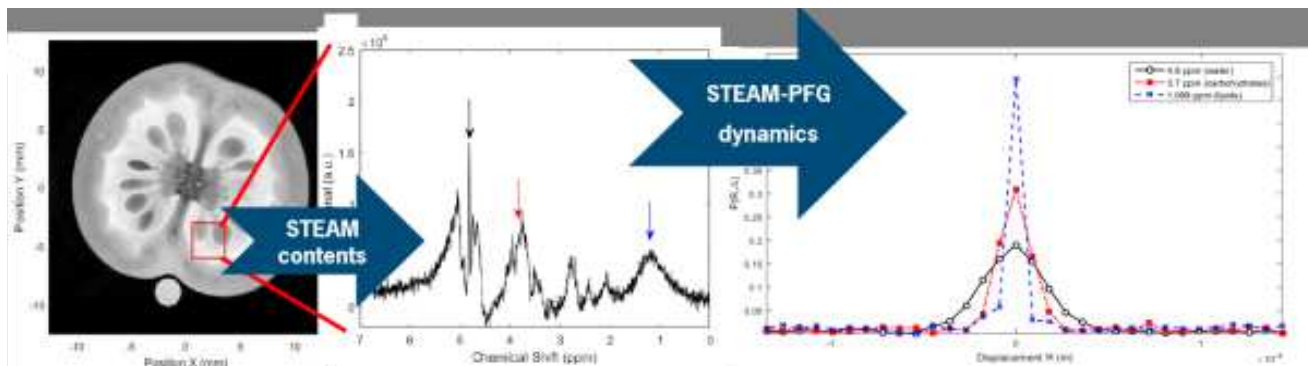
## Localized propagator measurements of metabolites by STEAM-PFG

H. Van As<sup>\*</sup>, S van Kesteren and FJ Vergeldt, Lab of Biophysics, Wageningen University, Stippeneng 4, 6708 WE Wageningen, NL.

MRI flowmetry is the gold standard to measure flow in plants, both xylem (transpiration stream from root to leaves) and phloem (transport of photosynthetic products from source leaves to sink tissues)<sup>1</sup>. Up till now methods have been used that do not discriminate on chemical shift information and therefore the data reflects mainly water transport. Metabolite transport (such as sugars, the main photosynthetic products) in the phloem is of great interest, since phloem transport is still not well understood and challenging. Here we present a NMR approach to quantify the flow of sucrose in the phloem of a plant and at the same time distinguish between the flowing sucrose in the phloem elements and stationary sucrose in the surrounding tissue. The technique combines flowmetry based on the full propagator measurement by PFG with the localized spectroscopy sequence STEAM: STEAM-PFG. The sequence results in chemical shift resolved displacement or propagator distributions. The technique is demonstrated on phantoms, which show that the technique is capable of accurately measuring the diffusion coefficients of sucrose and water and can distinguish between sucrose and water in a flowing solution, measuring the predicted flow-profile and velocities. In vivo application of STEAM-PFG in the gel/seed region of a tomato fruit shows that even in a more complex system the diffusion of water, carbohydrates and lipids can be determined (see figure).

First results obtained in a live tomato plant at our 3T intact plant MRI system are promising. The velocities of water in both phloem and xylem measured with STEAM-PFG correspond well to flow-velocities as observed by PFG-SE-TSE imaging<sup>1</sup>. In addition, STEAM-PFG was successful to measure sucrose flow. The velocity of the sucrose transport in the phloem was very comparable to that of water. We now can start to study the diurnal behaviour.

1. Van As, H. (2007) *J. Exp Bot.* 58, 743-756.

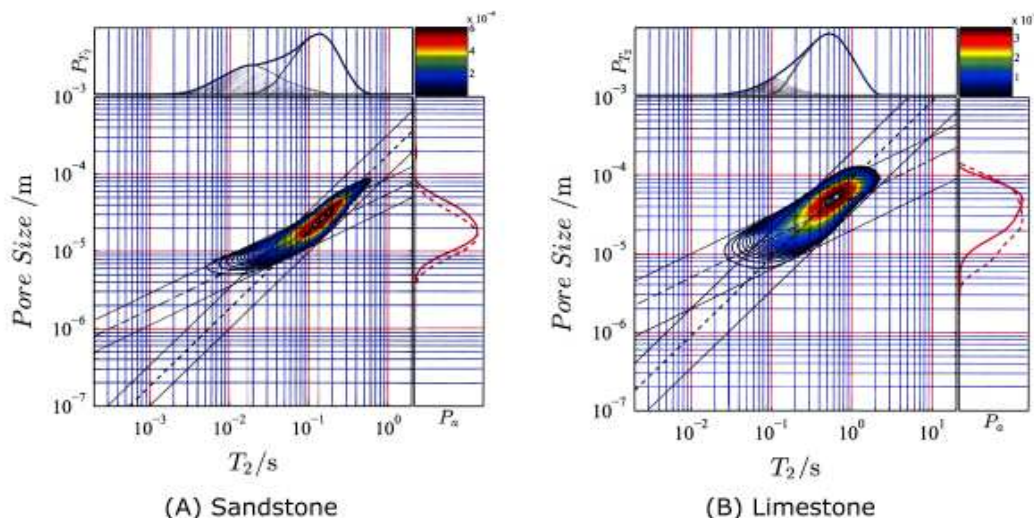


## Experimental Evidence of Both Fast and Slow Diffusion Regimes in a Sandstone Core Plug by 2D NMR Relaxometry and Diffusometry Correlation

A. Afrough, L Romero-Zerón and B J Balcom<sup>\*s</sup>, University of New Brunswick.

Brownstein and Tarr (Phys. Rev. A, 19, 2446; 1979) showed that the total nuclear magnetization decay in media with surface relaxation centers can be described as a multiexponential decay. Their approach is based on normal mode analysis and is valid for both  $T_1$  and  $T_2$  relaxation. In the fast diffusion regime, applicable to sedimentary rocks, the 0<sup>th</sup> mode of the multiexponential decay dominates. Liu et al. (J. Mag. Res., 246, 110; 2014), employing the method developed by Song (Phys. Rev. Lett., 85, 3878; 2000), removed the effect of the 0<sup>th</sup> mode of  $T_1$  decay and correlated the results with a CPMG measurement. Their experiments were performed on a 2 MHz instrument on sandstone and limestone core plugs. The results are shown in Fig. A and B, where  $T_1$  distribution is rescaled to pore size. Liu et al. ascribed changing slopes in different pore regimes to heterogeneous surface properties. We demonstrate that this anomaly is because of the 0<sup>th</sup> mode in the slow diffusion regime for the sandstone sample.

The 0<sup>th</sup> mode of the fast diffusion regime is  $T_{2,0} = a/\alpha\rho_2$ , where  $a$  is the pore size,  $\alpha$  is a pore geometry constant, and  $\rho_2$  is transverse relaxation surface relaxivity. Other modes, both in the fast and slow diffusion regimes, are in the form of  $T_{2,n} = a^2/D f^2(n)$ , where  $D$  is the pore fluid diffusivity, and  $f(n)$  is a constant function of mode number. In a log-log plot of pore size versus  $T_2$ , the 0<sup>th</sup> mode of the fast diffusion regime aligns with a straight line of unity slope and all other modes align with a straight line of slope  $\frac{1}{2}$ . Straight lines of slope unity on the dominant part of the correlation function demonstrate the fast diffusion regime. The portions of the correlation functions aligned with  $\frac{1}{2}$  slope lines can potentially represent either the 0<sup>th</sup> mode of slow diffusion or the 1<sup>st</sup> mode of fast diffusion. However, if they were the 1<sup>st</sup> mode of fast diffusion, their contribution to the net magnetization would be approximately 10% of the 0<sup>th</sup> mode of fast diffusion's. According to the  $T_2$  distribution on top of Fig. A, the contributions of both modes are comparable in magnitude. In Fig. A, based on the intercept, the diffusivity of water in the slow diffusion regime is expected to be on the order of  $10^{-10}$  m<sup>2</sup>/s. The exact value of diffusivity can be calculated based on a more rigorous analysis of raw data. In summary, this work demonstrates that the 0<sup>th</sup> order of both the fast and slow diffusion regimes are observed in a sandstone rock sample. This observation can be because of either a different water diffusivity in small pores, or the bound layer covering pore surfaces. In the case of limestone, the small contribution of the  $\frac{1}{2}$  slope section leaves the question open whether it is the 1<sup>st</sup> mode of fast diffusion or the 0<sup>th</sup> mode of slow diffusion.



**MRI measurement of flowing and stationary water in a spray setup**

S. Ahmadi, Department of Physics,, University of New Brunswick, Fredericton,NB E3B5A3 Canada; I.V. Mastikhin, Department of Physics,, University of New Brunswick, Fredericton,NB E3B5A3 Canada.

## MRI measurement of flowing and stationary water in a spray setup

MRI is a new promising technique to study sprays. Its non-invasive nature does not interfere with the gas-liquid interface. It is inherently a 3D imaging method, and the data comes directly from the bulk of the sample. Low spin density of sprays means low Signal-to-Noise, resulting in a long acquisition time. Reduction of the geometry of the system from 3D to 2D would considerably reduce acquisition time. But before reduction, it is necessary to find out the ratio of signal from the spray zone and the signal from the stationary water accumulated on the walls of the experimental setup.

We performed a series of measurements with 3D Conical-SPRITE to quantify the amount of water on the walls. The 3D data were integrated in longitudinal (spray) and axial directions. After analyzing the data, it was found that the signal intensity from the walls was comparable to the one from spray zone. Therefore, non-slice selective 2D images of sprays would be contaminated with signal from stationary water accumulated on the walls.

However, for an RF probe length of  $L$  and the average spray speed  $V$ , if  $TR > L/V$ , then we can use 90 flip angles as water in spray will leave completely the RF region before the next RF pulse so we will always excite the unsaturated magnetization. At the same time, the stationary water will be inside the probe all the time and its magnetization will become saturated following the steady-state equation:  $M_z/M_0 = (1 - \exp(-TR/T_1))$ .

To measure the range of velocities  $V$ , the motion-sensitized 3D Conical-SPRITE experiment was used for velocity mapping of water in the spray and on the walls. Average velocity values were then employed to estimate optimal parameters ( $TR$  and  $T_1$ ) for 2D measurements of sprays with good SNR and saturated stationary water magnetization.

## Comparison of the Gas and Liquid Phase Flow of Foam using PFG-Readout Velocity Mapping

A. Adair and B. Newling\*, University of New Brunswick, Fredericton, Canada.

The focus of this study is the behaviour of foam flow, in particular, the flow field of both the gas and liquid phases of a foam. Foams have a wide range of commercial applications (oil recovery, food products, and cosmetics, for example). An advantage of magnetic resonance imaging to the study of foam flow over other common flow measurement techniques is its non-optical and non-invasive nature -- foams are often both optically opaque and physically delicate. Motion-sensitised MRI can be used to study the flow field of the foam through velocity mapping. Velocity mapping measurements can be performed while separately analysing the gas and liquid phase signal from the foam. Comparing the flow fields of the two phases can yield interesting information about the relative behaviour of the phases.

Measurements were performed using a 4.7 T vertical bore superconducting magnet. A glass pipe with an inner diameter of 17.3 mm was placed within the magnet such that a constriction in the pipe (inner diameter of 5.7 mm) was within the region of study. Foam was generated below the magnet and flowed vertically upward through the pipe (Fig.1). The foaming liquid used was a mixture of water, glycerol, and a surfactant [1]. Foam was created by bubbling sulfur hexafluoride through the liquid, with typical bulk foam flow rates on the order of cm/s.

Velocity mapping was performed by using a preparation-readout style of measurement. The preparation was accomplished using pulsed field gradients (PFG) and readout was via a modified SPRITE sequence. Measurements at different PFG amplitudes were used to create velocity maps of the flow [2]. Velocity mapping of the two phases of the foam may be carried out by consecutive measurements on the same foam flow using separate  $^1\text{H}$  and  $^{19}\text{F}$  RF probes. The probe mountings were modified to allow for either probe to be used without disrupting the flow of the foam sample (Fig.1).

The velocity maps that were acquired show the behaviour of the foam as it flowed through the pipe constriction. In addition, the velocity maps were analysed in conjunction with each other to study the relative behaviour of the two phases and look for differences in the flow fields.

[1] K. Bos, K.G. Wilson, B. Newling, *Diffus. Fund.* 18 5 (2013) 1-4.

[2] K. Romanenko, D. Xiao, B.J. Balcom, *J. Magn. Reson.* 223 (2012) 120-128.

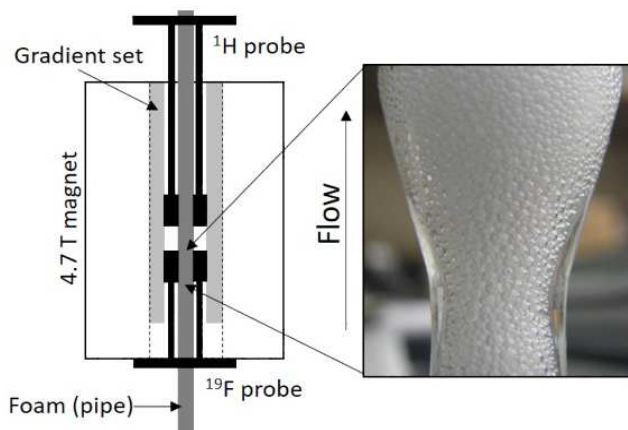


Figure 1: [Left] A diagram of the vertical bore magnet and apparatus. The foam flows upward through the pipe inside the magnet. The position of the probes can be translated to allow for the study of either the  $^1\text{H}$  (liquid phase) or  $^{19}\text{F}$  (gas phase) signal. [Right] A photograph of the foam sample in the pipe constriction (ID = 5.7 mm).

## Assessing the feasibility of measuring the diffusion exchange of water in nerve tissue using diffusion exchange spectroscopy (DEXSY)

J.O. Breen-Norris<sup>a,b</sup>, B. Siow<sup>a,b,c</sup>, T.A. Roberts, A. Ianus and S. Walker-Samuel<sup>s</sup>, <sup>a</sup>Centre for Advanced Biomedical Imaging, UCL, London, U.K; B. Hipwell, I. Hill, M.F. Lythgoe and D. Alexander, <sup>b</sup>Microstructure Imaging Group, Centre for Medical Imaging Computing, UCL, London, U.K; <sup>c</sup>The Francis Crick Institute, London, U.K.

**Introduction:** We present numerical simulations demonstrating the feasibility of measuring the diffusion exchange of water in nerve tissue using DEXSY<sup>[1]</sup>. Permeability varies in both health and disease, in particular oncology and neurology<sup>[2]</sup>. Measurement of diffusion exchange, using apparent exchange rate (AXR), has been linked to gene expression<sup>[3][4]</sup>. DEXSY may be more effective as, unlike AXR, it is a model-free approach. DEXSY MRI has previously been used to measure exchange in biological contexts<sup>[5][6][7]</sup>, but the underlying physical mechanism has not been validated.

**Methods:** We simulate a wide range of permeabilities in a nerve tissue model<sup>[8]</sup> using the CAMINO diffusion tool-kit<sup>[9]</sup>. **Tissue model:** 100 cylinders with gamma distribution of radii, shape and scale parameters of 5.3316 and  $1.0242 \times 10^{-7}$  respectively, lattice size of  $1.65 \times 10^{-5}$  m, and 23 permeabilities  $p=0-0.1$ . **DEXSY:**  $\delta=15$  ms,  $\Delta=17$  ms,  $t_m=100$  ms,  $G_1 \& G_2=0-900$  mT/m in  $16 \times 16$  steps. 2D Inverse Laplace transform<sup>[10]</sup> software, kindly provided by Petrik Galvosas, was used to give diffusion-diffusion (D-D) exchange plots.

**Results:** Figure 1(left): A representative D-D exchange plot for  $p=0.00025$ . Diagonal peaks represent diffusion within different compartments (here, intracellular and extracellular) and cross-peaks represent diffusion exchange between compartments. Diagonal peaks and cross-peaks can only be observed over  $p=0.0001$  to  $0.00055$ . At  $p=0.1$  only one compartment can be seen. Figure 1(right): The ratio of cross peaks to diagonal peaks increases monotonically with permeability.

**Conclusion:** This suggests that DEXSY is an appropriate technique for studying nerve cell membrane permeability in-vivo. Further studies will investigate DEXSY in-vitro and in-vivo experiments.

**References:** [1] P. T. Callaghan, *J. Chem. Phys.*, 120(8):4032-4038, (2004), [2] S. Lasic et al, *Magn. Reson. Med*, 66:356-365 (2011), [3] A. Mukherjee et al, *Nat. Commun.* 7, 13891 (2016), [4] F. Schilling et al. *Nature Biotechnol.* 35, 7580 (2017), [5] B Siow et al., *Proc. ICMRM 12*, Cambridge, UK (2013), P43, [6] B. Siow et al., *Proc. MRPM 12*, Wellington, NZ, (2014), P06, [7] D. Benjamini et al., *Phys. Rev. Lett.* 118, 158003 (2017), [8] Alexander et al, *Magnetic Resonance in Medicine* 52 (4), 1374-1389, (2010), [9] M. Hall et al, *IEEE Trans.*, 28(9):1354, (2009), [10] Y.-Q.-Song et al, *Magn. Reson. Med.* 154:261-268 (2002).

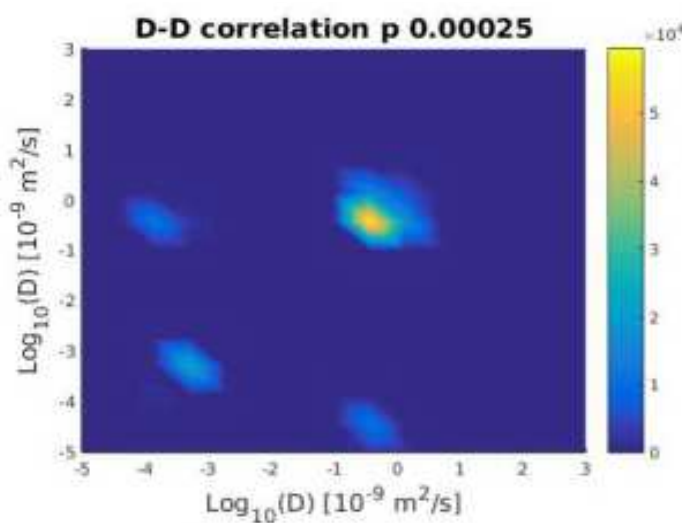
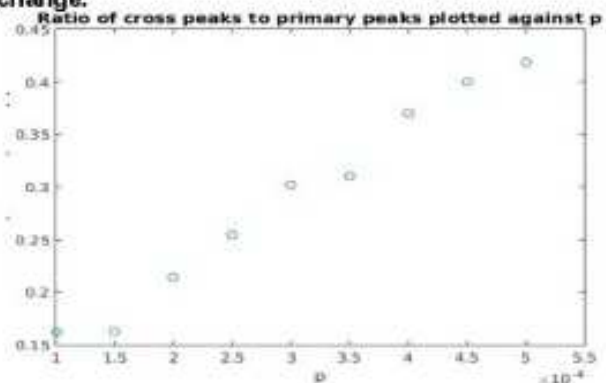


Figure 1: (left) a D-D correlation plot where the probability ( $p$ ) of water crossing the barrier is  $p=0.00025$ . (right) A graph of the ratio of cross peak height to primary peak height, plotted against  $p$ , showing that this ratio is a potential marker for quantifying diffusion exchange.





## Magnetic resonance imaging with variable field magnet, Variation of $B_0$ to control sensitivity and susceptibility mismatch effects

Razieh Enjilela\*, Bryce MacMillan, Sarah Vashaee and Bruce.J Balcom, Department of Physics, MRI Center, University of New Brunswick, Fredericton, New Brunswick, Canada.

Fluid saturated porous materials in presence of external uniform magnetic field creates a so called "internal magnetic field gradient" inside the pore space due to magnetic susceptibility mismatch ( $\Delta\chi$ ) difference between filled pores and solid matrix [1]. It is important to know what is the best field for rock core samples studies to trade-off greater sensitivity at high field versus  $T_2^*$  lifetime decreases due to susceptibility effects. We have recently installed a new cryogen free superconducting variable field magnet. This magnet provides an opportunity to undertake MR/MRI measurements for saturated rock cores with high sensitivity while controlling  $T_2^*$  transverse lifetime decreases due to susceptibility mismatch. Bulk Free Induction Decay (FID) and 3D MRI Centric Scan SPRITE [2] have been undertaken over a wide range of rock core samples saturated with 2% brine solution to show the sensitivity and  $T_2^*$  lifetime variation at three different fields (0.79, 1.5, and 3T). A single exponential  $T_2^*$  decay was observed for all rock samples as expected by theory [1]. Results showed  $T_2^*$  lifetime is generally shorter at higher field for all samples. Figure 1 shows the linewidth ( $1/\pi T_2^*$ ) measured at different magnetic field strength ( $B_0$ ) for five rock core samples saturated with brine. The slope is determined by susceptibility mismatch ( $\Delta\chi$ ) of solid matrix and fluid and  $B_0$  field.

The single exponential  $T_2^*$  behavior of fluid saturated rock cores is important for successful proton density weighted Centric Scan SPRITE imaging since the local image intensity has simple  $T_2^*$  contrast. Sensitivity variation results showed SNR is higher for the samples which have a longer  $T_2^*$ .

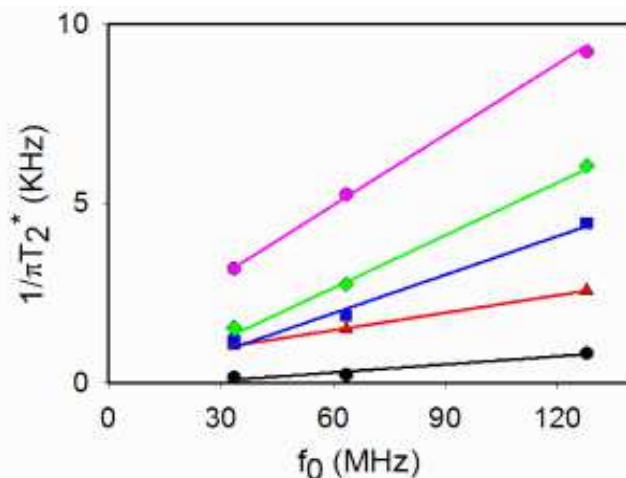


Figure 1. The linewidth ( $1/\pi T_2^*$ ) measured at different fields for (●) Bentheimer, (▲) Nugget, (■) Buff Berea, (◆) Berea, and (●) Wallace sandstones.

### References

- [1]. Q. Chen, A.E. Marble, B.G. Colpitts, B.J. Balcom, *J. Magn. Reson.* 175 (2005) 300-308.
- [2]. M. Halse, D.J. Goodyear, B. MacMillan, P. Szomolanyi, D. Matheson, B.J. Balcom, *J. Magn. Reson.* 165 (2003), 219-229.



## A Magnetic Resonance Study of Low Salinity Waterflooding for Enhanced Oil Recovery

M. Li<sup>a,b</sup>, S Vashaee, F Marica and B Balcom<sup>\*</sup>, <sup>a</sup>MRI Research Centre, Department of Physics, University of New Brunswick, Fredericton, Canada; L Romero-Zerón, <sup>b</sup>Department of Chemical Engineering, University of New Brunswick, Fredericton, Canada.

Low salinity waterflooding (LSF) has been proposed to improve oil recovery, with major projects in progress worldwide. There is however no consensus on the mechanisms of LSF for enhanced oil recovery (EOR). Wettability change is the most widely accepted mechanism. In this work, magnetic resonance (MR) and magnetic resonance imaging (MRI) were employed to monitor oil displacement processes during model laboratory scale LSF experiments. The MR and MRI measurements permit evaluation of putative LSF mechanisms.

Two clay-coated sand packs, one with non-swelling kaolinite, the other with swelling montmorillonite, were prepared as model porous media for LSF. The interactions between pore fluids (oil and water) and the clay-coated pore surfaces were evaluated with relaxation time measurements. A MRI methodology, SE-SPI, was employed to spatially resolve the  $T_2$  distribution along the sand pack. The oil saturation profiles were determined from SE-SPI measurements. A new differential relaxation time distribution method was proposed in this work for oil saturation estimation. The pore fluid self-diffusion coefficients were measured. The mechanism of wettability change for LSF is suggested based on the oil diffusion coefficient variations with LSF. The similarities and differences between the kaolinite and montmorillonite behaviors are discussed.

This work demonstrates that MR and MRI are robust tools to monitor oil displacement processes, with the potential to reveal the mechanisms of LSF and other procedures for enhanced oil recovery.

## Development of a field camera system for a 1.5T/280 mm superconducting magnet system

Y. Kobayashi, K. Kose and Y. Terada\*, Institute of Applied Physics, University of Tsukuba, Japan.

In many MRI applications, it is crucial to reduce acquisition times and there is an increasing demand for fast imaging methods, such as EPI and spiral acquisitions. However, these methods require high fidelity of hardware, and often suffer from image distortion, blurring, or other imaging artifacts due to the infidelity of imaging gradient and other hardware imperfections. Therefore, the implementation of the fast imaging methods is practically limited to advanced systems with improved hardware. In this study, we developed a field camera system [1,2] that monitors the k-space trajectory and field inhomogeneity for a 1.5T/280mm superconducting magnet system. We demonstrated that the field camera enables to recover artifact-free images, even in the presence of large hardware imperfections.

As a field camera system, 4  $^1\text{H}$ -NMR probes were built and mounted on a birdcage RF coil (60 mm in diameter) (Figs. 1(a) and (b)). The size of each probe was 51 mm (length)  $\times$  41 mm (width)  $\times$  23 mm (height). Each probe consisted of a capillary glass (inner diameter = 0.5 mm) filled with  $\text{CuSO}_4$ -doped water and a 3-turn solenoid coil. The probe lifetime was 30 ms and maximum resolution was  $(500 \text{ m})^{-1}$ . The FID signal of the 4 probes were used to analyze the k-trajectory and field drift using a first-order spherical-harmonic model with four basis function [1]. A spiral scan (32 interleaves and acquisition time = 9 ms) for a structured cylindrical phantom was monitored by the field camera.

Figures 1(c) and (d) show the nominal and monitored k-space trajectories, respectively. The monitored trajectory was significantly distorted because of the large residual eddy-current fields. The phantom image reconstructed with the nominal trajectory (Fig. 1(f)) was also distorted, compared with the spin echo image (Fig. 1(e)). The artifact was successfully removed in the image reconstructed with the monitored trajectory (Fig. 1(g)). These results showed the validity of the method.

References: [1] C. Barmet et al., MRM 60 (2008) 187.

[2] C. Barmet et al., MRM 62 (2009) 269.

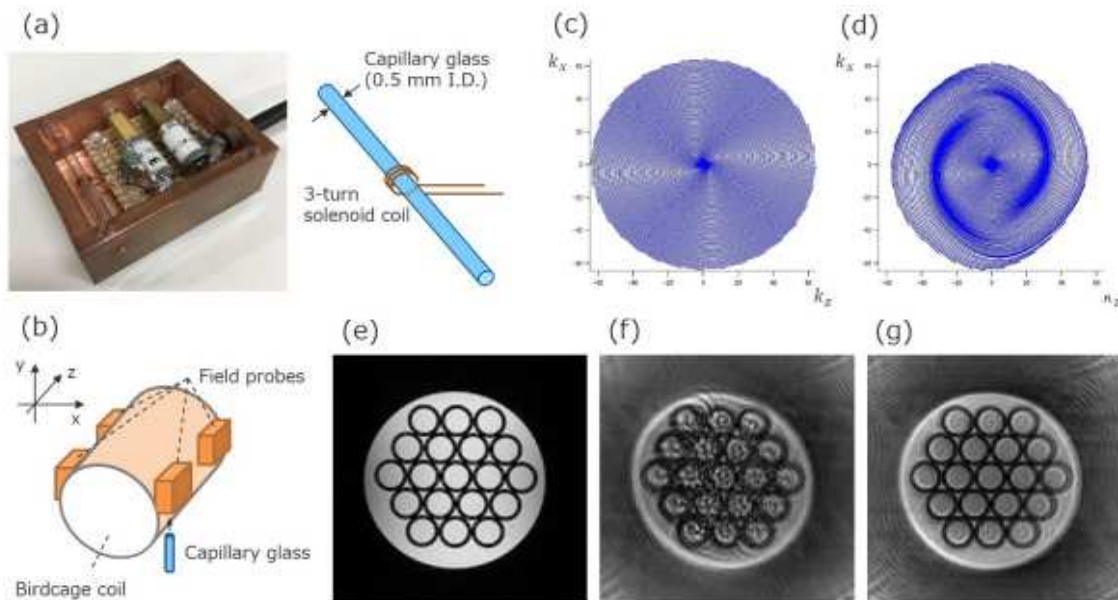


Fig. 1 (a) Home-built field probe. (b) Arrangement of the birdcage coil and field probes. (c) and (d) K-space trajectories of spiral imaging. (c) Nominal and (d) monitored trajectories. (e)-(g) Phantom images reconstructed with (e) the Cartesian trajectory and (f) the nominal and (g) monitored spiral trajectories. Matrix sizes of the reconstructed images =  $128 \times 128$ . FOV = 64 mm  $\times$  64 mm. Slice thickness = 10 mm. TE/TR = 10 ms/1000 ms.

## An Open PXIe Platform for MRI Instrumentation Development

R. Dykstra<sup>\*§</sup>, A Ang, M Bourne and S Obruchkov, School of Engineering and Computer Science, Victoria University of Wellington, New Zealand.

The entry barrier for MRI system development is often high due to the system complexity and the high speed interconnect requirements. Often, a modular approach is taken either using a high cost standard commercial backplane or developing a simple custom backplane [1,2]. PXIe [3] is a good backplane option as the data rate of the PCIe serial bus is beyond any NMR receiver requirements and being a standard allows one to make use of modules provided by many vendors. However, until now, PXIe platforms and modules are usually expensive and contain proprietary Intellectual Property (IP) so system developers have no choice but to purchase a complete vendor platform or if developing own hardware still have to pay for IP. This, as well as the system complexity, is a potential barrier to a lot university based researchers who want to develop their own MRI system hardware.

With the release of high performance integrated processor/FPGA devices from vendors such as Xilinx [4] and the availability of open source Linux operating systems has made it significantly easier to develop complex systems. The Xilinx ZYNQ series are a single chip device that contains a dual core ARM processor, FPGA fabric and dedicated PCIe peripheral units. This device combined with Linux is an elegant solution for implementing a PXIe system controller. The ZYNQ device, or just one of the newer FPGA devices with PCIe peripheral units can be used as the basis for the required RF transceiver or gradient controller modules. Now to implement a PXIe solution one still needs to develop the PCIe communications hardware for the modules as well as a device driver for the operating system. There are several vendors offering FPGA IP and device drivers but at a significant cost. The focus of this work was to develop freely available IP, a device driver and example designs so that other researchers can easily build their own MRI or other instrumentation systems.

To make it even easier to develop systems, some component distributors such as Avnet [5] have developed plug in System On Module (SOM) solutions that are basically a small board that contains either a ZYNQ device or just a FPGA, some memory, communications interfaces as well as a connector to interface with a carrier board. In our case, this carrier board is either a system controller or peripheral module and plugs directly into a standard PXIe chassis such as those provided by National Instruments [6]. This therefore allows the rapid development of Instrumentation systems.

PXIe system controller and peripheral boards have been developed including IP for the peripheral board and an associated Linux device driver for the system controller. The device driver can support multiple peripheral modules and it manages communications in both directions using either single word or DMA transfers with a maximum block size of 8MB. The device driver, FPGA IP and PCB schematics are available via GitHub. Also to be developed in the near future are, backplanes, a system timing board and a full MRI implementation.

[1] [www.magritek.com/products/kea/](http://www.magritek.com/products/kea/) [2] [mrsrl.stanford.edu/~medusa/hardware/](http://mrsrl.stanford.edu/~medusa/hardware/) [3] [www.pxisa.org/Default.aspx](http://www.pxisa.org/Default.aspx) [4] [www.xilinx.com](http://www.xilinx.com) [5] [www.avnet.com/en-us/Pages/default.aspx](http://www.avnet.com/en-us/Pages/default.aspx) [6] [www.ni.com](http://www.ni.com)

## An MRI System for Cerebral Stroke Monitoring

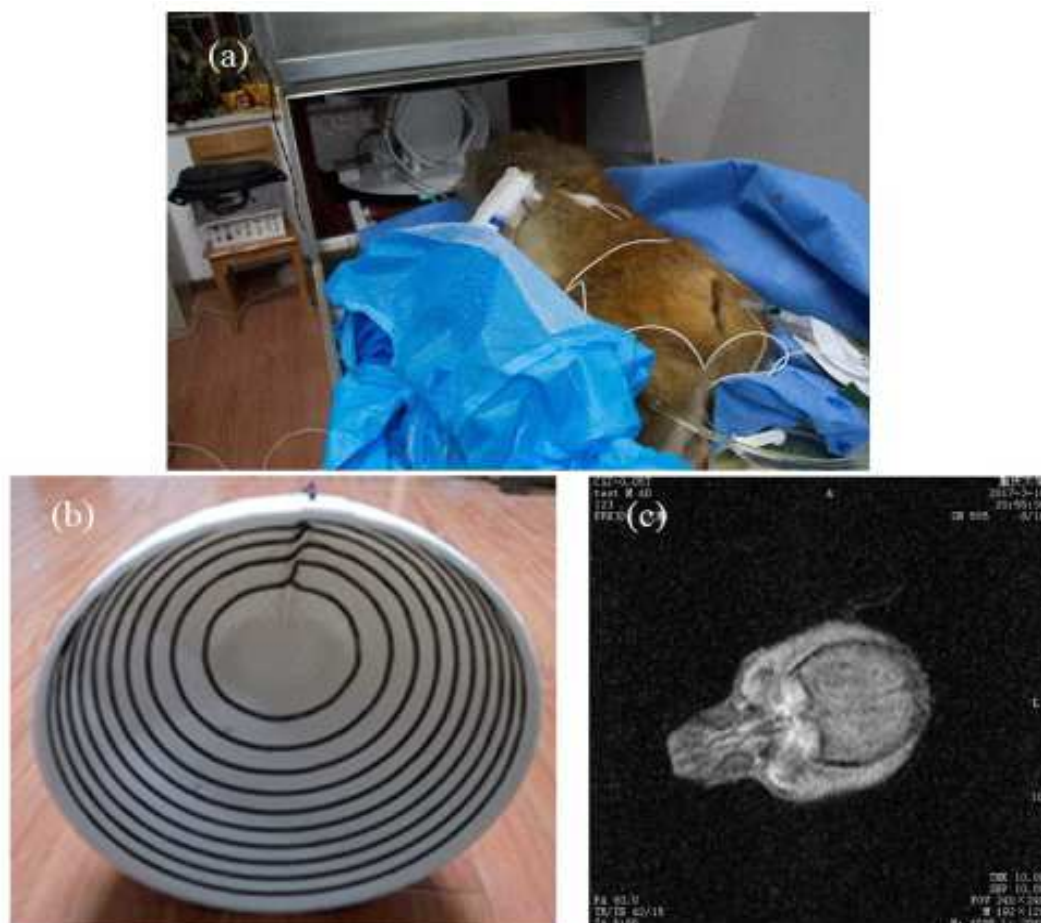
Y. He, W. He, Z. Xu, J. Wu and L. Zhang, State Key Laboratory of Power Transmission Equipment & System Security and New Technology, Chongqing University, Chongqing 400044, China.

The research data which was reported in the Lancet by the National center for chronic and Noncommunicable Disease Control and prevention of China indicated that the cerebrovascular disease was the first most common cause of death in china. The CT and MRI are effective method to diagnose the condition of stroke patients. CT has radioactivity, and traditional MRI device was pretty heavy (weighting dozens of ton) and expensive (1 million per 1 Tesla). So they couldn't be used to monitoring. Now, there have no effective image monitoring system in the clinical to monitoring the changes of stroke patient.

Since the advantage of noninvasive and resolution of image, a light-weight MRI system(50mT) was set up to achieve the monitoring of cerebral stroke. The magnet is consisted by permanent magnet (total weight: 220kg, uniformity: 50ppm in DSV 200mm). It can be push in the N-ICU (Neurologic Intensive Care Unit).

In order to achieve the purpose of monitoring, the half-open head RF (Radio Frequency) coils was designed. The PSO (particle swarm optimization) was used to optimize half-open head RF coil. Its optimized object is the distance of circular current loop. The real coil was shown in Fig.1(b).

On the basis of this system, the rhesus monkey was used to make the animal cerebral hemorrhage model. The model was used to research the ultra-low field imaging technologies for cerebral stroke monitoring. The experimental picture and MRI image were shown in Fig.1(a) and Fig.1(c).



## Magnetic Resonance Imaging with a Variable Field Superconducting Magnet that can be rotated for Vertical or Horizontal Operation

S. Vashae<sup>s</sup>, B MacMillan, M Li, F Marica\* and BJ Balcom, UNB MRI Research Centre, Department of Physics, University of New Brunswick, E3B 5A3, Canada; DP Green, Green Imaging Technologies, Inc., 520 Brookside Drive, Suite B Fredericton, NB, E3A 8V2, Canada.

Magnetic Resonance (MR) is employed in the petroleum industry for down-hole logging and for laboratory core analysis. Sensitivity of MR experiment to fluid type and fluid environment makes it well suited to these applications. The same advantages should accrue to Magnetic Resonance Imaging (MRI) measurements of core flooding experiments.

Bulk  $^1\text{H}$  relaxation time measurements are undertaken at low magnetic field to reduce magnetic susceptibility mismatch effects. These fields, typically 0.05 T, are too low for MRI studies. Higher magnetic fields (2.4 T and above) are commonly employed for biomedical MRI studies with superconducting magnets. Susceptibility mismatch effects at these field strengths can be severe for many core plugs. The best field for core plug MRI studies is sample dependent as one seeks to balance greater sensitivity at high field with susceptibility effects which decrease the transverse signal lifetimes ( $T_2$  and  $T_2^*$ ) as field increases.

New generation superconducting magnets, actively cooled rather than passively cooled, are permanently connected to the magnet power supply and thus have the possibility of variable field operation. We have recently installed such a magnet. It permits operation in the field range 0.01 T to 3 T. One can maximize the sample magnetization for high sensitivity core flooding MRI measurements, while controlling the effect of susceptibility mismatch on the signal lifetime. Because of the elimination of liquid cryogenes the new magnet is a fraction of the size and weight of conventional superconducting magnets. The magnet can easily be rotated, from horizontal to vertical, by one person.

Variable field operation permits MRI measurement of other nuclei of importance in core flooding studies. The gyromagnetic ratio of sodium  $^{23}\text{Na}$  and fluorine  $^{19}\text{F}$  are each less than that of hydrogen  $^1\text{H}$ . One can increase the static field strength to compensate for the decrease in gyromagnetic ratio such that the RF probe employed to excite and detect the signal has an unchanged frequency. This provides the experimentalist a new way to undertake multi-nuclear MRI studies of core plug systems.



The Gifford-McMahon (GM) cryocooler permits vertical or horizontal operation (indeed any orientation) unlike a pulse tube cryocooler. The magnet may be easily rotated by one person.



## Enhancements for Low-field NMR systems

J.Z. Zhen, P.L. Stanwix, M.W. Legg, K.T. O'Neill, E.O. Fridjonsson and M.L. Johns, School of Mechanical and Chemical Engineering, University of Western Australia, AUSTRALIA.

Although low-field NMR is an attractive platform for the development of sensors from the perspective of cost, size, and portability, it is well known that potential applications are limited by low signal-to-noise ratio (SNR). This low SNR is the result of poor spin polarisation, relatively long sequence delays, and increased sensitivity to changes in the ambient field as the operating field-strength is reduced. The first of these has received significant attention, with improvements to spin polarisation generally achieved through the use of pre-polarising fields or dynamic nuclear polarisation. In this work we focus on the latter two systematic limitations and present the results of two modular solutions that have been developed for an Earth's field NMR system [1] to minimise dead-time and compensate for changes in the ambient field.

The high-Q probes used in typical low-field NMR systems result in long ring-down times, requiring a long wait time (up to 25 ms) before signal acquisition can be initiated. This excludes applications with relaxation processes that occur over shorter timescales, for example high-velocity flow measurements [2]. We have developed a resistive Q-switch that reduces probe ring-down time, shortening the signal acquisition delay from 25 ms to 9 ms on an Earth's magnetic field system. The system works by switching on a resistive load to the probe immediately after the excitation radio frequency (RF) pulse is terminated. This damping process works by lowering the Q and hence speeds up the dissipation of residual stored energy in the probe, resulting in a shorter ring-down time.

Magnetic-field inhomogeneity (arising from the introduction of a sample and also the surrounding environment) strongly affects the signal amplitude of NMR systems. Therefore, it is typically compensated for prior to measurement through shimming. For example, in the Earth's field system used in this work, shimming is performed by applying small offset currents to a 3-axis gradient set, where the optimisation of the shim is achieved through a iterative gradient-ascent algorithm that can take up to 10 minutes to complete. Whilst small changes to the ambient field have a minimal effect on high-field spectrometers, they can have a relatively strong influence on homogeneity in such low-field systems. Changes may be caused by simply moving ferro-magnetic objects within the immediate vicinity, requiring the shim optimisation to be repeated. We have developed a passive magnetometer array based on simple 3-axis sensors that monitors changes in the ambient field and adjusts the shimming currents accordingly. This shim-feedback can be performed within seconds, making it suitable to apply during long measurements, between acquisitions, where the area surrounding the low-field NMR system cannot be controlled.

### References

- [1] Terranova-MRI: Earth's Field MRI Teaching System, <http://www.magritek.com/products/terranova/>
- [2] K.T. O'Neill, E.O. Fridjonsson, P.L. Stanwix, M.L. Johns, Quantitative velocity distributions via nuclear magnetic resonance flow metering, *Journal of Magnetic Resonance*, 269 (2016) 179-185.



## Pattern Recognition for Comparison of NMR Depth Profiles of Mortar from Wall-Paintings

C. Rehorn\*, W. Zia and B. Blümich<sup>§</sup>, Institut für Technische und Makromolekulare Chemie (ITMC), RWTH Aachen University, Aachen, Germany; C. Kehlet and E. Del Federico, Department of Mathematics and Science, Pratt Institute, Brooklyn, USA; T. Meldrum, The College of William & Mary, Integrated Science Center, Williamsburg, USA.

Recently, both commercial and scientific interest in artificial intelligence is on a steady rise. The algorithms developed today could soon be used to redefine what is considered a repetitive task that can be performed by the computer. One of the most important aspects in human and machine learning is the ability to recognize patterns in data and describe them in a way that is simple and intuitive to understand.

In our work, we present a recently developed MATLAB toolkit that is optimized to compare NMR depth profiles, i.e. one-dimensional imaging data acquired with unilateral NMR sensors such as the MOUSE [1,2]. It is applied to compare mortar stratigraphy of wall paintings acquired in a variety of houses in the ruins of Herculaneum. Like Pompeii, the town of Herculaneum was situated in immediate proximity of Mount Vesuvius and was engulfed in ashes and lava shortly after its infamous eruption in the year 79 AD. To this day, the preserved ruins are studied with great interest in the painting and preparation techniques of the ancient roman craftsmen [3]. The stratigraphy is thought to be correlated with the function of the room and the social standing of the estate owners [4].

In this work, we used three distinct methods to calculate and display the pattern recognition. Principal Component Analysis serves as an unsupervised algorithm, while Linear Discriminant Analysis can be employed when information on the class structure is already available and inter-class scatter needs to be observed. To include the possibility of varying layer thicknesses in the stratigraphy, Dynamic Time Warping is included into the toolkit. The application of these methods to a collection of more than 60 depth profiles simplifies the evaluation by increasing the information density. Separation and overlap of houses and building complexes are recognized. By manually grouping the profiles regarding to their place of origin, between-class and within-class scatter are examined.

The work was financed by The National Centre for Research and Development in Poland (contract No. STRATEGMED2/265761/10/NCBR/2015).

### References

- [1] G. Eidmann, R. Savelsberg, P. Blümler, B. Blümich, , J. Magn. Reson. A 122 (1996) 104109.
- [2] B. Blümich, J. Perlo, F. Casanova, Prog. Nucl. Magn. Reson. Spectrosc. 52 (2008) 197169.
- [3] J. R. Clarke, The Houses of Roman Italy, 100 B.C.-A.D. 250: Ritual, Space, and Decoration, University of California Press, Los Angeles (1991).
- [4] A. Wallace-Hadrill, Houses and Society in Pompeii and Herculaneum, Princeton, University Press, Princeton (1996).

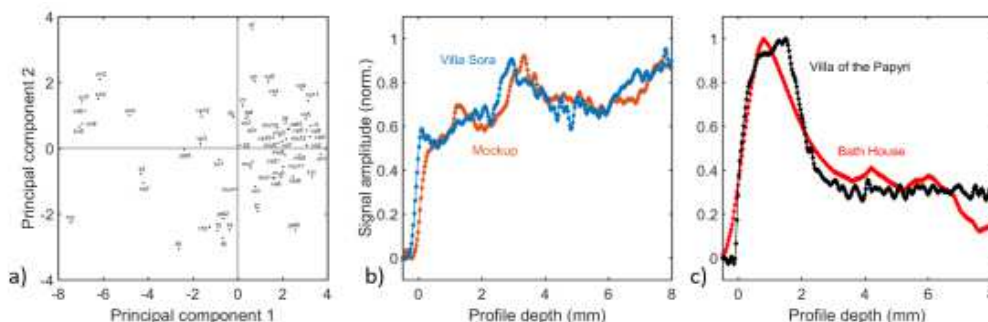


Figure 1: Principal Component Analysis (a) can help to find patterns in the data. Profiles that are recognized to match can be found in proximity (b, c). When profiles do not seem similar, the distance between the points is large.

### Development of portable MRI for early detection of baseball elbow

K. Tanabe, K. Katsumi and Y. Terada\*, Institute of Applied Physics, University of Tsukuba, Japan; Y. Okamoto, Institute of Clinical Medicine Department of Diagnostic and Interventional Radiology, University of Tsukuba, Japan.

Okamoto et al. have reported that a low-field MRI system dedicated for small joints is useful for early detection of baseball elbow [1]. However, the scanner used was not portable, and the subjects were limited to nearby players. Having a portable elbow MRI would allow MRI screening at a remote baseball ground and expand the availability of the screening. In this study, we developed a portable MRI system for early detection of baseball elbow.

We used a 0.2 T permanent magnet (NEOMAX Engineering, Japan; 200 kg; 16 cm gap; 44 cm x 50 cm x 36 cm, 10 ppm over 10 cm diameter of spherical volume) (Fig. 1(a)), a home-built RF coil, gradient, and shim coils, which are portable using a hand lift. An MRI console consisted of a digital transceiver (DTRX4, MRTechnology, Japan), a gradient driver (20 V, 10 A, DST Inc., Japan), and a transmitter (150 W, DST Inc., Japan), which were installed in a 19-inch rack (56 cm x 77 cm x 60 cm, 80 kg) (Fig. 1(b)) and portable manually. All the devices can be mounted on the car (total space is only approx. 160 cm x 220 cm). A multislice gradient echo was used (coronal plane, FOV = 256 mm x 128 mm, 11 slices, slice thickness = 3mm, TR = 1200 ms, TE = 16ms, scan time = 2 min 4 s, matrix size = 256 x 128). Fig. 1(c) shows an MRI elbow image of a 22-year-old male (Fig. 1(d)). The anatomical structures are visible. We developed a local shield (both on the shoulder and wrist sides) and reduced external noise (Fig. 1(e)), which led to the improved image quality. We will also perform the elbow imaging to verify the validity of the elbow examination with the portable MRI.

[1] Y. Okamoto et al., Incidence of elbow injuries in adolescent baseball players: screening by a low field magnetic resonance imaging system specialized for small joints, *Jpn. J. Radiol.* 34 (2016) 300-6.

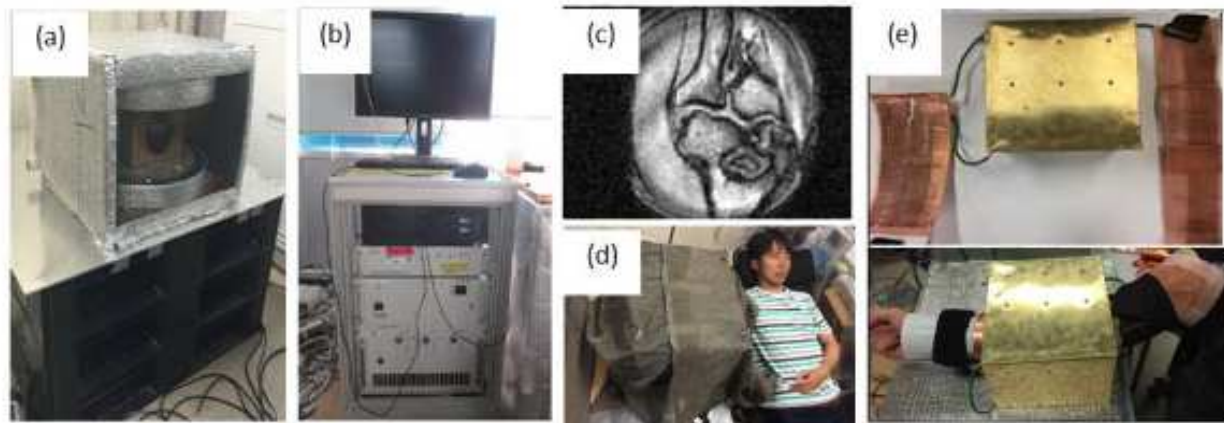


Fig. 1: (a), (b) Portable elbow MRI system. (c) Cropped image (85mm x 128mm). (d) MRI examination. (e) Local shield.

### ILT analysis of porous soft matter

D. Jaschtschuk<sup>\*</sup>, C. Rehorn and B. Blümich<sup>§</sup>, Institut für Technische und Makromolekulare Chemie,, RWTH Aachen University, 52074 Aachen.

Single-sided NMR sensors, such as the NMR-MOUSE<sup>®</sup>, are a powerful tool for non-invasive investigation of several porous biological and synthesized soft matter materials. Depth profiles of violins and tire samples were acquired by mounting the NMR-MOUSE<sup>®</sup> to a step-motor driven lift and retracting the sensor in decrements of 100  $\mu\text{m}$  to 150  $\mu\text{m}$  away from the sample. Effectively, the distribution of  $T_2$  times can be employed to gain additional contrast. This can be realized through a weight function, which assigns a value derived from a multi-echo sequence to each depth increment by dividing the amplitude sum of the first few echoes by that of all the rest. This parameter is intrinsically unstable as it depends on the choice of both divisors. A cleaner method is presented here, where Inverse Laplace Transform (ILT) data are analyzed at each depth. By calculating and using the integrals of peaks in chosen  $T_2$  ranges to calculate the weight parameter, we obtain a more stable contrast that also has physical instead of arbitrary meaning (Fig. 1 a). The method is very sensitive to changes in the ratio of shorter and longer  $T_2$  times, which makes it possible to detect short relaxation time components even though their amplitude may be small, which makes it a formidable tool to observe thin layers such as varnish or just to observe effects of brittle surfaces.

It is also possible to create  $T_2$  distribution profiles to gain insight into the variation of different molecular components indicated by their transverse relaxation times (Fig. 1 b). One can distinguish between different components, even within one layer. Furthermore, changings in the molecular properties within the transition zone of layers can be observed due to changes in the relaxation behavior.

The work was financed by The National Centre for Research and Development in Poland (contract No. STRATEGMED2/265761/10/NCBR/2015).

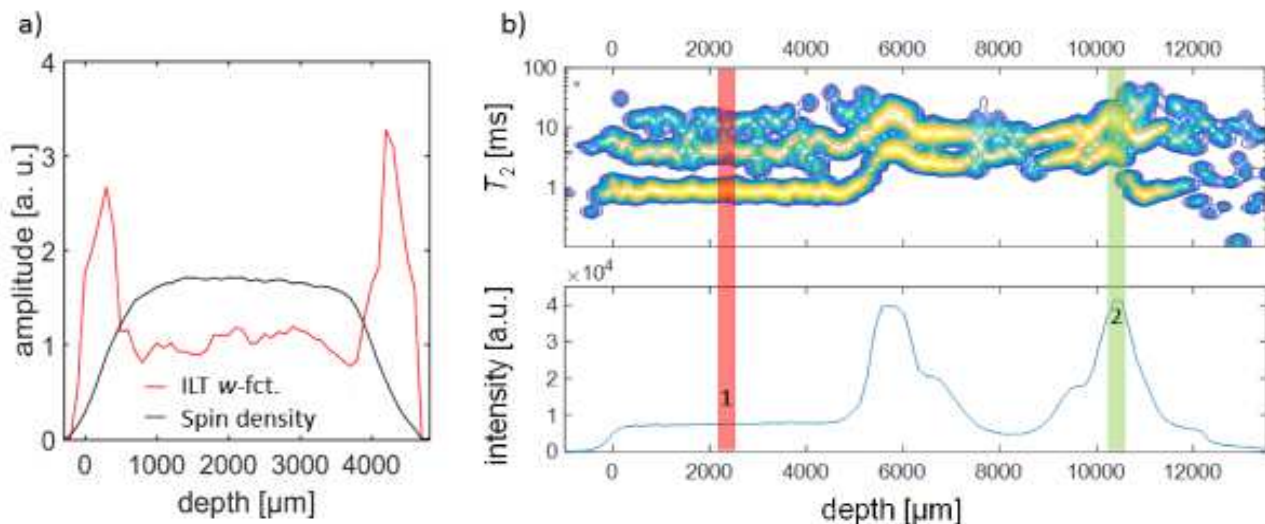


Figure 1: a) Spin density and ILT weighting function profile of a violin. The ILT w-fct. indicates treatment of the wood on both surfaces. b)  $T_2$  distribution profile (top) and the corresponding spin density profile (bottom) of a tire. The number of components and the  $T_2$  times vary over the whole profile of the tire.

**Developing magnetic resonance imaging (MRI) by studying batteries**

Y. AlZahrani, J. Bray and M. Britton, School of Chemistry, University of Birmingham, Birmingham B15 2TT, UK.

There is significant interest in the development of improved energy storage devices, in particular, the development of high performance advanced batteries. In order to improve such energy storage devices, a full understanding of the distribution of chemical species, ion transport, side reactions and structural changes of the electrodes, *in operando*, is required.

Magnetic resonance imaging (MRI) is a promising tool to visualize and understand the electrochemical processes inside batteries and it can provide significant insight in a non-invasive way<sup>1</sup>. There have been <sup>7</sup>Li MRI studies of lithium-ion batteries<sup>2-4</sup>. Potential replacements for Li-ion batteries are zinc and aluminium based batteries<sup>5</sup>. However, in order to study zinc and aluminium batteries, an alternative method should be developed to study the electroactive species using <sup>1</sup>H NMR signal from the electrolyte<sup>6</sup>.

This project focuses on using MRI techniques to determine the speciation and distribution of electroactive zinc species in novel electrolytes, such as room temperature ionic liquids (RTILs) and deep eutectic solvents (DESS). Studying the effect of Zn<sup>2+</sup> on the NMR parameters, such as  $T_1$  and  $T_2$  relaxation times, of the electrolyte will facilitate visualization of the distribution of zinc species in RTILs or DESS based batteries.

**References:**

1. M. Britton, *Chem. Phys. Chem.*, 2014, 15, 17311736.
2. S. Chandrashekar, N. Trease, H. Chang, L. Du, C. Grey, A. Jerschow, *Nat. Mater.*, 2012, 11, 311315
3. H. Chang, A. Ilott, N. Trease, M. Mohammadi, A. Jerschow, C. Grey, *J. Amer. Chem. Soc.*, 2015, 137 (48), 1520915216.
4. A. Ilott, M. Mohammadi, H. Chang, C. Grey, A. Jerschow, *Proc. Nati. Acad. Sci. U.S.A.*, 2016, 113 (39), 1077910784.
5. M. Lin, M. Gong, B. Lu, Y. Wu, D. Wang, M. Guan, M. Angell, C. Chen, J. Yang, B. Hwang, H. Dai, *Nature*, 2015, 520, 324-328.
6. M. Britton, P. Bayley, P. Howlett, A. Davenport, M. Forsyth, *J. Phys. Chem. Lett.* 2013, 4, 3019-3023.

**Plasma Viscosity measurements in Sickle Cell Disease and Multiple Myeloma employing NMR**

M. A. Lores Guevara, J. C. García Naranjo and Y. M. Torres, Centro de Biofísica Médica, Universidad de Oriente, Patricio Lumumba S/N. CP: 90500. Santiago de Cuba. Cuba; N Rodríguez Suárez, Chemistry Department. Natural Sciences Faculty. Universidad de Oriente, Patricio Lumumba S/N. CP: 90500. Santiago de Cuba. Cuba; L. C. Suárez Beyrio, M. A. Marichal Felue, T Simón Brada and I. C. Rodríguez Reyes, General Hospital "Dr. Juan Bruno Zayas Alfonso", Carretera del Caney S/N. Santiago de Cuba. Cuba; J. Philippé, Department of Clinical Chemistry, Immunology and Microbiology, Ghent University, Ghent, Belgium.

Measuring viscosity is an important tool for diagnosis in medical applications. NMR methods can be applied for measuring this parameter provided some considerations are assumed. In this work a NMR based experimental procedure to determine the dynamic viscosity ( $\eta$ ) in plasma solutions is presented. An equation relating  $\eta$  and the transversal proton magnetic relaxation time ( $T_2$ ) is obtained after considering a fast exchange between the free and associated water inside the plasma solution, the dominant role of the associated water in proton magnetic relaxation, the characteristic mobility of the plasma proteins and the magnetic field employed. Carr-Purcell-Meiboom-Gill pulse sequence was employed for measuring  $T_2$  in a magnetic resonance console coupled to a homogeneous magnetic system (0,095 T). A  $\eta$  value of  $1.66 \pm 0.05$  mPas was obtained in 27 control individuals, which statistically match with the value obtained in the same samples using the Oswald viscometer ( $1.62 \pm 0.03$  mPas).  $\eta$  was determined in 166 patients with Multiple Myeloma ( $2.24 \pm 0.07$  mPas) and 54 with Sickle Cell Disease ( $1.92 \pm 0.05$  mPas) showing a statistically significant increase over the control individuals. The results show the utility of this NMR method to estimate dynamic viscosity in Plasma with medical purpose.

**References**

1. Rosencranz, R., Bogen, S. A.: *A m. J. Clin. Pathol.* 125, S78-S86 (2006)
2. Hong, R., Cima, M.J., Weissleder, R., Josephson, L.: *Magnetic Resonance in Medicine.* 59, 515-5120 (2008)



## Multi-Temperature In Situ Magnetic Resonance Imaging of Polarization and Salt Precipitation in Li-Ion Battery Electrolytes

J. David Bazak, S. A. Krachkovskiy and G. R. Goward\*, Department of Chemistry, McMaster University, Hamilton, Ontario, Canada.

The parameterization and validation of accurate electrochemical models for lithium-ion batteries in automotive applications is an important milestone in their widespread deployment. Much effort has been focused on the mass transport characteristics of the electrode domains, but a significant fraction of overall polarization stems from concentration gradients that form in the electrolyte domain and their attendant effect on the mass transport parameters, which have recently been shown by *in situ* MRI to be quite significant.<sup>1</sup> The effect of temperature on these concentration gradients remains to be explored by *in situ* MRI.

A comparison of the salt concentration profiles at a series of temperatures was therefore conducted using <sup>19</sup>F chemical shift imaging (CSI) of the PF<sub>6</sub><sup>-</sup> anions in the electrolyte, to assess how the magnitudes of the gradients varied with temperature and to confirm agreement with magnitudes predicted from *ex situ* transport measurements. In order to quantitatively make this comparison, a robust means of imaging is required

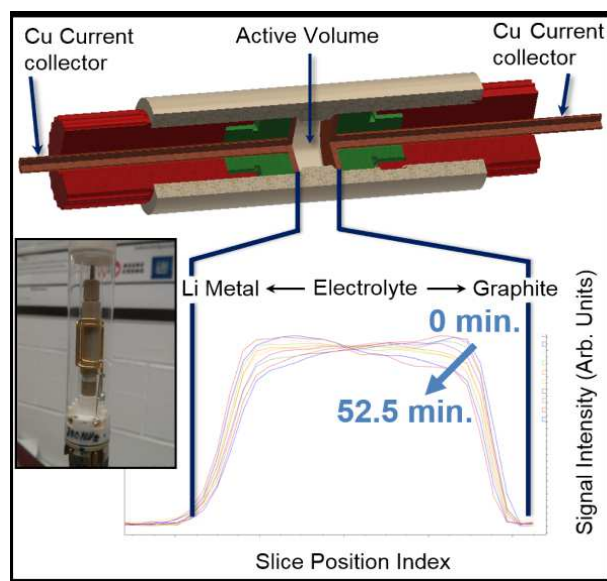
to calibrate the active volume sizing for CSI, which exhibits 'dead space' near the conductive parts of the *in situ* cell.<sup>2</sup> This was achieved with the pure-phase-encoding, low-tip-angle centric scan SPRITE imaging technique.<sup>3</sup> Conventional frequency-encoding techniques are ill-suited to the significant susceptibility variations across the cell, rapid acquisition times notwithstanding. CSI, which is phase-encoding, yields much sharper images than frequency-encoding techniques, even with only two scans per gradient step, and much better SNR than SPRITE, but still exhibits artifacts from field inhomogeneity to which only SPRITE is immune. Within 3 $\sigma$  confidence intervals, agreement was found between the concentration gradients measured by *in situ* MRI and the *ex situ* methods, directly demonstrating that *in situ* MRI can generate transport parameters relevant to real battery modelling efforts.

A surprising outcome of these studies was that at 10°C, a conventional electrolyte mixture exhibited anomalous concentration gradient formation with a modest current density, whereas the same mixture could be polarized without difficulty at room temperature. On comparing raw CS images from before the polarization and after the relaxation of the disrupted concentration gradient, it is clear that the overall signal intensity is lower whilst the shape of the profile is retained, which is a direct indicator that salt precipitation has occurred and a result that would be difficult to confirm without the use of *in situ* MRI.

(1) Krachkovskiy, S. A.; Bazak, J. D.; Werhun, P.; Balcom, B. J.; Halalay, I. C.; Goward, G. R.. J. Am. Chem. Soc. 2016, 138 (25), 79927999.

(2) Sethurajan, A. K.; Krachkovskiy, S. A.; Halalay, I. C.; Goward, G. R.; Protas, B. J. Phys. Chem. B 2015, 119 (37), 1223812248.

(3) Halse, M.; Goodyear, D. J.; MacMillan, B.; Szomolanyi, P.; Matheson, D.; Balcom, B. J. J. Magn. Reson. 2003, 165 (2), 219229.





### Carbonation front in cement paste and mortar detected by low-field unilateral NMR

F. Diaz-Diaz and P. F. de Cano-Barrita\*, CIIDIR Unidad Oaxaca/Instituto Politecnico Nacional, Calle Hornos No. 1003, Sta. Cruz Xoxocotlan, Oaxaca, Mexico; B. J. Balcom<sup>§</sup>, Department of Physics, MRI Center, University of New Brunswick, Fredericton, New Brunswick, E3B 5A3, Canada.

Carbonation is one of the main causes of steel corrosion in reinforced concrete structures [1]. The aim of the present work was to use low-field unilateral NMR to observe the carbonation front in cement pastes and mortars subject to accelerated carbonation and to compare the results with the phenolphthalein test. Cement paste (6 cm long) and mortar (5 cm long) samples at water-to-cement ratios of 0.60, 0.50, and 0.40 were prepared and moist cured for 60 days. After moist curing and conditioning at 75% RH and 30 °C, the samples were subjected to accelerated carbonation with 4% by volume CO<sub>2</sub> at 75% RH and 30 °C. A three-magnet array [2] with a 4.5 cm diameter and 0.25 cm long solenoid coil were used to obtain the CPMG decay at different positions along the samples. The samples were displaced inside the solenoid in 0.5 cm steps. The results show that carbonation increases the T<sub>2</sub> lifetime and reduces the signal intensity, compared with the noncarbonated region/control samples (Fig. 1). A reduction in total porosity and changes in the pore structure/surface chemistry are caused by carbonation [3]. The position with the highest rate of T<sub>2</sub> change was in agreement with the fully carbonated front determined by the phenolphthalein test.

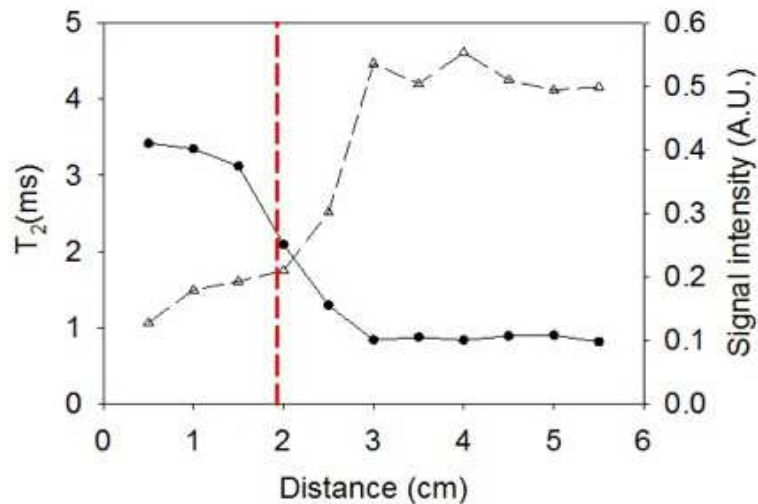


Figure 1. Long T<sub>2</sub> lifetime component (solid line) and signal intensity (dashed line) versus distance in a 6 cm long 0.40 w/c Portland cement paste. The samples were vacuum saturated after carbonation to perform the CPMG measurements.

#### REFERENCES

1. Neville AM (2012) Properties of Concrete, 5th ed. USA
2. García-Naranjo JC, Guo P, Marica F, et al (2014) Magnetic resonance core-plug analysis with the three-magnet array unilateral magnet. *Petrophysics* 55:229–239.
3. Cano-Barrita PF de J, Balcom BJ, Castellanos F (2017) Carbonation front in cement paste detected by T<sub>2</sub> NMR measurements using a low field unilateral magnet. *Materials and Structures* 50:150.

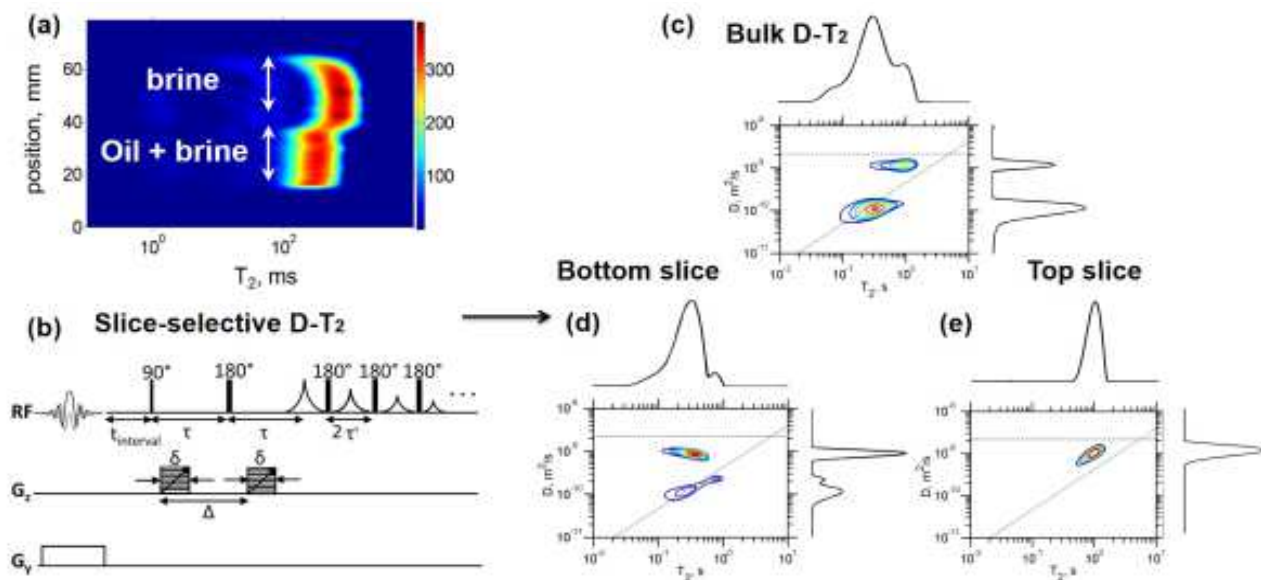
## Local Diffusion and Diffusion- $T_2$ Distribution Measurements in Porous Media

S. Vashaei, B Newling, B MacMillan, F Marica, M Li and BJ Balcom, UNB MRI Centre, Department of Physics, University of New Brunswick, Fredericton, New Brunswick, E3B 5A3, Canada.

Slice-selective pulsed field gradient (PFG) and PFG- $T_2$  measurements are developed to measure spatially-resolved molecular diffusion and diffusion- $T_2$  distributions. A spatially selective adiabatic inversion pulse was employed for slice-selection. The slice-selective pulse is able to select a coarse slice, on the order of 1 cm, at an arbitrary position in the sample.

The new method can be employed to characterize oil-water mixtures in porous media. The new technique has an inherent sensitivity advantage over phase encoding imaging based methods due to signal being localized from a thick slice. The method will be advantageous for magnetic resonance of porous media at low field where sensitivity is problematic.

Experimental CPMG data, following PFG diffusion measurement, were compromised by a transient  $\Delta B_0(t)$  field offset. The off resonance effects of  $\Delta B_0(t)$  were examined by simulation. The  $\Delta B_0(t)$  offset artifact in D- $T_2$  distribution measurements may be avoided by employing real data, instead of magnitude data.



(a) A  $T_2$  spatially-resolved map of fully saturated Bentheimer injected with S6 oil, generated with SE-SPI method. The bottom of the sample (bottom of the image) includes a mixture of S6 oil and brine, but the top of the sample is still fully brine-saturated. (b) Adiabatic inversion SE-PFG- $T_2$  for slice-selective D- $T_2$  measurements of regions of interest.

(c) Bulk D- $T_2$  contour plot for S6 oil/brine-Bentheimer system, measured with bulk SE-PFG- $T_2$ . The brine and S6 oil are clearly separated. (d) The D- $T_2$  plot for a slice chosen from the bottom of the sample (bottom of the image) which includes both brine and S6 oil. (e) The D- $T_2$  plot for a slice chosen from the top of the sample which is fully brine-saturated.

**Optimization of a Parallel Plate Resonator for High Resolution Thin Film Imaging in Lithium Ion Batteries.**

A. Ramirez Aguilera<sup>\*a,b</sup>, B. MacMillan and B. J Balcom, <sup>a</sup>UNB MRI Centre, , Department of Physics, , University of New Brunswick, , Fredericton, New Brunswick, , Canada E3B 5A3; <sup>b</sup>Centro de Biofísica Médica, , Universidad de Oriente, , Patricio Lumumba s/n, , Santiago de Cuba, , Cuba 90500; G. R. Goward, Department of Chemistry, , McMaster University, , Hamilton, Ontario, , Canada L8S 4L8.

Choosing the right NMR probe with the correct dimensions plays an important role in magnetic resonance imaging, especially for high resolution thin film imaging. In this work a parallel plate resonator, that is intended to work as part of a lithium ion battery, has been optimized in order to do high resolution imaging in the electrochemical device. The design of the probe and the optimization process was performed using CST Micro Wave Studio. A capillary tube of 400  $\mu\text{m}$ , filled with doped water was used for testing the optimized probe in a 2.4 T magnet. It is shown that increasing the width of the connections of the plate produce an increase of up to 75 % in the homogeneity of the  $\mathbf{B}_1$  field. The best approach was to keep the dimensions constant and use additional capacitors at the device corners to distribute the current. This approach produce a  $\mathbf{B}_1$  field stronger at the centre of the plate and increases the area of homogeneity in the plate up to 80%. The experimental result show that it is possible to achieve 10  $\mu\text{m}$  depth resolution using the optimized probe. The parallel plate resonator will be tested as part of a working lithium ion battery.

**References**

1. Ziheng Zhang, Andrew E. Marble, Rodney P. MacGregor, Jonathan Martin, Haijiang Wang, Bruce J. Balcom, "Zero-mode TEM parallel-plate resonator for high-resolution thin film magnetic resonance imaging" *Can. J. Chem.*, 89:745-753 (2011).
2. Ziheng Zhang, Jonathan Martin, Jinfeng Wu, Haijiang Wang, Keith Promislow, Bruce J. Balcom, "Magnetic resonance imaging of water content across the Nafion membrane in an operational PEM fuel cell", *Journal of Magnetic Resonance*, 193(2):259-266 (2008).

## Characterizing heterogeneous water populations by Overhauser DNP enhanced relaxometry and diffusometry

T. Überrück and B. Blümich<sup>s</sup>, RWTH Aachen University, Institut für Technische und Makromolekulare Chemie, Worringerweg 1, 52074 Aachen, Germany; O. Neudert\* and S. Stapf, Technical University Ilmenau, Institut für Physik, Unterpörlitzer Straße 38, 98693 Ilmenau, Germany; J. Granwehr, Forschungszentrum Jülich, Institut für Energie- und Klimaforschung, Ostring 10, 52425 Jülich, Germany; S. Han, University of California Santa Barbara, Department of Chemistry and Biochemistry, Santa Barbara, CA 93106, USA

There are many materials systems for which the interaction between the material and the solvent water is essential to their function. A strategic use of nitroxide radical based spin probes coupled with Overhauser dynamic nuclear polarization (ODNP) provides an opportunity to selectively enhance the relaxation or diffusion properties of the solvent in direct contact with the spin probe that is associated with the material. The use of ODNP is a common method in Biochemistry, but there are other aqueous non-biological systems this technique can be applied to. One field of special interest are membrane materials that are applied in e.g. fuel cells. A better insight into the water conduction properties of those membrane materials would enable new perspectives in improving their efficiencies. A previous published study has shown that 4-Amino-TEMPO, 4-Hydroxy-TEMPO and TEMPO display significantly different partitioning within a water-soaked Nafion membrane system. Based on the differential partitioning of 4-Amino-TEMPO to the sulfonated Nafion surface and 4-Hydroxy-TEMPO to the solvent channel, differential solvent dynamic properties in direct contact with the Nafion surface vs channel have been derived. However, this interpretation has been questioned in the light of whether these spin probes alter the properties of Nafion.

Here, we present a proof of principle, as well as critical study on the example of water-soaked Nafion membranes into which various mono nitroxide radical probes are imbibed to showcase the benefit and detriment of ODNP-enhanced relaxometry and diffusometry for providing insight into the material-solvent-spin probe interaction that is otherwise difficult to gain.

In short, we find that (i) the spin probes even at relatively modest concentration dramatically alter the function-relevant properties of Nafion, while (ii) specific spin probes are highly surface-active and dehydrate Nafion's surface water, while the structural properties of Nafion remain unaltered as seen by SAXS.

The work was financed by The National Centre for Research and Development in Poland (contract No. STRATEGMED2/265761/10/NCBR/2015).

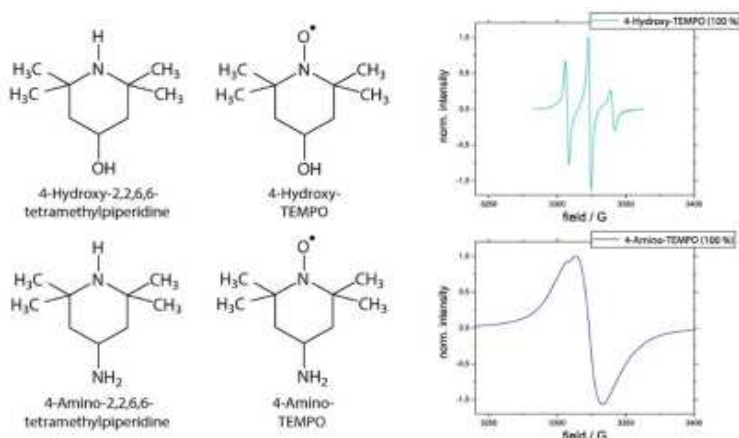


**Fig.1:** Chemical structure of the paramagnetic spin probes 4-Hydroxy- and 4-Amino-TEMPO and their diamagnetic equivalents. The EPR spectrum for 4-Hydroxy-TEMPO shows three distinct lines indicating a mobile environment for the spin probes, whereas 4-Amino-probes show reduced mobility resulting in a single Heisenberg exchanged EPR line.